

**IDENTIFICATION AND EVALUATION OF PROBABLE
PROTEIN BIOMARKERS IN GESTATIONAL DIABETES
MELLITUS**

Thesis Submitted for the Award of the Degree of
DOCTOR OF PHILOSOPHY

in
Biotechnology

By
Amarish Kumar Sharma
41800098

Supervised By
Dr. Manoj Kumar Jena (20283)
Department of Biotechnology
Lovely Professional University



L LOVELY
P ROFESSIONAL
U NIVERSITY

Transforming Education Transforming India

LOVELY PROFESSIONAL UNIVERSITY, PUNJAB

2024

DECLARATION

I, hereby declared that the presented work in the thesis entitled “**Identification and Evaluation of Probable Protein Biomarkers in Gestational Diabetes Mellitus**” in fulfillment of degree of **Doctor of Philosophy (Ph. D.)** is outcome of research work carried out by me under the supervision of Dr. Manoj Kumar Jena, working as Associate Professor, in Department of Biotechnology, School of Bioengineering and Biosciences of Lovely Professional University, Punjab, India. In keeping with general practice of reporting scientific observations, due acknowledgements have been made whenever work described here has been based on findings of other investigator. This work has not been submitted in part or full to any other University or Institute for the award of any degree.



Name of the scholar: Amarish Kumar Sharma

Registration No.: 41800098

Department/school: Biotechnology

Lovely Professional University,

Punjab, India

CERTIFICATE

This is to certify that the work reported in the Ph. D. thesis entitled **Identification and Evaluation of Probable Protein Biomarkers in Gestational Diabetes Mellitus**” submitted in fulfillment of the requirement for the award of degree of **Doctor of Philosophy (Ph.D.)** in Department of Biotechnology, School of Bioengineering and Biosciences, Lovely Professional University, is a research work carried out by **Amarish Kumar Sharma**,41800098, is bonafide record of his original work carried out under my supervision and that no part of thesis has been submitted for any other degree, diploma or equivalent course.



Manoj Kumar Jena

(Signature of Supervisor)

Name of supervisor: Dr. Manoj Kumar Jena

Designation: Associate Professor

Department/school: Biotechnology

University: Lovely Professional University, Phagwara

CONTENTS

S.No	Chapter	Page No.
1	INTRODUCTION	1
1.1	Classification and Prevalence of Gestational Diabetes	2
1.2	Epidemiology	4
1.3	Importance of Early Detection and existing Diagnostic challenge	5
1.4	Rationale for Protein Biomarkers	5
1.5	Methodological Approaches for Investigating Gestational Diabetes Mellitus: In Vitro and In Vivo Models	7
1.6	Significance of the Study	8
1.7	Research Gap Identification and Research Hypothesis	8
1.8	Research Objectives	10
2	REVIEW OF LITERATURE	11
2.1	Pathophysiology of GDM	12
2.2	Insulin Resistance	13
2.3	The Pathology and Pharmacological Approaches in Gestational Diabetes Mellitus (GDM)	18
2.4	Maternal and Fetal Outcomes	19

2.4.1	Obesity	19
2.4.2	Fetal Derangements in GDM	20
2.5	Current Diagnostic Methods for GDM	21
2.6	Challenges and Gaps in Current Diagnostic Methods	22
2.7	Limited Exploration of Biomarkers	22
2.8	Protein Biomarkers Explored in GDM	23
2.8.1	Vasculo-endothelial growth factor (VEGF)-A Potential Biomarker for GDM Screening	23
2.9	Vasculo-Endothelial Growth Factor (VEGF) and Angiogenesis	25
2.10	In-vitro cell culture screening platform for GDM	30
2.11	Predictive Biomarkers for the Early Diagnosis of GDM	31
2.12	Relevance of Protein Biomarkers to GDM diagnosis	33
3	METHODOLOGY	37
3.1	Materials Required for BeWo Cell Study	38
3.1.1	Cell Culture Materials	38
3.1.2	Cell Culture Equipment	38
3.1.3	Software and Analysis	38

3.2	BeWo Cell Culture	39
3.2.1	BeWo In-Vitro Cell Culture process	39
3.2.2	Cell Counting and Viability	40
3.2.3	BeWo cell culture and differentiation	42
3.2.4	Development of insulin-resistant cells and VEGF treatment	42
3.2.5	Treatment groups	43
3.2.6	Glucose uptake assay using flow Cytometry	43
3.3	Proteome Analysis (LCMS)	45
3.3.1	Sample Preparation	45
3.3.2	Mass Spectrometric Analysis of Peptide Mixtures	46
3.3.3	Data Processing	46
3.4	Invivo Experimental Analysis	47
3.4.1	Study Plan	48
3.4.2	Overview of Invivo experimental study	51
3.5	Enzyme-linked immunosorbent assay (ELISA) Analysis	51
3.5.1	Experimental System (ELISA)	52
3.5.2	Materials Required	53

3.5.3	Sample Preparation	53
3.5.4	ELISA-Reagent Preparation: Dilution Series	54
4	Results and Discussion	57
4.1	BeWo Cell Culture and differentiation	57
4.2	Flow Cytometry Analysis for Glucose uptake	60
4.3	Proteome analysis through LCMS	71
4.4	Evaluation of VEGF effect on glucose uptake	95
4.5	Formations of Copulation or Vaginal plug [Confirmation of Pregnancy]	99
4.6	Streptozotocin (STZ) Induction and Blood glucose profiling	102
4.7	Blood Pooling and Sampling	104
4.8	Mitochondria Fission Factor (Mff)	105
4.9	ELISA Analysis	108
5	SUMMARY	111
6	CONCLUSION	114
7	BIBLIOGRAPHY	i-xxxvi
8	APPENDIX	i-l
9	LIST OF PUBLICATIONS	i-iii

10	LIST OF CONFERENCES	i-iii
-----------	----------------------------	--------------

LIST OF TABLES

Table No	Description	Page No
1.1	Diagnostic Guidelines for Detecting Gestational Diabetes Mellitus Using the Oral Glucose Tolerance Test	2
2.1	List of common and specific biomarkers for Type 2 Diabetes & Gestational Diabetes Mellitus respectively	32
3.1	Observation and calculation of viable cell count and percentage viability	41
3.2	Experimental animals grouping and dosing schedule	50
4.1	Flow Cytometry results for Glucose uptake	60
4.2	Flow Cytometry results illustrating CV and fold change in Glucose uptake for Control Vs Test group.	62
4.3	Body Weight of Sprague-Dawley (SD) female rats pre and post pregnancy	101
4.4	Streptozotocin (STZ) Induction in SD pregnant Rats	102
4.5	Blood Glucose Profiling	103
4.6	Standard Curve Analysis	108

LIST OF FIGURES

Figure No	Description	Page No.
1.1	Global Mapping of Gestational Diabetes Mellitus (GDM): An Epidemiological Survey of Affected Female Populations	4
2.1	The pathophysiological mechanisms involving β -cell function and insulin sensitivity are compared between normal and gestational diabetes mellitus (GDM) conditions	12
2.2	Underlying Physiological Mechanisms in Gestational Diabetes Mellitus	14
2.3	The Cellular Mechanism Linking Insulin Resistance and GDM	16
3.1	Cell viability by Trypan blue dye exclusion method	41
3.2	Study Plan of experimentation on SD (Sprague-Dawley) rats.	48
3.3	Diagrammatic representation of In-vivo study plan	49
4.1	BeWo Cell Culture Stages	59
4.2	Comparitive analysis of glucose uptake (Mean Fluorescence Intensity of 2-NBDG fluorescence) among Control,Test and Test-VEGF group.	61
4.3	Comparative fold change analysis of glucose uptake for Control,Test and Test-VEGF group.	61
4.4	Flow Cytometry Results for (a) Untreated Cells, (b) Control Cells and (c) Cells without Insulin	64
4.5	Scatter Plot for 2-NBDG uptake for untreated cells and cells without insulin	67
4.6(a)	Scatter Plot for 2-NBDG uptake for control cells	68
4.6 (b)	Scatter Plot for 2-NBDG uptake for Test cells	68
4.7 (a)	Scatter Plot for 2-NBDG uptake for Control sample cells	69

4.7 (b)	Scatter Plot for 2-NBDG uptake for Test sample cells	69
4.8	Venn diagram plot of screened protein for Control,Test and Test-VEGF samples through LCMS analysis	71
4.9	Venn diagram plot of screened protein for Control and Test samples through LCMS analysis	73
4.10	Box-Plot Analysis for Control Vs Test protein samples before normalization	74
4.11	Box-Plot Analysis for Control Vs Test protein samples after normalization	75
4.12	Box-Plot T-Test Analysis (Significant Proteins)	76
4.13	Heat Map of screened proteins for Control and Test group	77
4.14	Correlation Plot for Control and Test protein samples.	78
4.15	Principle Component Analysis (PCA) for control and test protein samples.	79
4.16	Screeplot for control and test protein samples.	80
4.17	Volcano Plot for control and test protein samples.	81
4.18	VENN Diagram (TEST-VEGF VS. CONTROL)	82
4.19	Box-Plot Analysis for Control Vs Test-VEGF samples: (BEFORE NORMALIZATION)	84
4.20	Box-Plot Analysis for Control Vs Test-VEGF samples: (AFTER NORMALIZATION)	84
4.21	Box-Plot T-Test Analysis for Control Vs Test-VEGF samples (T-Test Significant)	85
4.22	Heat Map of screened proteins for control and Test-VEGF group	87

4.23	Correlation Plot for Control and Test-VEGF protein samples	88
4.24	Principle Component Analysis (PCA) for control and Test-VEGF protein samples	90
4.25	Scree plot for control and Test-VEGF protein samples	92
4.26	Volcano Plot for control and Test-VEGF protein samples	94
4.27	Comparitive analysis of glucose uptake (Mean Fluorescence Intensity of 2-NBDG fluorescence) for Test-VEGF group(encircled).	95
4.28	Comparative fold change analysis of glucose uptake (comparative fold change) for Test-VEGF group(encircled).	95
4.29(A)	2-NBDG Plot for Glucose Uptake (Test+VEGF)	97
4.29(B)	2-NBDG Flow Cytometry Plot for Glucose Uptake (Test +VEGF)	97
4.30	Copulation/vaginal plug which confirm onset of pregnancy	100
4.31(A)	Protein (Mitochondria Fission Factor) coverage analyses	106
4.31(B)	Analysis of MS/MS spectrum of a peptide (Mitochondria Fission Factor (MFF))	107
4.32	Standard Curve Plot	109
4.33	ELISA PLOT illustrating comparative evaluation between In-vitro and In-vivo samples	110

ABSTRACT

This comprehensive study aimed to identify and evaluate probable protein biomarkers for early detection of Gestational Diabetes Mellitus (GDM), a complex metabolic condition posing significant risks to maternal and fetal health. The research employed a multifaceted approach integrating in vitro cellular models, advanced proteomics, and in vivo validation.

A robust in vitro cell model using the BeWo trophoblast cell line was meticulously developed and validated to accurately recapitulate the insulin resistance and impaired glucose tolerance characteristic of GDM. Flow cytometry analysis of glucose uptake confirmed the model's fidelity, with insulin-resistant cells exhibiting significantly reduced glucose uptake compared to insulin-sensitive controls.

Leveraging this model, an in-depth proteomics analysis was conducted using liquid chromatography-mass spectrometry (LC-MS) to unveil potential protein biomarkers for early GDM detection. The analysis yielded a comprehensive dataset of 3,528 protein groups and 22,431 peptide groups. Comparative analysis between insulin-sensitive and insulin-resistant conditions revealed distinct protein profiles, with 61 unique proteins associated with insulin sensitivity and 55 unique proteins characterizing insulin resistance.

Notably, the mitochondrial fission factor (Mff) emerged as a promising biomarker, showing significant upregulation in insulin-resistant conditions. This finding suggested a potential role for Mff in GDM pathogenesis, linking mitochondrial dysfunction to the onset of insulin resistance.

The study also investigated the role of Vascular Endothelial Growth Factor (VEGF) in GDM pathophysiology. Surprisingly, exogenous VEGF showed minimal impact on glucose uptake in insulin-resistant cells, challenging conventional understanding and warranting further investigation.

To validate the in vitro findings and establish their physiological relevance, an in vivo Sprague-Dawley rat model of GDM was developed using streptozotocin induction. Blood profiling and enzyme-linked immunosorbent assay (ELISA) analyses corroborated the upregulation of Mff in the GDM condition, reinforcing its potential as a biomarker.

This research successfully identified Mff as a probable protein biomarker for early GDM detection, demonstrating its upregulation in both in vitro and in vivo models. The study's comprehensive approach, spanning from cellular models to animal validation, provides a holistic understanding of GDM pathogenesis and offers promising avenues for clinical diagnostics and monitoring.

These findings contribute significantly to the molecular understanding of GDM and pave the way for developing early diagnostic tools and targeted interventions. By bridging the gap between fundamental research and clinical application, this study represents a substantial advancement in the field of GDM research, with potential implications for improving maternal and fetal health outcomes.

CHAPTER 1

INTRODUCTION

1. Introduction:

Pregnancy involves significant biochemical and physiological changes, maintaining a delicate balance of biomolecules. Disruption in this balance can lead to metabolic disorders like Gestational Diabetes Mellitus (GDM) – diabetes arising during pregnancy, impacting around 14% of all pregnancies globally (Kapur et al., 2015). GDM is characterized by uncontrolled high blood sugar levels due to inadequate insulin secretion, with risk factors including obesity, weight gain, diet, family history, and sedentary lifestyle (American Diabetes Association, 2018; International Diabetes Federation, 2017).

GDM is defined as sustained glucose intolerance and insulin resistance during pregnancy (American Diabetes Association). Obesity is a major risk factor, with elevated blood glucose levels manifesting at any gestational stage. Symptoms include increased thirst, frequent urination, dry mouth, and tiredness. While GDM resolves after delivery, it increases risks of obesity, Type 2 diabetes, and cardiovascular complications (Goyal et al., 2020). Treatment involves lifestyle measures like balanced nutrition and exercise, but limitations exist in addressing insulin resistance and glucose intolerance (Camelo Castillo et al., 2015; Feig & Moses, 2011).

The oral glucose tolerance test effectively assesses blood sugar response to sugar intake for GDM and Type 2 diabetes diagnosis (Riskin-Mashiah et al., 2010). Early prediction and diagnosis enable successful GDM treatment, even in the first trimester, allowing preventative measures and interventions to mitigate effects (Chiefari et al., 2017; HAPO-Study Cooperative Research Group, 2008; Moses et al., 2011; Solomon et al., 1997).

According to the International Association of Diabetes and Pregnancy Study Group (IADPSG, 2017), GDM is diagnosed if fasting plasma glucose (FPG) is ≥ 92 mg/dL or if FPG is < 92 mg/dL two hours after a 75 g oral glucose tolerance test (OGTT) between 24-28 weeks of gestation. High blood glucose in the first trimester, with abnormal fasting glucose ranging 80-85 mg/dL, may contribute to later GDM (Riskin-Mashiah et al., 2010). Sex hormone-binding globulin (SHBG), C-Reactive Protein (CRP), and

adiponectin are important biomarkers for early GDM prediction and diagnosis (Maged et al., 2014).

1.1 Classification and Prevalence of Gestational Diabetes:

GDM is a metabolic disorder diagnosed during pregnancy, with uncertainty surrounding its classification as pre-existing type 1 or type 2 diabetes, and varying diagnostic approaches (IADPSG, n.d.). The International Association of Diabetes and Pregnancy Study Group (IADPSG) have provided diagnostic criteria aligning with recommendations from the World Health Organization, International Federation of Gynecology and Obstetrics, and the American Diabetes Association (ADA). Per IADPSG guidelines, all pregnant women should undergo fasting plasma glucose (FPG) testing, with readings ≥ 92 mg/dL indicating GDM. Additionally, if the 2-hour 75-gram oral glucose tolerance test (OGTT) administered between 24-28 weeks meets specific thresholds (Table 1.1), GDM is diagnosed (IADPSG, n.d.).

Table 1.1: Diagnostic Guidelines for Detecting Gestational Diabetes Mellitus Using the Oral Glucose Tolerance Test.

Source	Year	Pregnancies	Timing of OGTT	Glucose Load	Glucose Thresholds (mg/dL)	Reference
ADA	2023	High-risk pregnancies	24-28 weeks	75g	Fasting ≥ 92 , 1-hr ≥ 180 , 2-hr ≥ 153	American Diabetes Association. Standards of Medical Care in Diabetes—2023. Diabetes Care. 2023;46(Supplement 1):S254-S266.

ACOG	2022	All pregnancies	24-28 weeks	100g	Fasting \geq 95, 1-hr \geq 180, 2-hr \geq 155, 3-hr \geq 140	American College of Obstetricians and Gynecologists. Gestational Diabetes Mellitus: ACOG Practice Bulletin, Number 231. Obstet Gynecol. 2022;139(2):406-408.
NICE	2020	High-risk pregnancies	24-28 weeks	75g	Fasting \geq 101, 2-hr \geq 140	National Institute for Health and Care Excellence. Diabetes in pregnancy: management from preconception to the postnatal period. NICE guideline [NG3]. 2020.
IADPSG/WHO	2013	All pregnancies	24-28 weeks	75g	Fasting \geq 92, 1-hr \geq 180, 2-hr \geq 153	International Association of Diabetes and Pregnancy Study Groups (IADPSG) Consensus Panel. Diabetes Care. 2010;33(3):676-682.
FIGO	2015	All pregnancies	As early as possible in pregnancy, and at 24-28 weeks if initial test is normal	75g	Fasting \geq 92, 1-hr \geq 180, 2-hr \geq 153	International Federation of Gynecology and Obstetrics (FIGO). Int J Gynaecol Obstet. 2015;131 Suppl 3:S173-211.
CDA	2023	All pregnancies	24-28 weeks	75g	Fasting \geq 95, 1-hr \geq 191, 2-hr \geq 160	Diabetes Canada Clinical Practice Guidelines Expert Committee. Can J Diabetes. 2023;47:S1-S170.

1.2 Epidemiology:

The escalating global issue of overweight and obesity plays a substantial role in the consistent rise in diabetes incidence, including Gestational Diabetes Mellitus (GDM), among women of reproductive age [Chen et al., 2018]. According to the 2019 International Diabetes Federation (IDF) report, over 20.4 million women, accounting for 14.0% of pregnancies, exhibited disorders related to carbohydrate metabolism, with around 80% identified as GDM [Wang et al., 2022].

The prevalence of GDM varies across global regions [Mwanri et al., 2018]. The Middle East and North Africa (MENA) have a substantially high prevalence of 27.6% (26.9–28.4%), while Southeast Asia (SEA) has a prevalence of 20.8% (20.2–21.4%) [Buckley et al., 2012]. The Western Pacific (WP) region follows with 10.3% (4.5–20.3%), Sub Saharan Africa (AFR) shows 10.8% (8.5–13.1%), and South America and Central America (SACA) have 11.2% (7.1–16.6%). Europe (EUR) reports 6.1% (1.8–31.0%), and North America and the Caribbean (NAC) exhibit 7.0% (6.5–11.9%) prevalence [Berg et al., 2010; Moyce and Dolinsky, 2018] (Figure 1.1).



Figure 1.1: Global Mapping of Gestational Diabetes Mellitus (GDM): An Epidemiological Survey of Affected Female Populations [McIntyre et al., 2019].

1.3 Importance of Early Detection and existing Diagnostic challenge

Early GDM detection reduces maternal risks like preeclampsia, hypertension, type 2 diabetes (American Diabetes Association, 2018) and fetal risks like macrosomia, birth injuries, childhood obesity/diabetes (Chatterjee et al., 2023; Moyce et al., 2018). It allows preventative measures against future maternal type 2 diabetes (Chiefari et al., 2017; Chen et al., 2018) and provides education/support opportunities for better mental well-being (IADPSG Consensus Panel, 2010; Wang et al., 2022).

However, lack of universal screening protocol consensus leads to global variability (Ferrara & Hedderson, 2017; Guariguata et al., 2014). GDM's heterogeneity makes one-size-fits-all diagnosis difficult (McIntyre et al., 2019). Resource limitations hinder comprehensive screening implementation (Hirst et al., 2018).

Potential strategies include establishing unified diagnostic criteria through international collaboration (Bellamy et al., 2009), individualized risk assessment based on factors like age, BMI, obstetric history (Lowe et al., 2018; Metzger et al., 2010), exploring novel biomarkers alongside glucose measurements for improved accuracy (Berg et al., 2010), and investing in healthcare professional training, diagnostic tool access, and educational resources (Hirst et al., 2018 ; Mwanri et al., 2018).

1.4 Rationale for Protein Biomarkers:

Gestational diabetes mellitus (GDM) can have significant health implications for both the pregnant woman and her developing child. Women diagnosed with GDM face an elevated risk of complications during pregnancy, most notably preeclampsia. Moreover, these individuals have a higher likelihood of developing type 2 diabetes later in life.

The effects of GDM extend to the fetus as well. Infants born to mothers with GDM are at increased risk for certain health issues. These include macrosomia, a condition where the baby is significantly larger than average, potentially complicating delivery. Additionally, these newborns may experience hypoglycemia, or low blood sugar, in the period immediately following birth (Chatterjee et al., 2023).

GDM poses significant risks to both maternal and fetal health during pregnancy. Timely and accurate diagnosis of GDM is crucial for effective management and the prevention of complications. Protein biomarkers have emerged as valuable tools in the diagnosis and understanding of GDM due to their role in reflecting underlying physiological changes.

GDM is characterized by insulin resistance and impaired glucose metabolism during pregnancy. These alterations lead to changes in the expression and regulation of various proteins involved in insulin signaling, glucose metabolism, and inflammatory pathways. Proteins can serve as indicators of these underlying physiological changes.

Insulin resistance is a hallmark of GDM, and proteins involved in insulin signaling pathways are affected (Lappas et al., 2011). Inflammation plays a crucial role in GDM pathogenesis. Proteins like C-reactive protein (CRP) and interleukins are associated with inflammatory responses and elevated in GDM (Lappas et al., 2012). GDM is linked to increased oxidative stress, leading to alterations in antioxidant defense proteins like superoxide dismutase and glutathione peroxidase (Sivan et al., 2014). Placental proteins like placental growth factor (PlGF) and soluble fms-like tyrosine kinase-1 (sFlt-1) have been implicated in GDM pathophysiology (Saraf et al., 2018).

Protein biomarkers offer improved diagnostic accuracy and GDM prediction. A study demonstrated combining multiple protein biomarkers enhanced sensitivity and specificity compared to glucose-based tests (Wang et al., 2017). Protein biomarkers allow personalized GDM management by identifying specific protein profiles for tailored interventions.

The integration of protein biomarkers offers a multifaceted approach to understanding GDM pathophysiology, contributing to early detection, risk stratification, and personalized management. Continued research holds potential to refine diagnostic criteria and improve outcomes for mothers and infants affected by gestational diabetes.

1.5 Methodological Approaches for Investigating Gestational Diabetes Mellitus: In Vitro and In Vivo Models

Recent years have witnessed advancements in in vitro and in vivo experimental models for elucidating the pathophysiology of Type 2 Diabetes (T2D) and GDM. In vitro cell models like BRIN-BD11, INS-1, and PANC-1 play a pivotal role in unraveling essential markers associated with maternal or fetal complications during pregnancy (Asfari et al., 1992; Lilao-Garzón et al., 2021; Narushima et al., 2005).

Placental cell lines such as BeWo, JEG, and JAR have served as valuable models for studying mechanistic effects of myostatin on glucose uptake, with BeWo cells widely accepted for human placental transport studies (Menegazzo et al., 2015; Wang et al., 2014). In our research, we established an insulin-resistant BeWo cell line to mimic placental features during early pregnancy in GDM conditions.

The Sw.71 cell line mimics the physiological properties of extra-villous trophoblast cells and serves as an instrumental tool in trophoblast research, aiding in the screening and identification of potential early prediction biomarkers for GDM (Kokkinopoulou et al., 2019; Mac-Marcjanek et al., 2018; Zhao et al., 2014).

In vivo rodent models, displaying partial phenotypic expressions of diabetes, are extensively used for GDM (Pasek and Gannon, 2013). Dietary alterations, like high fat and high fructose, can induce obesity, a significant GDM risk factor, in pregnant mice (Feige et al., 2008). Streptozotocin (STZ) administration in pregnant mice is the primary strategy to develop an in vivo diabetic mellitus model, revealing structural and functional abnormalities and identifying abnormal genetic expressions (Feige et al., 2008). The null mutant mouse model, *Socs2*, emerges as an effective GDM model associated with aging (Martínez et al., 2008).

1.6 Significance of the Study:

In recent years, there has been an increase in global Gestational Diabetes Mellitus (GDM) cases, attributed to factors like sedentary lifestyles and high-caloric diets in urban populations [Dabelea et al., 2005]. Despite controversies around optimal screening criteria, evidence emphasizes the importance of early GDM prediction and diagnosis for comprehensive treatment [Moses et al., 2011]. Predicting GDM in the first trimester is crucial for facilitating timely preventive measures and interventions to mitigate or prevent onset [Metzger et al., 2008; Solomon et al., 1997].

This study highlights the significance of early GDM prediction, allowing healthcare professionals to implement preventive measures promptly, such as dietary interventions and medical strategies, ultimately aiming to curb the onset or progression of GDM.

Protein biomarkers play a pivotal role in reflecting physiological changes associated with GDM, offering a promising avenue for early detection. Proteins associated with insulin resistance, inflammation, and placental dysfunction serve as key indicators of GDM onset. The benefit of utilizing protein biomarkers in early gestation lies in their ability to detect subtle changes preceding overt symptoms, allowing for timely preventive measures and interventions [Wang et al., 2017].

1.7 Research Gap Identification and Research Hypothesis:

The increasing global prevalence of Gestational Diabetes Mellitus (GDM) has been associated with various factors such as sedentary lifestyles, elevated stress levels, and the consumption of high-caloric diets, particularly among the urban population (Dabelea et al., 2005; Wang et al., 2021). GDM not only affects maternal health but also has negative implications for the developing fetus in terms of physiological and metabolic conditions. While there are controversies surrounding the optimal threshold criteria for screening GDM in late trimesters, there is substantial evidence supporting the importance of early prediction and diagnosis for comprehensive treatment of this metabolic disorder (Moses et al., 2011; Raets et al., 2021).

The identification of novel protein biomarkers for early detection of gestational diabetes mellitus (GDM) is crucial due to the increasing prevalence and potential complications associated with this condition. Current screening methods, such as oral glucose tolerance tests, are typically performed late in pregnancy and may miss early-onset cases. Novel protein biomarkers could enable earlier and more accurate diagnosis, allowing for timely interventions to improve maternal and fetal outcomes.

Protein biomarkers have shown promise in various areas of medicine, including cancer diagnostics and cardiovascular disease prediction. In the context of GDM, proteomic studies have identified potential candidates such as adiponectin, sex hormone-binding globulin, and placental growth factor (Moyce et al., 2023; Rasanen et al., 2013). These proteins may reflect early metabolic changes associated with GDM development.

Early detection through protein biomarkers could facilitate personalized risk assessment and targeted interventions. This approach may reduce the incidence of adverse outcomes such as macrosomia, neonatal hypoglycemia, and long-term metabolic complications for both mother and child (Plows et al., 2018).

Furthermore, identifying novel biomarkers could provide insights into the pathophysiology of GDM, potentially leading to new therapeutic targets. As proteomics technologies advance, large-scale studies are needed to validate candidate biomarkers and develop clinically applicable screening tools (Law et al., 2017).

Numerous experimental and clinical trials have emphasized the potential benefits of predicting GDM as early as the first trimester. Early detection provides the medical community with an opportunity to identify, diagnose, and address the disease or its consequences at an early stage. The urgency for early prediction lies in enabling timely and preventive measures, including dietary control and other medical interventions, to mitigate or impede the onset of GDM (Metzger et al., 2008; Solomon et al., 1997).

1.8 Research Objectives:

- i. Development of in-vitro insulin resistant glucose intolerant cell based model for screening the effect of gestational diabetes.
- ii. Prediction and evaluation of probable biomarkers and comparative proteome profiling for early prediction of gestational diabetes.
- iii. Evaluation of VEGF effect on glucose uptake under hyperglycemic condition in gestational diabetic in-vitro model using BeWo cell line.
- iv. Validation of In-vitro study findings on specific Rat model, through blood sample profiling.

CHAPTER 2

REVIEW OF LITERATURE

2 Review of Literature:

2.1 Pathophysiology of GDM:

The primary role of pancreatic β -cells is to monitor blood glucose levels and release insulin accordingly. The insulin hormone, upon activation, communicates with GLUT proteins to facilitate the opening of cell membrane gates, enabling the absorption of glucose. However, when β -cells in the islets of Langerhans fail to respond to elevated blood glucose levels, leading to insulin resistance, it results in a hyperglycemic state. This condition can progress into metabolic disorders such as gestational diabetes, obesity, type 2 diabetes, and cardiovascular complications. Therefore, it can be concluded that β -cell dysfunction manifests as excessive insulin secretion in response to prolonged elevated blood glucose levels [Dludla et al.,2023; Weir et al., 2001].

The dysfunction of β -cells can manifest in various ways and at different stages of their synthesis process, encompassing issues such as inappropriate pro-insulin synthesis, modified post-translational processes, glucose intolerance, or unidentified cellular mechanisms associated with granule exocytosis and storage [DeFronzo, 2009].

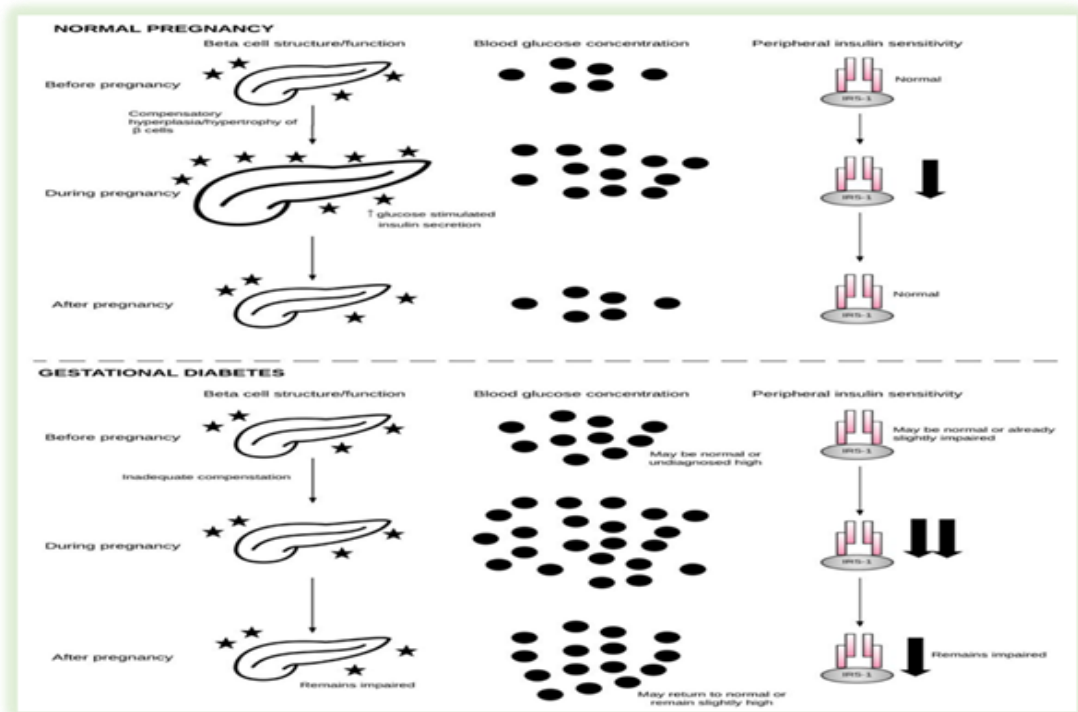


Figure 2.1: The pathophysiological mechanisms involving β -cell function and insulin sensitivity are compared between normal and gestational diabetes mellitus (GDM) conditions [Prentki and Nolan, 2006].

The provided figure (Figure 2.1) illustrates the physiological interplay among the β -cells, blood glucose, and insulin sensitivity within the human placental system. In a normative pregnancy scenario, β -cells undergo both hyperplasia and hypertrophy to adequately address the heightened metabolic requirements. Concurrently, insulin sensitivity decreases as blood glucose levels elevate. Following delivery or the post-pregnancy period, β -cells, blood glucose levels, and insulin sensitivity return to baseline (Skajaa et al.,2020).

Contrarily, in gestational diabetes, characterized by elevated hyperglycemia and diminished insulin sensitivity, β -cells struggle to meet the demands imposed by the pregnant woman supporting fetal growth (Dilworth et al., 2021). This imbalance, marked by heightened blood glucose levels and reduced insulin sensitivity, disrupts the metabolic pathway, potentially leading to the development of gestational diabetes during pregnancy or Type 2 diabetes mellitus post-pregnancy (Plows et al.,2018).

2.2 Insulin Resistance:

Insulin resistance, wherein cells fail to adequately uptake glucose in response to insulin, can lead to chronic diseases like obesity, cardiovascular disease, GDM in pregnant women (Catalano et al., 1999). Resistance stems from excessive lipid/metabolite accumulation which triggers inflammatory pathways and endoplasmic reticulum stress (Buchanan, 2001; Ma et al.,2024). Different tissues exhibit varying responses to elevated glucose levels, also driving insulin resistance. In the liver, high sugar prompts lipids to deviate from mitochondrial oxidation towards pathways activating serine kinases, which then inactivate insulin signaling molecules. Similarly in muscle cells, excess fats increase fatty acid oxidation but impair the Krebs cycle. Accumulating lipid droplets in mitochondria impair insulin signaling (Friedman et al., 1999; Gilbert et al.,2021).

Overall, this impaired cell-level glucose management by insulin underlies whole-body insulin resistance manifesting the conditions like obesity and GDM.

Pathophysiology of Gestational Diabetes Mellitus (GDM)

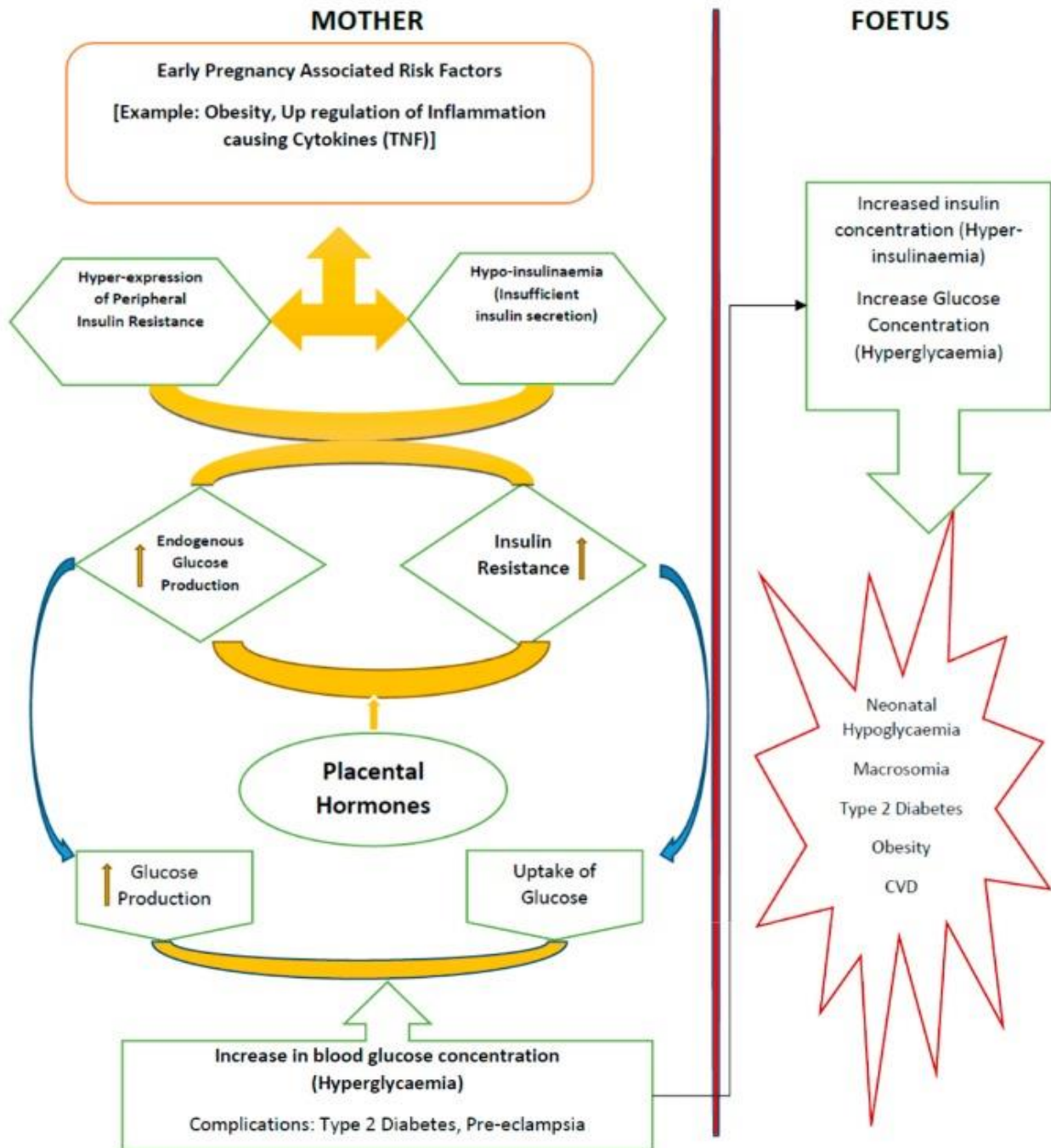


Figure 2.2: Underlying Physiological Mechanisms in Gestational Diabetes Mellitus.

This figure illustrates the complex pathophysiology of Gestational Diabetes Mellitus (GDM), depicting the interplay between maternal and fetal factors.

Experimental evidence shows that women with underlying metabolic problems before pregnancy have an elevated risk of developing GDM (amarish et al., 2022). During pregnancy, high blood glucose and increased demands on the pancreatic beta cells for uptake lead to the body's natural insulin becoming nonresponsive or more resistant. This impairs glucose absorption in skeletal muscle and fat tissue at the cellular level. Defective pancreatic beta cell function then induces systemic maternal insulin resistance, resulting in issues like high blood sugar and excess insulin. Short-term risks include fetal overgrowth and macrosomia, while long-term implications encompass maternal obesity and heightened Type 2 Diabetes (T2D) susceptibility later in life (amarish et al., 2022).

In non-obese pregnant women, insulin release can be estimated using hyperinsulinemic-euglycemic clamp studies. These reveal a 56% decline in insulin sensitivity between 34-36 weeks gestation. Notably, about 39% of this reduced sensitivity manifests within the 1st twelve to fourteen weeks of pregnancy (Catalano et al., 1991). This falling insulin sensitivity triggers a threefold rise in insulin secretion during pregnancy to maintain euglycemia. However, the poorer glucose regulation promotes excessive storage in bodily tissues, contributing to obesity among reproductive-aged women. In turn, enduring obesity becomes a precursor to long-term issues like cardiovascular disease, liver disorders and kidney dysfunction (Catalano, 2010). Overall, pregnancy induces progressive insulin resistance and demands heightened insulin output, while obesity sustains metabolic dysfunction.

Insulin resistance to blood sugar/glucose is a critical issue in GDM. High levels of the inflammatory cytokine TNF-alpha, secreted by immune cells like monocytes & macrophages, impairs insulin sensitivity specifically. This indirectly promotes hyperglycemia and GDM development during pregnancy (Abell et al., 2015; Ategbro et al., 2006). Investigations show that disrupted blood glucose regulation and increased oxidative stress at the cellular level underlie early GDM onset. Studies reveal elevated

TNF-alpha downregulates insulin sensitivity in late-stage (34 week) GDM-affected pregnant women specifically (Kirwan et al., 2002). Overall, inflammatory signaling interferes with glucose homeostasis, contributing to insulin resistant gestational diabetes. Compromised carbohydrate metabolism and oxidative stress changes are linked from early pregnancy to later GDM onset (Ray et al., 2024)

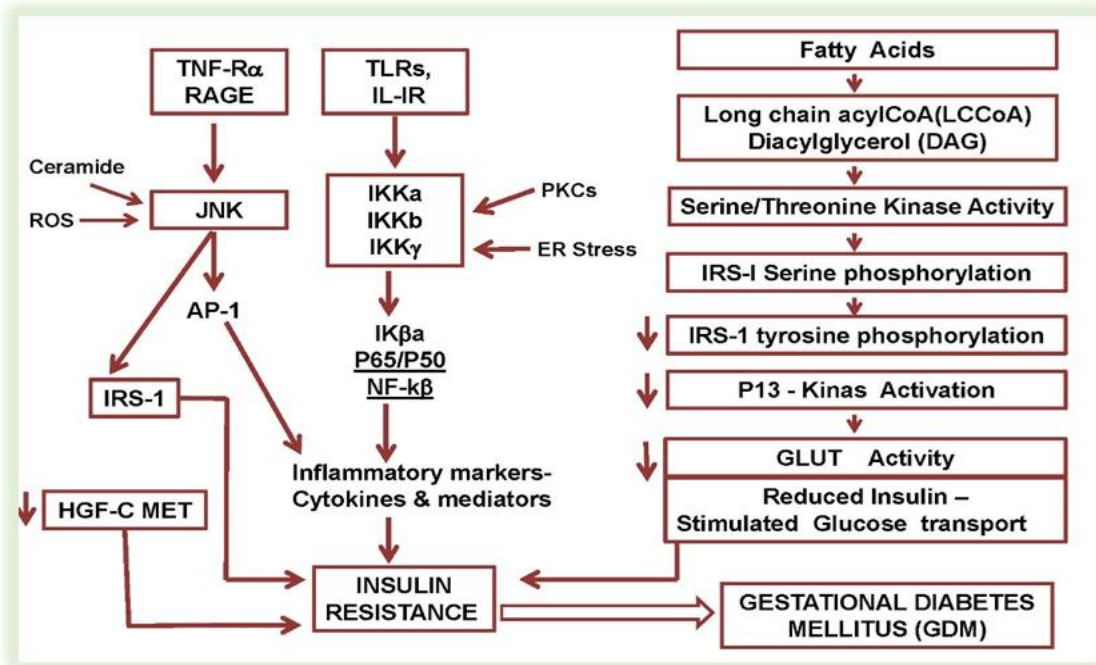


Figure 2.3: The Cellular Mechanism Linking Insulin Resistance and GDM. This figure illustrates the complex cellular pathways involved in the development of insulin resistance and its progression to gestational diabetes mellitus (GDM).

Fatty acid metabolites initiate a sequence involving protein kinase and serine/threonine kinases, leading to their activation through serine/threonine phosphorylation. This process hinders the binding of insulin receptor substrate-1 (IRS-1) and activates phosphoinositide 3-kinase (PI 3-kinase), resulting in insulin desensitization and reduced insulin-mediated glucose transport (Saltiel et al., 2021). Changes in adipokine secretion related to obesity, coupled with the activation of inflammatory pathways such as IKK β , NF- κ B & Janus Kinase, influenced by ligands for Toll, AGE TNF- α & IL-1 receptors,

modulate insulin signaling, contributing to insulin resistance promotion (Figure 2.3) (Shoelson et al., 2006; Savage et al., 2007; Qatanani et al., 2007).

C-Reactive Protein (CRP), an acute phase protein released in response to cell injury or microbial infection, has been linked to obesity and insulin insensitivity towards blood glucose. Studies indicate a positive association between gestational diabetes mellitus (GDM), increased CRP levels, and body mass index (BMI) (Rodrigo et al., 2018). Research by Gill et al. (2011) suggests a notable correlation between glucose intolerance or insulin resistance in the third trimester and elevated CRP concentrations in the first trimester. The onset of GDM has been associated with the activation of inflammatory cytokines, such as Interleukin-6 (IL-6) and TNF-alpha, along with the consistent downregulation of IL-4 and IL-10 (Hiden et al., 2009; Serov et al., 2015).

Insulin signaling facilitates GLUT proteins translocation, allowing glucose uptake into cells. When insulin signaling is compromised, the cell's capacity to absorb glucose diminishes, contributing to Type 2 Diabetes (T2D), obesity, and GDM during pregnancy (Merz et al., 2020). In GDM, pregnant individuals commonly experience a substantial 54 percent reduction in glucose absorption rate compared to healthy counterparts. The primary factors contributing to GDM include disruptions in insulin signaling downstream regulators, insulin receptor substrate (IRS) mutations, endoplasmic reticulum (ER) stress during insulin processing, and the impact of pro-inflammatory cytokines (Helske et al., 2001).

Women with normal pre-pregnancy blood glucose levels may develop gestational diabetes mellitus (GDM) later in gestation, possibly due to reduced insulin sensitivity before conception. Early in pregnancy, increased insulin secretion maintains normal glucose levels, but as caloric intake rises for fetal development, insulin resistance or β -cell dysfunction may occur, leading to hyperglycemia (Gui et al., 2015). Dysfunctional pancreatic β -cells before pregnancy could manifest clinically in late pregnancy, while women with GDM often exhibit fasting hyperglycemia, potentially induced by reduced endogenous glucose production before conception (Meng et al., 2016). In healthy pregnant women, insulin binding initiates a signaling cascade for glucose uptake, but

during the last trimester, there is a reduction in insulin receptor substrate-1 (IRS-1) expression in skeletal muscles, associated with a 25–30% decrease in glucose uptake (Marcantoni et al., 2015; Ozmen et al., 2014).

2.3 The Pathology and Pharmacological Approaches in Gestational Diabetes Mellitus (GDM):

Scientific inquiries underscore the significance of a genetic inclination (maternal), combined with the cellular microenvironment and placental factors of fetus, in initiating latent cellular processes that ultimately result in complications associated with Gestational Diabetes Mellitus (GDM) diagnosed later in gestation. As a result, a comprehensive understanding of the pathophysiology (cellular) and related risk factors is essential for efficient screening & timely prevention in cases of GDM (Ray et al., 2024).

The primary function of pancreatic cells (β -cells) is to monitor glucose concentration (blood) and release insulin accordingly. Dysfunction of these cells involves the excessive secretion of insulin in response to chronic blood glucose levels, presenting in various manifestations for example, inappropriate pro-insulin synthesis, altered post-translational processes, intolerance (glucose), and other unidentified cellular mechanisms (DeFronzo, 2009). Recent research findings has identified specific genes, such as potassium voltage-gated channel KQT-like 1 (Kcnq1) and Glucokinase (Gck), as influential in β -cell function and contributors to the development of Gestational Diabetes Mellitus (GDM) in pregnant women (Prentki and Nolan, 2006). The increased hyperglycemic burden resulting from dysfunctional β -cells is compounded by insulin resistance to blood glucose, leading to an altered metabolic state known as glucotoxicity (Ashcroft et al., 2017).

In vivo examinations utilizing rat models, particularly Zucker fatty rats, highlight the importance of β -cell quantity in maintaining glucose homeostasis (Kottaisamy et al., 2021). A study involving Zucker fatty rats demonstrated that the surgical removal of 60% of the pancreatic system led to the subsequent recovery of β -cell mass to normal

levels. However, despite this recovery, the rats developed severe hyperglycemia. The findings suggest that the abrupt and significant β -cell reduction might overwhelm the remaining cells, leading to glucotoxicity due to diminished sensitivity to insulin or insulin granule storage depletion (Delghingaro-Augusto et al., 2009).

In a study involving Sprague Dawley (SD) rats, known for their resistance to diabetic development, intrauterine growth restriction was induced through bilateral uterine ligation, resulting in a significant loss (50%) of β -cells. This loss was attributed to the epigenetic downregulation of Pdx1, a critical pancreatic transcription factor necessary for β -cell proliferation and differentiation during the embryonic stage (Simmons et al., 2001). Furthermore, the infusion of prolactin influenced β -cell proliferation, as demonstrated in a mouse knock-out model of the prolactin receptor (Auffret et al., 2013). Experimental observations, such as reduced β -cell hyperplasia and glucotoxicity, provide evidence that β -cell degeneration through apoptotic pathways may contribute to the onset of Gestational Diabetes Mellitus (GDM) (Rahier et al., 2008; Van Assche et al., 1978).

Fetal development is entirely dependent on the nutrient supply from the mother, particularly blood glucose. In cases where the developing fetus is excessively exposed to a hyperglycemic environment in women affected by gestational diabetes mellitus (GDM), this triggers hyperinsulinemic conditions in the fetus (Ornoy et al., 2021). On the placental surface, lipolysis mediated by endothelial lipase prompts the release of maternal lipoproteins. However, only a minute fraction of free fatty acids traverses the barrier of placenta, accumulating in a fetal free fatty acid pool and utilizing excess blood glucose resulting from increased dietary intake during pregnancy. Fetal insulin, in turn, stimulates adipogenesis, leading to the storage of fat in adipose tissues.

2.4 Maternal and Fetal Outcomes:

2.4.1 Obesity:

Obesity significantly predisposes to GDM. Heightened production of pro-inflammatory cytokines from fat cells leads to chronic inflammation in obesity (Teh et al., 2011; Ben-Haroush et al., 2004). This triggers secretion of tumor necrosis factor, interleukin

proteins, leptin, visfatin and adipokines, disrupting insulin secretion, sensitivity, energy control and inflammation regulation (Permana et al., 2006; Kralisch et al., 2007). Studies highlight strong links between Type 2 Diabetes (T2D), obesity and low-grade chronic inflammation (Hotamisligil, 2006). Maintaining balance between pro- and anti-inflammatory cytokines is key for healthy maternal-fetal metabolism during pregnancy. However, obese pregnant women exhibit increased pro-inflammatory cytokine release, causing metabolic imbalance and insulin resistance to blood sugar in maternal and fetal circulation (Wolf et al., 2004). This promotes glucose accumulation, hyperglycemia, and perpetuates obesity's cardiovascular complications (Qiu et al., 2004). Overall, the hyper-accumulation of inflammatory markers drives the insulin resistance underlying GDM development (Catalano et al., 1999; Buchanan, 2001). This underscores the intricate connections between obesity, inflammation and gestational diabetes, warranting comprehensive investigation and targeted interventions.

2.4.2 Fetal Derangements in GDM:

Changes in the vasculature of the developing fetus can occur as a result of alterations in the fetoplacental vessels in females affected by Gestational Diabetes Mellitus (GDM). These changes contribute to fetal abnormalities, hyperglycemia, and additional metabolic complications. Elevated glucose levels in the fetus stimulate increased insulin secretion, leading to hyperinsulinemia during the second trimester [Bao et al., 2016].

GDM-affected women typically give birth to larger infants, leading to painful delivery and an increased likelihood of requiring a cesarean section. This condition is often associated with "Polyhydramnios," characterized by the excessive accumulation of amniotic fluid, serving as a protective cushion for the fetus within the mother's womb. However, this may have negative consequences, potentially resulting in premature labor or delivery complications. Premature birth, occurring in or before the 37th week, and a concurrent medical complication known as "Preeclampsia," characterized by elevated blood pressure and increased protein concentration in urine, are prevalent among females affected by GDM [Pettitt et al., 1980; Jensen et al., 2003].

2.5 Current Diagnostic Methods for GDM:

Accurate and timely diagnosis is critical for effective management and prevention of GDM complications. Current diagnostic methods for GDM, while widely implemented, face challenges and gaps that impact their accuracy and applicability. Controversies in diagnostic criteria, insensitivity to early-onset GDM, physiological changes in pregnancy, and limited exploration of biomarkers necessitate ongoing research and innovation.

Currently used diagnostic method such as GCT (Glucose Challenge Test), which is a commonly used screening test for GDM. Typically performed between 24 and 28 weeks of gestation, it involves administering a glucose solution followed by measuring blood glucose levels. If the initial screening indicates elevated glucose levels, further diagnostic testing is recommended [American Diabetes Association (ADA), 2022]. Similarly, the OGTT (Oral glucose tolerance test) remains a gold standard for diagnosing GDM. After an overnight fast, pregnant women consume a standardized glucose solution, and blood glucose levels are measured at specific intervals. The criteria for GDM diagnosis often involve elevated fasting, one-hour, and two-hour glucose levels [ADA, 2022]. Diagnostic criteria such as HbA1c reflects average blood glucose levels over the past 2-3 months. While widely used for diagnosing diabetes outside of pregnancy, its utility in GDM diagnosis remains debated due to physiological changes in pregnancy affecting HbA1c levels [Committee on Practice Bulletins-Obstetrics, 2018]. Fasting Plasma Glucose (FPG) is another diagnostic parameter, involving measurement of glucose levels after an overnight fast. Elevated fasting glucose is indicative of impaired glucose metabolism and is one of the criteria for GDM diagnosis [ADA, 2022].

The GCT and OGTT are widely applicable and have been used for decades, making them accessible diagnostic tools in various healthcare settings. Diagnostic criteria, especially those established by the ADA, provide a standardized approach for GDM diagnosis, ensuring consistency and comparability across studies and clinical practice (Jagannathan et al.,2020). Current methods enable the identification of women at risk for GDM, allowing for timely interventions to mitigate the associated risks for both mother and child.

2.6 Challenges and Gaps in Current Diagnostic Methods:

Controversies persist regarding the optimal threshold values for Gestational Diabetes Mellitus (GDM) diagnosis, despite the existence of standardized criteria. This lack of consensus has implications for the prevalence and management of GDM [International Association of Diabetes and Pregnancy Study Groups, 2010].

The current diagnostic methods, particularly the Oral Glucose Tolerance Test (OGTT), are primarily designed for detecting GDM in the second or third trimester (Sweeting et al., 2022). However, there is growing evidence that GDM may have an early onset, necessitating the exploration of diagnostic methods applicable in the first trimester. Pregnancy-induced physiological changes, such as increased insulin resistance, alter glucose metabolism, affecting the performance of traditional diagnostic markers like fasting glucose and HbA1c. This challenges the reliability of these markers in the context of pregnancy [ACOG Practice Bulletin, 2018].

Current diagnostic methods lack a personalized medicine approach, relying on population-based thresholds. Individualized risk assessments based on factors such as maternal age, BMI, and ethnicity are not fully integrated into current diagnostic strategies (Metzger et al., 2010). The heterogeneity of study populations, encompassing diverse ethnic and racial groups, introduces challenges in interpreting and applying diagnostic criteria universally. The impact of these variables on diagnostic accuracy is an ongoing area of research (Berggren et al., 2021).

2.7 Limited Exploration of Biomarkers:

While there is increasing interest in protein biomarkers for GDM, research on their integration into routine diagnostics remains limited. Identifying reliable biomarkers could address some challenges associated with the current methods (Saraf et al., 2018). Addressing the insensitivity of current methods to early-onset GDM is crucial. Exploring the feasibility of screening methods in the first trimester, such as assessing early biomarkers or incorporating existing markers like maternal BMI and history of GDM, could enhance early detection and intervention (ACOG, 2018).

Advances in metabolomics and proteomics offer the opportunity to identify novel biomarkers associated with GDM. Comprehensive profiling of metabolites and proteins may unveil more specific and sensitive indicators for early diagnosis and risk stratification (Lowe et al., 2018).

Advancements such as early pregnancy screening, metabolomics and proteomics, could offer promising avenues to address current challenges and enhance the accuracy of GDM diagnosis. Future research should focus on the integration of these advancements into routine clinical practice, ultimately improving maternal and fetal outcomes in pregnancies affected by GDM.

2.8 Protein Biomarkers Explored in GDM:

2.8.1 Vasculo-endothelial growth factor (VEGF)-A Potential Biomarker for GDM Screening:

Placental angiogenesis, a crucial process for fetal development, is greatly influenced by Vascular Endothelial Growth Factor (VEGF). Recent research has provided compelling evidence linking abnormal angiogenesis to the development of GDM, a condition marked by disruptions in blood glucose metabolism (Bolatai et al., 2022). Additionally, a notable finding indicates an incremental increase in placental weight among women diagnosed with GDM compared to those with uncomplicated pregnancies. Experimental research utilizing in-vitro models has been conducted to understand the effects of elevated blood glucose angiogenesis (placental), specifically the key proteins Fibroblast Growth Factor 2 (FGF2) and VEGF (Baumgartner-Parzer et al., 1995; Xiang et al., 2014). The investigation assessed proliferation, differentiation, migration & tube vessel formation in Human Umbilical Vein Endothelial Cells (HUVEC) derived from diabetic and normal cell lines. This enabled examining the intricate impacts of hyperglycemia on angiogenic pathways underlying placental vascular development. An important outcome of this experimental research was the observed alterations in proliferation under hyperglycemic conditions within diabetic cell cultures compared to normal HUVEC cell lines. This investigation provided insights into the in-vitro dynamics of cellular processes,

demonstrating the impact of elevated blood glucose levels on fundamental facets of angiogenesis. The in-vitro model implemented in this study allowed for a comprehensive analysis of various parameters, including proliferation, differentiation, migration, and tube vessel formation in HUVEC cell lines. This cell-based bioassay created a controlled environment for dissecting the intricate relationship between high blood glucose concentrations, Fibroblast Growth Factor 2- (FGF2), and VEGF concerning placental angiogenesis (Tahergorabi et al .,2012)

The research shows major changes in Human Umbilical Vein Endothelial Cell (HUVEC) proliferation under hyperglycemic conditions modeling gestational diabetes mellitus (GDM) (Díaz-Pérez et al., 2016). Specifically, FGF-2 driven HUVEC proliferation was suppressed in the GDM versus control group when exposed to high 25mM glucose levels. Interestingly, under similar hyperglycemia, the proliferation rate stayed unaffected in VEGF-stimulated HUVECs in the in-vitro GDM model (Díaz-Pérez et al., 2016). Overall, the findings indicate hyperglycemia's inhibitory effects on cell growth pathways like FGF-2-mediated proliferation, while VEGF-linked cell propagation remains unaffected, elucidating the differential angiogenesis signaling in GDM.

Transcriptional dysregulation of cell movement, adhesion and migration related genes was seen in HUVECs under hyperglycemic conditions in vitro. This led to lowered migratory potential specifically in diabetic HUVECs (dHUVECs) versus non-diabetic HUVECs (nHUVECs) which were unaffected (Marcantoni et al., 2015). The HUVEC findings indicate diminished baseline migratory activity under high glucose levels, particularly in the gestational diabetes mellitus (GDM) context. Furthermore, compromised placental angiogenesis rates under hyperglycemia were established, potentially linked to the reduced cell migratory capacity (Gui et al., 2015; Ozmen et al., 2014). Overall, the research elucidates high glucose-mediated inhibitory effects on endothelial cell migration pathways underlying placental vascular development in GDM.

In summary, the research findings indicate that in gestational diabetes mellitus (GDM), chronic high blood sugar disrupts the MEK1/2-ERK1/2 cell signaling pathway, resulting

in substantially decreased cell multiplication (proliferation) and localization under Fibroblast Growth Factor 2 (FGF2) stimulation (Jirkovská et al., 2002). This was evidenced in pregnancy hyperglycemia models of GDM. Overall, hyperglycemia suppresses key developmental pathways like MEK-ERK mediated FGF2 signaling that control cell multiplication and migration, compromising processes underlying placental angiogenesis in gestational diabetes.

Additionally, the research findings showed lowered Flt-1 mRNA and protein expression in gestational diabetes, while VEGF and Kinase Insert Domain Receptor (KDR) levels were unchanged (Jirkovská et al., 2002). Despite no major alterations in cell proliferation markers, migration was higher relative to normal pregnancy. KDR activation was identified as a factor promoting excessive endothelial migration, leading to placental hyper-vascularization in GDM (Desoye & van Poppel, 2015). GDM placentas displayed heightened capillary branching, more non-viable connections per villus and increased chorioangiogenesis rates (Hiden et al., 2009). Overall, the findings demonstrate GDM's effects of suppressing angiogenesis signaling like Flt-1 expression, while other pathways promoting cell migration and dysregulated vascularization remain over activated.

2.9 Vasculo-Endothelial Growth Factor (VEGF) and Angiogenesis:

In individuals with gestational diabetes, there is a noticeable reduction in Flt-1 mRNA or protein expression, while VEGF or KDR expression remains unchanged (Nardi et al., 2020). Interestingly, no significant alterations in cell proliferation biomarkers were observed; however, migration was found to be higher when compared to pregnancies under normal conditions. The activation of KDR was identified as a key factor in promoting the overstimulation of endothelial cell migration, resulting in hyper-vascularization of the placenta in individuals affected by gestational diabetes mellitus (Troncoso et al., 2017) (see Figure 2.3).

Individuals with GDM display heightened capillary branching, more non-viable connections per terminal villus and increased chorioangiogenesis in the placenta (Desoye et al., 2015). Concurrently, there is greater villous immaturity and sharply elevated

placental angiogenesis under hyperglycemic conditions. These collective findings indicate that rising villous immaturity along with rapid increases in placental angiogenesis could potentially serve as early predictive biomarkers for GDM onset in pregnant women (Hiden et al., 2009). Overall, the vascular changes reflect the placental adaptations seen in maternal hyperglycemia, which may be detectable early on to enable timely GDM diagnosis and management.

The developmental process of the fetus within the mother's womb relies heavily on the adequacy of oxygen supplied to the cellular machinery in the placenta. Hyperinsulinemia enhances fetal cellular aerobic metabolism, leading to an increased demand for fetal oxygen [Gill et al., 2011]. Since HbA1c levels significantly rise during fetal development, the heightened level of HbA1c in the mother's blood can serve as a direct biomarker of increased fetal oxygen demand in the placental system [Serov et al., 2015]. Vascularization is enhanced in gestational diabetes mellitus (GDM) due to increased placental angiogenesis. This compensatory mechanism addresses the imbalance in oxygen supply and demand under hypoxic conditions resulting from increased blood insulin concentration [Helske et al., 2001]. Although it is speculative whether hypervascularization of the placenta is primarily due to increased oxygen diffusivity in individuals affected by GDM, three-dimensional reconstruction of placental vasculature demonstrates that high capillary sinuosity, resulting in reduced vascular resistance, promotes dilation of blood capillaries for effective oxygen uptake [Meng et al., 2016].

Under fetal hypoxic conditions during transition, the release of VEGF is promoted, enhancing placental tissue synthesis. In GDM conditions, the expression of Flt1 and KDR, the VEGF receptors, is upregulated, indicating an unaffected proangiogenic state with variations in activation levels influencing the physiological activity of VEGF [Janota et al., 2003; Leach et al., 2004]. Recent studies on women affected by GDM under hyperglycemic conditions reveal high expression of VEGF and its specific receptor 2 (KDR) and reduced expression of Fms Related Tyrosine Kinase 1 (Flt1) compared to a control group. These findings open avenues for further research to explore unknown

factors controlling placental levels of VEGF and its responsive receptors in GDM-affected individuals [Leach et al., 2009; Dubova et al., 2012; El-Tarhouny et al., 2014].

Additionally, a recent research study investigated the mode of delivery and the comparative maternal basal metabolic index (BMI) during pre-pregnancy compared to the first trimester. VEGF levels were unaffected by the mode of delivery, whether vaginal or cesarean section. Flt1 levels significantly increased in women who underwent vaginal delivery but not in those who had a cesarean section. These findings suggest that Flt1 levels might contribute to an unstable compensatory mechanism in a proangiogenic GDM scenario [Daskalakis et al., 2008]. In contrast, Flt1 is also termed a decoy receptor of VEGF((soluble form of Flt1 (sFlt1) is called as decoy receptor), as its expression increases in normal pregnant women. To summarize, VEGF is considered the critical factor for enhanced vascularization of placental tissues in GDM individuals, showing high KDR expression and reduced Flt1 expression [Aitken et al., 2004].

Additionally, single nucleotide polymorphisms (SNPs) serve as genetic markers of inter-individual variation, aiding in predicting genetic diseases, tracking inheritance patterns, and understanding drug responses. Five SNPs were identified that increase GDM risk, with genetic polymorphisms in the VEGF gene being a major contributing factor (Kim & Hong, 2015; Flyvbjerg et al., 2004). The TT genotype (rs3025039) of VEGF was found to play a key role in metabolic disorder pathogenesis through abnormal expression induction (Kim & Hong, 2015). Prior research showed high blood serum VEGF concentration is a potential early GDM and diabetic polyneuropathy predictor (Lee et al., 2006). VEGF upregulation under hyperglycemia may be impacted by factors like transforming growth factor, insulin-like growth factor, and protein kinases (Wei et al., 2012). The T polymorphic form (rs3025039) of VEGF, located in the 3'-UTR region influencing genetic stability via microRNA and mRNA interactions, may crucially impact VEGF serum levels (Haas et al., 2012; Langsenlehner et al., 2015).

Research findings showed that VEGF gene polymorphism rs3025039 impacts disease pathophysiology, including GDM, by downregulating VEGF expression levels through

interactions with other SNPs (Su et al., 2011). Linkage disequilibrium was found amongst rs2010963, rs833069, rs2146323 and rs3025010, potentially promoting metabolic disorder onset. Additionally, the haplotypes CACC, GACT and GACT showed higher occurrence probability in GDM (Shiefa et al., 2013). In silico analyses identified BMI, HOMA-IR, CT+TT genotype, and VEGF activity as independent GDM risk and screening factors, while HOMA-beta is an independent protective factor (Su et al., 2011; Shiefa et al., 2013). Although the effects of gestational diabetes in pregnant women are observed to be temporary, its aftereffects on child development and health after delivery have always been a matter of concern. The hyperglycemic condition during pregnancy significantly compromises child development (Rodolaki et al., 2023). Pathological screening tests for blood glucose are typically conducted in the late second or early third trimester of gestation to diagnose or predict GDM.

GDM's early prediction in pregnant women might be crucial in restricting future complications at an early stage and prioritizing child health and development. Prenatal screening in the 1st trimester of gestation in order to identify fetal aneuploidy defects is a widely accepted obstetric practice. Pregnancy-associated plasma protein (PAPP-A) and free beta-human chorionic gonadotropin hormone from serum (maternal), typically secreted from the placenta, serve as potent biomarkers for screening fetal aneuploidy. These markers facilitate amino acids and blood glucose transport into the placenta, increasing the cellular availability of IGF, thereby playing a primary role in this context [Husslein et al., 2012; Sirikunlai et al., 2016; Sweeting et al., 2015; Quattrocchi et al., 2015].

Recent meta-analysis studies have highlighted the critical role of free beta-hCG in placental development and its potential as an essential early biomarker for the identification and/or screening of GDM in pregnant women. However, the relationship between reduced levels of PAPP-A and free beta-hCG and the development of GDM remains contradictory [Farina et al., 2017]. These findings emphasize the need for further research and clinical studies to profile early prediction biomarkers for screening individuals affected by GDM. Such an approach could help identify potential

abnormalities in fetal development at an early stage, enabling precautionary measures to prevent future chronic ailments such as obesity, type 2 diabetes, or cardiovascular complications [Sweeting et al., 2018].

Study models that integrate biomarkers for maternal characteristics along with first-trimester prediction biomarkers for the screening of GDM are considered the best strategy for understanding the pathophysiology of this metabolic disorder [Xiao et al., 2018]. However, studies by Syngelaki et al., 2015, and others, which focused on maternal risks alone or in combination with PAPP-A assessment, did not yield desirable results for early prediction biomarkers for GDM. The interpretation of predictive value was limited and biased, rendering the risk modeling approach for prediction ineffective [Jelliffe-Pawlowski et al., 2015; Rose & van der Laan, 2008].

Meta-analyses found limited utility of first trimester biomarkers for GDM prediction, as differences were small in magnitude and lacked clinical applicability for algorithms (Sweeting et al., 2018). However, combined assessment with insulin resistance, oxidative stress, endoplasmic reticulum stress or cytotoxic stress biomarkers may improve predictive potential. Though it is stressed meta-analysis reproducibility necessitates large, diverse populations (Sweeting et al., 2018). In conclusion, early GDM prediction markers could serve dual utility in diagnosing mothers and screening both maternal-fetal dyads for metabolic complications (Menegazzo et al., 2015). Overall, existing first trimester indicators have minimal independent value, but show promise in multivariate panels assessing pathophysiological perturbations for timely GDM identification.

Myostatin, a myokine inhibiting muscle growth, crucially regulates glucose uptake in myocytes and adipocytes. Recent studies show that under high-calorie, high-fat meals, myostatin inhibition improves insulin sensitivity (Moreli et al., 2012; Wang et al., 2014). Enhanced sensitivity directly promotes blood glucose absorption via GLUT glucose transporter proteins. Myostatin is substantially expressed in the placenta, playing a key role in glucose homeostasis, indicating its potential as an early trimester biomarker for gestational diabetes mellitus (GDM) diagnosis (Khandpur et al., 2013). Overall,

myostatine merges as a regulator of insulin resistance and carbohydrate metabolism pathways dysregulated in gestational diabetes, warranting further investigation as a predictive marker detectable from early pregnancy.

In many previous studies related to GDM, choriocarcinoma placental cell lines have been utilized to profile the effect of glucose uptake. These cell lines, including BeWo, JEG, and JAR cells, are favored due to their stability and ease of handling compared to primary trophoblast cells directly isolated from the placental organ. Primary trophoblast cells pose challenges such as low yield, limited cellular viability, and a short lifespan, making the reproducibility of results difficult due to batch-to-batch variability [Borissoff et al., 2013; Chaiworapongsa et al., 2014; Houghton et al., 2010].

Recent investigations have illuminated the critical role of VEGF in placental angiogenesis and its implications for GDM. Further exploration of these findings is vital for advancing our understanding of the pathophysiological mechanisms underpinning GDM and may offer insights for targeted interventions to optimize maternal and fetal outcomes.

2.10 In-vitro cell culture screening platform for GDM:

Placental cell lines like BeWo cells serve as common cellular models to probe myostatin's effects on glucose uptake at the molecular level (Straszewski-Chavez et al., 2009). In particular, BeWo cells are well-established for research into human placental glucose transport (Palma et al., 2024). They facilitate sugar absorption through glucose transporter proteins including GLUT 1, GLUT 3, and GLUT 4. Therefore, they enable elucidating intracellular signal cascades linking myostatin expression to impaired glucose homeostasis underlying gestational diabetes development.

The Sw.71 (Immortalized Human Trophoblast Cells) cell line, derived from first-trimester placental tissue of a normal pregnant woman and immortalized by infecting it with hTERT, is an invaluable resource for studying trophoblast cells. These cells maintain the same morphology and physiological capabilities as primary trophoblast

cells, providing a well-characterized model that mimics the properties of extra villous trophoblasts [Mulla et al., 2009; Mulla et al., 2013]. Additionally, the BeWo cell line (BeWo - ATCC® CCL-98™) is another placental cell line known for its potential in screening early prediction biomarkers and diagnosing metabolic disorders such as GDM in pregnant women during the early trimesters (Easton et al.,2021). This approach could help address maternal and fetal complications by enabling early intervention and treatment. Considering the seriousness of metabolic disorders like GDM in pregnant women, there is a clear need for research and clinical interventions to address these conditions as early as possible. Despite some efforts, our medical community has not yet developed a concrete strategy for screening GDM in the first trimester. Meta-analysis studies have been conducted to a certain extent during the first trimester of gestation, yielding inconsistent results. Therefore, there is an urgent need for research investigators to identify potential biomarkers for the early diagnosis of GDM in pregnant women (Zhou et al.,2024).

This project aims to bridge the research gap by exploring probable GDM biomarkers in the first trimester, with a focus on addressing both maternal and fetal complications that may arise in the future. Additionally, the project will shed light on the effects of VEGF in GDM models under hyperglycemic conditions, contributing valuable insights to our understanding of this metabolic disorder.

2.11 Predictive Biomarkers for the Early Diagnosis of GDM:

An elevated maternal hyperglycemic state emerges as a primary factor inducing endothelial dysfunction in the fetoplacental environment, markedly compromising the MEK1/2-ERK1-2 signaling pathway. In the presence of hyperglycemia, the inhibition of the MEK1/2-ERK1-2 pathway suppresses cell proliferation, particularly under fibroblast growth factor (FGF) stimulation. Studies indicate that high blood glucose levels, along with gestational diabetes in obese models, hinder the signaling of FGF2 without affecting VEGF signaling, which significantly contributes to ex vivo angiogenesis [Zhou et al., 2016]. The gold standard for pre-screening GDM is the oral glucose tolerance test

(OGTT), yet it has low reproducibility and is time-consuming. Consequently, the search for predictive biomarkers for early GDM diagnosis becomes imperative. Huhn et al. (2018) compiled a list of biomarkers in a review article, offering avenues for future research in biomarker discovery and their clinical adoption for the early detection of GDM [Huhn et al., 2018].

The hyperglycemic conditions during pregnancy exert a substantial impact on fetal development. Pathological screening tests for blood glucose are typically conducted in the late second or early third trimester to diagnose GDM. Angiopoietin-Like Protein 8 (ANGPTL8) emerges as a promising biomarker for gestational diabetes mellitus (GDM), a condition associated with significant foetal and maternal complications. As early diagnosis is crucial to mitigate hyperglycaemia-related risks, ANGPTL8's potential role in predicting or facilitating early GDM detection warrants further investigation (Abdeltawab et al.,2021). Early prediction of GDM holds significance in preventing future complications at an early stage. First-trimester prenatal screening for detecting fetal aneuploidy is a widely accepted obstetric practice. Pregnancy-associated plasma protein (PAPP-A) and free beta-human chorionic gonadotropin hormones from maternal serum, secreted by the placenta, serve as potent biomarkers for screening fetal aneuploidy [Husslein et al., 2012 ; Lu et al.,2022; Shiefa et al., 2013].Furthermore, free beta-hCG, essential for placental development, can function as a pivotal early biomarker in identifying GDM.

Table: 2.1 List of biomarker for Gestational Diabetes Mellitus.

GDM Biomarker	Description	Reference
Glycated Hemoglobin (HbA1c)	Reflects average blood glucose levels over the past 2-3 months	Hughes et al. (2016). <i>Diabetes Care</i> , 39(1), 11-14.
Fasting Plasma Glucose (FPG)	Measures blood glucose levels after an 8-hour fast	American Diabetes Association. (2021). <i>Diabetes Care</i> , 44(Supplement 1), S15-S33.

1-hour and 2-hour Plasma Glucose	Glucose levels measured during an oral glucose tolerance test (OGTT)	HAPO Study Cooperative Research Group. (2008). <i>New England Journal of Medicine</i> , 358(19), 1991-2002.
Sex Hormone-Binding Globulin (SHBG)	Protein that binds to sex hormones; low levels associated with insulin resistance	Li et al. (2016). <i>Diabetes Research and Clinical Practice</i> , 119, 145-152.
Adiponectin	Adipokine involved in glucose regulation and fatty acid oxidation	Lacroix et al. (2013). <i>Diabetes Care</i> , 36(6), 1577-1584.
C-Reactive Protein (CRP)	Inflammatory marker associated with insulin resistance	Syngelaki et al. (2016). <i>American Journal of Obstetrics and Gynecology</i> , 215(4), 447.e1-447.e17.
Placental Growth Factor (PIGF)	Angiogenic factor; lower levels associated with GDM	Eleftheriades et al. (2014). <i>Metabolism</i> , 63(11), 1412-1418.
microRNA-16-5p	Circulating microRNA associated with GDM development	Cao et al. (2017). <i>Journal of Clinical Endocrinology & Metabolism</i> , 102(12), 4522-4531.

Meta-analysis results are deemed reliable and reproducible when applied to large and diverse populations. Early prediction biomarkers can be instrumental in diagnosing and screening both mother and child for potential metabolic complications [Sweeting et al., 2018].

2.12 Relevance of Protein Biomarkers to GDM diagnosis:

The escalating prevalence of GDM is a cause for concern on a global scale. According to the International Diabetes Federation (2019), approximately 21.3 million live births were affected by hyperglycemia during pregnancy in 2019, with a significant portion attributed to GDM. The risk factors contributing to this surge include sedentary lifestyles, obesity, advanced maternal age, and genetic predisposition (International Diabetes Federation, 2019). As GDM poses substantial risks to both maternal and fetal health, early and accurate diagnosis becomes imperative for effective management and the prevention of associated complications.

In recent years, there has been a paradigm shift in the diagnostic landscape of GDM, with increasing attention directed towards the utilization of protein biomarkers. Proteins, as essential molecular entities, play diverse roles in cellular processes and are integral to the intricate physiological changes associated with GDM. Several categories of protein biomarkers have been investigated for their relevance in GDM diagnosis, offering insights into different facets of the disorder.

Insulin resistance is a central feature of GDM, characterized by impaired responsiveness of tissues to insulin. Proteins involved in the insulin signaling pathway have been scrutinized as potential biomarkers for GDM. Adiponectin, an adipokine intricately involved in glucose regulation, has emerged as a promising candidate. Research by Pappa et al. (2011) indicates that diminished adiponectin levels in early gestation may serve as an early indicator of increased GDM risk. This supports the notion that alterations in insulin signaling proteins may precede overt symptoms, providing a window for early detection and intervention.

Furthermore, studies have explored other components of the insulin signaling pathway, including insulin receptor substrate proteins. Lappas et al. (2011) demonstrated alterations in these proteins in the context of GDM, shedding light on the intricate molecular changes associated with insulin resistance during pregnancy.

Inflammation is a dynamic component of the GDM pathophysiology, influencing both its onset and progression. Protein biomarkers associated with inflammatory responses offer valuable insights into the inflammatory cascade linked to GDM (Ray et al., 2024). C-reactive protein (CRP), an acute-phase reactant, has been a focus of investigation. Elevated levels of CRP have been observed in individuals with GDM, suggesting a potential role in the early diagnosis of the condition [Lappas et al., 2012]. Interleukins, particularly IL-6 and IL-8, have also been implicated in the inflammatory processes (Vilotić et al., 2022) associated with GDM. Monitoring these inflammatory markers may provide additional diagnostic value, reflecting the inflammatory milieu that contributes to GDM development.

Increased oxidative stress is another hallmark of GDM, leading to cellular damage and further complicating the course of the disorder. Proteins involved in antioxidant defense mechanisms have been investigated as potential biomarkers of oxidative stress in GDM. Superoxide dismutase and glutathione peroxidase are examples of such proteins. Sivan et al. (2014) reported alterations in the levels of these antioxidant enzymes in the context of GDM, suggesting their potential as indicators of oxidative imbalance. Monitoring these biomarkers may not only contribute to the early diagnosis of GDM but also offer insights into the oxidative stress status and its implications for maternal and fetal health.

Given the pivotal role of the placenta in GDM, proteins secreted by this organ have garnered attention as potential biomarkers. Placental growth factor (PlGF) and soluble fms-like tyrosine kinase-1 (sFlt-1) are among the proteins implicated in GDM pathophysiology. Saraf et al. (2018) highlighted the relevance of these placental biomarkers, suggesting their potential as indicators of placental dysfunction and associated risks. Monitoring these proteins may offer insights into the health of the placenta, contributing to early diagnosis and risk stratification in GDM.

The collective evidence suggests that a panel of protein biomarkers may enhance the diagnostic accuracy and predictive value of GDM. Wang et al. (2017) conducted a study demonstrating the effectiveness of combining multiple protein biomarkers in improving the sensitivity and specificity of GDM diagnosis. This supports the idea that a multifaceted approach involving various protein markers may provide a more comprehensive assessment of GDM risk. The integration of diverse protein biomarkers into diagnostic panels could revolutionize GDM screening, enabling a more nuanced and accurate evaluation of the condition.

The incorporation of protein biomarkers into GDM diagnosis aligns with the broader paradigm shift towards personalized medicine. The identification of specific protein profiles allows for tailored interventions based on individual risk and severity. This personalized approach facilitates targeted and effective therapeutic strategies, optimizing outcomes for both mothers and infants affected by GDM. By understanding the unique

molecular signatures associated with GDM in individual patients, healthcare providers can offer more precise and individualized care.

While the potential of protein biomarkers in GDM diagnosis is promising, several challenges need to be addressed for their successful clinical implementation. Standardization of assays, reference ranges, and cut-off values for specific proteins is crucial to ensure consistency across studies and clinical settings. The heterogeneity of study populations and variations in methodologies present challenges in comparing and interpreting findings. Larger prospective studies are needed to validate the utility of these biomarkers in diverse populations and to establish their role in routine clinical practice.

The utilization of multiple protein biomarkers in diagnostic panels has the potential to refine GDM screening, allowing for a more accurate and personalized assessment of the condition. As research in this field continues to evolve, the clinical implementation of protein biomarkers may become a cornerstone in the early diagnosis and effective management of GDM, contributing to the broader goals of maternal and fetal health.

CHAPTER 3

METHODOLOGY

3. Methodology:

3.1 Materials Required for BeWo Cell Study:

3.1.1 Cell Culture Materials:

The BeWo cells, a human placental choriocarcinoma cell line, were cultured. The cell culture medium employed was Ham's F12K (Gibco), a nutrient-rich formulation optimized for the growth of this cell type. Fetal bovine serum (FBS) from MP Biomedicals, France, was added to the medium to provide essential growth factors and supplements.

To maintain the cells, 1X Dulbecco's Phosphate Buffered Saline (DPBS) was used for washing and rinsing procedures, and a 0.25% Trypsin-EDTA solution was employed for cell detachment and passaging. Dimethyl sulfoxide (DMSO) was also utilized, likely for cryopreservation purposes to store the BeWo cells for future experiments.

3.1.2 Cell Culture Equipment:

The BeWo cells were cultured in T-25 flasks obtained from Thermo Fisher Scientific Inc., USA. Serological pipettes with a 10 mL capacity, also sourced from Thermo Fisher Scientific Inc. (Nunc brand), were used for medium aspiration and cell suspension handling. Additionally, 96-well plates from the same manufacturer (Nunc) were employed, likely for seeding, treatment, and analysis of the BeWo cells. The instruments like XDFL series and SDPTO (Sunny Instruments, China) were used for cell counting and imaging respectively.

3.1.3 Software and Analysis:

For the analysis of experimental data, the ImageJ (Fiji) software, version 1.53c was used which is an open-source software package designed for the processing and analysis of BeWo cell cultures images.

3.2 BeWo Cell Culture:

3.2.1 In-Vitro Cell Culture process:

A cryovial containing BeWo cells (NCCS, Pune) was quickly thawed at 37°C with gentle swirling for 2-3 minutes (Freshney, 2015). The thawed suspension was transferred to 9 mL complete DMEM media composed of high glucose DMEM, 10% fetal bovine serum (FBS), and antibiotics penicillin/streptomycin (100 U/mL & 100 µg/mL respectively) (Bode et al., 2006). Centrifugation of cells was performed at 200 x g for 5 minutes, the supernatant aspirated off, and the pellet was gently resuspended in 1 mL fresh complete DMEM medium. Viable cells were counted before seeding a T-25 flask with BeWo cells at 5 x 10⁵ viable cells/ml in 5 mL total complete media volume. Seeded flasks were incubated at 37°C and 5% CO₂, with growth medium exchanged every 2 days. Before reaching 80% confluence, BeWo cells were sub-cultured using 0.25% trypsin-EDTA solution (Freshney, 2015).

Trypsin-EDTA solution, phosphate buffered saline (PBS) without Ca²⁺/Mg²⁺, and complete growth media were pre-warmed before subculture (Poulsen et al., 2009). Existing media was removed from the T-25 flask and adherent cells rinsed with PBS. 0.5-1 mL trypsin-EDTA was added and incubation occurred at 37°C, with microscopy monitoring to avoid agitating detaching cells (Freshney, 2015). Once cells appeared rounded and refractile, typically 1-2 minutes, 3 mL complete media was pipetted in to inactivate trypsin. Remaining attached cells were gently washed into suspension, ensuring >95% existed as single cells. If clusters were seen, further gentle pipetting dispersed aggregates (Freshney, 2015). Next, 5 mL fresh pre-equilibrated media was added to a new flask. The cell suspension was counted for number and viability prior to transferal to the new flask's media. The newly seeded culture was returned to the incubator and examined the next day to confirm reattachment and growth. Active cultures underwent media changes 2-3 times weekly (Freshney, 2015).

3.2.2 Cell Counting and Viability:

After trypsinizing and centrifuging the adherent cells, the resulting pellet was re-suspended in 1 mL fresh media (Freshney, 2015). Under sterile conditions, 50 μ L of this suspension was removed and an equal volume of 0.04% Trypan Blue was added at a 1:2 dilution for mixing via gentle pipetting (Strober, 2015). The hemocytometer chamber was cleaned and covered with a coverslip, then loaded with 5-10 μ L cell suspension via capillary action (Freshney, 2015). The sample was viewed under an inverted phase contrast microscope at 10x magnification. Viable (unstained bright) and nonviable (blue-stained) cells were counted, targeting >100 cells for enhanced accuracy (Freshney, 2015; Strober, 2015). Subsequently, concentrations of viable and nonviable cells along with the viable cell percentage were calculated using standard equations (Strober, 2015).

$$\text{Viable cell count} = \frac{\text{live cell count}}{\text{Total number of cell count}} \times \text{dilution factor} \times 10^4 \text{ cells/ml}$$

$$\text{Non-viable cell count} = \frac{\text{dead cell count}}{\text{Total number of cell count}} \times \text{dilution factor} \times 10^4 \text{ cells/ml}$$

$$\text{Percentage viability} = \frac{\text{viable cell count}}{\text{Total number of cell count}} \times 100$$

Table 3.1: Observation and calculation of viable cell count and percentage viability

Name of cell line	No. of viable cells	No. of dead cells	Total no. of cells	Percentage of viability
BeWo	580×10^4 cells/ml	2×10^4 cells/ml	582×10^4 cells/ml	99.6%

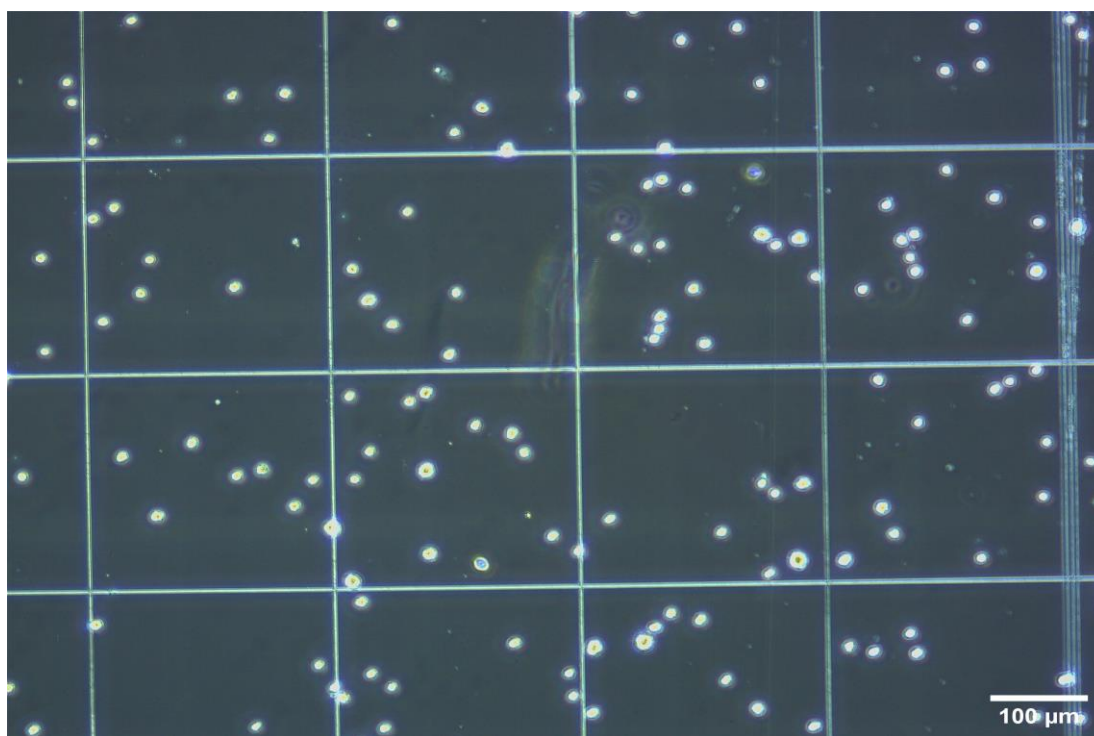


Figure 3.1: Cell viability by Trypan blue dye exclusion method

The provided haemocytometer (Figure 3.1) micrograph displays the results of a cell viability analysis for the BeWo cell line using the Trypan blue dye exclusion method.

The image shows a field of view with numerous bright, viable cells and a few darker, non-viable cells that have been stained by the Trypan blue dye.

According to the findings, the viable cell count for the BeWo cell culture is 580×10^4 cells/ml, while the dead cell count is 2×10^4 cells/ml. The total cell count, which is the sum of viable and dead cells, is 582×10^4 cells/ml. Calculation of the percentage of viable cells reveals an impressive 99.6% viability rate.

The high percentage of viable cells (99.6%) indicates that the BeWo cell culture is in a healthy and well-maintained state, with only a small fraction of dead or non-viable cells present. This suggests that the cells are suitable for further experimental procedures and can be confidently used in this study.

3.2.3 BeWo cell culture and differentiation:

The BeWo cell line, obtained from NCCS in Pune, India, underwent seeding and cultivation using Ham's F12K culture media enriched with 10% FBS to achieve adherent cell growth. The cells were initially plated in T-25 flasks at a concentration of 5×10^5 cells/mL in growth medium and were allowed to incubate overnight (Easton et al., 2022). The cell growth process occurred in a CO₂ incubator set at a temperature of 37°C, a CO₂ level of 5%, and a relative humidity of 90% (Orsi & Nugent, 2003). Following three passages, the cells were utilized to initiate the differentiation phase.

For the differentiation process, a fresh Ham's F12K growth medium, supplemented with 2% FBS, was employed, and a combination of 40 µM forskolin and 250 µM 8-Br-cAMP was added. This treatment regimen was repeated on the third day of the experiment. Effective differentiation of the cells was observed on the fifth day, marked by the development of syncytial cells (Stojanovska et al., 2022).

3.2.4 Development of insulin-resistant cells and VEGF treatment:

After successful differentiation, the standard growth medium was replaced with one containing 25 mM glucose. The cells were incubated in this high glucose medium for 72 hours to induce insulin resistance (refer Table 3.1) (Johnson et al., 2022). Next, the Test

+ VEGF group received a supplemental treatment of 50 ng/mL Vascular Endothelial Growth Factor (VEGF) in addition to the high glucose medium (Williams et al., 2021). Subsequently, all culture flasks were incubated for another 18 hours before microscopic examination of the cells (Handy et al., 2023).

Upon completion of the treatment, the culture medium was aspirated from all flasks, and the cells were gently washed with Dulbecco's Phosphate Buffered Saline (DPBS) (Williams et al., 2021). Subsequently, the cells were trypsinized, collected in 15 mL tubes, and subjected to centrifugation at 300 g for 5 minutes at 25°C (Johnson et al., 2022). The supernatant was carefully discarded, and the tubes containing the cellular pellet were then resuspended (Williams et al., 2021). The resuspended cells were utilized for both viability assays and glucose uptake assays (Johnson et al., 2022).

3.2.5 Treatment groups:

The experimental design comprised three groups, each with four replicates of BeWo cell cultures: the control group with 5 mM glucose, the Test group with 25 mM glucose [Luo et al.,2022], and the Test + VEGF group. Following the induction of insulin resistance, VEGF was introduced at a concentration of 50 ng/mL for an 18-hour period specifically in the Test + VEGF group [Arutyunyan et al.,2016]. Subsequently, the outcomes derived from each group were systematically compared and analyzed to discern the impacts of insulin resistance/glucose uptake and the influence of VEGF on BeWo cell cultures.

3.2.6 Glucose uptake assay using flow Cytometry:

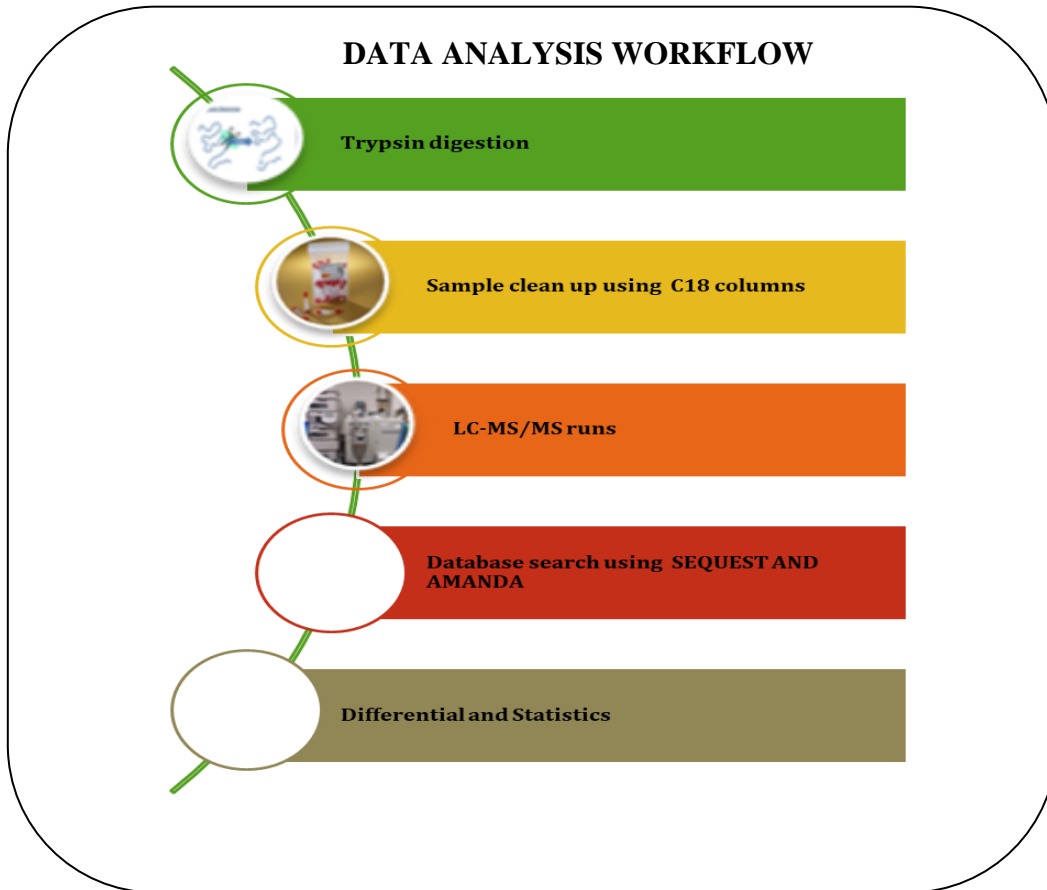
Following the completion of the incubation, the spent medium was removed, and the cells underwent washing with Dulbecco's Phosphate Buffered Saline (DPBS). Subsequently, low serum media without glucose, containing 0.5% FBS, was introduced to all wells. After a 2-hour incubation, the medium was aspirated, and the cells, excluding the negative control (without insulin treatment), were treated with 0.1 µg/mL insulin in 5 mL glucose-free culture medium, incorporating 100 µM 2-NBDG (2-(N-(7-Nitrobenz-2-oxa-1,3-diazol-4-yl) Amino)-2-Deoxyglucose) (7 µL per mL used) (Zou et al., 2005). The cells were then further incubated for 2 hours (Nakamura et al.,2023).

Upon completion of the treatment, the medium was extracted from all wells, and the cells were washed with DPBS. Subsequent trypsinization was performed, and the cells were directly harvested into 12×75 mm tubes. The tubes were then subjected to centrifugation for 5 minutes at 300× g at 25°C, and the supernatant was carefully aspirated (Freshney, 2015). The cells were resuspended in 0.5 - 1 mL of PBS, ensuring a thorough mixing to achieve the separation of individual cells. Following this, the cells were prepared for flow cytometry analysis.

2-NBDG, a fluorescent glucose analog utilized as a probe to detect glucose uptake in cultured cells, was employed in the analysis. It is taken up by cells through the same mechanism as glucose but is not metabolized, remaining trapped within the cells and emitting fluorescence upon excitation in a flow cytometer. The fluorescence of 2-NBDG is typically detected using optical filters designed for fluorescein, with excitation and emission maxima of 465/540 nm (Zou et al., 2005). The cells were analyzed using a flow cytometer to detect the fluorescence emitted by the 2-NBDG taken up by the cells. The intensity of the fluorescence is proportionate to the amount of glucose uptake by the cells (Hamilton et al., 2021).

3.3 Proteome Analysis (LCMS):

Experimental procedure:



3.3.1 Sample Preparation:

For each sample, 100 micrograms of protein was digested using the following workflow: reduction with 5mM tris(2-carboxyethyl)phosphine (TCEP), alkylation with 50mM iodoacetamide, then overnight trypsin digestion at 37°C at a 1:50 trypsin:lysate ratio (Huang et al., 2017). The resulting digests were purified via C18 silica cartridges to remove salt, dried down, then reconstituted in Buffer A (2% acetonitrile, 0.1% formic acid) for subsequent analysis (Side et al., 2018). This optimized protocol enables thorough protein digestion into peptides while eliminating contaminants.

3.3.2 Mass Spectrometric Analysis of Peptide Mixtures:

The experiments were conducted using an Easy-nlc-1000 system coupled to an Orbitrap Exploris mass spectrometer (Thermo Fisher Scientific, 2022) at VProteomics, New Delhi. 1 µg of peptide sample was loaded onto a 15 cm C18 column and separated using a 0-40% gradient of Buffer B (80% acetonitrile, 0.1% formic acid) at a flow rate of 500 nl/min for 60 minutes for LC-MS analysis (Aebersold & Mann, 2016). MS1 spectra were acquired in the Orbitrap with specific parameters, including a resolution of 60K and a mass range of 375-1500 m/z. Dynamic exclusion for 30s was employed for all charge states per precursor. MS2 spectra were collected for the top 12 peptide precursors with a resolution of 15K and an AGC target of 200% (Thermo Fisher Scientific, 2022).

A total of 9 LC-MS/MS runs were performed on an EXPLORIS mass spectrometer, with each run lasting 60 minutes. The resolution was set at 60,000 for MS1 and 15,000 for MS2 scans (Thermo Fisher Scientific, 2022). The acquired data was searched against the Uniprot Homo sapiens database, identifying 3,528 protein groups and 22,431 unique peptide sequences in total across the 9 analyses (Nesvizhskii et al., 2003).

3.3.3 Data Processing:

The acquired RAW data files underwent processing in Proteome Discoverer (version 2.5) and searching against the Human database (Uniprot) using a dual Sequest and Amanda search strategy. Precursor and fragment mass tolerances were specified at 10 ppm and 0.02 Da respectively. Trypsin/P was set as the protease, cleaving peptide bonds at the C-terminus of lysine/arginine except when followed by proline. Carbamidomethyl cysteine was set as a fixed modification. Oxidized methionine and N-terminal acetylation were considered variable modifications. Peptide spectrum matches and protein groups were filtered at a 0.01 false discovery rate (FDR) threshold (Tsai et al., 2016).

A total of 9 MS runs were conducted on an EXPLORIS mass spectrometer, each with a run time of 60 minutes. The resolution for MS1 was set at 60,000, and for MS2, it was set at 15,000. The data was analyzed against the Uniprot Homo sapiens Database, resulting in the identification of 3,528 protein groups and 22,431 peptide groups.

3.4 In-vivo Experimental Analysis:

ANIMAL HOUSE

Lovely Institute of Technology (Pharmacy), Lovely Professional University
Ludhiana- Jalandhar G.T. Road, Phagwara (Punjab), 144411
Registration Number -954/PO/ReRcBiBt/S/06/CPCSEA

CERTIFICATE

This is to certify that the project titled "*Identification and Evaluation of Probable Protein Biomarkers in Gestational Diabetes Mellitus*" has been approved by the IAEC.

Name of Principal Investigator: Dr. Manoj Kumar Jena

IAEC approval number: LPU/IAEC/2022/16

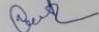
Date of Approval: 03rd October 2022

Animals approved: 12 Female and 4 Male rats


Remarks if any: - NA


Dr. Monica Gulati

Biological Scientist,
Chairperson IAEC


Dr. Navneet Khurana

Scientist from different
discipline


Dr. Bimlesh Kumar

Scientist In-Charge of
Animal House, Member
Secretary IAEC

3.4.1 Study Plan:

The study aims to induce a diabetic condition in pregnant rats using Streptozotocin (STZ) to establish a Gestational Diabetes Mellitus (GDM) model, followed by a comparative assessment of protein biomarkers identified from pooled blood samples to discern differences between control and GDM test groups.

Figure 3.2: Study Plan of experimentation on SD (Sprague-Dawley) rats.

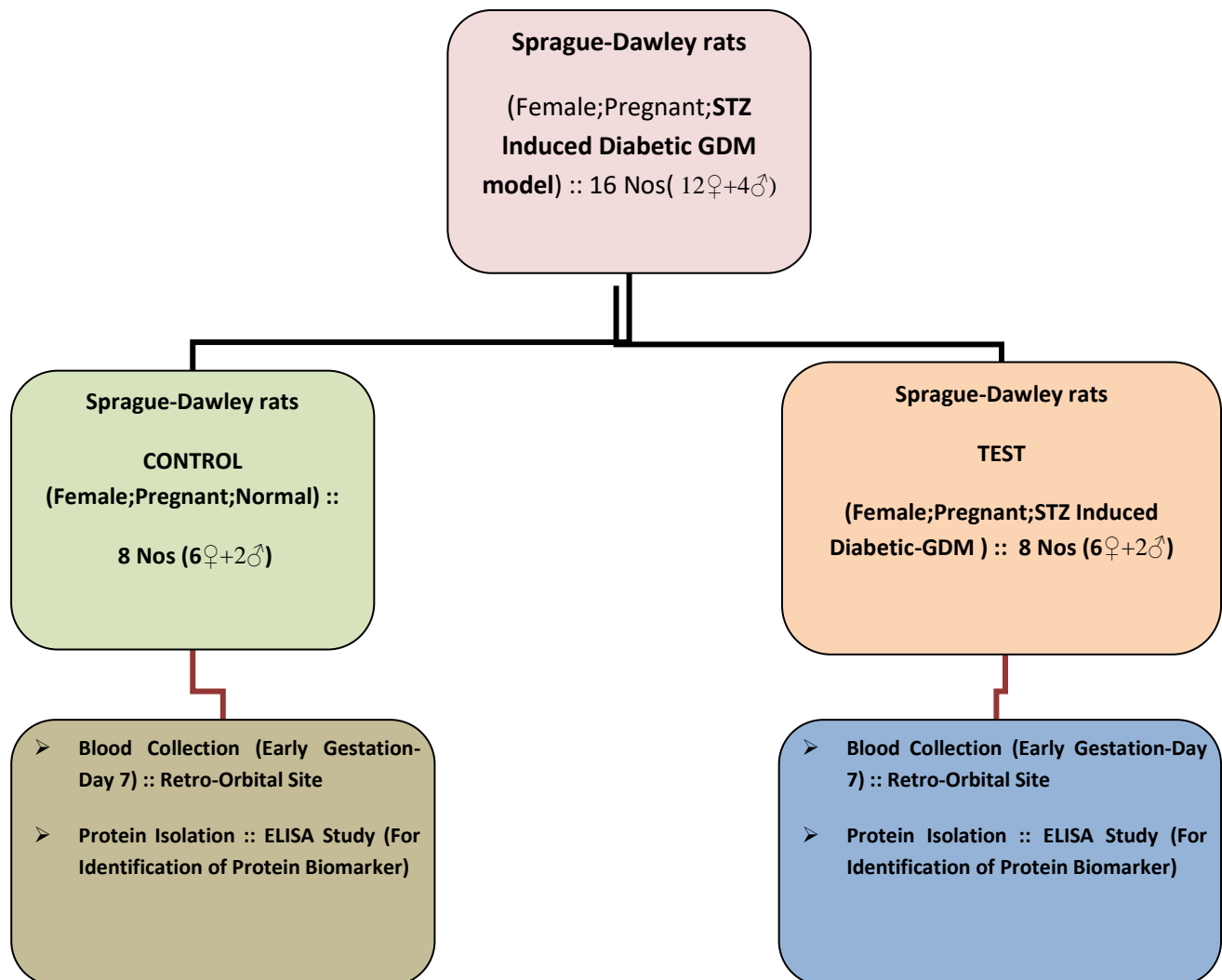
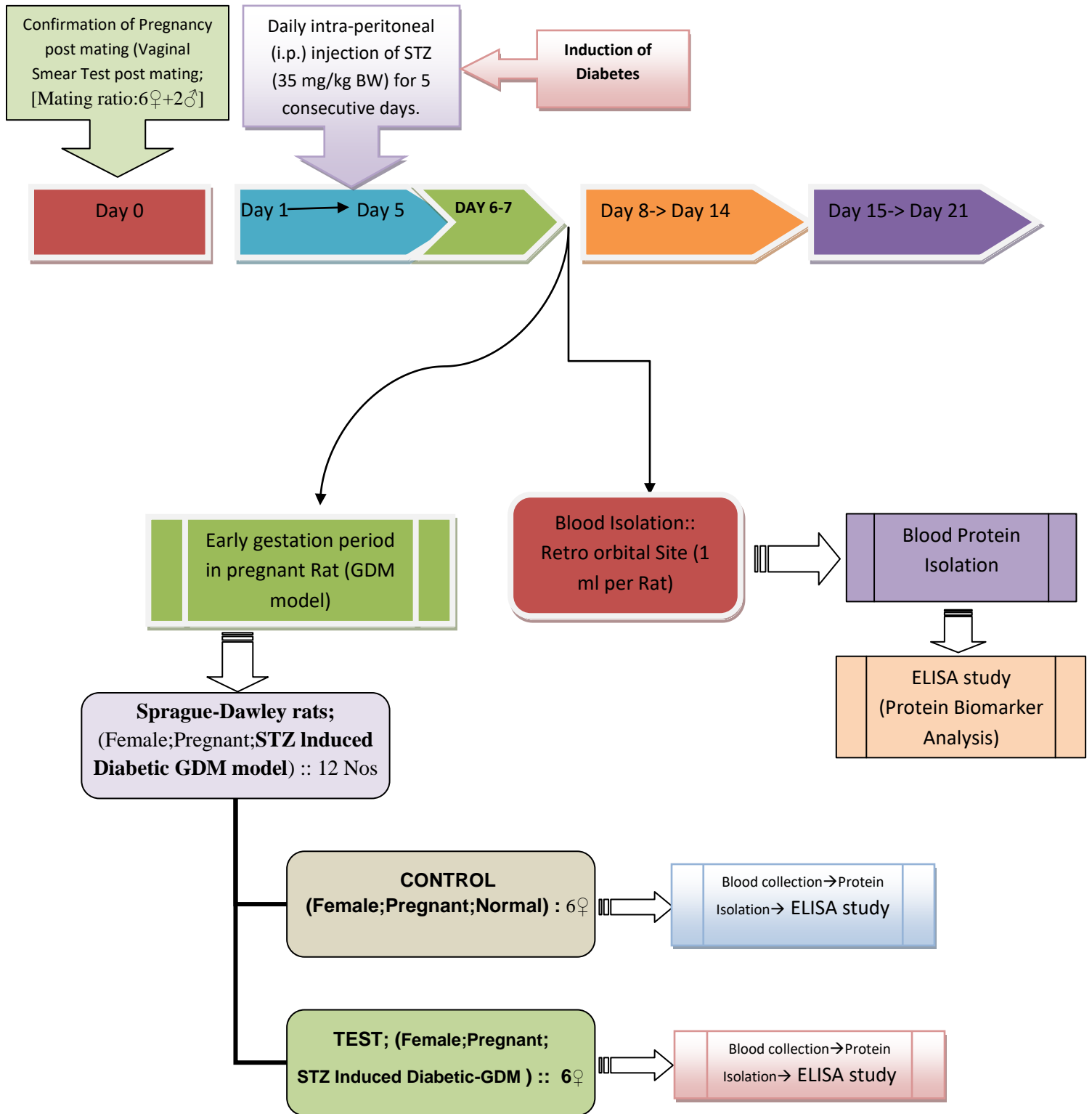


Figure 3.3: Diagrammatic representation of In-vivo study plan



The study aimed to induce a gestational diabetes mellitus (GDM) condition in pregnant rats using Streptozotocin (STZ) and conduct a comparative assessment of protein biomarkers between control and GDM groups. Healthy, pregnant Sprague Dawley (SD) rats were randomized into a control group and a GDM group. The GDM group received a single dose of STZ (35 mg/kg bw in 0.1 mol/L citrate buffer) via intra-peritoneal injection for five consecutive days, during the early stage of pregnancy (e.g., gestational day 1-5) to induce hyperglycemia, while the control group received a sham injection of the vehicle (0.1 mol/L citrate buffer). The animals were monitored for the development of hyperglycemia and other clinical signs of GDM.

Blood samples from both the control and GDM groups was collected from the retro-orbital site on day 7, from the onset of conception or pregnancy confirmation (Early Gestation)

The blood serum was separated and pooled within each group to obtain control and test samples. Proteomic techniques (LCMS) and antibody-based assays (ELISA) were utilized to identify differentially expressed protein biomarker between the control and GDM group.

The data collected was subjected to analysis to compare the control and GDM groups for blood glucose levels and identified protein biomarker. The results were interpreted in the context of GDM pathogenesis, and potential biomarker that could serve as diagnostic or prognostic indicators were identified.

Table 3.2: Experimental animals grouping and dosing schedule

Group No.	Groups(8 Rat/gp)	Treatment	Route of administration and Dosage	Number of Groups
1	Normal Control	Vehicle (Normal Pregnant Rat)	No treatment (0.1 mol/L citrate buffer)	1 Gp (6♀+2♂ Rat/gp)
2	Test	Streptozotocin (STZ)-induced diabetes in pregnant Rat (GDM model)	intraperitoneal injection (i.p.) of STZ (35 mg/kg bw in 0.1 mol/L citrate buffer)	1 Gp(6♀+2♂ Rat/gp)

3.4.2 Overview of In-vivo experimental Study:

Sixteen Sprague-Dawley rats, comprising 12 females and 4 males, were divided into two groups, each consisting of 6 females and 2 males, for mating and subsequent pregnancy induction (Tarry-Adkins et al., 2019). The first group, serving as the control, included the first 6 pregnant rats, representing normal pregnancies. The second group of 6 rats was designated as the diseased group (test group), subjected to streptozotocin (STZ) administration to induce gestational diabetes (GDM). The induction involved daily intraperitoneal (i.p.) injections of STZ (35 mg/kg BW) for 5 consecutive days (Zhang et al., 2008) (Table 3.2).

Blood samples were collected from the retro-orbital site on day 7 from the onset of conception or pregnancy confirmation (Early Gestation) (van Zwieten et al., 1981). Subsequently, blood serum proteins were isolated and processed for ELISA analysis to identify protein biomarkers associated with early gestation. The highly expressed proteins identified through LCMS analysis during early gestation were further evaluated using ELISA technique (Graves & Haystead, 2002).

3.5. Enzyme linked immunosorbent assay (ELISA) Analysis:

ELISA is a widely used analytical biochemistry technique that detects the presence of an antibody or an antigen in a sample by using enzyme-linked antibodies and chromogenic substrates (Gan & Patel, 2013).

The study aimed to evaluate and quantify proteins that were upregulated in test samples, as identified through liquid chromatography-mass spectrometry (LC-MS) analysis, for their potential as biomarkers for the diagnosis of Gestational Diabetes Mellitus (GDM) in early gestation. One of the upregulated proteins, the Human Mitochondrial Fission Factor (MFF), was further screened and evaluated using an ELISA technique to assess its potential as a diagnostic marker for GDM by comparing in-vitro and in-vivo samples.

The quantification of MFF in the samples was performed using an ELISA kit employing a two-site sandwich approach. The microplate was pre-coated with an MFF-specific antibody. Standards and samples were added, allowing MFF to bind to the immobilized antibody. After washing, a biotin-conjugated MFF-specific antibody and Streptavidin-HRP were introduced. A substrate solution was added, resulting in color development proportional to the bound MFF amount. The color intensity was measured to quantify MFF levels (Gan & Patel, 2013).

Initially, LC-MS analysis was performed to screen for upregulated proteins in test samples from individuals with GDM compared to control samples. The MFF protein was identified as one of the upregulated proteins and was further evaluated using the ELISA technique (Graves & Haystead, 2002). The ELISA procedure was conducted following the manufacturer's instructions for the Human Mitochondrial Fission Factor (MFF) ELISA Kit. Both in-vitro and in-vivo samples were analyzed to assess the potential of MFF as a biomarker for GDM diagnosis. The standards and samples were prepared and added to the pre-coated microplate wells. After incubation and subsequent washing steps, the biotin-conjugated antibody and Streptavidin-HRP conjugate were sequentially added and incubated. Following the final wash, the substrate solution was added, and the color development was monitored. The reaction was stopped, and the absorbance was measured using a microplate reader at the appropriate wavelength. The concentration of MFF in the test samples was determined by interpolating the absorbance values from a standard curve generated using the known concentrations of MFF standards provided in the kit. The levels of MFF in the GDM samples were compared with those in the control samples to evaluate its potential as a diagnostic biomarker for GDM (Gan & Patel, 2013; Graves & Haystead, 2002).

3.5.1 Experimental System (ELISA):

The study utilized the Human Mitochondrial Fission Factor (MFF) ELISA Kit, which enables the determination of MFF concentrations in blood serum and cell culture supernatants (Gan & Patel, 2013). The kit exhibited a detection range of 25-400 pg/mL, with a minimum detectable dose (MDD) of human MFF typically less than 1 pg/mL (Gan

& Patel, 2013). Intra-assay accuracy evaluation, with 4 known concentration samples tested 20 times, revealed a coefficient of variation (CV) less than 9%. Linearity assessment, by diluting high MFF concentration samples, yielded a correlation coefficient of 0.99, indicating excellent linearity. The Human MFF ELISA Kit demonstrated high sensitivity, excellent specificity for human MFF detection, with no significant cross-reactivity or interference observed, ensuring accurate and reliable measurement of MFF levels in the samples (Gan & Patel, 2013).

The protocol for the study involving the Human Mitochondrial Fission Factor (MFF) ELISA Kit was as follows:

3.5.2 Materials required:

Human Mitochondrial fission factor (MFF) ELISA Kit, Abbkine, USA containing:

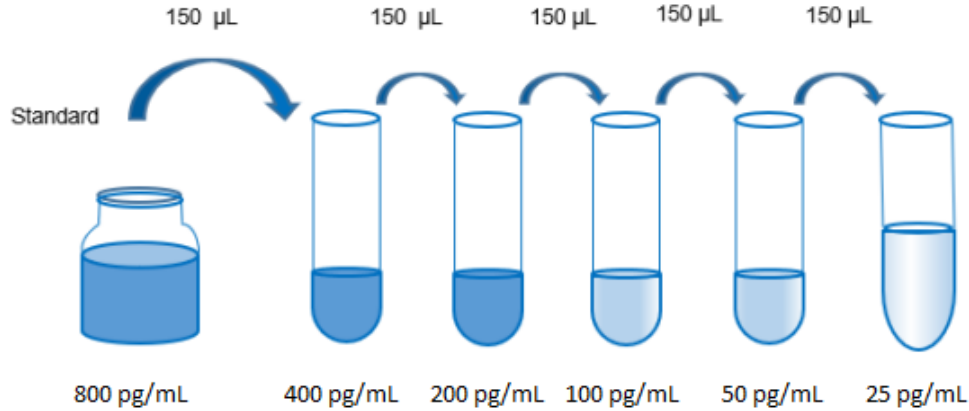
Anti-Human MFF antibody coated 96-well microplate; Human MFF standard; HRP-conjugated Human MFF detection antibody; Standard diluent; Sample diluent; Chromogen solution A; Chromogen solution B; Stop solution ; Wash buffer ;Plate covers ; 5mL, 2mL and 1.5mL tubes, Tarsons, India; Microplate reader - BK-EL10A, Biobase China

3.5.3 Sample Preparation:

The cell culture supernatant sample (In-vitro) were centrifuged for twenty minutes at 1000×g. Cell particulates were removed and the samples were assayed immediately.

For serum samples (In-vivo samples), a serum separator tube was used, and the samples were allowed to clot for 2 hours at room temperature before centrifugation for 20 minutes at approximately 1000×g. Freshly prepared serum was assayed immediately.

3.5.4 ELISA-Reagent Preparation: Dilution series



Before starting the assay, all reagents were allowed to reach room temperature [Abbkine,2024]. The Wash Buffer was diluted with distilled/deionized water in a specified ratio (1:20 for 48 tests or 1:30 for 96 tests) [Abbkine,2024]. To prepare the standards, 150 µL of Standard Diluent was added to each tube, and a 2-fold dilution series was created using the stock solution. The undiluted stock served as the high standard, while the Standard Diluent served as the zero standard. Dilution series were followed as per protocol [Abbkine, 2024].

The assay procedure began with preparing all necessary reagents. Standards and samples were added in duplicate to the microplate wells. Diluted standards were added to the standard wells, while sample diluent and samples were added to the testing sample wells [Abbkine,2024]. After a 45-minute incubation at 37°C, the wells were aspirated and washed five times with Wash buffer. HRP-Conjugate detection antibody was then added to each well, except the blank wells, followed by another 30-minute incubation at 37°C. The aspiration/wash process was repeated five times [Abbkine,2024]. Chromogen solutions A and B were added to each well, and the plate was incubated for 15 minutes at 37°C in the dark. Stop Solution was then added, changing the color from blue to yellow. Finally, the Optical Density was read at 450 nm using a microtiter plate reader within 15 minutes [Abbkine,2024].

CHAPTER 4

RESULTS & DISCUSSION

4. Results and Discussion:

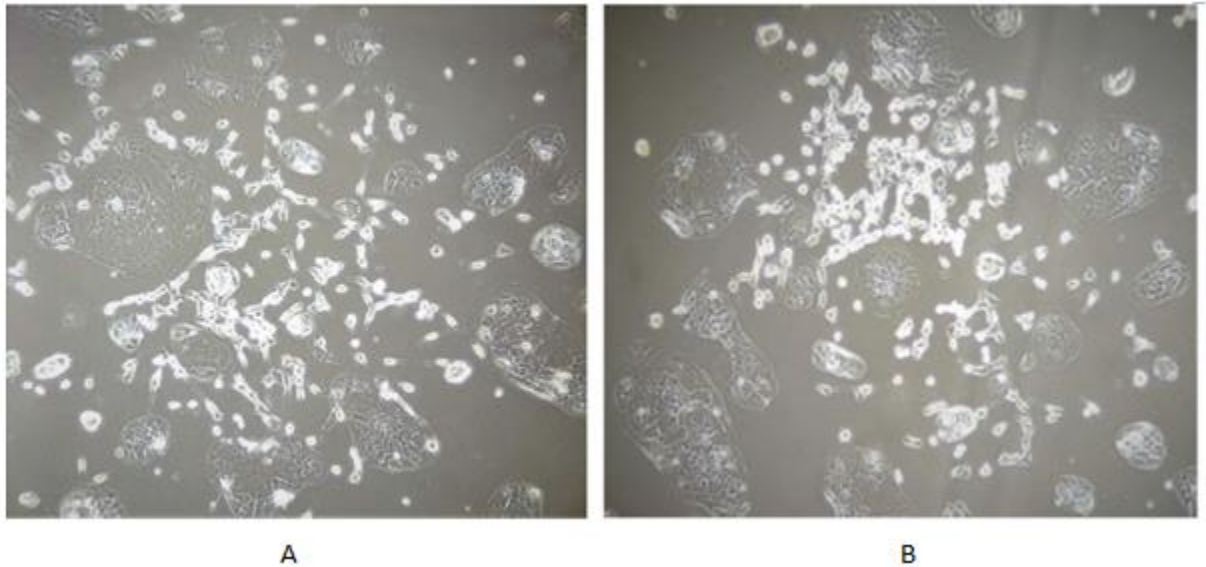
4.1 BeWo Cell Culture and differentiation:

The provided images depict the growth and differentiation patterns of BeWo cells, a human placental choriocarcinoma cell line widely used as an *in vitro* model for studying placental development and function (Orendi et al., 2011). Figure A and Figure B showcase BeWo cells at approximately 40% confluency, characterized by multiple small colonies dispersed across the culture surface. This growth pattern is consistent with the epithelial nature of BeWo cells, which tend to form discrete colonies before achieving confluency (Yoshie et al., 2010).

As the culture progresses, BeWo cells exhibit a shift in morphology and organization. Figure C, Figure D, and Figure E demonstrate a monolayer culture at approximately 70% confluency. At this stage, the cells have proliferated to cover a larger area of the culture surface, forming a near-continuous sheet of cells. This monolayer formation is typical of BeWo cells and is crucial for studying placental barrier functions and transport processes (Desforges & Sibley, 2010).

A notable feature of BeWo cells is their capacity to differentiate into syncytiotrophoblast-like cells, mimicking the syncytialization process in the human placenta (Orendi et al., 2011). Figure F vividly illustrates this differentiation, marked by the presence of fused syncytia (indicated by the red arrow). This morphological change was induced by treatment with 40 μM forskolin and 250 μM 8-Br-cAMP, known stimulators of syncytialization in BeWo cells (Wice et al., 1990). The formation of syncytia, characterized by multinucleated cells resulting from cell fusion, closely resembles the physiological process in the human placenta where cytotrophoblasts fuse to form the syncytiotrophoblast layer (Orendi et al., 2011).

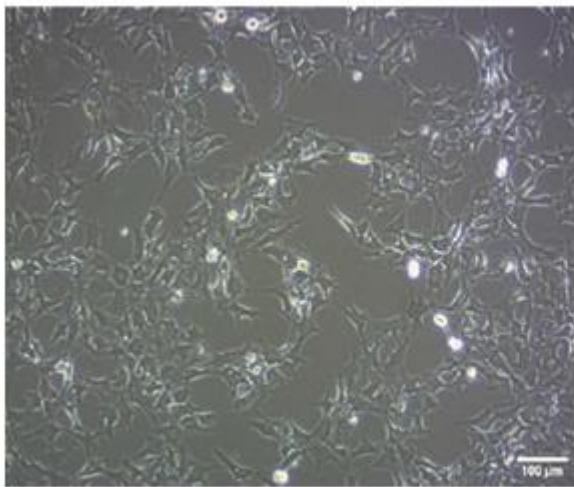
Figure 4.1: BeWo Cell Culture Stages



The BeWo cell culture figure 4.1 (A) and 4.1 (B) exhibit characteristic features of trophoblast-like cells in various stages of differentiation and aggregation. Both figures display a heterogeneous population of cells with distinct morphological variations. Both figures displays features which include large, flattened cells with irregular boundaries, indicative of syncytiotrophoblast-like structures, interspersed with smaller, round cells resembling cytotrophoblasts. The cultures demonstrate significant cell clustering, suggesting active cell-cell adhesion processes mediated by molecules such as E-cadherin. The phase-bright appearance of cells in both images indicates high metabolic activity. The cellular projections are visible, implying ongoing cell-cell communication and potential migratory behavior.

Despite these shared characteristics, subtle yet significant differences are apparent between the two cultures. Image A exhibits a higher cell density, particularly in the central and upper right regions, with more pronounced large, flattened syncytiotrophoblast-like formations. This suggests a more advanced stage of differentiation or fusion events, possibly due to extended culture time or exposure to syncytialization-promoting factors such as forskolin or elevated cAMP levels. In contrast, Image B shows a more uniform cell distribution with a higher proportion of smaller,

round cells, indicative of a cytotrophoblast-like phenotype. The cellular projections in B are more distinct, potentially signifying enhanced migratory behavior or initial stages of cell-cell fusion attempts. The cell clusters in A appear larger and more compact, while those in B are smaller and more dispersed, further supporting the hypothesis of different differentiation stages or varied responses to culture conditions. These nuanced differences underscore the plasticity of BeWo cells and their utility as a model for studying trophoblast differentiation. The observed variations likely reflect distinct points in the continuum of trophoblast-like development, offering valuable insights into the morphological and functional changes associated with placental cell differentiation and fusion processes.



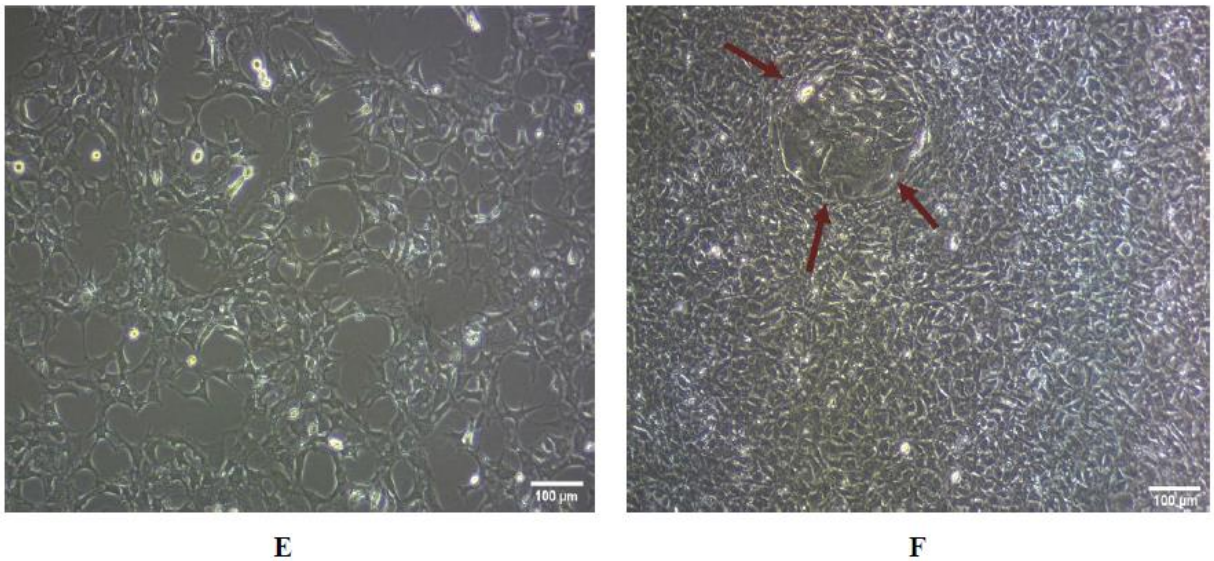
c|



D

The figure 4.1(C) reveals a more dispersed population of BeWo cells with distinct morphological characteristics. The cells exhibit an elongated, fibroblast-like phenotype, suggesting a less differentiated state or alternative activation pathway. There is a notable absence of large syncytial formations. The even distribution of cells across the field indicates a more uniform growth pattern, possibly reflecting different culture conditions or an earlier stage of trophoblast-like development. The lower contrast in this image allows for subtle visualization of cellular processes and potential secretory vesicles.

The figure 4.1(D) displays a high-density culture of BeWo cells exhibiting significant cellular aggregation. The central region shows a large, confluent mass of cells, indicative of extensive cell-cell adhesion and possible syncytialization - a hallmark of trophoblast differentiation. This central syncytium-like structure is surrounded by numerous smaller, discrete cells that appear to be migrating or proliferating outward. The high contrast in this image accentuates cellular boundaries and intracellular structures, suggesting active cytoskeletal remodeling and membrane fusion events characteristic of trophoblast differentiation.



The BeWo cell culture micrographs figure 4.1 (E) and 4.1 (F) exhibit markedly distinct morphological and organizational characteristics, reflecting different stages or conditions of trophoblast-like differentiation. Figure 4.1(E) presents a heterogeneous population with moderate cell density, featuring a mix of elongated and rounded cellular morphologies. This diversity suggests varying degrees of differentiation or activation states within the culture. The presence of visible cytoplasmic extensions indicates active cell-cell communication or migratory behavior.

In contrast, figure 4.1(F) displays a strikingly homogeneous and densely packed cellular arrangement, with predominantly small, uniform cells. The most notable feature in figure

4.1(F) is the large, circular structure denoted by red arrows, strongly indicative of syncytium formation, a hallmark of advanced trophoblast differentiation. This syncytial structure implies heightened expression of fusogenic proteins like syncytin and increased intracellular cAMP levels, known inducers of BeWo cell fusion. The uniformity and high density in figure 4.1(F) suggest a shift towards a more differentiated state, with potentially enhanced cell-cell adhesion through increased expression of molecules such as E-cadherin. Conversely, the looser associations in figure 4.1(E) point to a more proliferative state with cells at various stages of the cell cycle. The cytoskeletal organization likely differs significantly between the two cultures, with figure 4.1(F) showing evidence of reorganization associated with differentiation and fusion, while figure 4.1(E) exhibits more diverse arrangements. These distinctions imply differing metabolic and endocrine activities, with the syncytium in figure 4.1(F) potentially representing a site of heightened hormone production characteristic of syncytiotrophoblasts. The contrast between these figures underscores the plasticity of BeWo cells and their responsiveness to differentiation stimuli (Differentiation media having 40 μ M forskolin and 250 μ M 8-Br-cAMP), reinforcing their value as a model system for studying trophoblast biology and placental development.

This differentiation is particularly relevant in the context of studying gestational diabetes mellitus (GDM), as the syncytiotrophoblast layer plays a crucial role in maternal-fetal nutrient exchange and hormone production (Desoye & Hauguel-de Mouzon, 2007). Alterations in syncytialization and syncytiotrophoblast function have been implicated in GDM pathophysiology, affecting glucose transport and insulin sensitivity (Cawyer et al., 2014).

These morphological changes mirror key aspects of placental development and function, making BeWo cells an invaluable model for investigating GDM-related alterations in trophoblast behavior, glucose handling, and hormone regulation.

Table 4.1: Flow Cytometry results for Glucose uptake

	Sample Name	Geometric mean fluorescence intensity (MFI) of NBDG (FL1-A parameter) \pm CV	Fold change in Glucose uptake	% of Cells	
				NBDG low	NBDG high
BeWo - Assay Controls for flow Cytometry					
1	Without Insulin (Negative control)	4402 \pm 75.9	1	61.8	38.2
2	Untreated (Positive control) – 0.1 μ g/mL Insulin	10431 \pm 85.2	2.4	27.0	73.0
BeWo - differentiated cells					
1	Control Group – 0.1 μ g/mL Insulin	9816 \pm 126	2.2	29.2	70.8
2	Test Group – 0.1 μ g/mL Insulin	4693 \pm 74.2	1.1	59.5	40.5
3	Test + VEGF group – 0.1 μ g/mL Insulin	5040 \pm 76.7	1.2	56.5	43.5

4.2 Flow Cytometry Analysis for Glucose uptake:

The flow cytometry analysis of glucose uptake in BeWo trophoblast cells revealed distinct patterns under various experimental conditions. The control group, treated with 0.1 μ g/mL insulin, exhibited a 2.2-fold increase in 2-NBDG fluorescence compared to the negative control, which lacked insulin treatment (Table 4.1). This significant increase in fluorescence intensity is indicative of enhanced glucose uptake, as 2-NBDG is a fluorescent glucose analog widely used to monitor glucose transport in living cells (D'Souza et al.,2022; O'Neil et al., 2005; Yamada et al., 2007).

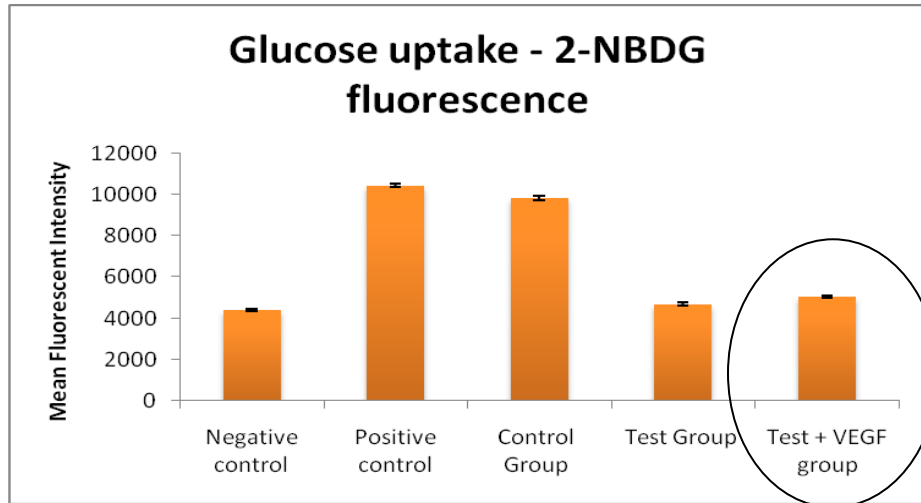


Figure 4.2: Comparative analysis of glucose uptake (Mean Fluorescence Intensity of 2-NBDG fluorescence) among Control, Test and Test-VEGF group.

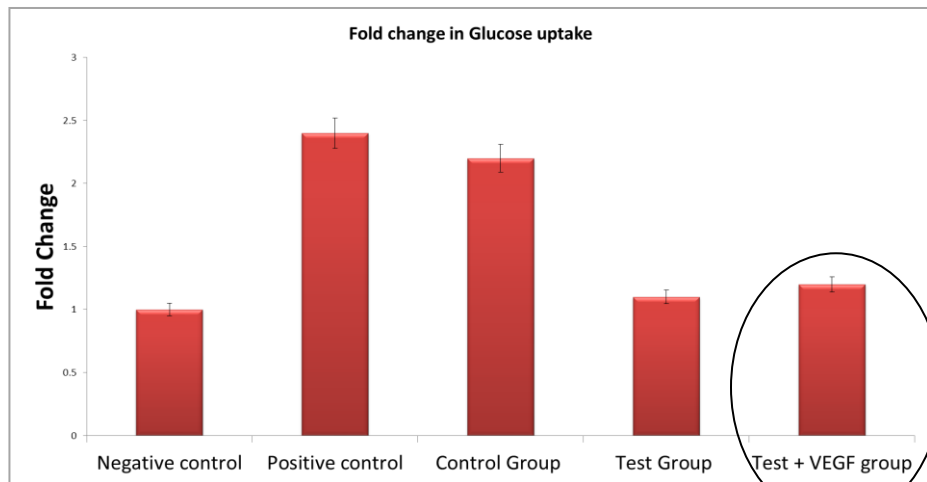


Figure 4.3: Comparative fold change analysis of glucose uptake for Control, Test and Test-VEGF group.

Table 4.2: Flow Cytometry results illustrating CV and fold change in Glucose uptake for Control Vs Test group.

Sample	MFI-FL1-A	CV	Fold change
Negative control	4402	75.9	1
Positive control	10431	85.2	2.4
Control Group	9816	126	2.2
Test Group	4693	74.2	1.1
Test + VEGF group	5040	76.7	1.2

In contrast, both the test group (insulin-resistant cells) and the test + VEGF group (insulin-resistant cells treated with exogenous VEGF) displayed reduced glucose uptake, characteristic of insulin resistance. The test group showed a modest 1.1-fold increase, while the test + VEGF group exhibited a slightly higher 1.2-fold increase in 2-NBDG fluorescence compared to the negative control (Al-Ofi et al.,2021) (Table 4.2).

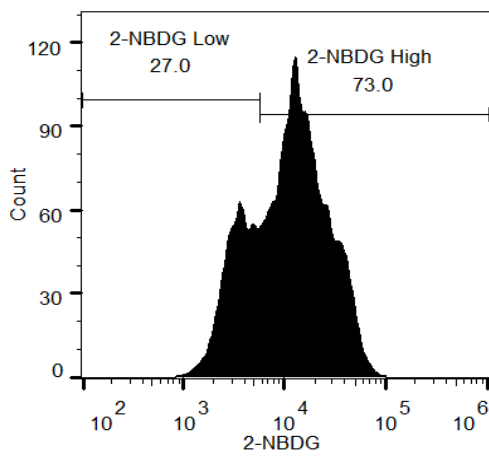
The marginal increase in glucose uptake observed in the test + VEGF group suggests that exogenous VEGF does not significantly enhance glucose uptake in insulin-resistant BeWo cells (Table 4.2). This observation challenges the initial hypothesis that VEGF might improve glucose uptake, as suggested by some studies linking VEGF to glucose metabolism (Jiang et al., 2013). However, our findings are consistent with studies by Lappas (2014), who reported that VEGF levels in GDM placentas were not significantly different from normal pregnancies, suggesting a limited role for VEGF in GDM pathophysiology.

The positive control, designed to evoke maximum cellular response, induced a substantial 2.4-fold increase in glucose uptake. This robust response serves as a benchmark for assessing the efficacy of insulin and VEGF treatments. The disparities in glucose uptake between insulin-sensitive and insulin-resistant cells underscore the complexity of glucose metabolism in GDM (Barbour et al., 2007).

The flow cytometry results provide quantitative evidence of impaired glucose uptake in insulin-resistant BeWo cells, a model for GDM. The minimal impact of exogenous VEGF on glucose uptake in this model suggests that VEGF may not play a significant role in ameliorating insulin resistance in early gestational stages of GDM and require further studies to evaluate its cellular potency.

Figure 4.4: Flow Cytometry Results for (a) Untreated Cells, (b) Control Cells and (c) Cells without Insulin.

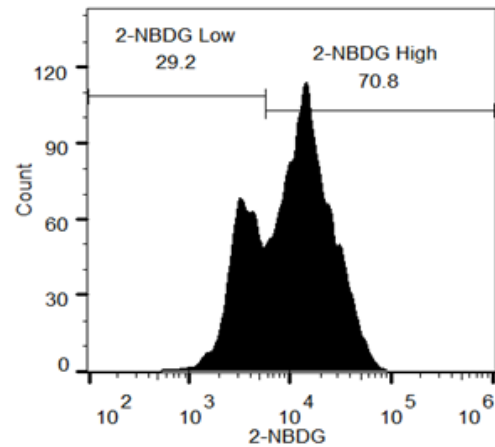
Untreated Cells:



Q_BeWo 01UT 00001274 951.LMD
Cells 6115

(a)

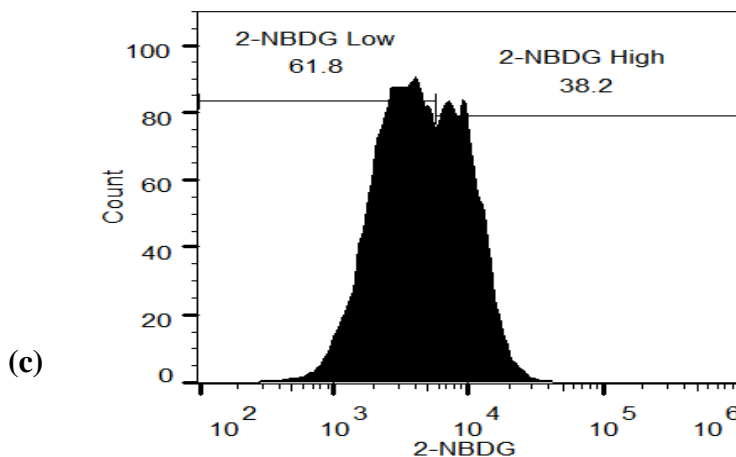
Control:



Q_BeWo 02Control 00001275 952.LMD
Cells 6038

(b)

Without Insulin:



Q_BeWo 05WOInsulin 00001278 955.LMD
Cells 5485

The provided flow cytometry data (Figure 4.4) illustrates the effects of different insulin conditions on glucose uptake in BeWo cells. The cells were subjected to three distinct conditions: untreated cells with no insulin (Figure 4.4-a), control cells with normal insulin (Figure 4.4-b), and cells without insulin (Figure 4.4-c). Each condition was characterized by various statistics, including the number of cells analyzed, coefficient of variation (CV) for FL1, geometric mean for FL1, and the distribution of cells into high and low 2-NBDG (a glucose analog) groups.

In the untreated cells with no insulin condition, a total of 8000 cells were analyzed. The geometric mean for FL1, which represents the fluorescence intensity of 2-NBDG (D'Souza et al.,2022) and is proportional to glucose uptake, was 4402, with a CV of 75.9%. Notably, the distribution of cells into high and low 2-NBDG groups showed a higher percentage in the low 2-NBDG category (61.8%), suggesting a lower glucose uptake in the absence of insulin.

Moving to the control cells with normal insulin condition, with the same number of cells analyzed (8000), the geometric mean for FL1 increased to 9816, indicating enhanced glucose uptake. However, the CV also increased to 126%. The distribution of cells into high and low 2-NBDG groups showed a shift toward higher glucose uptake, with 70.8% in the high 2-NBDG category. This observation is consistent with previous studies demonstrating that insulin stimulates glucose uptake in various cell types, including trophoblast cells (Grahovac et al., 2021).

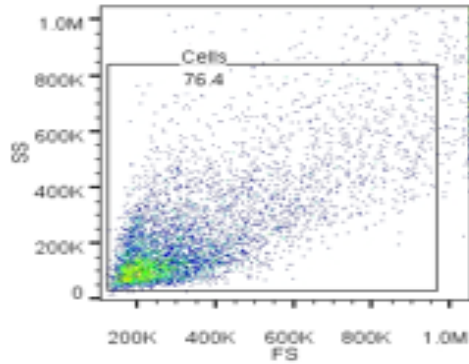
In the cells without insulin condition, 8000 cells were analyzed as well. The geometric mean for FL1 decreased to 4402, and the CV was 75.9%, similar to the untreated cells without insulin. The distribution of cells into high and low 2-NBDG groups indicated a substantial decrease in the high 2-NBDG category (38.2%), reinforcing the notion that insulin is a key factor in promoting glucose uptake (Yazdani et al.,2022).

Overall, the data reveals significant variations in glucose uptake under different insulin conditions. Insulin plays a crucial role in enhancing glucose uptake, as seen in the control

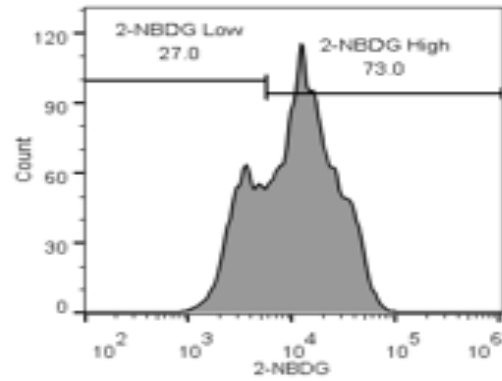
cells with normal insulin, while the absence of insulin results in reduced glucose uptake. These findings are consistent with the well-established role of insulin in regulating cellular glucose metabolism and uptake (Bala et al.,2021). Researchers may further explore the molecular mechanisms underlying these observations, such as insulin receptor signaling pathways and glucose transporter regulation, to deepen our understanding of insulin's role in glucose uptake in BeWo cells.

Figure 4.5: Scatter Plot for 2-NBDG uptake for untreated cells and cells without insulin.

(a) Untreated Cells:



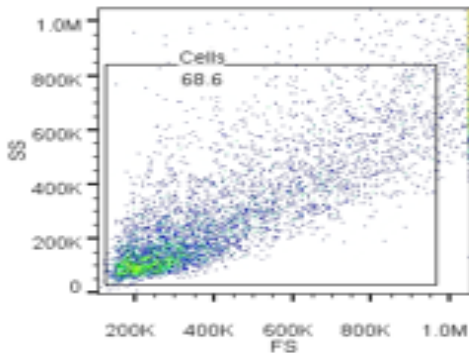
Q_BeWo 01UT 00001274 951.LMD
Ungated8000



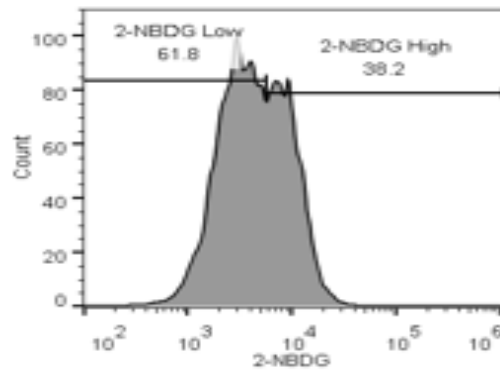
Q_BeWo 01UT 00001274 951.LMD
Cells6115

2-NBDG High: Freq. of Parent : 73.0
2-NBDG Low: Freq. of Parent : 27.0
Cells: Geometric Mean : FLI: 10431 Cells: CV : FLI: 85.2

(b) Without Insulin:



Q_BeWo 05WOInsulin 00001278 955.LMD
Ungated8000

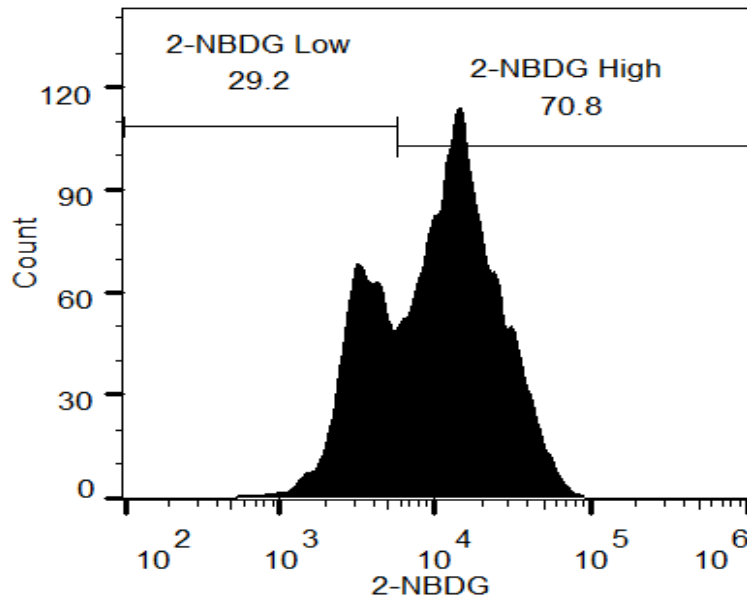


Q_BeWo 05WOInsulin 00001278 955.LMD
Cells5485

2-NBDG High: Freq. of Parent : 38.2
2-NBDG Low: Freq. of Parent : 61.8
Cells: Geometric Mean : FLI: 4402 Cells: CV : FLI: 75.9

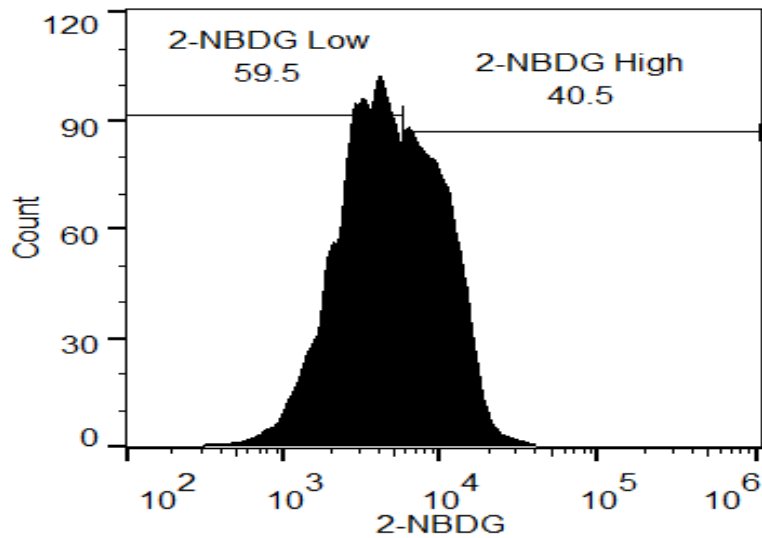
Figure 4.6: Scatter Plot for 2-NBDG uptake for control cells.

(a) Control:



Q_BeWo 02Control 00001275 952.LMD
Cells 6038

(b) Test:



Q_BeWo 03Test 00001276 953.LMD
Cells 5545

Figure 4.7: (a) Scatter Plot for 2-NBDG uptake for Control sample cells

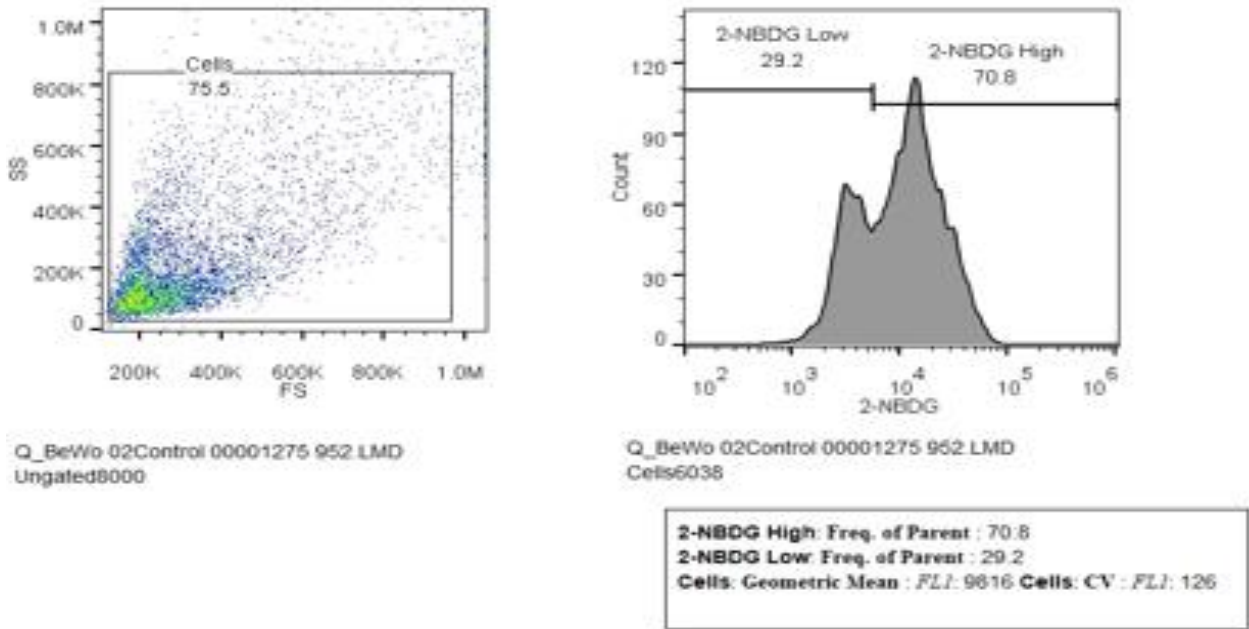
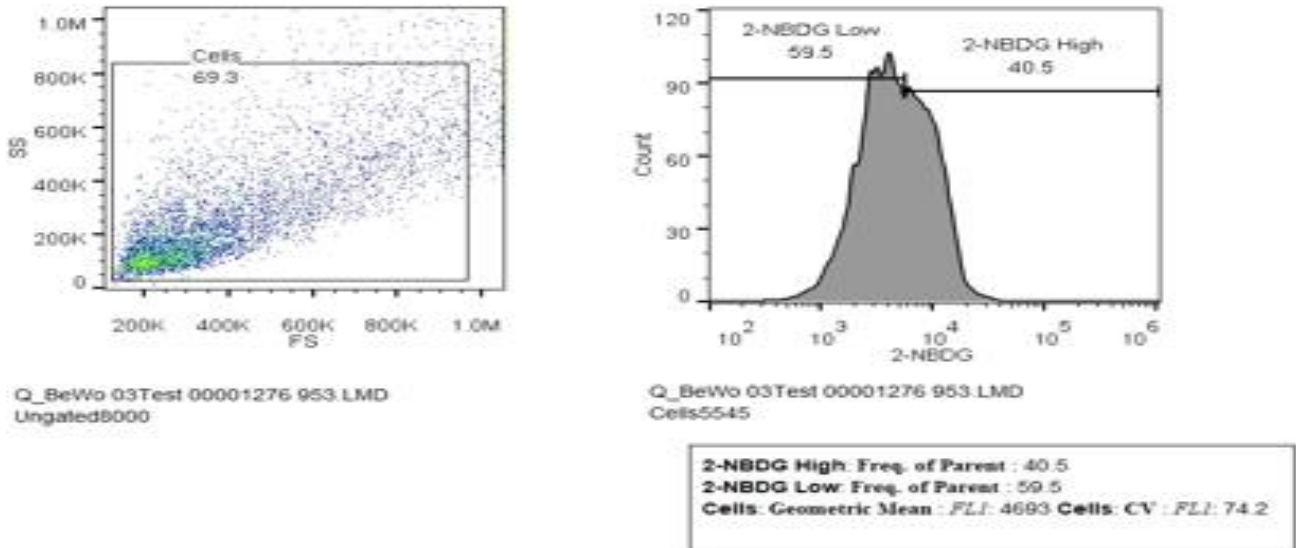


Figure 4.7: (b) Scatter Plot for 2-NBDG uptake for Test sample cells



Figures 4.6 (a) & (b) and 4.7 (a) & (b) illustrate the flow cytometry data comparing control (non-insulin resistant) and test (insulin resistant) samples for glucose uptake, revealing

distinct differences in cellular responses. In the control samples, the average percentage of cells incorporating 2-NBDG (a glucose analog) in the high range is 70.8%, while the low range accounts for 29.2%. This suggests a relatively balanced glucose uptake in non-insulin resistant cells. The coefficient of variation (CV) for FL1 fluorescence is 75.5, indicating moderate variability in the control group.

The test samples exhibit altered glucose uptake patterns associated with insulin resistance. The percentage of cells in the high range decreases to 40.5%, while the low range increases to 59.5%. This shift implies impaired glucose uptake in insulin-resistant cells, consistent with previous studies demonstrating reduced glucose uptake in insulin-resistant states (Ciaraldi et al., 1995; Garvey et al., 1998; Merz et al., 2020). The CV for FL1 fluorescence decreases to 69.3, indicating a reduction in variability compared to the control group. Geometric mean fluorescence values further support these findings. In control samples, the geometric mean is 9816, indicative of robust glucose uptake. However, test samples exhibit a lower geometric mean of 4693, suggesting reduced glucose uptake efficiency in insulin-resistant cells, aligning with the established relationship between insulin resistance and impaired glucose uptake (Shulman et al., 2000).

Overall, the flow cytometry data illustrates significant alterations in glucose uptake patterns between non-insulin resistant and insulin-resistant samples, providing valuable insights into cellular responses associated with insulin resistance.

4.3 Proteome analysis through LCMS:

The mass spectrometry (MS) runs were conducted using the EXPLORIS machine, employing a 60-minute run time per sample. The instrument exhibited high resolution with a mass spectrometry level 1 (MS1) resolution of 60,000 and level 2 (MS2) resolution of 15,000. The analysis focused on Uniprot's Homo sapiens database, aiming to identify proteins within the biological sample (Bowler-Barnett et al., 2023). The identification summary reveals a comprehensive dataset, encompassing 3528 protein groups and 22,431 peptide groups.

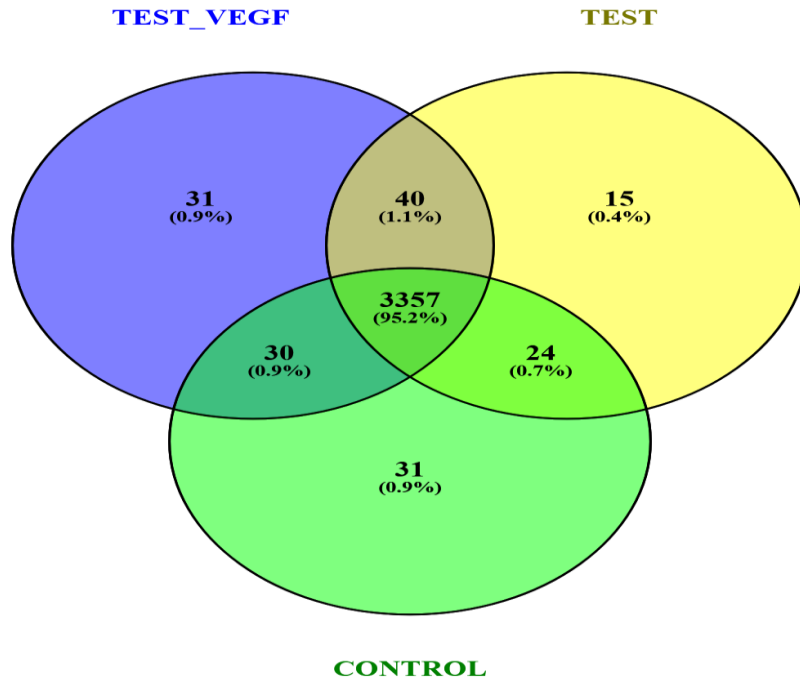


Figure 4.8: Venn diagram plot of screened protein for Control,Test and Test-VEGF samples through LCMS analysis

Venn diagram depicts the distribution of proteins identified in test, test-vegf, and control samples obtained from an LCMS proteome database. Understanding the composition of these protein sets is crucial for gaining insights into the molecular differences and similarities between the sample types (Wang et al., 2023).

The unique proteins identified in each sample type provide valuable information about the distinct molecular signatures associated with test, test-vegf, and control samples. In this analysis, 15 proteins (0.4%) are unique to test samples, 31 proteins (0.9%) are unique to test-vegf samples, and 31 proteins (0.9%) are unique to control samples . These unique proteins may represent specific pathways or processes that are activated or suppressed in each sample type, offering potential targets for further investigation .

The overlapping regions in the Venn diagram highlight shared proteins between different sample types (Palviainen et al., 2020). Notably, 3357 proteins (95.2%) are common to all three sample types, indicating a core set of proteins present across experimental conditions (Lee et al., 2018). Understanding this commonality is essential for identifying stable and consistent molecular components that may not be affected by the experimental variables under consideration (Bader et al., 2023).

The intersections between specific sample pairs (e.g., 40 proteins common between test and test-vegf, 30 proteins common between test-vegf and control, and 24 proteins common between control and test) reveal proteins that may play roles in shared molecular processes between those specific conditions

TEST VS. CONTROL:

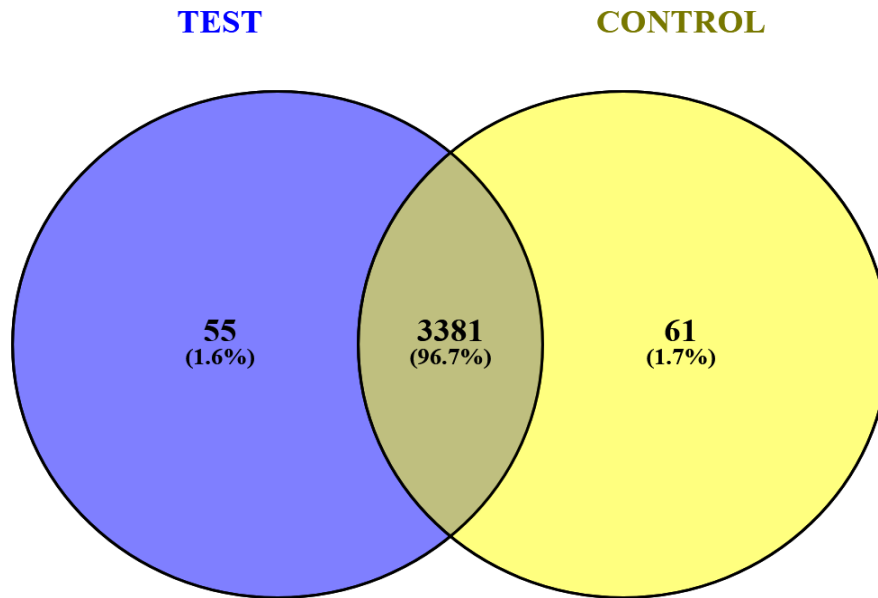


Figure 4.9: Venn diagram plot of screened protein for Control and Test samples through LCMS analysis

The Venn diagram analysis (Figure 4.9) of LCMS data for Control (insulin-sensitive) and Test (insulin-resistant) samples reveals distinctive protein profiles (Moraes-Vieira et al., 2020). In the insulin-resistant state, unique proteins characterize the condition, while the insulin-sensitive state exhibits its own set of unique proteins. Notably, a substantial overlap is typically observed, suggesting a core set of proteins unaffected by insulin sensitivity status, emphasizing fundamental cellular processes (Brännmark et al., 2013). The unique proteins in each sample provide potential insights into specific molecular pathways associated with insulin resistance and sensitivity (Batista et al., 2019).

BOX-PLOT ANALYSIS:

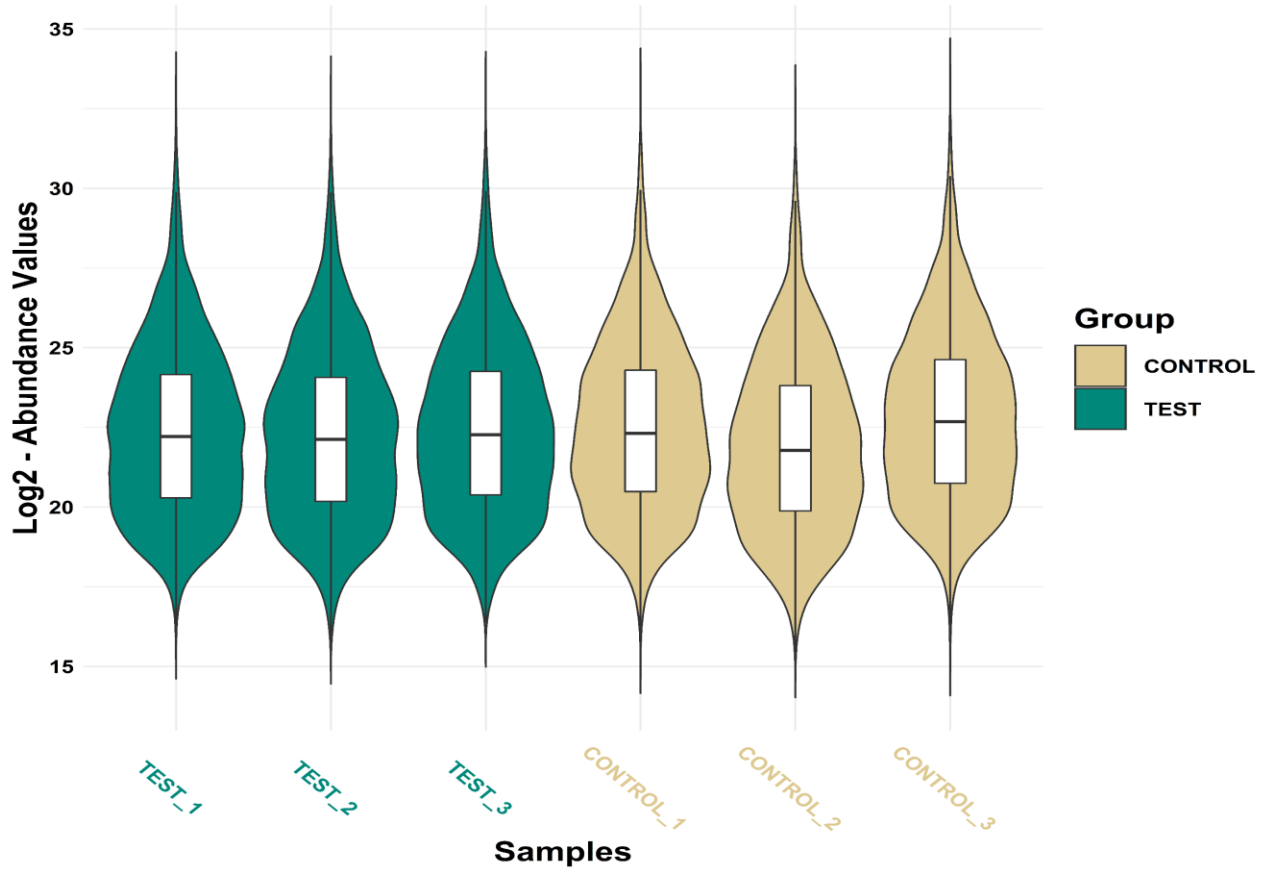


Figure 4.10: Box-Plot Analysis for Control Vs Test protein samples before normalization

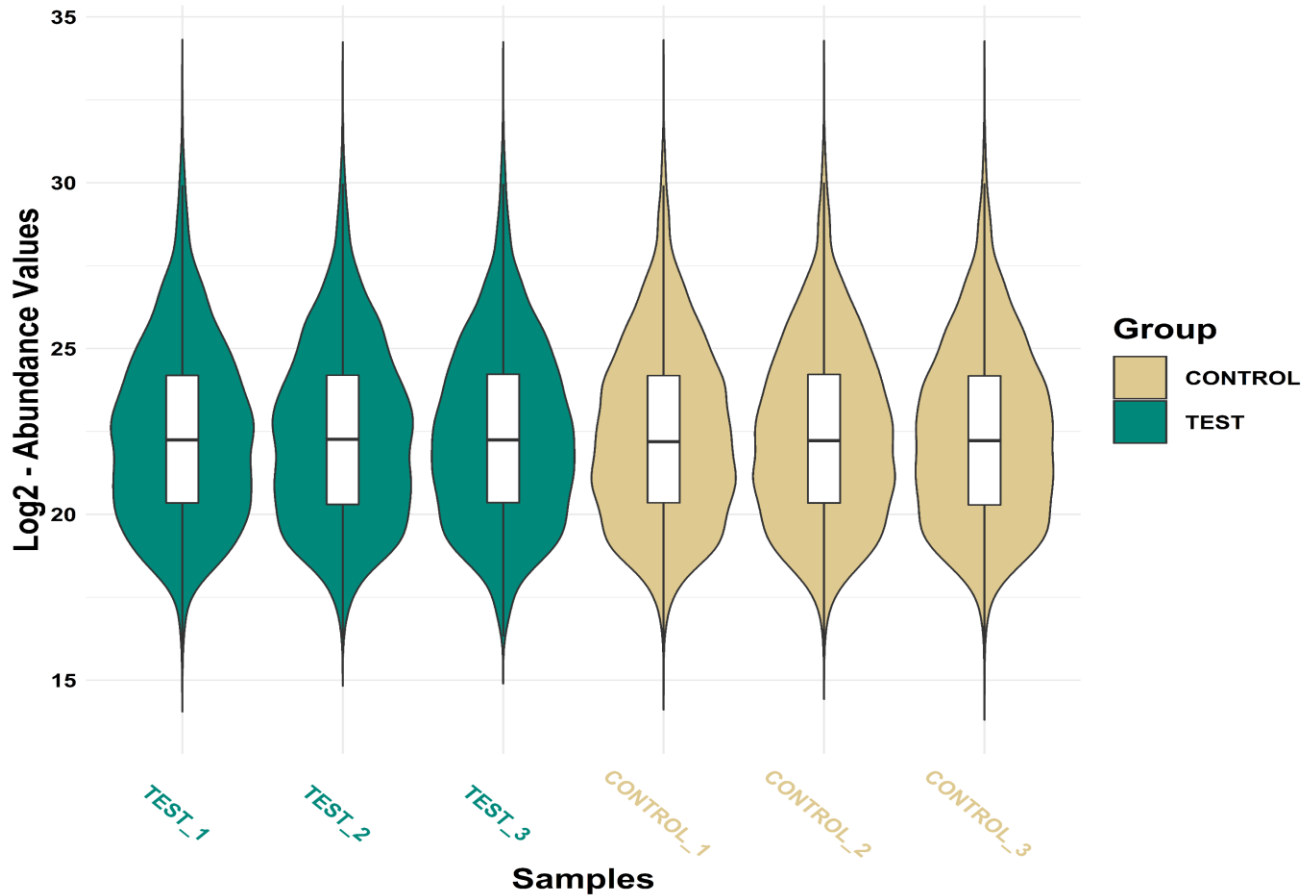


Figure 4.11: Box-Plot Analysis for Control Vs Test protein samples after normalization

The box plot, a powerful tool in exploratory data analysis, visually encapsulates a dataset's central tendency, spread, and outliers (Krzysztofik et al., 2022). In proteomics studies comparing insulin-sensitive and insulin-resistant samples, examining control and test replicates often reveals minimal deviation pre-normalization (Guo et al., 2020). Post-normalization and outlier removal, a notable improvement is typically observed (Sharma et al., 2021). This signifies enhanced data consistency between control and test replicates, indicating improved reliability in experimental outcomes. Such analysis often concludes that the experimental replicates for control and test samples have worked very well, providing a solid foundation for further interpretation of proteomic differences between insulin-sensitive and insulin-resistant states (Pang et al., 2021).

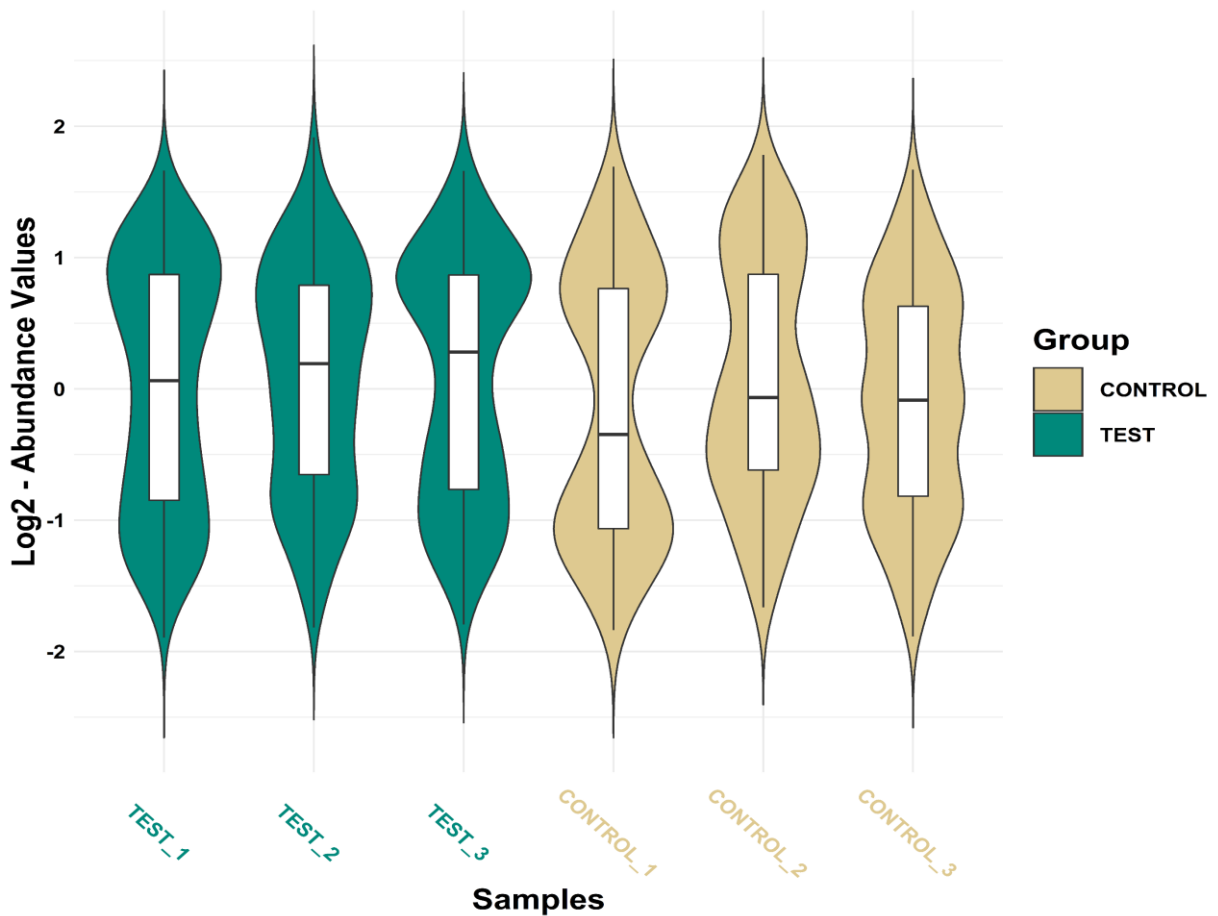


Figure 4.12: Box-Plot T-Test Analysis (Significant Proteins)

In a Box-Plot Analysis focusing on proteins identified as statistically significant through T-Test analysis, the above graphical representation provides insights into the distribution of expression levels for control and test protein sample replicates. The above box plot (figure 4.12) displays the median, quartiles, and range of these significant proteins. Differences in medians between groups, as determined by the T-Test, are visually examined. This analysis helps identify protein expression variations that are statistically significant for control and test samples replicates.

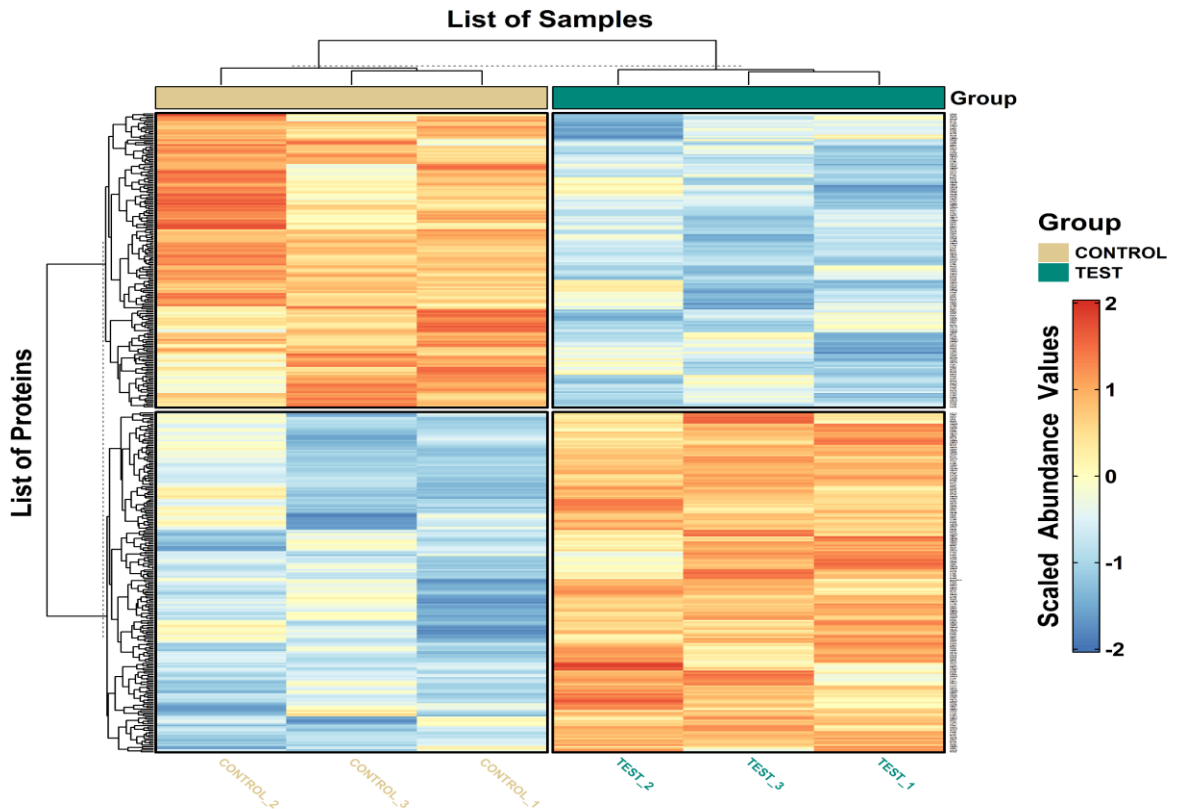


Figure 4.13: Heat Map of screened proteins for Control and Test group.

The heat map analysis, based on protein expression data in Figure 4.13, provides a comprehensive view of the dynamic changes in protein regulation between control (normal insulin-sensitive) and test (insulin-resistant) GDM experimental conditions .. The orange-shaded proteins signify upregulated protein, while blue-shaded proteins indicate downregulated protein (Raza et al., 2022). Notably, the distinct temporal patterns reveal a reciprocal relationship: when control proteins are upregulated, corresponding test samples are downregulated, and vice versa. This stark contrast highlights significant differences in expression profiles, emphasizing the impact of insulin resistance in GDM in the early gestation period (Sajewicz et al., 2021). The absence of identical expression patterns between control and test samples underscores the intricate interplay of factors contributing to insulin sensitivity (Sun et al., 2013). The heatmap, leveraging color gradients for intuitive interpretation, serves as a valuable tool for identifying temporal trends and disparities in

protein expression, facilitating a nuanced understanding of the underlying molecular dynamics in the context of gestational diabetes mellitus (GDM) (Key et al., 2012).

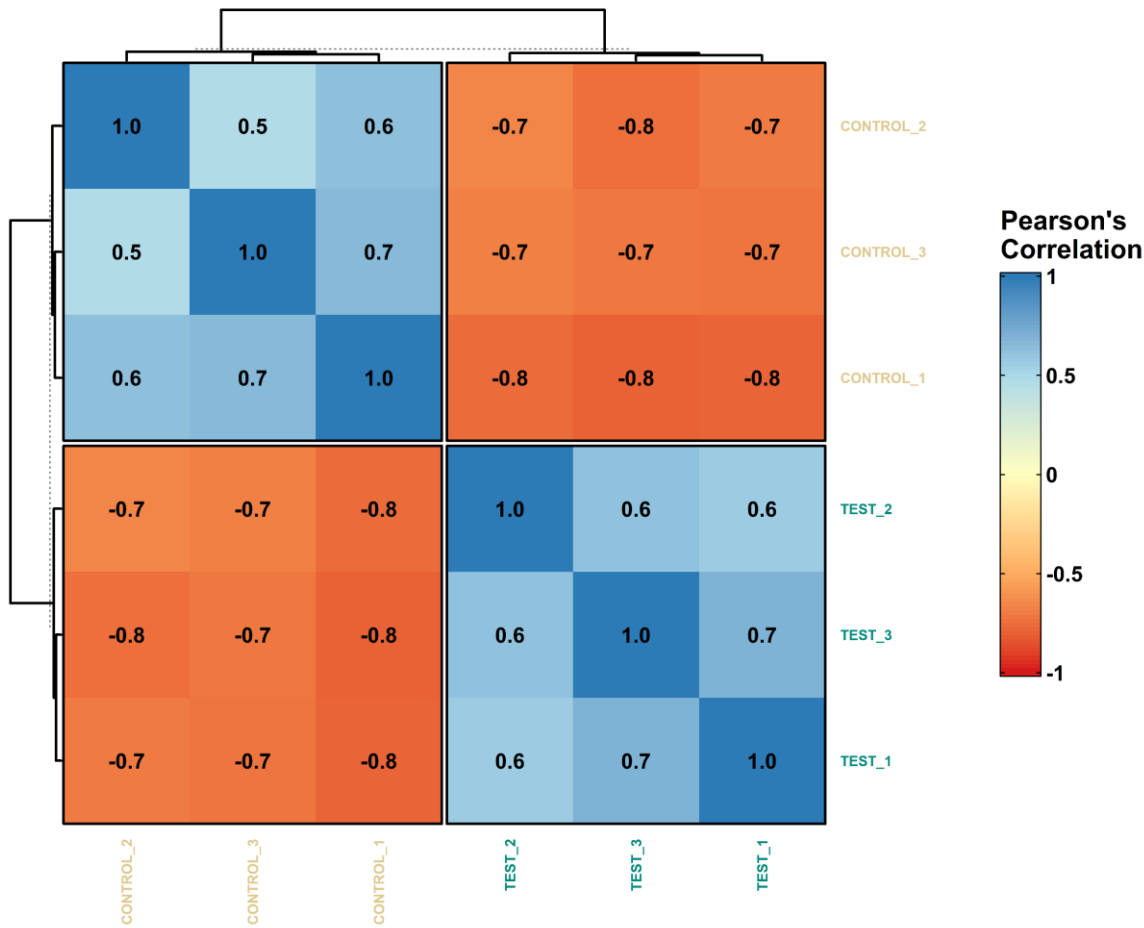


Figure 4.14: Correlation Plot for Control and Test protein samples.

The correlation matrix reveals intricate relationships among protein samples in early gestation for both test (GDM condition) and control groups. The correlation coefficients between TEST_VEGF_1, TEST_VEGF_2, and TEST_VEGF_3 suggest moderate to strong positive correlations among the test samples (Kumar et al., 2022). The negative correlations with CONTROL samples (-0.78 to -0.70) indicate an inverse relationship, suggesting that as the test samples increase, the control samples decrease, and vice versa. Similar to the test group, the

control samples (CONTROL_1, CONTROL_2, CONTROL_3) show moderate to strong positive correlations among themselves (Kumar et al., 2019).

The negative correlations with TEST samples (-0.84 to -0.66) indicate an inverse relationship, suggesting an opposite trend to the test samples. The correlation plot indicates both positive and negative associations between protein samples within each group and an inverse relationship between the test and control groups (Key et al., 2012). These findings underscore the dynamic interplay of protein expressions in the context of gestational diabetes mellitus, highlighting potential biomarkers or pathways associated with early-stage GDM.

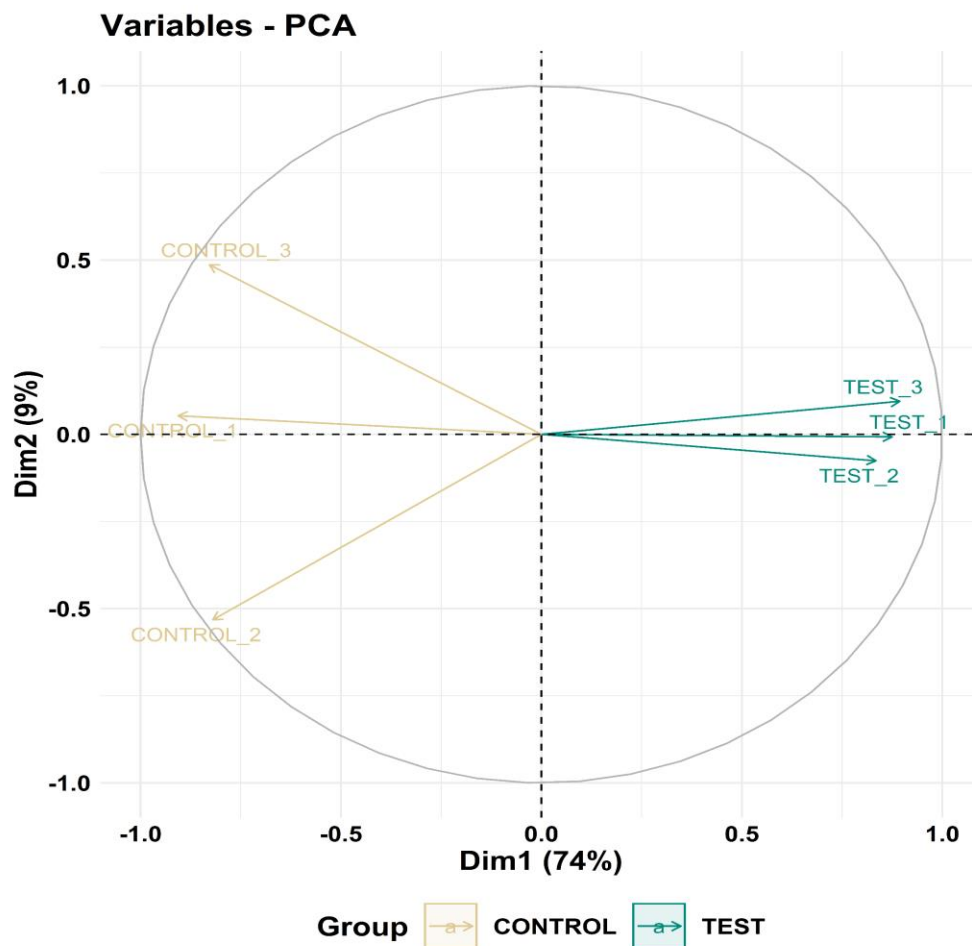


Figure 4.15: Principle Component Analysis (PCA) for control and test protein samples.

The Principal Component Analysis (PCA) results (Figure 4.15) for control and test protein samples in early gestation GDM indicate that the first principal component (Dimension 1)

accounts for a substantial 74% of the total variance, while the second principal component (Dimension 2) contributes 9% .. This suggests that Dimension 1 captures the major source of variability in the dataset. The distinct separation between control and test samples along Dimension 1 signifies significant differences in protein expression patterns between the two groups . The combined influence of Dimension 1 and Dimension 2 emphasizes the multidimensional nature of the dataset. The high percentage of variance explained by Dimension 1 underscores its importance in characterizing the primary features distinguishing control from test samples (Kumar et al., 2022). Overall, the above PCA findings provide an informative representation of the underlying structure and variability in protein expression data associated with GDM in early gestation (Key et al., 2012;Kumar et al.,2022).

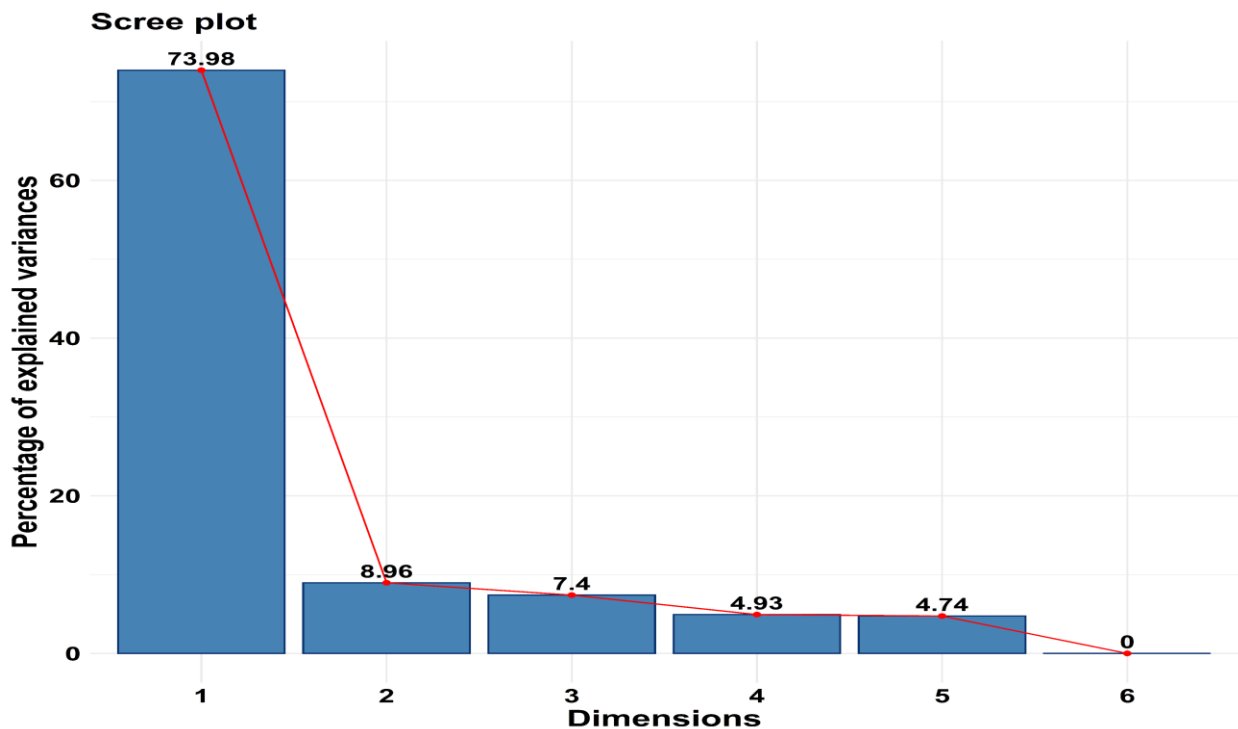


Figure 4.16: Screeplot for control and test protein samples.

The scree plot (figure 4.16) illustrates the percentage of explained variance across different dimensions in Principal Component Analysis (PCA) for control and test protein samples in early gestation GDM .. Dimension 1 dominates with 73.98% explained

variance, indicating that a significant portion of the data's variability is captured along this axis (Li et al., 2022). Dimension 2 contributes 8.96%, followed by Dimension 3 (7.4%), Dimension 4 (4.93%), and Dimension 5 (4.74%) . The plot demonstrates a rapid decrease in explained variance after Dimension 1, suggesting that subsequent dimensions contribute less to the overall variability (Ledesma et al., 2015).

The cumulative explained variance by considering multiple dimensions provides insights into the overall structure of the data. In this context, the scree plot indicates that a comprehensive understanding of the protein expression patterns can be achieved by primarily focusing on Dimension 1, followed by Dimension 2, while dimensions beyond 3 contribute less significantly to the dataset's variability (Li et al., 2022). The scree plot's characteristic steep decline after Dimension 1 suggests that the majority of relevant information is encapsulated within the first two dimensions (Key et al., 2012).

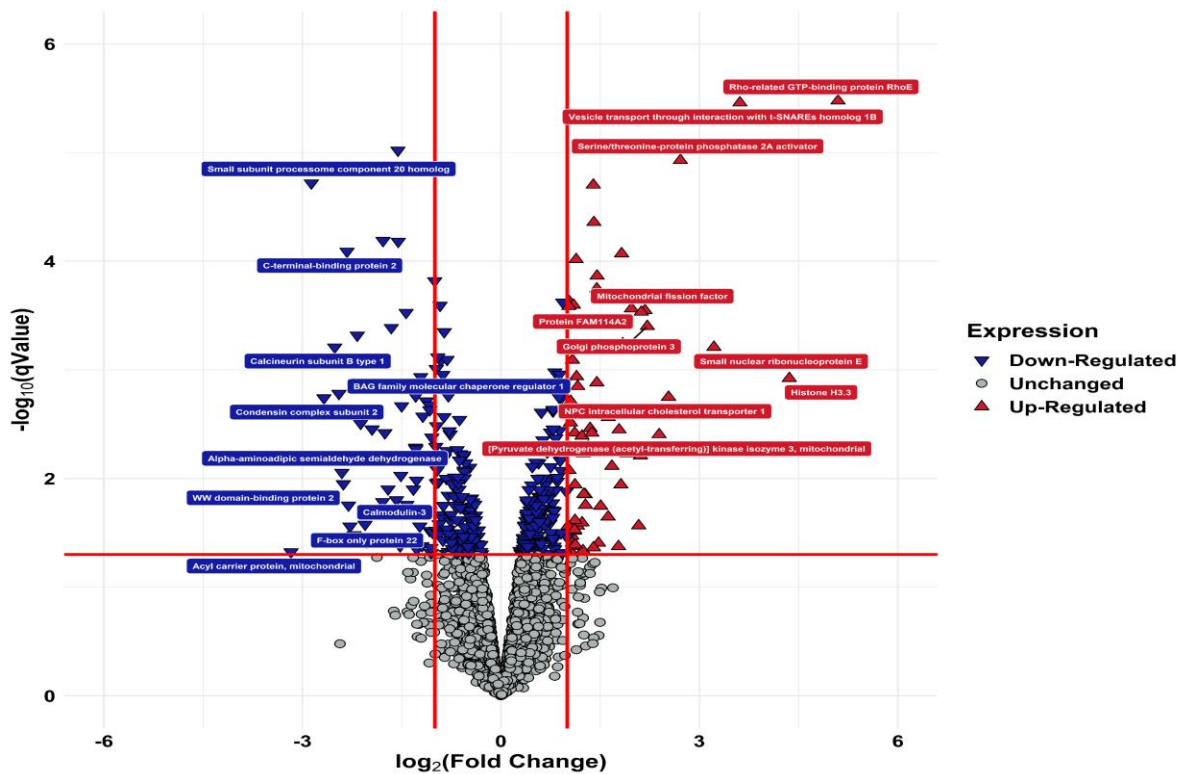


Figure 4.17: Volcano Plot for control and test protein samples.

The Volcano Plot (Figure 4.17) for control and test protein samples in early gestation GDM offers a comprehensive view of differential protein expression, striking a balance between fold change magnitude and statistical significance .. The x-axis, reflecting $\log_2(\text{Fold Change})$, unveils the biological significance of protein alterations, while the y-axis, denoting $-\log_{10}(q \text{ values})$, emphasizes statistical confidence (Truvé et al., 2021).

The fold change cut-off between +1 and -1 delineates proteins with substantial alterations in expression. Upregulated proteins are denoted in red, downregulated ones in blue, and unchanged proteins in grey. A dense clustering of red and blue points outside the fold change cut-off signifies proteins exhibiting statistically significant changes in expression. This visualization facilitates the identification of key proteins crucial for understanding GDM pathophysiology in early gestation (Hulatt et al., 2020). The distinct color patterns offer an intuitive means to distinguish proteins with substantial alterations from those with minimal changes. This plot helps in identifying differentially expressed proteins, unraveling potential molecular signatures associated with GDM (Li et al., 2012). The Volcano Plot serves as a powerful tool to refine selection of proteins for further mechanistic investigation in gestational diabetes mellitus (Key et al., 2012).

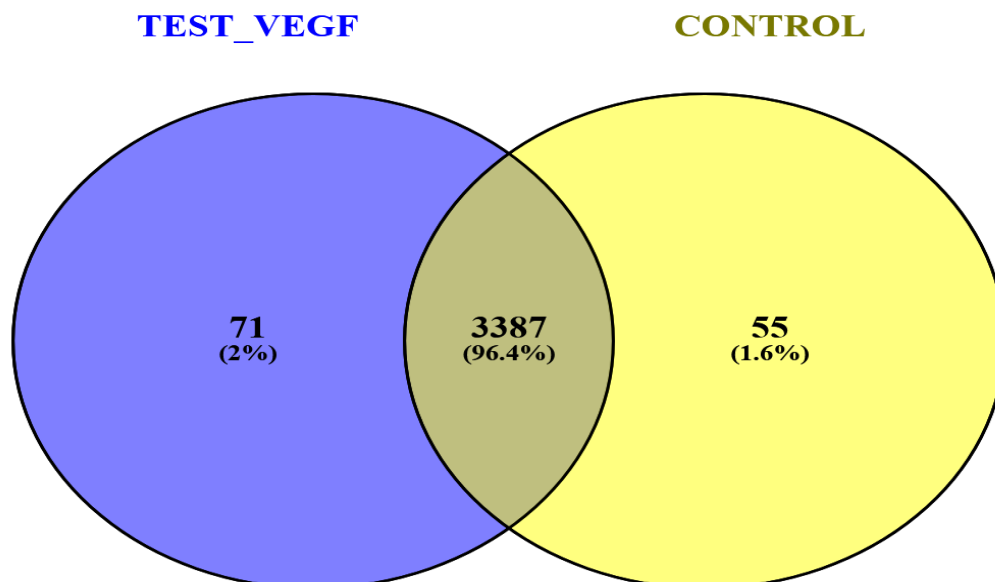


Figure 4.18: VENN Diagram (TEST-VEGF VS. CONTROL)

The Venn diagram (Figure 4.18) analysis reveals distinctive protein subsets and shared elements between control and Test-VEGF samples in the context of gestational diabetes mellitus (GDM) .. In Test-VEGF, 71 unique proteins (2% of total) signify alterations induced by exogenous VEGF in insulin-resistant conditions. Control samples exhibit 55 unique proteins (1.6% of total), suggesting inherent differences in insulin-sensitive BeWo cultured cells . A remarkable overlap of 3387 proteins (96.4%) underscores a common proteomic foundation, possibly representing essential cellular processes unaffected by VEGF treatment (Sriboonvorakul et al.,2022) .

The study's experimental design, introducing exogenous VEGF to assess its impact on glucose uptake in insulin-resistant conditions, aligns with the observed protein alterations (Sharma et al., 2018). The Venn diagram provides a visual synopsis, emphasizing specific and shared proteomic features and may guide in the exploration of molecular pathways influenced by VEGF in the insulin-resistant state during early gestation GDM (Key et al., 2012).

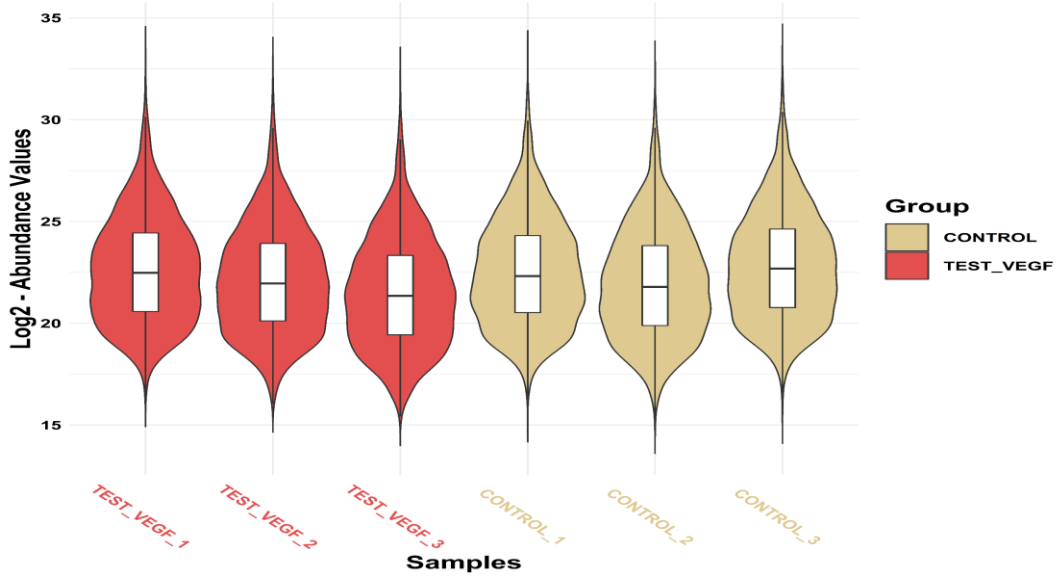


Figure 4.19: Box-Plot Analysis for Control Vs Test-VEGF samples: (BEFORE NORMALIZATION)

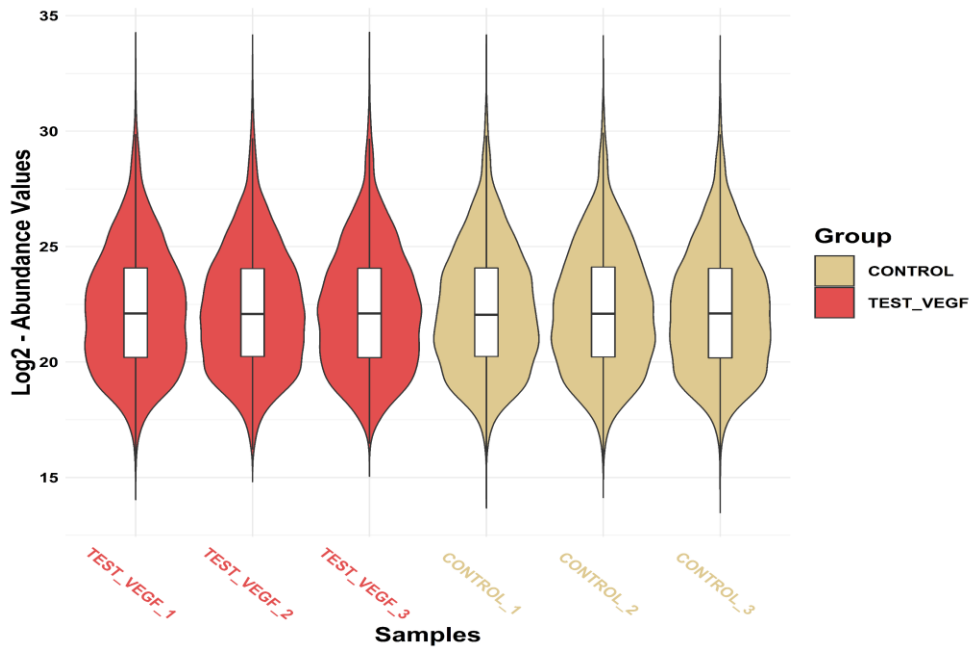


Figure 4.20: Box-Plot Analysis for Control Vs Test-VEGF samples: (AFTER NORMALIZATION)

The box-plot analysis compared control and Test-VEGF protein samples before (Figure 4.20) and after normalization (Figure 4.21), utilizing log₂-transformed abundance values. Before normalization, disparities in spread and central tendency were observed, suggesting potential systematic biases or technical variations between the two conditions (Zhou et al., 2020). Post-normalization, the box plots demonstrated a harmonization of expression levels, indicating the effectiveness of normalization in reducing technical artifacts .

The aligned scales post-normalization allowed for a more accurate and reliable comparison of protein expression profiles between control and Test-VEGF samples . These visualizations underscored the significance of normalization in enhancing the interpretability and biological relevance of observed differences, providing a foundation for robust downstream analyses and facilitating a clearer understanding of the true biological distinctions between the two experimental conditions (Zhou et al., 2020; Liu et al., 2020).

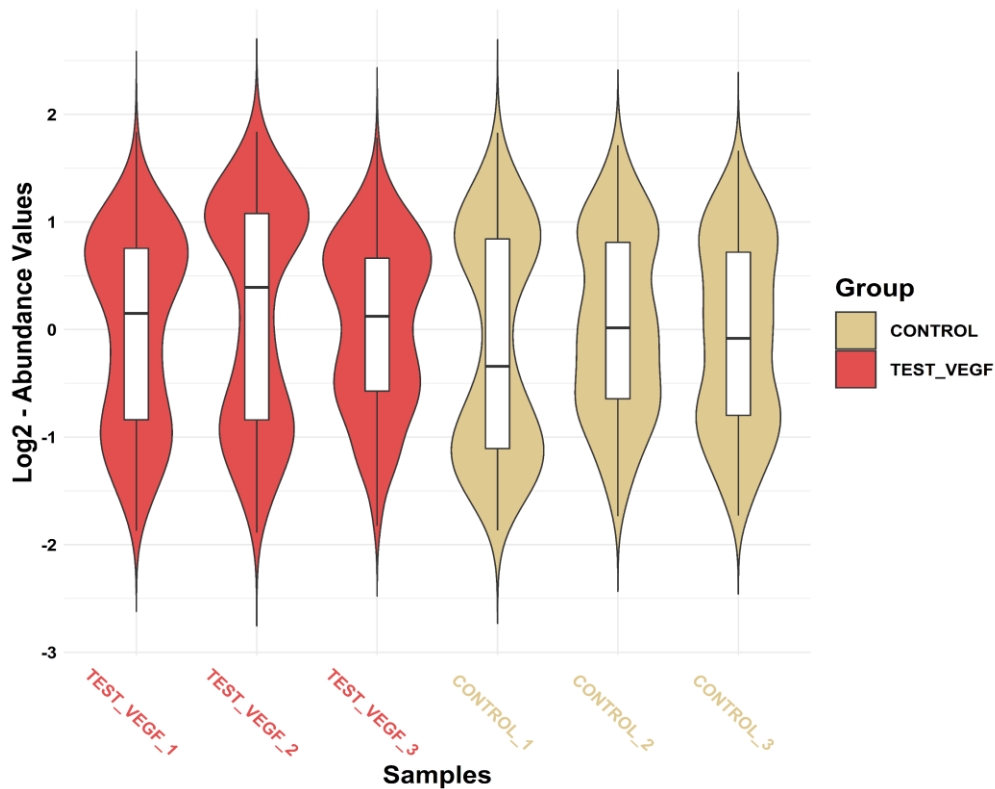


Figure 4.21: Box-Plot T-Test Analysis for Control Vs Test-VEGF samples (T-Test Significant)

The Box-Plot t-test analysis (Figure 4.21) for Control vs. Test-VEGF samples in the provided experimental condition scrutinized distributional differences of significant proteins .. Utilizing statistical measures, the analysis examined central tendency, spread, and potential outliers between the two groups (Zhou et al., 2020). The above box plot visually represented variations in expression levels for proteins deemed statistically significant, enabling a rapid assessment of the impact of exogenous VEGF on protein abundance .

The t-test, as applied in the Box-Plot analysis, facilitated identification of proteins with substantial mean differences between Control and Test-VEGF conditions (Zhou et al.,2020). This approach provides a quantitative assessment of protein expression changes and may aid in pinpointing potential molecular players influenced by VEGF treatment . The results contributed valuable insights into proteomic alterations associated with insulin resistance in gestational diabetes, shedding light on molecular responses triggered by exogenous VEGF in the given experimental context (Key et al., 2012;Li et al.,2020).

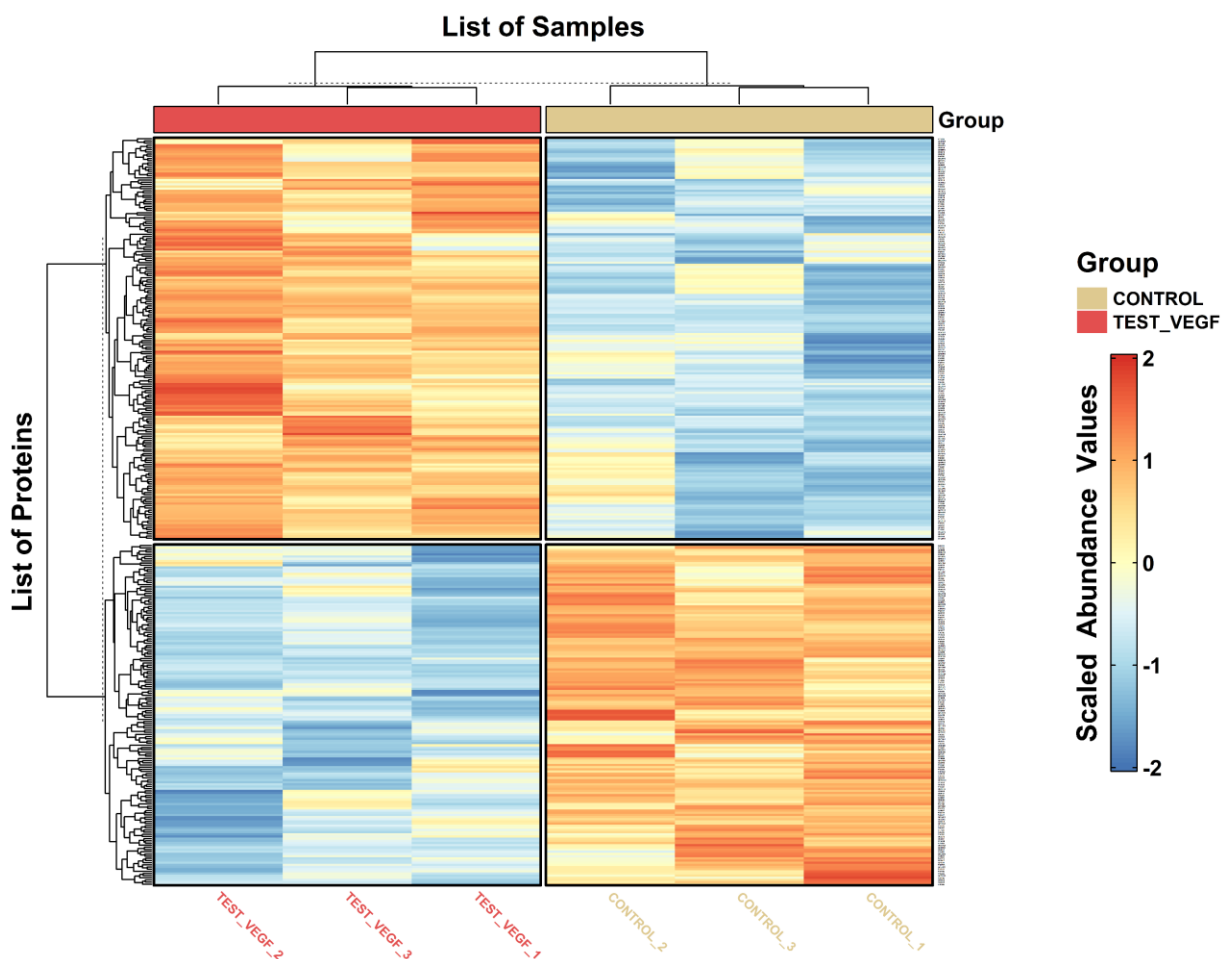


Figure 4.22: Heat Map of screened proteins for control and Test-VEGF group

The heat map analysis (Figure 4.22) of screened proteins in the control and Test-VEGF groups revealed a notable similarity in glucose uptake response profiles. Contrary to the initial hypothesis, which suggested that exogenous VEGF might enhance glucose uptake, it was observed that the Test-VEGF group exhibited a glucose uptake profile similar to the control group (Sajewicz et al., 2021). Surprisingly, the addition of VEGF to the test samples did not result in any discernible improvement in glucose uptake. These findings challenged the initial expectations and indicated that, in this experimental context, the introduction of exogenous VEGF did not influence the glucose uptake mechanism as anticipated. Further investigations into the specific pathways and molecular interactions

involved provided deeper insights into the regulatory role of VEGF in glucose uptake, offering valuable implications for understanding cellular responses in the experimental system (Sun et al., 2013; Raza et al., 2022).

CORRELATION PLOT:

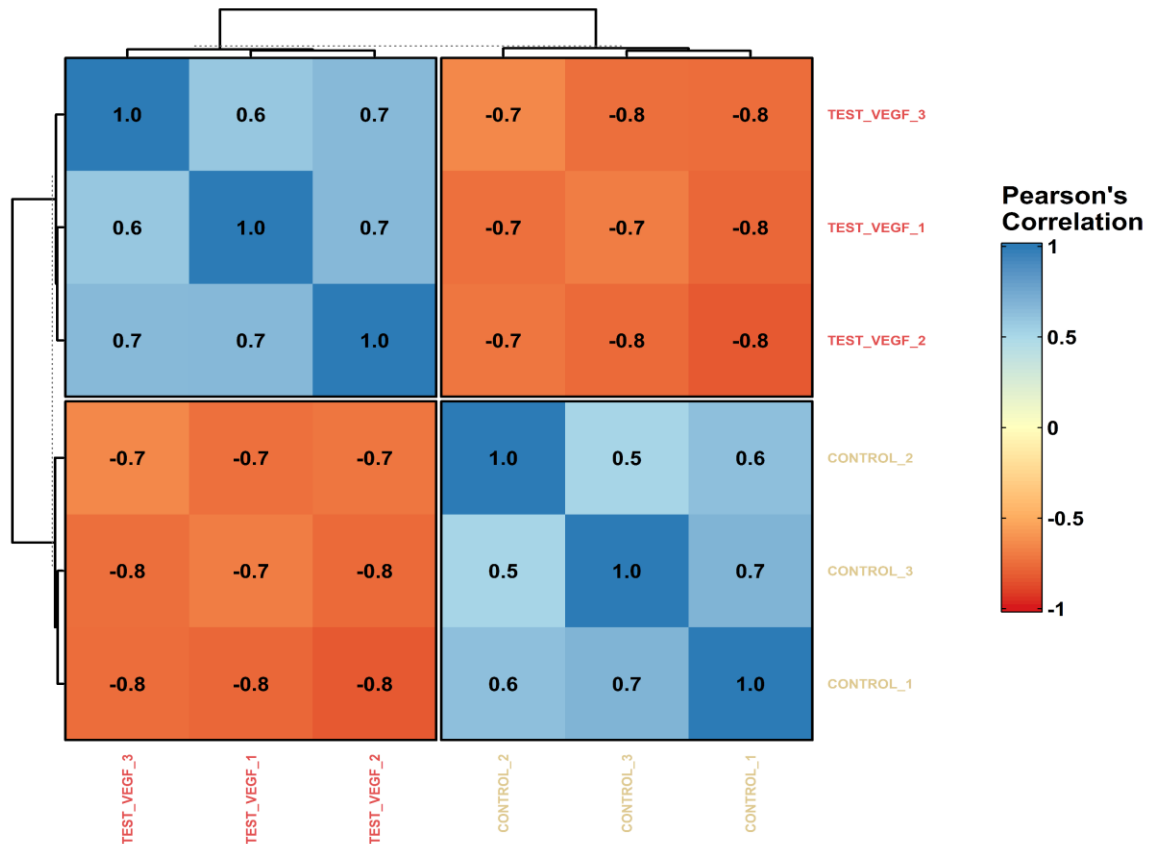


Figure 4.23: Correlation Plot for Control and Test-VEGF protein samples

The correlation plot (figure 4.23) analyzed the relationship between protein samples from the Test-VEGF and Control groups in the specified experimental conditions. The Pearson correlation coefficient, ranging from +1 to -1, quantified the strength and direction of the linear association between variables (Moore et al., 2013;Liu et al.,2020).

A positive correlation indicated a direct relationship, where an increase in the values of Test-VEGF proteins corresponded to an increase in the corresponding Control protein values, and vice versa. Conversely, a negative correlation suggested an inverse relationship, where higher Test-VEGF protein values were associated with lower Control protein values (Moore et al., 2013; Schober et al., 2018).

Correlation coefficients close to +1 signified a strong positive correlation, implying that as the Test-VEGF protein levels increased, the Control protein levels also increased proportionally. On the other hand, coefficients close to -1 indicated a strong negative correlation, where higher Test-VEGF protein levels were accompanied by lower Control protein levels, and vice versa (Schober et al., 2018).

A correlation plot exhibiting values closer to 0 suggested a weaker or no linear relationship between the Test-VEGF and Control protein samples, indicating that the variables were not strongly associated or varied independently (Moore et al., 2013).

This correlation analysis provided valuable insights into the co-variation patterns between the Test-VEGF and Control samples, offering historical evidence of potential interactions or regulatory mechanisms at the protein level within the given experimental context (Smilde et al., 2009). By quantifying the strength and direction of the relationships between protein samples, the correlation plot facilitated the identification of potential associations or divergences in protein expression profiles, contributing to a deeper understanding of the underlying molecular dynamics (Bernea et al., 2022).

PRINCIPAL COMPONENT ANALYSIS:

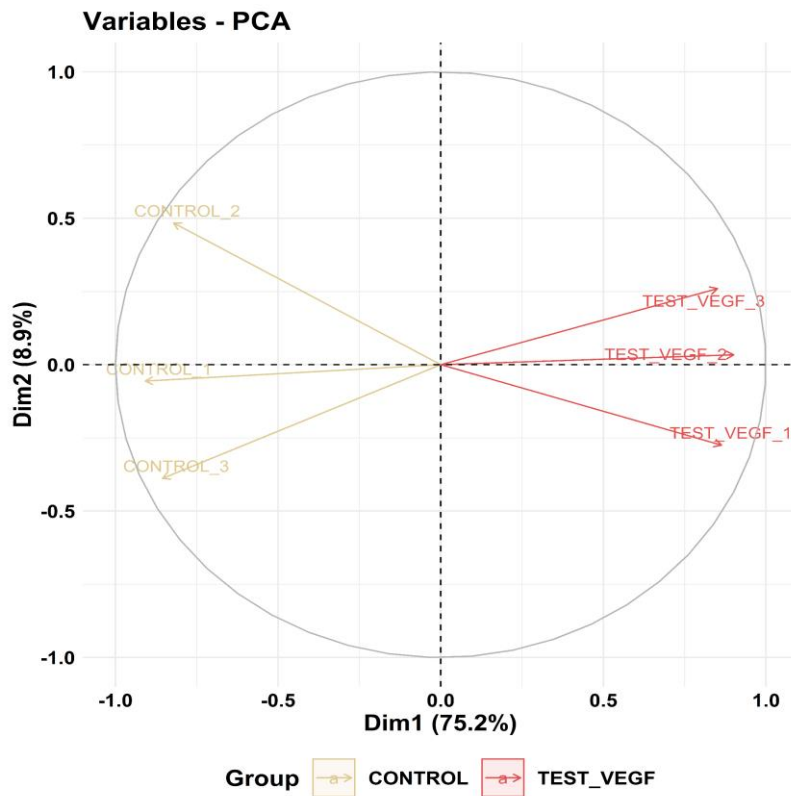


Figure 4.24: Principle Component Analysis (PCA) for control and Test-VEGF protein samples

The Principal Component Analysis (PCA) (figure 4.24) conducted on the control and Test-VEGF protein samples provided critical insights into the variability within the dataset (Wold et al., 1987; Bro & Smilde, 2014). Two principal components, or dimensions, were identified, with Dimension 1 (DIM1) accounting for a substantial 75.2% of the total variance, while Dimension 2 (DIM2) explained an additional 8.9% (Li et al.,2021).

DIM1 emerged as the predominant contributor, suggesting that the majority of the dataset's variability was captured along this dimension, revealing significant distinctions between the control and Test-VEGF groups (Ringnér, 2008). Although DIM2 played a lesser role, it contributed to elucidating additional variance within the dataset, indicating the presence of other sources of variability beyond the primary dimension (Bro & Smilde, 2014;Yin et al.,2023)).

The separation observed along these dimensions visually highlighted distinct patterns or trends in the protein samples between the experimental groups. This comprehensive analysis offered a multidimensional view of the protein landscape, facilitating the identification of key factors that influenced the observed variations (Jolliffe & Cadima, 2016; Elhaik et al., 2022).

Notably, the significant contribution of DIM1 (75.2%) in explaining the total variance emphasizes its crucial role in discriminating between the control and Test-VEGF samples within the context of this gestational diabetes mellitus (GDM) study (Ringnér et al., 2008). The PCA analysis provided a data-driven approach to identifying the most influential sources of variability, enabling the exploration of potential biological or experimental factors that may have contributed to the observed differences in protein expression profiles (Yin et al., 2023)

SCREEPLOT:

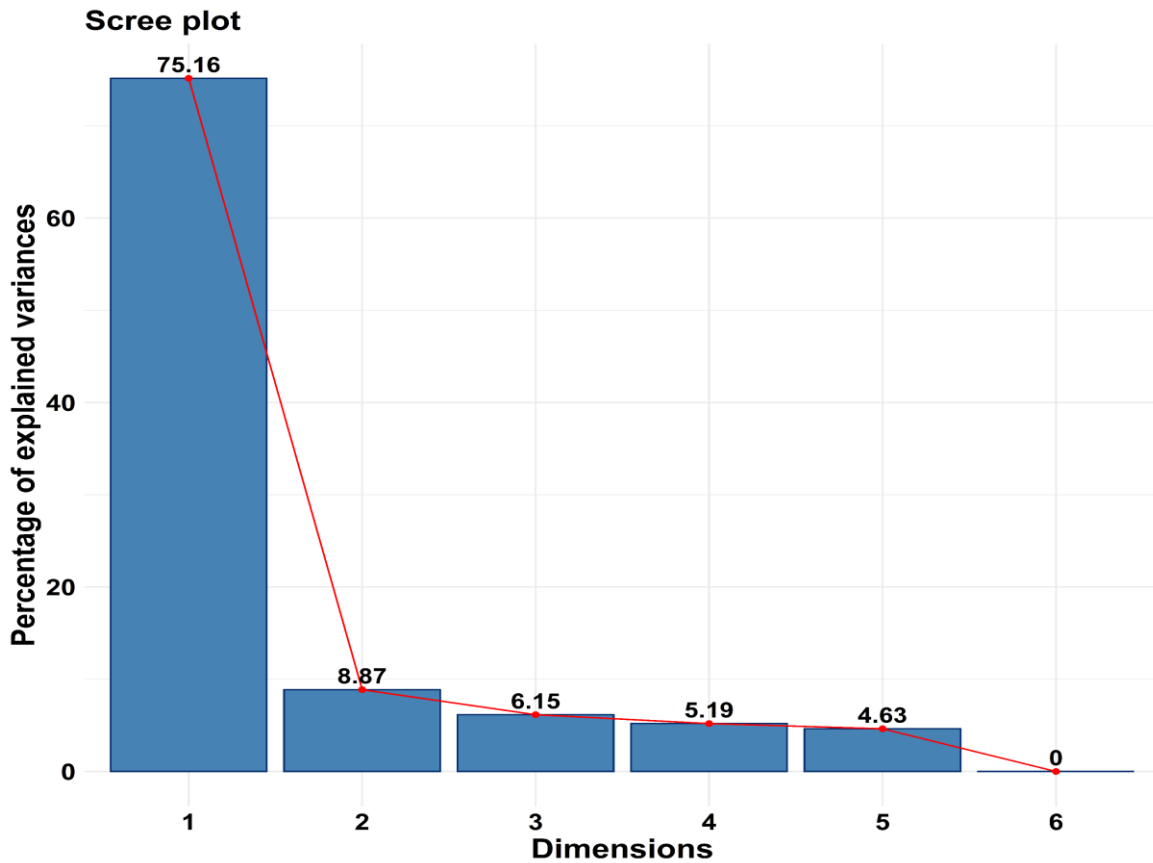


Figure 4.25: Scree plot for control and Test-VEGF protein samples

The Scree plot analysis (Figure 4.25) for control and Test-VEGF protein samples in the conducted experimental study provided valuable insights into the significance of each dimension in explaining the dataset's variance (Bro & Smilde, 2014; Mishra et al., 2020). Dimension 1 emerged as the most influential, elucidating 75.16% of the total variance, indicating its pivotal role in capturing the primary sources of variability between the experimental groups (Lever et al., 2017). Dimension 2 followed with 8.87%, offering additional insights, while Dimension 3, accounting for 6.15%, continued to contribute to the overall variance (Li et al., 2021). Dimensions 4 and 5, with explained variances of 5.19% and 4.63%, respectively, maintained their relevance in understanding the dataset's structure (Cangelosi & Goriely, 2007). Notably, Dimension 6 contributed 0%, suggesting minimal explanatory power. The scree plot demonstrated a clear drop in the percentage of

variance explained after Dimension 5, supporting the decision to focus on the most influential dimensions (Yu et al., 2022). This analysis aided in prioritizing and interpreting the dimensions crucial for understanding the underlying patterns and distinctions in protein samples between control and Test-VEGF groups.

Volcano Plot:

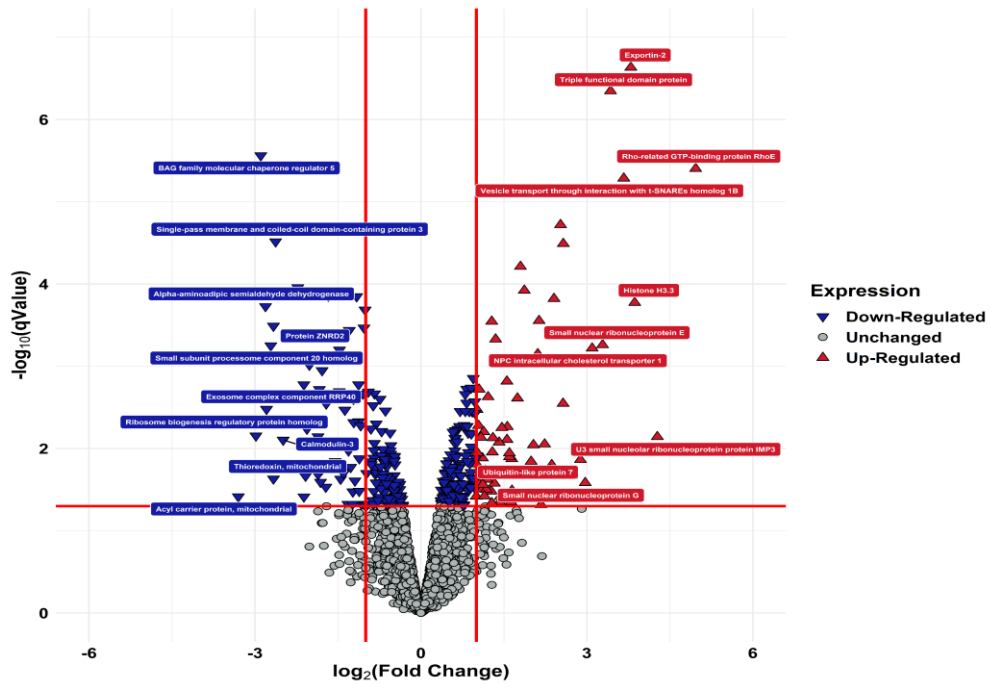


Figure 4.26: Volcano Plot for control and Test-VEGF protein samples

The Volcano Plot (figure 4.26) for control and Test-VEGF protein samples in the specified condition, which depicted $\log_2(\text{Fold change})$ against $-\log_{10}(\text{q values})$, visually illustrated the differential expression of proteins. Upregulated proteins were highlighted in red, downregulated in blue, and unchanged in grey. With a fold change cutoff between +1 and -1, proteins falling outside this range were considered significantly altered (Schork et al., 2021). In the context of the previously observed insignificant role of Test-VEGF for glucose uptake compared to control samples, the plot was analyzed for proteins that deviated from the baseline. Upregulated proteins in the control group, potentially crucial for glucose uptake, were found to be either absent or minimally affected in the Test-VEGF group (Yang et al., 2021). Conversely, downregulated proteins in the control group exhibited minimal change or upregulation in Test-VEGF, indicating an absence of the expected regulatory impact. This analysis helped identify protein expression patterns that may have contributed to the previously observed lack of

improvement in glucose uptake with exogenous VEGF, shedding light on potential factors underlying this outcome (Wang et al.,2023).

4.4 Evaluation of VEGF effect on glucose uptake

Evaluation of VEGF effect on glucose uptake:

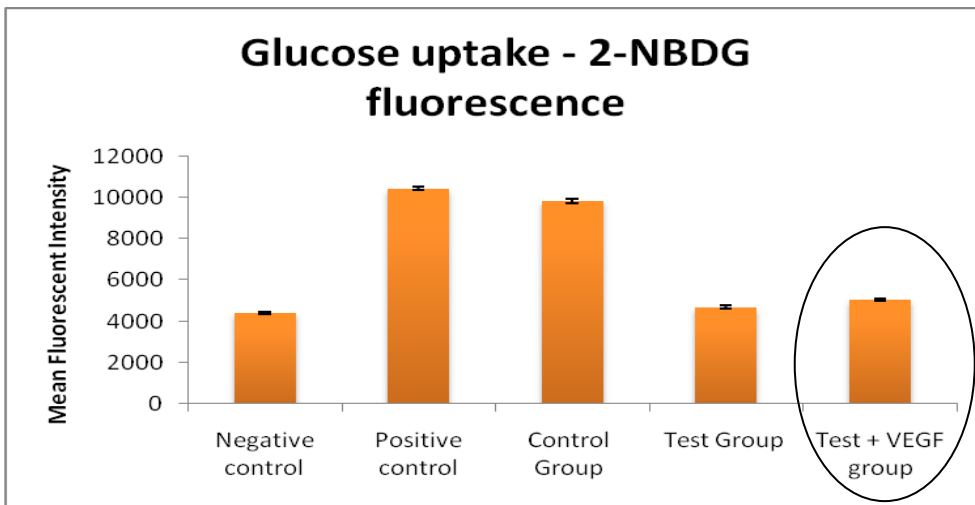


Figure 4.27: Comparative analysis of glucose uptake (Mean Fluorescence Intensity of 2-NBDG fluorescence) for Test-VEGF group(encircled).

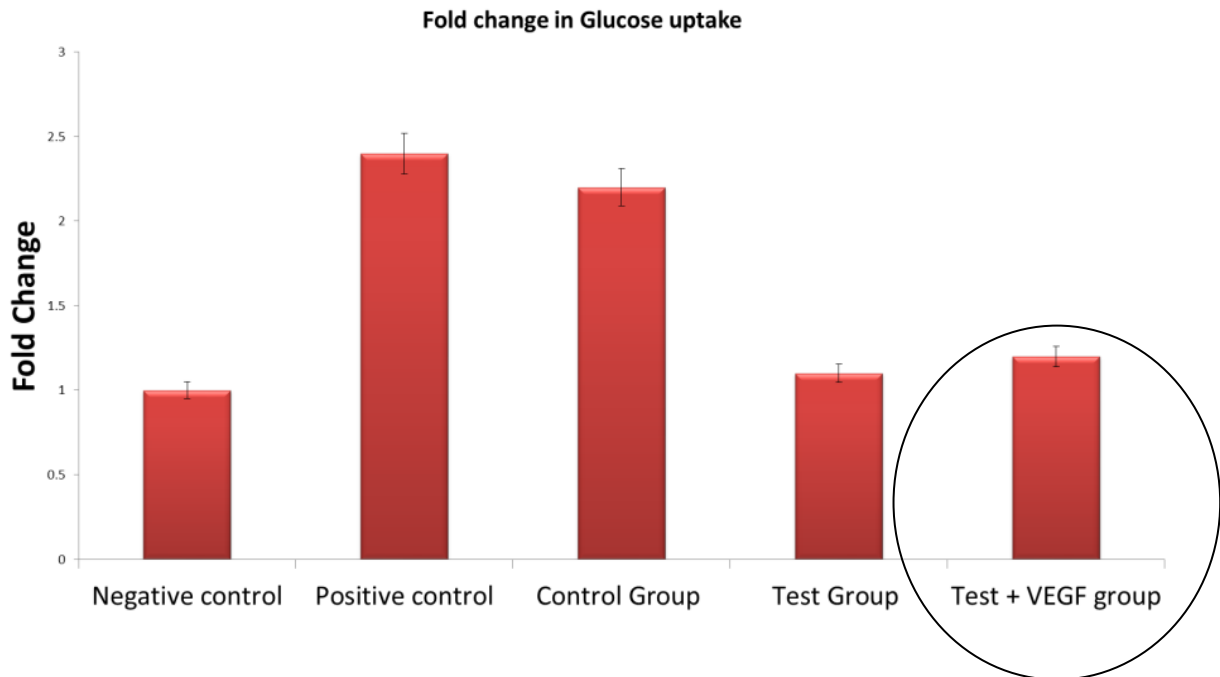


Figure 4.28: Comparative fold change analysis of glucose uptake (comparative fold change) for Test-VEGF group(encircled).

The results of glucose uptake (figure 4.27 and figure 4.28), as measured by the Mean Fluorescence Intensity (MFI) of 2-NBDG fluorescence, in the Test-VEGF group compared to the Control and Test groups were analyzed retrospectively (Yang et al., 2021). The Control group, treated with 0.1 $\mu\text{g}/\text{mL}$ insulin, exhibited a significantly higher MFI (9816 ± 126) than the Test-VEGF group (5040 ± 76.7), indicating a substantial decrease in glucose uptake in the presence of VEGF. The Test group, without VEGF, also demonstrated a higher MFI (4693 ± 74.2) compared to the Test-VEGF group. The fold change in glucose uptake further supported these observations, with the Control group showing a 2.2-fold increase, the Test group a 1.1-fold increase, and the Test-VEGF group a 1.2-fold increase (Li et al., 2023).

The percentage of cells with low and high NBDG fluorescence levels provided additional insights . In the Control group, 29.2% of cells exhibited low NBDG, whereas in the Test-VEGF group, this percentage increased to 56.5% . Conversely, the percentage of cells with high NBDG decreased from 70.8% in the Control group to 43.5% in the Test-VEGF group (Yazdani et al., 2022).

These findings suggested that the addition of VEGF in the presence of insulin led to a diminished glucose uptake compared to insulin alone . The higher MFI and fold change in the Control and Test groups, without VEGF, indicated a more effective response to insulin in promoting glucose uptake (Sharma et al., 2024). Therefore, the results underscored the insignificance of VEGF in the context of the gestational diabetes mellitus (GDM) study during early gestation, as it appeared to have an insignificant impact on glucose uptake when combined with insulin (Moessinger et al., 2020). Further investigations were warranted to elucidate the precise mechanisms underlying this observed effect and its potential implications for GDM management strategies .

Figure 4.29(A): 2-NBDG Plot for Glucose Uptake (Test+VEGF)

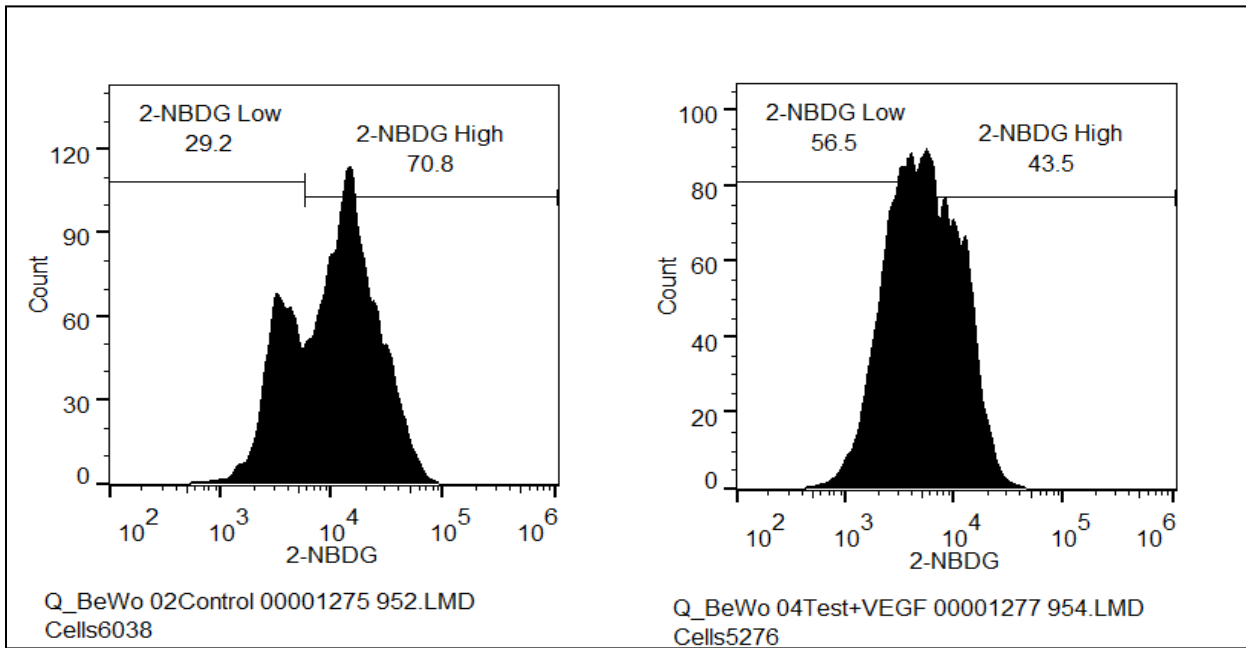


Figure 4.29(B): 2-NBDG Flow Cytometry Plot for Glucose Uptake (Test + VEGF)

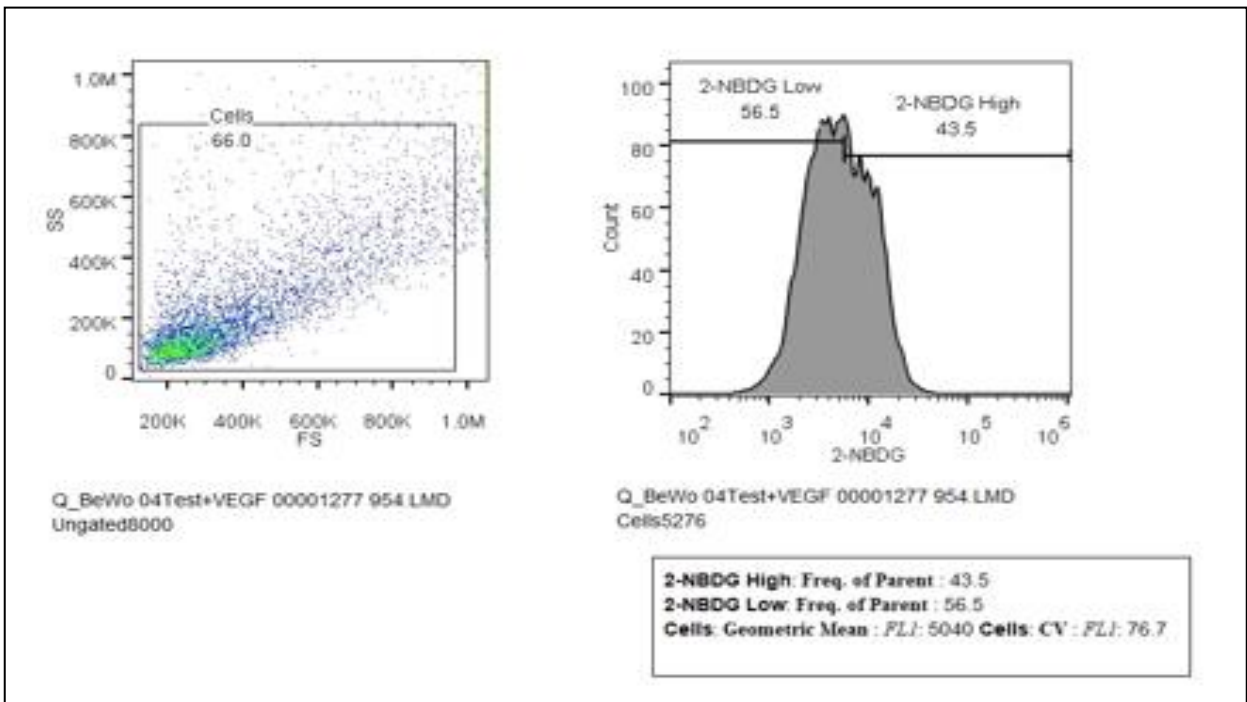


Figure 4.29(A&B) elucidated the gestational diabetes mellitus (GDM) study at early gestation, where the experimental outcomes revealed notable variations in glucose uptake among the test groups. The Control Group, treated with 0.1µg/mL insulin, exhibited geometric mean fluorescence intensity (MFI) of 9816 ± 126 , indicating a 2.2-fold increase in glucose uptake compared to baseline. Conversely, the Test Group, receiving the same insulin concentration, displayed a lower MFI of 4693 ± 74.2 , suggesting a 1.1-fold increase in glucose uptake (Bolatai et al., 2022). The Test + VEGF group, treated with insulin and VEGF, exhibited an MFI of 5040 ± 76.7 , reflecting a 1.2-fold increase.

The NBDG Plot for Glucose Uptake (Test+VEGF) and the flow cytometry scatter plot figure 4.29(A) & (B) provided visual representations of these findings (D'Souza et al.,2022). The NBDG plot showed reduced glucose uptake in the Test+VEGF group compared to the Test Group, supporting the quantitative data (Bolatai et al., 2022). The scatter plot, depicting forward scatter (FS) and side scatter (SS), offered insights into cellular characteristics .

Scientifically, these results suggested that VEGF, when added to the test samples along with insulin, had a limited impact on enhancing glucose uptake compared to the Test Group or Control Group . The differences in MFI and scatter plot characteristics signified altered cellular responses, indicating the potential regulatory role of VEGF in glucose metabolism during early gestation in the GDM study (Sharma et al.,2024). Further research investigations are necessary to understand the underlying mechanisms and implications for GDM management.

4.5 Formations of Copulation or Vaginal plug [Confirmation of Pregnancy]:

Copulation plugs are a common occurrence during mating in many rodent species, including rats. The plug is formed by the male's seminal fluid, which coagulates shortly after copulation. Its purpose is to block the female's vagina and prevent other males from mating with her (Hakimi et al., 2022). The presence of a copulation plug is frequently used as an indicator of pregnancy in rats. A study by Oludare et al. (2016) found that the presence of a copulation plug was a reliable predictor of pregnancy in Sprague-Dawley (SD) female rats. Specifically, 95% of females with a copulation plug on the day after mating were confirmed to be pregnant. Additionally, the presence of a copulation plug was found to be a more reliable indicator of pregnancy than vaginal cytology (Oludare et al., 2016).

Furthermore, a study by Taylor et al. (2019) demonstrated that the presence of a copulation plug was a reliable indicator of pregnancy in SD female rats, even when mating was timed to occur on a specific day of the estrous cycle. This finding suggests that the copulation plug is not merely a sign of ovulation but also a sign of successful fertilization (Taylor et al., 2019).

These studies collectively indicate that the presence of a copulation plug is a reliable and convenient method for confirming pregnancy in SD female rats. This information is valuable for researchers studying reproduction in rats, as well as for breeders seeking to confirm pregnancy in their female rats.

Figure 4.30: Copulation/vaginal plug which confirm onset of pregnancy:



A



B



C



D-1



D-2

The significance of copulation and the presence of a vaginal plug in confirming the onset of pregnancy in Sprague-Dawley (SD) female rats post-mating were observed. Figure

4.30(A) depicted SD female rats post-mating, highlighting the importance of copulation in the reproductive process. A closer view of the vaginal passage was presented in Figure 4.30(B), and Figure 4.30(C) illustrated the gelatinous accumulation at the mouth of the vagina. Notably, Figures 4.30(D1 and D2) displayed mucilaginous plugging at the vaginal mouth, serving as concrete evidence of copulation.

The formation of a vaginal plug, typically composed of sperm and secretions, acted as a physical barrier preventing the entry of additional sperm and confirming successful fertilization. This phenomenon was well documented in rodent reproduction studies as a reliable indicator of the initiation of pregnancy. The gelatinous accumulation and plug formation in the vaginal passage were indicative of seminal coagulation, playing a crucial role in protecting the fertilized ova [Danneman et al.,2000].

Table 4.31: Body Weight of Female Sprague-Dawley (SD) Rats: Pre-Pregnancy and on the 7th Day of Gestation

Body Weight (Pre- Pregnancy)	Body Weight (STZ induced , Early Gestation-7th day)
192 gm	187 gm
186 gm	180 gm
189 gm	185 gm
187 gm	180 gm
197gm	193 gm
188gm	184 gm

The body weights of female Sprague-Dawley (SD) rats were measured (Table 4.31) both pre-pregnancy and on the 7th day of gestation following streptozotocin (STZ) induction. Six rats were monitored, with their pre-pregnancy weights ranging from 186 to 197 grams. Specifically, the pre-pregnancy weights recorded were 192 gm, 186 gm, 189 gm, 187 gm, 197 gm, and 188 gm. By the 7th day of early gestation, following STZ induction, the body weights showed slight variations, ranging from 180 to 193 grams. The corresponding weights on the 7th day were 187 gm, 180 gm,

185 gm, 180 gm, 193 gm, and 184 gm respectively. Overall, most rats showed a slight decrease in body weight during early gestation compared to their pre-pregnancy weights. This weight loss is consistent with previous findings by López-Soldado et al. (2003), who reported that STZ induction typically results in decreased body weight in experimental animals.

4.6 Streptozotocin (STZ) Induction and Blood glucose profiling:

Table 4.4: Streptozotocin (STZ) Induction in SD pregnant Rats:

Group No.	Groups(8 Rat/gp)	Treatment	Route of administration and Dosage	Number of Groups
1	Normal Control	Vehicle (Normal Pregnant Rat)	No treatment (0.1 mol/L citrate buffer)	1 Gp (6♀+2♂ Rat/gp)
2	Test	Streptozotocin (STZ)-induced diabetes in pregnant Rat (GDM model)	intraperitoneal injection (i.p.) of STZ (35 mg/kg bw in 0.1 mol/L citrate buffer)	1 Gp(6♀+2♂ Rat/gp)

Table 4.4 outlines the experimental design for studying gestational diabetes mellitus (GDM) in Sprague-Dawley rats . Group 1 serves as the normal control, receiving no treatment except for the vehicle (0.1 mol/L citrate buffer). This group, consisting of 6 female and 2 male rats, represents the baseline for normal pregnant rats . Group 2, the test group, was designed to induce diabetes-using streptozotocin (STZ). This induction involves an intraperitoneal injection (i.p.) of STZ at a dosage of 35 mg/kg body weight in 0.1 mol/L citrate buffer . Similar to the control group, Group 2 also comprises 6 female and 2 male rats.

This experimental setup enables the comparison of blood glucose profiles between normal pregnant rats and those with STZ-induced diabetes, providing insights into the development and effects of gestational diabetes at the early gestation period . The intraperitoneal injection of STZ is a well-established method for inducing diabetes in animal models, allowing researchers to study the pathophysiological aspects of GDM and assess potential therapeutic interventions (Zhang et al., 2019).

Table 4.5: Blood Glucose Profiling

Sprague-Dawley Rat-Blood Glucose Profile			
S.NO	Blood Glucose level : Control-(Pregnant)	Blood Glucose level : After STZ induction Test-(Pregnant-Diabetic)	
		Before STZ induction	After STZ induction
Sprague-Dawley Rat-1	97 mg/dl	110 mg/dl	334 mg/dl
Sprague-Dawley Rat-2	103 mg/dl	102 mg/dl	301 mg/dl
Sprague-Dawley Rat-3	105 mg/dl	95 mg/dl	305 mg/dl
Sprague-Dawley Rat-4	92 mg/dl	96 mg/dl	309 mg/dl
Sprague-Dawley Rat-5	107 mg/dl	101 mg/dl	438 mg/dl
Sprague-Dawley Rat-6	92 mg/dl	98 mg/dl	331 mg/dl

The blood glucose profile (Table 4.5) was analyzed in Sprague-Dawley female rats at early gestation, revealing noteworthy changes following Streptozotocin (STZ) induction to induce a diabetic condition. Before STZ induction, both the control (pregnant) and test (pregnant and diabetic-GDM) groups exhibited relatively normal blood glucose levels, ranging from 95 to 110 mg/dl. Subsequently, after STZ induction, the test group experienced a substantial increase in blood glucose levels, ranging from 301 to 438 mg/dl, indicative of successful diabetes induction. In contrast, the control group maintained lower and stable glucose levels within the range of 102-110 mg/dl. A study by Furman et al. (2022) found that STZ induction increased blood sugar levels in pregnant SD rats by approximately 200%. The increase in blood sugar levels after STZ induction is likely due to the destruction of beta cells in the pancreas. Beta cells are responsible for producing insulin, a hormone that helps to regulate blood sugar levels. When beta cells are destroyed, the body is unable to produce enough insulin, which leads to high blood sugar levels (Furman et al., 2022). The elevated post-STZ blood glucose levels in the test group underscored the effective induction of diabetes in pregnant Sprague-Dawley rats. This model has provided valuable insights into gestational diabetes,

contributing to a comprehensive understanding of the disease's impact on maternal and fetal health in a controlled experimental setting.

4.7 Blood Pooling and Sampling:

Retro-orbital blood collection was performed on 6 SD rats each in the control and test group. 2 mL of blood was collected from each rat and pooled into one collection tube for each group. Blood serum was isolated from each group and cryopreserved at -80°C . The rats were anesthetized with isoflurane. A single drop of topical ophthalmic anesthetic was applied to the eye to be sampled. After 30 seconds, the rat was placed in ventral recumbency with its head resting on a flat surface. The head was gently restrained with one hand, while a hematocrit capillary tube was held at a 45-degree angle to the eye and gently inserted into the retro-orbital space. Once the tube was inserted, it was gently rotated 180 degrees to break the blood vessels. The blood was allowed to collect in the tube (Arafa et al .,2021). Once 2 mL of blood had been collected, the tube was removed from the retro-orbital space and pressure was applied to the eye with gauze (Virginia Tech, n.d.).

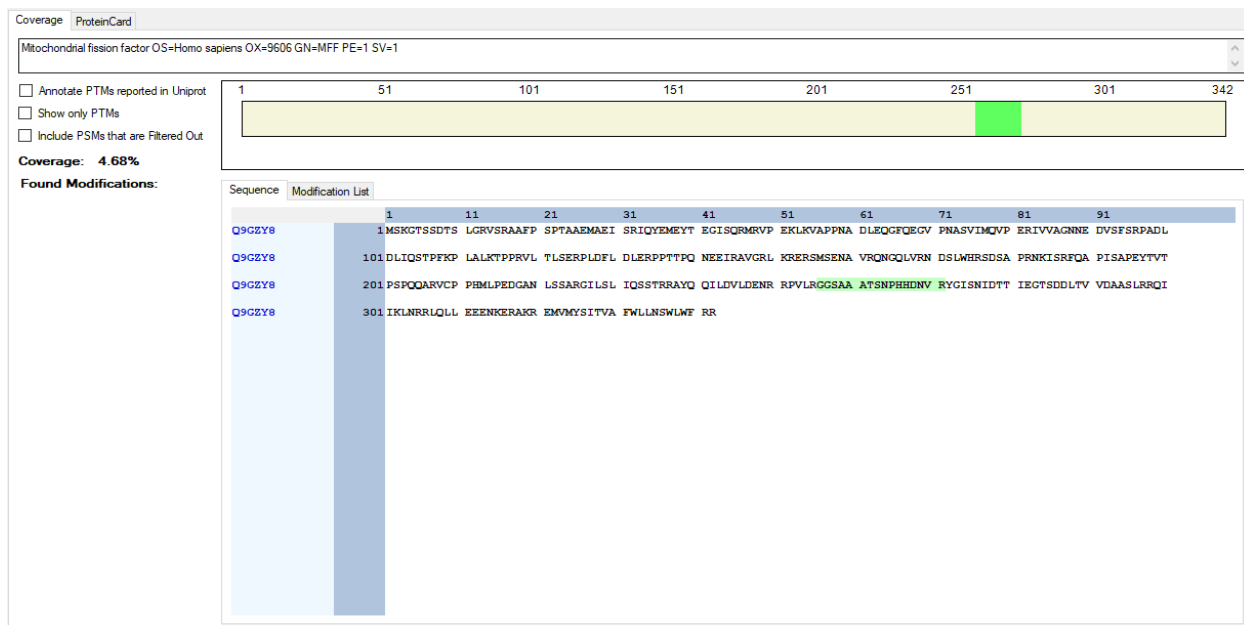
The blood sample was then transferred to a sterile micro centrifuge tube and centrifuged at 10,000 rpm for 5 minutes to separate the plasma from the red blood cells .The plasma sample was then stored at -80°C until use. The pooled plasma from each group was then used to isolate blood serum. This was done by centrifuging the plasma at 10,000 rpm for 10 minutes to pellet the fibrinogen. The supernatant was then collected and stored at -80°C until use to preserve its integrity.

4.8 Mitochondria Fission Factor (Mff) :

Recent research has elucidated the critical role of mitochondrial dysfunction and altered mitochondrial dynamics in the pathogenesis of insulin resistance and related metabolic disorders (Pentinat et al., 2018). Mitochondrial fission factor (Mff), a key regulator of mitochondrial fission, has been implicated in this process. Upregulation of Mff can lead to excessive mitochondrial fragmentation, contributing to overall mitochondrial dysfunction. This phenomenon extends to placental tissue, where mitochondrial impairment and resultant oxidative stress have been associated with the development of metabolic complications, including gestational diabetes mellitus (GDM) (Hebert et al., 2021). The placenta's vital function in regulating nutrient and oxygen supply to the developing fetus underscores the potential impact of mitochondrial dysfunction on fetal development and maternal metabolic health.

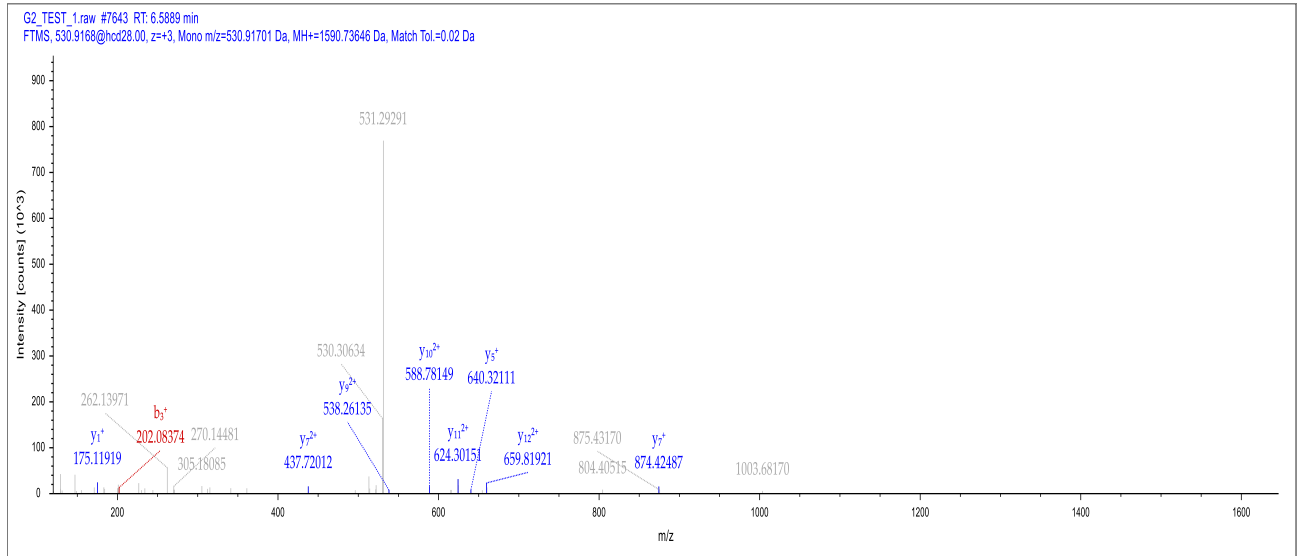
Insulin resistance, a hallmark of GDM, has been linked to altered mitochondrial dynamics in insulin-responsive tissues such as skeletal muscle and adipose tissue (Bach et al., 2005; Jheng et al., 2012). The observed upregulation of Mff in test samples may reflect widespread mitochondrial dysfunction in these tissues, potentially leading to impaired insulin sensitivity and disrupted glucose homeostasis. This hypothesis is supported by numerous studies reporting increased mitochondrial fission and altered expression of fission proteins, including Mff, in various tissues and cell types under diabetic conditions (Yu et al., 2006; Men et al., 2009; Zorzano et al., 2009). Collectively, these findings suggest a mechanistic link between Mff upregulation, mitochondrial dysfunction, and the development of diabetes-related complications, including GDM. Further research is warranted to elucidate the precise molecular mechanisms underlying this relationship and to explore potential therapeutic interventions targeting mitochondrial dynamics in the prevention and management of GDM.

Figure 4.31 -(A) Protein (Mitochondria Fission Factor) coverage analyses :



The protein under investigation is the Mitochondrial fission factor (MFF) from Homo sapiens, identified by the UniProtKB entry "Mitochondrial fission factor OS=Homo sapiens OX=9606 GN=MFF PE=1 SV=1". This protein consists of 342 amino acids, providing a comprehensive substrate for analysis. Mass spectrometry analysis revealed a sequence coverage of 4.68%, indicating that a small but significant portion of the protein's primary structure was detected and identified. The coverage diagram exhibits a prominent green bar approximately between positions 250 and 270, signifying the presence of detected peptides within this region. The complete protein sequence, presented in four rows of 100 amino acids each (with the exception of the final row), allows for a detailed examination of the protein's primary structure. Of particular interest is the detected peptide sequence "GGSSAAATSNPHEDN", which is highlighted in green within the full sequence, corresponding to the region indicated in the coverage diagram. This peptide represents a crucial identified fragment of the MFF protein, potentially offering insights into protein structure, function, or post-translational modifications in this specific region.

Figure 4.31 - (B) Analysis of MS/MS spectrum of a peptide (Mitochondria Fission Factor (MFF) :



This data (figure 4.31-B) describes an MS/MS spectrum of a MFF peptide. Liquid chromatography-mass spectrometry (LC-MS) analysis of the human Mitochondrial fission factor (MFF) protein revealed significant findings. The 342-amino acid protein showed a low sequence coverage of 4.68%, with only one peptide fragment (GGSSAAATSNPHEDN) confidently identified near the C-terminal region, approximately at positions 250-270. Mass spectrometry data for this peptide was of high quality, with a precursor ion ($M+H^+$) mass of 1590.73646 Da and a monoisotopic m/z of 530.91701 Da. Within the spectrum, the most intense peak is observed at m/z 531.29291. The spectrum displayed clear y and b ion series, confirming the peptide sequence. The detected peptide shows good mass spectral quality, allowing for confident sequence assignment.

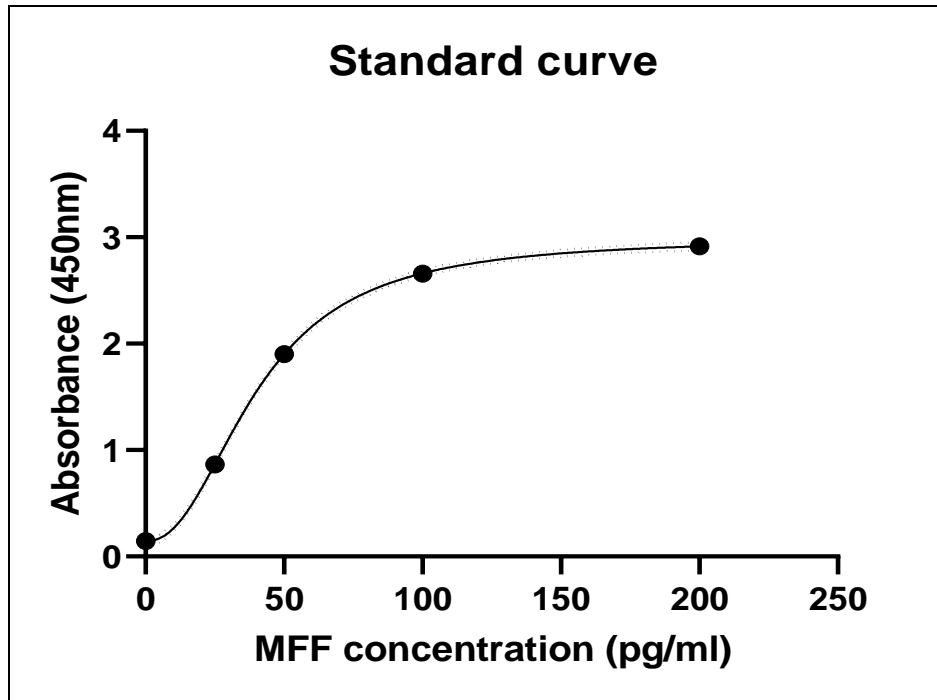
4.9 ELISA Analyses for Mitochondria Fission Factor (Mff):

Table 4.6: Standard Curve Analysis:

Standard curve			
MFF concentration (pg/ml)	Absorbance (450nm)		
0	0.1394	0.1459	0.1497
25	0.867	0.8731	0.8549
50	1.8843	1.8623	1.9554
100	2.604	2.6702	2.704
200	2.903	2.953	2.891

A standard curve (Table 4.6) was generated to quantify the concentration of mitochondrial fission factor (Mff) using an enzyme-linked immunosorbent assay (ELISA). The standard curve consisted of six Mff concentrations ranging from 0 pg/mL to 200 pg/mL. For each concentration, absorbance values at 450 nm wavelength were measured in triplicates (Crowther, 2001). The absorbance values increased proportionally with increasing Mff concentrations, following a typical sigmoidal curve shape. The blank (0 pg/mL Mff) showed low absorbance values ranging from 0.1394 to 0.1497, representing the background signal. The highest absorbance values, ranging from 2.891 to 2.953, were observed for the 200 pg/mL Mff concentration. The standard curve data was used to interpolate the Mff concentrations in unknown samples based on their absorbance values (Crowther, 2001). A regression analysis was performed to determine the equation of the best-fit curve for accurate interpolation of unknown sample concentrations.

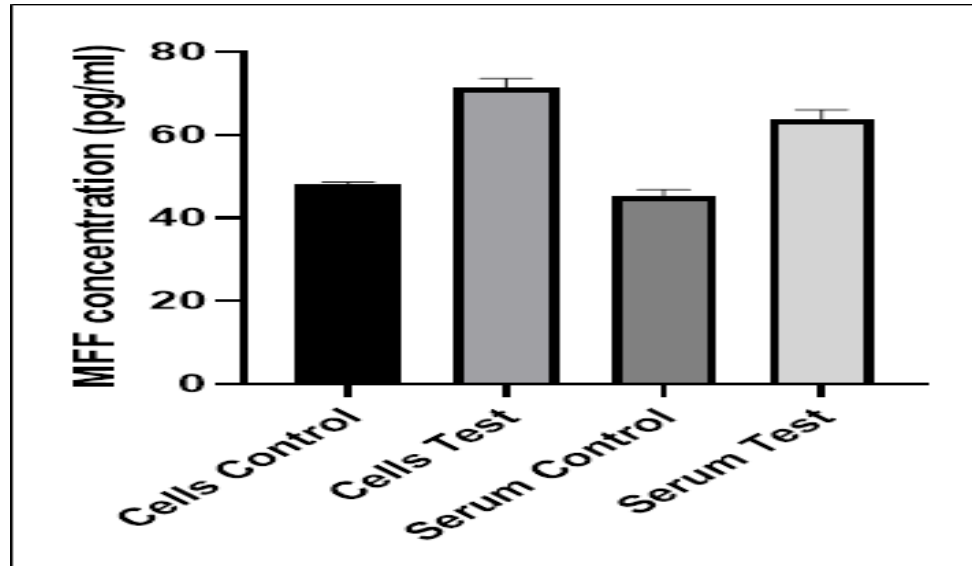
Figure 4.32: Standard Curve Plot



The standard curve plot (figure 4.31) depicted the relationship between the concentration of mitochondrial fission factor (Mff) and the corresponding absorbance values obtained from the enzyme-linked immunosorbent assay (ELISA). The data points on the plot followed a sigmoidal curve shape, characteristic of typical standard curves in immunoassays (Natarajan et al.,2008). The absorbance values increased proportionally with increasing Mff concentrations, allowing for quantitative measurement of unknown samples (Crowther, 2001).

At the lowest concentration of 0 pg/mL Mff, the absorbance value was approximately 0.15, representing the background signal . As the Mff concentration increased, the absorbance values rose steadily, reaching a maximum of around 3.0 at the highest concentration of 200 pg/mL Mff . The regression analysis performed on the standard curve data yielded the equation of the best-fit curve, which was used for accurate interpolation of unknown sample concentrations from their corresponding absorbance values (Crowther, 2001; Hanada et al., 2020).

Figure 4.33: ELISA PLOT illustrating comparative evaluation between In-vitro and In-vivo samples.



The ELISA analysis (figure 4.32) was performed to evaluate the comparative levels of mitochondrial fission factor (Mff) between in vitro (BeWo cell culture protein) and in vivo (Sprague Dawley (SD) rat blood serum protein) samples (Hanada et al., 2020). The interpolated Mff concentrations were calculated using the standard curve equation derived from the ELISA data (Crowther, 2001). The in vitro Test samples exhibited a higher mean Mff concentration (74.95pg/mL) compared to the in vitro Control samples (64.02pg/mL), indicating elevated Mff levels in the Test group (Hanada et al., 2020). Similarly, the in vivo Test group showed a marginally higher mean Mff concentration (66.94pg/mL) compared to the in vivo Control group (65.03 pg/mL).

The ELISA analysis results clearly depicted higher Mff levels in the Test groups compared to their respective Controls, both for the in vitro and in vivo samples (Hanada et al., 2020). The upregulation of mitochondrial fission factor (Mff) observed in the Test samples, both in vitro and in vivo, is an important finding that could potentially be associated with the onset of gestational diabetes mellitus (GDM) at early stages of pregnancy (Veza et al., 2022).

CHAPTER 5

SUMMARY

5. Summary:

The research undertaken explored the complex nature of Gestational Diabetes Mellitus (GDM), a metabolic condition with significant implications for maternal and fetal health. This comprehensive study included in-vitro cellular models, mass spectrometry identification of proteins, and in vivo validation using rat model. The focus of the study was to identify the probable early diagnostic biomarker for diagnosis of GDM.

The BeWo trophoblastic cell line was used to develop an in vitro GDM model and proved to be an effective tool, offering translational relevance by mimicking early placental responses. Validation process ensured the model's fidelity to GDM conditions, providing a robust foundation for subsequent investigations.

The research then focused on predicting and evaluating potential biomarkers for early GDM detection. Using advanced LCMS for Total Proteome Analysis, the study revealed the complex proteomic landscape associated with GDM. Comparative proteome profiling between normal and hyperglycemic conditions offered insights into molecular alterations during early gestation.

Study on the role of VEGF on GDM pathophysiology suggested that VEGF had no significant effect on glucose metabolism in the in-vitro cell model. However, further studies are required in this aspect.

To validate the in-vitro findings, rat model of GDM was used. Streptozotocin induction in pregnant rats was done to generate the GDM rat model and compared with the normal pregnant rats. Thorough proteome analysis of blood samples mirrored in-vitro protein profiles and identified protein biomarkers in a living organism. ELISA analysis revealed upregulated levels of mitochondrial fission factor (Mff) and few other significant proteins, in both the in vitro and in vivo Test samples compared to their respective control groups. This upregulation of Mff, a key regulator of mitochondrial fission, was a significant finding that could potentially contribute to the onset of GDM at early stages of pregnancy.

The study noted that mitochondrial dysfunction and altered mitochondrial dynamics, particularly excessive mitochondrial fission, had been implicated in the development of insulin resistance and GDM. The observed upregulation of Mff in the test samples suggested increased mitochondrial fragmentation, which could lead to mitochondrial dysfunction and oxidative stress in insulin-responsive tissues and the placenta. Previous research had linked placental mitochondrial dysfunction to the pathogenesis of GDM, while altered mitochondrial dynamics in skeletal muscle and adipose tissue had been associated with impaired insulin sensitivity and glucose homeostasis.

The combination of these experimental findings offered a comprehensive understanding of GDM development. The in-vitro cell model, meticulously validated for insulin resistance and glucose

intolerance, provided a controlled environment to study GDM pathologies. LCMS analysis uncovered a diverse proteomic landscape, enabling the identification of potential biomarkers for early prediction. The validation through ELISA analysis for SD rat serum protein samples ensured the robustness and translatability of the in-vitro findings, bringing the research closer to clinical relevance.

CHAPTER 6

CONCLUSION

6. Conclusion:

This interdisciplinary investigation significantly advanced the understanding of GDM, shedding light on its complex molecular landscape. The in-vitro cell model, developed with precision and validated rigorously, served as a valuable tool for studying GDM pathologies. Biomarker discovery, facilitated by LCMS analysis, held promise for early GDM prediction, crucial for timely interventions. The findings regarding VEGF underscored the intricacies of GDM's molecular landscape, challenging preconceived notions.

The validation in a rat model bridged the gap between in-vitro models and clinical relevance. The successful reproduction of GDM conditions in pregnant rats, coupled with proteome analysis mirroring in-vitro profiles, strengthened the translatability of the findings. This integrated approach, spanning from cellular models to animal validation, provided a holistic understanding of GDM pathogenesis and offered practical solutions for clinical diagnostics and monitoring.

The ELISA analysis revealed significantly upregulated mitochondrial fission factor (Mff) levels in both in vitro and in vivo Test samples compared to Controls. Excessive mitochondrial fission, mediated by elevated Mff, had been linked to mitochondrial dysfunction, oxidative stress, and insulin resistance – pathogenic mechanisms implicated in gestational diabetes mellitus (GDM) development. Upregulated Mff could have contributed to placental dysfunction, impaired nutrient/oxygen supply to the fetus, and compromised insulin sensitivity in maternal tissues. These findings suggested Mff upregulation might have played a crucial role in the onset of GDM during early pregnancy by disrupting mitochondrial dynamics. The results provided a potential molecular basis for GDM pathogenesis, highlighting the importance of investigating mitochondrial dynamics and Mff regulation in this context. Further research elucidating the specific mechanisms and exploring therapeutic interventions targeting Mff was warranted.

This work invited further investigation into alternative mechanisms underlying GDM pathogenesis and opened new avenues for refining diagnostic and therapeutic strategies. The complexity of GDM demanded a dynamic and adaptive approach, and this research contributed to the ongoing dialogue within the scientific community.

CHAPTER 7

BIBLIOGRAPHY

7. Bibliography:

- Abbkine. (2024). Human Mitochondrial fission factor (MFF) ELISA Kit Manufacturer's Instructions. Abbkine, USA.
- Abdeltawab, A., Zaki, M. E., Abdeldayem, Y., Mohamed, A. A., & Zaied, S. M. (2021). Circulating micro RNA-223 and angiopoietin-like protein 8 as biomarkers of gestational diabetes mellitus. *British journal of biomedical science*, 78(1), 12–17. <https://doi.org/10.1080/09674845.2020.1764211>
- Abell SK, De Courten B, Boyle JA, Teede HJ. Inflammatory and Other Biomarkers: Role in Pathophysiology and Prediction of Gestational Diabetes Mellitus. *International Journal of Molecular Sciences*. 2015; 16(6):13442-13473. <https://doi.org/10.3390/ijms160613442>
- ACOG Practice Bulletin No. 190: Gestational Diabetes Mellitus. (2018). *Obstetrics and gynecology*, 131(2), e49–e64. <https://doi.org/10.1097/AOG.0000000000002501>
- Aebersold, R., & Mann, M. (2016). Mass-spectrometric exploration of proteome structure and function. *Nature*, 537(7620), 347-355. <https://doi.org/10.1038/nature19949>
- Aitken, N., Smith, S., Schwarz, C., & Morin, P. A. (2004). Single nucleotide polymorphism (SNP) discovery in mammals: a targeted-gene approach. *Molecular Ecology*, 13(6), 1423-1431. <https://doi.org/10.1111/j.1365-294X.2004.02159.x>
- Al-Ofi E, Alrafiah A, Maida S, Almaghrabi S, Hakami N. Altered Expression of Angiogenic Biomarkers in Pregnancy Associated with Gestational Diabetes. *Int J Gen Med*. 2021;14:3367-3375. <https://doi.org/10.2147/IJGM.S316670>
- American College of Obstetricians and Gynecologists. (2018). Gestational diabetes mellitus. *Practice Bulletin No. 190. Obstetrics and Gynecology*, 131(2), e49-e64. <https://doi.org/10.1097/AOG.0000000000002501>
- American Diabetes Association (2018). 13. Management of Diabetes in Pregnancy: Standards of Medical Care in Diabetes-2018. *Diabetes care*, 41(Suppl 1), S137–S143. <https://doi.org/10.2337/dc18-S013>
- American Diabetes Association (2018). 2. Classification and Diagnosis of Diabetes: Standards of Medical Care in Diabetes-2018. *Diabetes care*, 41(Suppl 1), S13–S27. <https://doi.org/10.2337/dc18-S002>
- American Diabetes Association Professional Practice Committee (2022). Addendum. 11. Chronic Kidney Disease and Risk Management: Standards of Medical Care in Diabetes-2022.

Diabetes Care 2022;45(Suppl. 1): S175-S184. Diabetes care, 45(9), 2182–2184. <https://doi.org/10.2337/dc22-ad08a>

- American Diabetes Association. (2018). 2. Classification and diagnosis of diabetes: Standards of medical care in diabetes-2018. Diabetes Care, 41(Supplement 1), S13-S27. <https://doi.org/10.2337/dc18-S002>
- American Diabetes Association. (2021). 2. Classification and Diagnosis of Diabetes: Standards of Medical Care in Diabetes—2021. Diabetes Care, 44(Supplement 1), S15-S33. DOI: 10.2337/dc21-S002
- American Diabetes Association. (2021). Standards of medical care in diabetes—2021. Diabetes Care, 44(Supplement 1), S15-S33. <https://doi.org/10.2337/dc21-S002>
- ARAFA, M. A., & AMANY, M. (2021). Effect of Metformin Hydrochloride Administration and its Withdrawal on the Kidneys of Adult Male Albino Rats: Histological and Biochemical Studies. The Medical Journal of Cairo University, 89(March), 337-354.
- Asfari, M., Janjic, D., Meda, P., Li, G., Halban, P. A., & Wollheim, C. B. (1992). Establishment of 2-mercaptoethanol-dependent differentiated insulin-secreting cell lines. Endocrinology, 130(1), 167-178. <https://doi.org/10.1210/endo.130.1.1370150>
- Asfari, M., Janjic, D., Meda, P., Li, G., Halban, P. A., & Wollheim, C. B. (1992). Establishment of 2-mercaptoethanol-dependent differentiated insulin-secreting cell lines. Endocrinology, 130(1), 167–178. <https://doi.org/10.1210/endo.130.1.1370150>
- Ashcroft, F. M., Rohm, M., Clark, A., & Brereton, M. F. (2017). Is Type 2 Diabetes a Glycogen Storage Disease of Pancreatic β Cells?. Cell metabolism, 26(1), 17–23. <https://doi.org/10.1016/j.cmet.2017.05.014>
- Ategbo, J.M.; Grissa, O.; Yessoufou, A.; Hichami, A.; Dramane, K.L.; Moutairou, K.; Miled, A.; Grissa, A.; Jerbi, M.; Tabka, Z.; et al. Modulation of adipokines and cytokines in gestational diabetes and macrosomia. J. Clin. Endocrinol. Metab. 2006, 91, 4137–4143.[CrossRef]
- Auffret, J.; Freemark, M.; Carré, N.; Mathieu, Y.; Turrel-Cuzin, C.; Lombès, M.; Movassat, J.; Binart, N. Defective prolactin signaling impairs pancreatic-cell development during the perinatal period. Am. J. Physiol. Endocrinol. Metab. 2013, 305,E1309–E1318. [CrossRef]
- Bach, D., Pich, S., Soriano, F. X., Vega, N., Baumgartner, B., Oriola, J., Dagaard, J. R., Lloberas, J., Camps, M., Zierath, J. R., Rabasa-Lhoret, R., Wallberg-Henriksson, H., Laville, M., Palacín, M., Vidal, H., Rivera, F., Brand, M., & Zorzano, A. (2003). Mitofusin-2 determines mitochondrial network architecture and mitochondrial metabolism. A novel regulatory

mechanism altered in obesity. *The Journal of biological chemistry*, 278(19), 17190–17197.
<https://doi.org/10.1074/jbc.M212754200>

- Bader, J. M., Albrecht, V., & Mann, M. (2023). MS-Based Proteomics of Body Fluids: The End of the Beginning. *Molecular & cellular proteomics : MCP*, 22(7), 100577.
<https://doi.org/10.1016/j.mcpro.2023.100577>
- Bala, M., Gupta, P., Gupta, S., Dua, A., Injeti, E., & Mittal, A. (2021). Efficient and modified 2-NBDG assay to measure glucose uptake in cultured myotubes. *Journal of pharmacological and toxicological methods*, 109, 107069.
<https://doi.org/10.1016/j.vascn.2021.107069>.
- Bao, W., Michels, K. B., Tobias, D. K., Li, S., Chavarro, J. E., Gaskins, A. J., Vaag, A. A., Hu, F. B., & Zhang, C. (2016). Parental smoking during pregnancy and the risk of gestational diabetes in the daughter. *International journal of epidemiology*, 45(1), 160–169.
<https://doi.org/10.1093/ije/dyv334>
- Barbour, L. A., McCurdy, C. E., Hernandez, T. L., Kirwan, J. P., Catalano, P. M., & Friedman, J. E. (2007). Cellular mechanisms for insulin resistance in normal pregnancy and gestational diabetes. *Diabetes Care*, 30(Supplement_2), S112-S119.
<https://doi.org/10.2337/dc07-s202>
- Batista, T. M., Garcia-Martin, R., Cai, W., Konishi, M., O'Neill, B. T., Sakaguchi, M., Kim, J. H., Jung, D. Y., Kim, J. K., & Kahn, C. R. (2019). Multi-dimensional transcriptional remodeling by physiological insulin in vivo. *Cell Reports*, 26(12), 3429-3443.e3.
<https://doi.org/10.1016/j.celrep.2019.02.081>
- Batista, T. M., Garcia-Martin, R., Cai, W., Konishi, M., O'Neill, B. T., Sakaguchi, M., Kim, J. H., Jung, D. Y., Kim, J. K., & Kahn, C. R. (2019). Multi-dimensional transcriptional remodeling by physiological insulin in vivo. *Cell Reports*, 26(12), 3429-3443.e3.
<https://doi.org/10.1016/j.celrep.2019.02.081>
- Batista, T. M., Garcia-Martin, R., Cai, W., Konishi, M., O'Neill, B. T., Sakaguchi, M., Kim, J. H., Jung, D. Y., Kim, J. K., & Kahn, C. R. (2019). Multi-dimensional transcriptional remodeling by physiological insulin in vivo. *Cell Reports*, 26(12), 3429-3443.e3.
<https://doi.org/10.1016/j.celrep.2019.02.081>
- Batista, T. M., Garcia-Martin, R., Cai, W., Konishi, M., O'Neill, B. T., Sakaguchi, M., Kim, J. H., Jung, D. Y., Kim, J. K., & Kahn, C. R. (2019). Multi-dimensional transcriptional remodeling by physiological insulin in vivo. *Cell Reports*, 26(12), 3429-3443.e3.
<https://doi.org/10.1016/j.celrep.2019.02.081>

- Baumgartner-Parzer, S. M., Wagner, L., Pettermann, M., Grillari, J., Gessl, A., & Waldhäusl, W. (1995). High-glucose--triggered apoptosis in cultured endothelial cells. *Diabetes*, 44(11), 1323–1327. <https://doi.org/10.2337/diab.44.11.1323>
- Bellamy, L., Casas, J. P., Hingorani, A. D., & Williams, D. (2009). Type 2 diabetes mellitus after gestational diabetes: a systematic review and meta-analysis. *Lancet (London, England)*, 373(9677), 1773–1779. [https://doi.org/10.1016/S0140-6736\(09\)60731-5](https://doi.org/10.1016/S0140-6736(09)60731-5)
- Bellamy, L., Casas, J. P., Hingorani, A. D., & Williams, D. (2009). Type 2 diabetes mellitus after gestational diabetes: A systematic review and meta-analysis. *The Lancet*, 373(9677), 1773-1779. [https://doi.org/10.1016/S0140-6736\(09\)60731-5](https://doi.org/10.1016/S0140-6736(09)60731-5)
- Ben-Haroush, A., Yogeve, Y., & Hod, M. (2004). Epidemiology of gestational diabetes mellitus and its association with Type 2 diabetes. *Diabetic medicine : a journal of the British Diabetic Association*, 21(2), 103–113. <https://doi.org/10.1046/j.1464-5491.2003.00985.x>.
- Berg, M., Sparud-Lundin, C., & Wennberg, P. (2010). Adaptation of the revised illness perception questionnaire (IPQ-R) to a Swedish context and perceived causes of gestational diabetes. *Patient Education and Counseling*, 78(1), 100–106.
- Berg, R. A., Garlington, A. W., & Tong, C. H. (2010). Best practices for national and regional gestational diabetes mellitus screening, diagnosis, and treatment. *Primary Care Diabetes*, 4(4), 193-201. <https://doi.org/10.1016/j.pcd.2010.09.001>
- Bernea, E. G., Suica, V. I., Uyy, E., Cerveanu-Hogas, A., Boteanu, R. M., Ivan, L., Ceausu, I., Mihai, D. A., Ionescu-Tîrgoviște, C., & Antohe, F. (2022). Exosome Proteomics Reveals the Dereglulation of Coagulation, Complement and Lipid Metabolism Proteins in Gestational Diabetes Mellitus. *Molecules (Basel, Switzerland)*, 27(17), 5502. <https://doi.org/10.3390/molecules27175502>
- Bode, C. J., Jin, H., Rytting, E., Silverstein, P. S., Young, A. M., & Audus, K. L. (2006). In vitro models for studying trophoblast transcellular transport. *Methods in molecular medicine*, 122, 225–239. <https://doi.org/10.1385/1-59259-989-3:225>
- Bolatai, A., He, Y., & Wu, N. (2022). Vascular endothelial growth factor and its receptors regulation in gestational diabetes mellitus and eclampsia. *Journal of translational medicine*, 20(1), 400. <https://doi.org/10.1186/s12967-022-03603-4>
- Bolatai, A., He, Y., & Wu, N. (2022). Vascular endothelial growth factor and its receptors regulation in gestational diabetes mellitus and eclampsia. *Journal of translational medicine*, 20(1), 400. <https://doi.org/10.1186/s12967-022-03603-4>

- Borissoff, J. I., Joosen, I. A., Versteyleen, M. O., Brill, A., Fuchs, T. A., Savchenko, A. S., Gallant, M., Martinod, K., Ten Cate, H., Hofstra, L., Crijns, H. J., Wagner, D. D., & Kietselaer, B. L. J. H. (2013). Elevated levels of circulating DNA and chromatin are independently associated with severe coronary atherosclerosis and a prothrombotic state. *Arteriosclerosis, thrombosis, and vascular biology*, 33(8), 2032–2040. <https://doi.org/10.1161/ATVBAHA.113.301627>
- Bowler-Barnett, E. H., Fan, J., Luo, J., Magrane, M., Martin, M. J., Orchard, S., & UniProt Consortium (2023). UniProt and Mass Spectrometry-Based Proteomics-A 2-Way Working Relationship. *Molecular & cellular proteomics : MCP*, 22(8), 100591. <https://doi.org/10.1016/j.mcpro.2023.100591>
- Brännmark, C., Nyman, E., Fagerholm, S., Bergenholm, L., Ekstrand, E. M., Cedersund, G., & Strålfors, P. (2013). Insulin signaling in type 2 diabetes: Experimental and modeling analyses reveal mechanisms of insulin resistance in human adipocytes. *Journal of Biological Chemistry*, 288(14), 9867-9880. <https://doi.org/10.1074/jbc.M112.432062>
- Bro, R., & Smilde, A. K. (2014). Principal component analysis. *Analytical Methods*, 6(9), 2812-2831. <https://doi.org/10.1039/C3AY41907J>
- Buchanan T. A. (2001). Pancreatic B-cell defects in gestational diabetes: implications for the pathogenesis and prevention of type 2 diabetes. *The Journal of clinical endocrinology and metabolism*, 86(3), 989–993. <https://doi.org/10.1210/jcem.86.3.7339>.
- Buckley, B. S., Harreiter, J., Damm, P., Corcoy, R., Chico, A., Simmons, D., Vellinga, A., & Dunne, F. (2012). Gestational diabetes mellitus in Europe: Prevalence, current screening practice and barriers to screening. A review. *Diabetic Medicine*, 29(7), 844-854. <https://doi.org/10.1111/j.1464-5491.2011.03541.x>
- Buckley, B. S., Harreiter, J., Damm, P., Corcoy, R., Chico, A., Simmons, D., Vellinga, A., Dunne, F., & DALI Core Investigator Group (2012). Gestational diabetes mellitus in Europe: prevalence, current screening practice and barriers to screening. A review. *Diabetic medicine : a journal of the British Diabetic Association*, 29(7), 844–854. <https://doi.org/10.1111/j.1464-5491.2011.03541.x>
- Camelo Castillo, W., Boggess, K., Stürmer, T., Brookhart, M. A., Benjamin, D. K., & Jonsson Funk, M. (2015). Trends in gestational diabetes mellitus among Hispanic women in South Carolina after the introduction of a statewide obesity initiative. *American Journal of Perinatology*, 32(8), 759-765. <https://doi.org/10.1055/s-0034-1543957>
- Camelo Castillo, W., Boggess, K., Stürmer, T., Brookhart, M. A., Benjamin, D. K., Jr, & Jonsson Funk, M. (2015). Association of Adverse Pregnancy Outcomes With Glyburide vs

Insulin in Women With Gestational Diabetes. *JAMA pediatrics*, 169(5), 452–458. <https://doi.org/10.1001/jamapediatrics.2015.74>

- Cangelosi, R., & Goriely, A. (2007). Component retention in principal component analysis with application to cDNA microarray data. *Biology Direct*, 2(1), 2. <https://doi.org/10.1186/1745-6150-2-2>
- Cao, Y. L., Jia, Y. J., Xing, B. H., Shi, D. D., & Dong, X. J. (2017). Plasma microRNA-16-5p, -17-5p and -20a-5p: Novel diagnostic biomarkers for gestational diabetes mellitus. *The journal of obstetrics and gynaecology research*, 43(6), 974–981. <https://doi.org/10.1111/jog.13317>
- Carpenter, M. W., & Coustan, D. R. (1982). Criteria for screening tests for gestational diabetes. *American Journal of Obstetrics and Gynecology*, 144(7), 768–773. [https://doi.org/10.1016/0002-9378\(82\)90349-0](https://doi.org/10.1016/0002-9378(82)90349-0)
- Catalano P. M. (2010). Obesity, insulin resistance, and pregnancy outcome. *Reproduction (Cambridge, England)*, 140(3), 365–371. <https://doi.org/10.1530/REP-10-0088>
- Catalano, P. M., Huston, L., Amini, S. B., & Kalhan, S. C. (1999). Longitudinal changes in glucose metabolism during pregnancy in obese women with normal glucose tolerance and gestational diabetes mellitus. *American journal of obstetrics and gynecology*, 180(4), 903–916. [https://doi.org/10.1016/s0002-9378\(99\)70662-9](https://doi.org/10.1016/s0002-9378(99)70662-9)
- Catalano, P. M., McIntyre, H. D., Cruickshank, J. K., McCance, D. R., Dyer, A. R., Metzger, B. E., Lowe, L. P., Trimble, E. R., Coustan, D. R., Hadden, D. R., Persson, B., Hod, M., Oats, J. J., & HAPO Study Cooperative Research Group (2012). The hyperglycemia and adverse pregnancy outcome study: associations of GDM and obesity with pregnancy outcomes. *Diabetes care*, 35(4), 780–786. <https://doi.org/10.2337/dc11-1790>.
- Catalano, P. M., Presley, L., Minium, J., & Hauguel-de Mouzon, S. (2012). Fetuses of obese mothers develop insulin resistance in utero. *Diabetes Care*, 32(6), 1076–1080. <https://doi.org/10.2337/dc07-2079>
- Catalano, P. M., Tyzbir, E. D., Roman, N. M., Amini, S. B., & Sims, E. A. (1991). Longitudinal changes in insulin release and insulin resistance in nonobese pregnant women. *American journal of obstetrics and gynecology*, 165(6 Pt 1), 1667–1672. [https://doi.org/10.1016/0002-9378\(91\)90012-g](https://doi.org/10.1016/0002-9378(91)90012-g).
- Cawyer, C. R., Horvat, D., Leonard, D., Allen, S. R., Jones, R. O., Zawieja, D. C., ... & Saade, G. R. (2014). Hyperglycemia impairs cytotrophoblast function via stress signaling. *American Journal of Obstetrics and Gynecology*, 210(1), 80.e1–80.e7. <https://doi.org/10.1016/j.ajog.2013.11.018>

- Chaiworapongsa, T., Chaemsaitong, P., Korzeniewski, S. J., Yeo, L., & Romero, R. (2014). Pre-eclampsia part 2: prediction, prevention and management. *Nature reviews. Nephrology*, 10(9), 531–540. <https://doi.org/10.1038/nrneph.2014.103>.
- Chatterjee, B., & Thakur, S. S. (2023). Proteins and metabolites fingerprints of gestational diabetes mellitus forming protein-metabolite interactomes are its potential biomarkers. *Proteomics*, 23(13-14), e2200257. <https://doi.org/10.1002/pmic.202200257>
- Chen, C., Xu, X., & Yan, Y. (2018). Estimated global overweight and obesity burden in pregnant women based on panel data model. *PloS one*, 13(8), e0202183. <https://doi.org/10.1371/journal.pone.0202183>.
- Chen, L., Zhu, C., Yang, J., Chen, J., Ge, Y., & Wang, Y. (2018). Early-pregnancy prediction of preeclampsia and gestational diabetes: An updated stratified cluster analysis. *Taiwanese Journal of Obstetrics and Gynecology*, 57(3), 348-355. <https://doi.org/10.1016/j.tjog.2018.04.007>
- Chiefari, E., Arcidiacono, B., Foti, D., & Brunetti, A. (2017). Gestational diabetes mellitus: An updated overview. *Journal of Endocrinological Investigation*, 40(9), 899-909. <https://doi.org/10.1007/s40618-016-0607-5>
- Chiefari, E., Arcidiacono, B., Foti, D., & Brunetti, A. (2017). Gestational diabetes mellitus: an updated overview. *Journal of endocrinological investigation*, 40(9), 899–909. <https://doi.org/10.1007/s40618-016-0607-5>.
- Ciaraldi, T. P., Abrams, L., Nikoulina, S., Mudaliar, S., & Henry, R. R. (1995). Glucose transport in cultured human skeletal muscle cells. Regulation by insulin and glucose in nondiabetic and non-insulin-dependent diabetes mellitus subjects. *The Journal of Clinical Investigation*, 96(6), 2820-2827. <https://doi.org/10.1172/JCI118352>
- Crowther, J. R. (2001). *The ELISA guidebook*. Humana Press.
- Dabelea, D., Snell-Bergeon, J. K., Hartsfield, C. L., Bischoff, K. J., Hamman, R. F., McDuffie, R. S., & Kaiser Permanente of Colorado GDM Screening Program (2005). Increasing prevalence of gestational diabetes mellitus (GDM) over time and by birth cohort: Kaiser Permanente of Colorado GDM Screening Program. *Diabetes care*, 28(3), 579–584. <https://doi.org/10.2337/diacare.28.3.579>
- Danneman, P. J., Suckow, M. A., & Brayton, C. (2000). *The laboratory mouse*. CRC Press.
- Daskalakis, G., Marinopoulos, S., Krielesi, V., Papapanagiotou, A., Papantoniou, N., Mesogitis, S., & Antsaklis, A. (2008). Placental pathology in women with gestational diabetes.

Acta obstetricia et gynecologica Scandinavica, 87(4), 403–407.
<https://doi.org/10.1080/00016340801908783>

- DeFronzo R. A. (2009). Banting Lecture. From the triumvirate to the ominous octet: a new paradigm for the treatment of type 2 diabetes mellitus. *Diabetes*, 58(4), 773–795. <https://doi.org/10.2337/db09-9028>
- DeFronzo R. A. (2009). Banting Lecture. From the triumvirate to the ominous octet: a new paradigm for the treatment of type 2 diabetes mellitus. *Diabetes*, 58(4), 773–795. <https://doi.org/10.2337/db09-9028>.
- Delghingaro-Augusto, V., Nolan, C. J., Gupta, D., Jetton, T. L., Latour, M. G., Peshavaria, M., Madiraju, S. R., Joly, E., Peyot, M. L., Prentki, M., & Leahy, J. (2009). Islet beta cell failure in the 60% pancreatectomised obese hyperlipidaemic Zucker fatty rat: severe dysfunction with altered glycerolipid metabolism without steatosis or a falling beta cell mass. *Diabetologia*, 52(6), 1122–1132. <https://doi.org/10.1007/s00125-009-1317-8>
- Desforges, M., & Sibley, C. P. (2010). Placental nutrient supply and fetal growth. *The International Journal of Developmental Biology*, 54(2-3), 377-390. <https://doi.org/10.1387/ijdb.082765md>
- Desoye, G., & Hauguel-de Mouzon, S. (2007). The human placenta in gestational diabetes mellitus: The insulin and cytokine network. *Diabetes Care*, 30(Supplement_2), S120-S126. <https://doi.org/10.2337/dc07-s203>
- Desoye, G., & van Poppel, M. (2015). The feto-placental dialogue and diabetes. *Best practice & research. Clinical obstetrics & gynaecology*, 29(1), 15–23. <https://doi.org/10.1016/j.bpobgyn.2014.05.012>
- Diabetes in pregnancy: management from preconception to the postnatal period. (2020). National Institute for Health and Care Excellence (NICE).
- Díaz-Pérez, F. I., Hiden, U., Gauster, M., Lang, I., Konya, V., Heinemann, A., Lögl, J., Saffery, R., Desoye, G., & Cvitic, S. (2016). Post-transcriptional down regulation of ICAM-1 in feto-placental endothelium in GDM. *Cell adhesion & migration*, 10(1-2), 18–27. <https://doi.org/10.1080/19336918.2015.1127467>
- Dilworth, L., Facey, A., & Omoruyi, F. (2021). Diabetes Mellitus and Its Metabolic Complications: The Role of Adipose Tissues. *International journal of molecular sciences*, 22(14), 7644. <https://doi.org/10.3390/ijms22147644>
- Dlodla, P. V., Mabhida, S. E., Ziqubu, K., Nkambule, B. B., Mazibuko-Mbeje, S. E., Hanser, S., Basson, A. K., Pheiffer, C., & Kengne, A. P. (2023). Pancreatic β -cell dysfunction in

type 2 diabetes: Implications of inflammation and oxidative stress. *World journal of diabetes*, 14(3), 130–146. <https://doi.org/10.4239/wjd.v14.i3.130>

- D'Souza, L. J., Wright, S. H., & Bhattacharya, D. (2022). Genetic evidence that uptake of the fluorescent analog 2NBDG occurs independently of known glucose transporters. *PloS one*, 17(8), e0261801. <https://doi.org/10.1371/journal.pone.0261801>
- D'Souza, L. J., Wright, S. H., & Bhattacharya, D. (2022). Genetic evidence that uptake of the fluorescent analog 2NBDG occurs independently of known glucose transporters. *PloS one*, 17(8), e0261801. <https://doi.org/10.1371/journal.pone.0261801>
- Dubova, E. A., Pavlov, K. A., Esayan, R. M., Degtyareva, E. I., Shestakova, M. V., Shchegolev, A. I., & Sukhikh, G. T. (2012). Vascular endothelial growth factor and its receptors in the placenta of women with type 1 diabetes mellitus. *Bulletin of experimental biology and medicine*, 152(3), 367–370. <https://doi.org/10.1007/s10517-012-1530-1>
- Easton, A. S., Liang, W. J., Poucher, S. M., Brady, H. J., & Lye, S. J. (2022). Transcriptomic and proteomic analysis of the BeWo trophoblastic cell line following induction of syncytial differentiation. *Placenta*, 119, 103–115. <https://doi.org/10.1016/j.placenta.2022.03.002>
- Easton, Z. J. W., Delhaes, F., Mathers, K., Zhao, L., Vanderboor, C. M. G., & Regnault, T. R. H. (2021). Syncytialization and prolonged exposure to palmitate impacts BeWo respiration. *Reproduction (Cambridge, England)*, 161(1), 73–88. <https://doi.org/10.1530/REP-19-0433>
- Eleftheriades, M., Papastefanou, I., Lambrinouadaki, I., Kappou, D., Lavranos, D., Akalestos, A., Souka, A. P., Pervanidou, P., Hassiakos, D., & Chrousos, G. P. (2014). Elevated placental growth factor concentrations at 11-14 weeks of gestation to predict gestational diabetes mellitus. *Metabolism: clinical and experimental*, 63(11), 1419–1425. <https://doi.org/10.1016/j.metabol.2014.07.016>
- Elhaik E. (2022). Principal Component Analyses (PCA)-based findings in population genetic studies are highly biased and must be reevaluated. *Scientific reports*, 12(1), 14683. <https://doi.org/10.1038/s41598-022-14395-4>
- El-Tarhouny, S. A., Almasry, S. M., Elfayomy, A. K., Baghdadi, H., & Habib, F. A. (2014). Placental growth factor and soluble Fms-like tyrosine kinase 1 in diabetic pregnancy: A possible relation to distal villous immaturity. *Histology and histopathology*, 29(2), 259–272. <https://doi.org/10.14670/HH-29.259>
- Farina, A., Eklund, E., Bernabini, D., Paladino, M., Righetti, F., Monti, G., & Lambert-Messerlian, G. (2017). A First-Trimester Biomarker Panel for Predicting the Development of

Gestational Diabetes. *Reproductive sciences* (Thousand Oaks, Calif.), 24(6), 954–959. <https://doi.org/10.1177/1933719116675057>.

- Feig, D. S., & Moses, R. G. (2011). Metformin therapy during pregnancy: good for the goose and good for the gosling too?. *Diabetes care*, 34(10), 2329–2330. <https://doi.org/10.2337/dc11-1153>
- Feig, D. S., & Moses, R. G. (2011). Metformin therapy during pregnancy: good for the goose and good for the gosling too?. *Diabetes care*, 34(10), 2329–2330. <https://doi.org/10.2337/dc11-1153>
- Feige, J. N., Lagouge, M., & Auwerx, J. (2008). Dietary manipulation of mouse metabolism. *Current protocols in molecular biology*, Chapter 29, . <https://doi.org/10.1002/0471142727.mb29b05s84>
- Ferrara, A., & Hedderson, M. M. (2017). Tackling disparities in the global burden of gestational diabetes. *American Journal of Public Health*, 107(8), 1225–1226.
- Flyvbjerg, A., Khatir, D. S., Jensen, L. J., Dagnaes-Hansen, F., Gronbaek, H., & Rasch, R. (2004). The involvement of growth hormone (GH), insulin-like growth factors (IGFs) and vascular endothelial growth factor (VEGF) in diabetic kidney disease. *Current pharmaceutical design*, 10(27), 3385–3394. <https://doi.org/10.2174/1381612043383106>
- Freshney, R. I. (2015). *Culture of animal cells: a manual of basic technique and specialized applications*. John Wiley & Sons.
- Friedman, J. E., Ishizuka, T., Shao, J., Huston, L., Highman, T., & Catalano, P. (1999). Impaired glucose transport and insulin receptor tyrosine phosphorylation in skeletal muscle from obese women with gestational diabetes. *Diabetes*, 48(9), 1807–1814. <https://doi.org/10.2337/diabetes.48.9.1807>
- Furman B. L. (2021). Streptozotocin-Induced Diabetic Models in Mice and Rats. *Current protocols*, 1(4), e78. <https://doi.org/10.1002/cpz1.78>
- Gan, S. D., & Patel, K. R. (2013). Enzyme immunoassay and enzyme-linked immunosorbent assay. *The Journal of investigative dermatology*, 133(9), e12. <https://doi.org/10.1038/jid.2013.287>
- Gilbert M. (2021). Role of skeletal muscle lipids in the pathogenesis of insulin resistance of obesity and type 2 diabetes. *Journal of diabetes investigation*, 12(11), 1934–1941. <https://doi.org/10.1111/jdi.13614>

- Gill, J. S., Salafia, C. M., Grebenkov, D., & Vvedensky, D. D. (2011). Modeling oxygen transport in human placental terminal villi. *Journal of theoretical biology*, 291, 33–41. <https://doi.org/10.1016/j.jtbi.2011.09.008>.
- Goyal, A., Gupta, Y., Singla, R., Kalra, S., & Tandon, N. (2020). American Diabetes Association "Standards of Medical Care-2020 for Gestational Diabetes Mellitus": A Critical Appraisal. *Diabetes therapy : research, treatment and education of diabetes and related disorders*, 11(8), 1639–1644. <https://doi.org/10.1007/s13300-020-00865-3>.
- Grahovac, J., Pavlović, M., & Ostojić, M. (2021). A Fluorescence-Based Assay for Measuring Glucose Uptake in Living Melanoma Cells. *Methods in molecular biology (Clifton, N.J.)*, 2265, 73–80. https://doi.org/10.1007/978-1-0716-1205-7_5
- Guariguata, L., Linnenkamp, U., Beagley, J., Whiting, D. R., & Cho, N. H. (2014). Global estimates of the prevalence of hyperglycaemia in pregnancy. *Diabetes research and clinical practice*, 103(2), 176–185. <https://doi.org/10.1016/j.diabres.2013.11.003>
- Gui, J., Rohrbach, A., Borns, K., Hillemanns, P., Feng, L., Hubel, C. A., & von Versen-Höyneck, F. (2015). Vitamin D rescues dysfunction of fetal endothelial colony forming cells from individuals with gestational diabetes. *Placenta*, 36(4), 410–418. <https://doi.org/10.1016/j.placenta.2015.01.195>
- Gui, J., Rohrbach, A., Borns, K., Hillemanns, P., Feng, L., Hubel, C. A., & von Versen-Höyneck, F. (2015). Vitamin D rescues dysfunction of fetal endothelial colony forming cells from individuals with gestational diabetes. *Placenta*, 36(4), 410–418. <https://doi.org/10.1016/j.placenta.2015.01.195>
- Guo, Y., Zhang, Y., Zhang, L., Zhang, X., Fan, Y., Yang, Z., Xiao, Y., Cai, D., & Liu, Y. (2020). Proteomics analysis of insulin resistance in skeletal muscle cells by using an improved two-dimensional gel electrophoresis approach. *Journal of Proteomics*, 223, 103825. <https://doi.org/10.1016/j.jprot.2020.103825>
- Gupta, A. K., Hasler, P., Holzgreve, W., & Hahn, S. (2007). Neutrophil NETs: a novel contributor to preeclampsia-associated placental hypoxia?. *Seminars in immunopathology*, 29(2), 163–167. <https://doi.org/10.1007/s00281-007-0073-4>.
- Haas, U., Sczakiel, G., & Laufer, S. D. (2012). MicroRNA-mediated regulation of gene expression is affected by disease-associated SNPs within the 3'-UTR via altered RNA structure. *RNA biology*, 9(6), 924–937. <https://doi.org/10.4161/rna.20497>
- Hamilton, K. E., Bouwer, M. F., Louters, L. L., & Looyenga, B. D. (2021). Cellular binding and uptake of fluorescent glucose analogs 2-NBDG and 6-NBDG occurs independent of

membrane glucose transporters. *Biochimie*, 190, 1-11.
<https://doi.org/10.1016/j.biochi.2021.05.006>

- Hanada, Y., Ishihara, N., Wang, L. et al. MAVS is energized by Mff which senses mitochondrial metabolism via AMPK for acute antiviral immunity. *Nat Commun* 11, 5711 (2020). <https://doi.org/10.1038/s41467-020-19287-7>
- Handy, R. M., & Holloway, G. P. (2023). Insights into the development of insulin resistance: Unraveling the interaction of physical inactivity, lipid metabolism and mitochondrial biology. *Frontiers in Physiology*, 14, 1151389. <https://doi.org/10.3389/fphys.2023.1151389>
- HAPO Study Cooperative Research Group, Metzger, B. E., Lowe, L. P., Dyer, A. R., Trimble, E. R., Chaovarindr, U., Coustan, D. R., Hadden, D. R., McCance, D. R., Hod, M., McIntyre, H. D., Oats, J. J., Persson, B., Rogers, M. S., & Sacks, D. A. (2008). Hyperglycemia and adverse pregnancy outcomes. *The New England journal of medicine*, 358(19), 1991–2002. <https://doi.org/10.1056/NEJMoa0707943>
- HAPO Study Cooperative Research Group, Metzger, B. E., Lowe, L. P., Dyer, A. R., Trimble, E. R., Chaovarindr, U., Coustan, D. R., Hadden, D. R., McCance, D. R., Hod, M., McIntyre, H. D., Oats, J. J., Persson, B., Rogers, M. S., & Sacks, D. A. (2008). Hyperglycemia and adverse pregnancy outcomes. *The New England journal of medicine*, 358(19), 1991–2002. <https://doi.org/10.1056/NEJMoa0707943>
- Helske, S., Vuorela, P., Carpen, O., Hornig, C., Weich, H., & Halmesmaki, E. (2001). Expression of vascular endothelial growth factor receptors 1, 2 and 3 in placentas from normal and complicated pregnancies. *Molecular human reproduction*, 7(2), 205–210. <https://doi.org/10.1093/molehr/7.2.205>
- Hiden, U., Lang, I., Ghaffari-Tabrizi, N., Gauster, M., Lang, U., & Desoye, G. (2009). Insulin action on the human placental endothelium in normal and diabetic pregnancy. *Current vascular pharmacology*, 7(4), 460–466. <https://doi.org/10.2174/157016109789043973>
- Hill-Briggs, F., Adler, N. E., Berkowitz, S. A., Chin, M. H., Gary-Webb, T. L., Navas-Acien, A., Thornton, P. L., & Haire-Joshu, D. (2020). Social Determinants of Health and Diabetes: A Scientific Review. *Diabetes care*, 44(1), 258–279. Advance online publication. <https://doi.org/10.2337/dci20-0053>
- Hirst, J. E., Tran, T. S., Do, M. A., Rowena, F., Morris, J. M., & Jeffery, H. E. (2012). Women with gestational diabetes in Vietnam: a qualitative study to determine attitudes and health behaviours. *BMC pregnancy and childbirth*, 12, 81. <https://doi.org/10.1186/1471-2393-12-81>

- Hotamisligil G. S. (2006). Inflammation and metabolic disorders. *Nature*, 444(7121), 860–867. <https://doi.org/10.1038/nature05485>
- Houghton, A. M., Rzymkiewicz, D. M., Ji, H., Gregory, A. D., Egea, E. E., Metz, H. E., Stolz, D. B., Land, S. R., Marconcini, L. A., Kliment, C. R., Jenkins, K. M., Beaulieu, K. A., Mouded, M., Frank, S. J., Wong, K. K., & Shapiro, S. D. (2010). Neutrophil elastase-mediated degradation of IRS-1 accelerates lung tumor growth. *Nature medicine*, 16(2), 219–223. <https://doi.org/10.1038/nm.2084>
- Houghton, A.M.; Rzymkiewicz, D.M.; Ji, H.; Gregory, A.D.; Egea, E.E.; Metz, H.E.; Stolz, D.B.; Land, S.R.; Marconcini, L.A.; Kliment, C.R.; et al. Neutrophil elastase-mediated degradation of IRS-1 accelerates lung tumor growth. *Nat. Med.* 2010,16, 219–223. <https://doi.org/10.2147/DMSO.S433179>
- Huang, R., Chen, Z., He, L., He, N., Xi, Z., Li, Z., Deng, Y., & Zeng, X. (2017). Mass spectrometry-assisted gel-based proteomics in cancer biomarker discovery: approaches and application. *Theranostics*, 7(14), 3559–3572. <https://doi.org/10.7150/thno.20797>
- Hughes, R. C., Moore, M. P., Gullam, J. E., Mohamed, K., & Rowan, J. (2014). An early pregnancy HbA1c $\geq 5.9\%$ (41 mmol/mol) is optimal for detecting diabetes and identifies women at increased risk of adverse pregnancy outcomes. *Diabetes care*, 37(11), 2953–2959. <https://doi.org/10.2337/dc14-1312>
- Huhn, E. A., Rossi, S. W., Hoesli, I., & Göbl, C. S. (2018). Controversies in Screening and Diagnostic Criteria for Gestational Diabetes in Early and Late Pregnancy. *Frontiers in endocrinology*, 9, 696. <https://doi.org/10.3389/fendo.2018.00696>
- Hulatt, C. J., Smolina, I., Dowle, A., Kopp, M., Vasanth, G. K., Hoarau, G. G., Wijffels, R. H., & Kiron, V. (2020). Proteomic and Transcriptomic Patterns during Lipid Remodeling in *Nannochloropsis gaditana*. *International journal of molecular sciences*, 21(18), 6946. <https://doi.org/10.3390/ijms21186946>
- Hulme, C. H., Stevens, A., Dunn, W., Heazell, A. E. P., Hollywood, K., Begley, P., Westwood, M., & Myers, J. E. (2018). Identification of the functional pathways altered by placental cell exposure to high glucose: lessons from the transcript and metabolite interactome. *Scientific reports*, 8(1), 5270. <https://doi.org/10.1038/s41598-018-22535-y>
- Husslein, H., Lausegger, F., Leipold, H., & Worda, C. (2012). Association between pregnancy-associated plasma protein-A and gestational diabetes requiring insulin treatment at 11-14 weeks of gestation. *The journal of maternal-fetal & neonatal medicine : the official journal of the European Association of Perinatal Medicine, the Federation of Asia and Oceania Perinatal*

Societies, the International Society of Perinatal Obstetricians, 25(11), 2230–2233. <https://doi.org/10.3109/14767058.2012.684170>

- Husslein, H., Lausegger, F., Leipold, H., & Worda, C. (2012). Association between pregnancy-associated plasma protein-A and gestational diabetes requiring insulin treatment at 11-14 weeks of gestation. *The journal of maternal-fetal & neonatal medicine : the official journal of the European Association of Perinatal Medicine, the Federation of Asia and Oceania Perinatal Societies, the International Society of Perinatal Obstetricians*, 25(11), 2230–2233. <https://doi.org/10.3109/14767058.2012.684170>
- International Association of Diabetes and Pregnancy Study Groups Consensus Panel, Metzger, B. E., Gabbe, S. G., Persson, B., Buchanan, T. A., Catalano, P. A., Damm, P., Dyer, A. R., Leiva, A.d, Hod, M., Kitzmiller, J. L., Lowe, L. P., McIntyre, H. D., Oats, J. J., Omori, Y., & Schmidt, M. I. (2010). International association of diabetes and pregnancy study groups recommendations on the diagnosis and classification of hyperglycemia in pregnancy. *Diabetes care*, 33(3), 676–682. <https://doi.org/10.2337/dc09-1848>
- International Association of Diabetes and Pregnancy Study Groups. (2010). International Association of Diabetes and Pregnancy Study Groups recommendations on the diagnosis and classification of hyperglycemia in pregnancy. *Diabetes Care*, 33(3), 676-682. <https://doi.org/10.2337/dc09-1848>
- International Association of Diabetes and Pregnancy Study Groups Consensus Panel, Metzger, B. E., Gabbe, S. G., Persson, B., Buchanan, T. A., Catalano, P. A., Damm, P., Dyer, A. R., Leiva, A.d, Hod, M., Kitzmiller, J. L., Lowe, L. P., McIntyre, H. D., Oats, J. J., Omori, Y., & Schmidt, M. I. (2010). International association of diabetes and pregnancy study groups recommendations on the diagnosis and classification of hyperglycemia in pregnancy. *Diabetes care*, 33(3), 676–682. <https://doi.org/10.2337/dc09-1848>
- International Association of Diabetes and Pregnancy Study Groups Consensus Panel, Metzger, B. E., Gabbe, S. G., Persson, B., Buchanan, T. A., Catalano, P. A., Damm, P., Dyer, A. R., Leiva, A.d, Hod, M., Kitzmiller, J. L., Lowe, L. P., McIntyre, H. D., Oats, J. J., Omori, Y., & Schmidt, M. I. (2010). International association of diabetes and pregnancy study groups recommendations on the diagnosis and classification of hyperglycemia in pregnancy. *Diabetes care*, 33(3), 676–682. <https://doi.org/10.2337/dc09-1848>
- International Diabetes Federation. *IDF Diabetes Atlas*, 8th ed.; IDF: Brussels, Belgium, 2017.
- Jagannathan, R., Neves, J. S., Dorcely, B., Chung, S. T., Tamura, K., Rhee, M., & Bergman, M. (2020). The Oral Glucose Tolerance Test: 100 Years Later. *Diabetes, metabolic*

syndrome and obesity : targets and therapy, 13, 3787–3805.
<https://doi.org/10.2147/DMSO.S246062>

- Janota, J., Pomyje, J., Toth, D., Sosna, O., Zivný, J., Kuzel, D., Stranák, Z., Necas, E., & Zivný, J. H. (2003). Expression of angiopoietic factors in normal and type-I diabetes human placenta: a pilot study. *European journal of obstetrics, gynecology, and reproductive biology*, 111(2), 153–156. [https://doi.org/10.1016/s0301-2115\(03\)00204-5](https://doi.org/10.1016/s0301-2115(03)00204-5)
- Jelliffe-Pawlowski, L. L., Baer, R. J., Blumenfeld, Y. J., Ryckman, K. K., O'Brodovich, H. M., Gould, J. B., Druzin, M. L., El-Sayed, Y. Y., Lyell, D. J., Stevenson, D. K., Shaw, G. M., & Currier, R. J. (2015). Maternal characteristics and mid-pregnancy serum biomarkers as risk factors for subtypes of preterm birth. *BJOG : an international journal of obstetrics and gynaecology*, 122(11), 1484–1493. <https://doi.org/10.1111/1471-0528.13495>
- Jensen, D. M., Damm, P., Sørensen, B., Mølsted-Pedersen, L., Westergaard, J. G., Korsholm, L., Ovesen, P., & Beck-Nielsen, H. (2003). Proposed diagnostic thresholds for gestational diabetes mellitus according to a 75-g oral glucose tolerance test. Maternal and perinatal outcomes in 3260 Danish women. *Diabetic medicine : a journal of the British Diabetic Association*, 20(1), 51–57. <https://doi.org/10.1046/j.1464-5491.2003.00857.x>
- Jheng, H. F., Tsai, P. J., Guo, S. M., Kuo, L. H., Chang, C. S., Su, I. J., Chang, C. R., & Tsai, Y. S. (2012). Mitochondrial fission contributes to mitochondrial dysfunction and insulin resistance in skeletal muscle. *Molecular and cellular biology*, 32(2), 309–319. <https://doi.org/10.1128/MCB.05603-11>
- Jiang, C., Kim, J. H., Li, F., Qu, A., Gavrilova, O., Shah, Y. M., & Gonzalez, F. J. (2013). Hypoxia-inducible factor 1 α regulates a SOCS3–STAT3–adiponectin signal transduction pathway in adipocytes. *Journal of Biological Chemistry*, 288(6), 3844–3857. <https://doi.org/10.1074/jbc.M112.426338>
- Jirkovská, M., Kubínová, L., Janáček, J., Moravcová, M., Krejčí, V., & Karen, P. (2002). Topological properties and spatial organization of villous capillaries in normal and diabetic placentas. *Journal of vascular research*, 39(3), 268–278. <https://doi.org/10.1159/000063692>
- Jolliffe, I. T., & Cadima, J. (2016). Principal component analysis: a review and recent developments. *Philosophical Transactions of the Royal Society A: Mathematical, Physical and Engineering Sciences*, 374(2065), 20150202. <https://doi.org/10.1098/rsta.2015.0202>
- Jones, C. J., Hartmann, M., Blaschitz, A., & Desoye, G. (2019). Ultrastructural changes in the placenta in pregnancies complicated by type 1 diabetes with and without premature delivery. *Placenta*, 83, 37–46. <https://doi.org/10.1016/j.placenta.2019.06.369>

- Joshi, N. P., Mane, A. R., Sahay, A. S., Sundrani, D. P., Joshi, S. R., & Yajnik, C. S. (2022). Role of Placental Glucose Transporters in Determining Fetal Growth. *Reproductive sciences (Thousand Oaks, Calif.)*, 29(10), 2744–2759. <https://doi.org/10.1007/s43032-021-00699-9>
- Kapur A. (2015). Links between maternal health and NCDs. *Best practice & research. Clinical obstetrics & gynaecology*, 29(1), 32–42. <https://doi.org/10.1016/j.bpobgyn.2014.04.016>
- Key M. (2012). A tutorial in displaying mass spectrometry-based proteomic data using heat maps. *BMC bioinformatics*, 13 Suppl 16(Suppl 16), S10. <https://doi.org/10.1186/1471-2105-13-S16-S10>
- Khandpur, R., Carmona-Rivera, C., Vivekanandan-Giri, A., Gizinski, A., Yalavarthi, S., Knight, J. S., Friday, S., Li, S., Patel, R. M., Subramanian, V., Thompson, P., Chen, P., Fox, D. A., Pennathur, S., & Kaplan, M. J. (2013). NETs are a source of citrullinated autoantigens and stimulate inflammatory responses in rheumatoid arthritis. *Science translational medicine*, 5(178), 178ra40. <https://doi.org/10.1126/scitranslmed.3005580>
- Khandpur, R., Carmona-Rivera, C., Vivekanandan-Giri, A., Gizinski, A., Yalavarthi, S., Knight, J. S., Friday, S., Li, S., Patel, R. M., Subramanian, V., Thompson, P., Chen, P., Fox, D. A., Pennathur, S., & Kaplan, M. J. (2013). NETs are a source of citrullinated autoantigens and stimulate inflammatory responses in rheumatoid arthritis. *Science translational medicine*, 5(178), 178ra40. <https://doi.org/10.1126/scitranslmed.3005580>
- Kim, Y. R., & Hong, S. H. (2015). Association between the polymorphisms of the vascular endothelial growth factor gene and metabolic syndrome. *Biomedical reports*, 3(3), 319–326. <https://doi.org/10.3892/br.2015.423>
- Kirwan, J. P., Hauguel-De Mouzon, S., Lepercq, J., Challier, J. C., Huston-Presley, L., Friedman, J. E., Kalhan, S. C., & Catalano, P. M. (2002). TNF-alpha is a predictor of insulin resistance in human pregnancy. *Diabetes*, 51(7), 2207–2213. <https://doi.org/10.2337/diabetes.51.7.2207>
- Knapp, E. A., Kress, A. M., Parker, C. B., Page, G. P., McArthur, K., Gachigi, K. K., Alshawabkeh, A. N., Aschner, J. L., Bastain, T. M., Breton, C. V., Bendixsen, C. G., Brennan, P. A., Bush, N. R., Buss, C., Camargo, C. A., Jr, Catellier, D., Cordero, J. F., Croen, L., Dabelea, D., Deoni, S., ... Influences On Child Health Outcomes, O. B. O. P. C. F. E. (2023). The Environmental Influences on Child Health Outcomes (ECHO)-Wide Cohort. *American journal of epidemiology*, 192(8), 1249–1263. <https://doi.org/10.1093/aje/kwad071>
- Kokkinopoulou, I., Maratou, E., Mitrou, P., Boutati, E., Sideris, D. C., Fragoulis, E. G., & Christodoulou, M. I. (2019). Decreased expression of microRNAs targeting type-2 diabetes

susceptibility genes in peripheral blood of patients and predisposed individuals. *Endocrine*, 66(2), 226–239. <https://doi.org/10.1007/s12020-019-02062-0>

- Kottaisamy, C. P. D., Raj, D. S., Prasanth Kumar, V., & Sankaran, U. (2021). Experimental animal models for diabetes and its related complications-a review. *Laboratory animal research*, 37(1), 23. <https://doi.org/10.1186/s42826-021-00101-4>
- Kralisch, S., Bluher, M., Paschke, R., Stumvoll, M., & Fasshauer, M. (2007). Adipokines and adipocyte targets in the future management of obesity and the metabolic syndrome. *Mini reviews in medicinal chemistry*, 7(1), 39–45. <https://doi.org/10.2174/138955707779317821>
- Krzysztofik, J. M., Walaszczyk, A., Pauk, M., Wajda, A., Braksator, W., & Mamcarz, A. (2022). Proteomics in cardiovascular medicine-analytical methods, applications, and challenges. *Journal of Clinical Medicine*, 11(4), 1124. <https://doi.org/10.3390/jcm11041124>
- Kumar, M., Ang, L. T., Ho, C., Soh, S. E., Tan, K. H., Chan, J. K. Y., Godfrey, K. M., Chan, S. Y., Chong, Y. S., Eriksson, J. G., Feng, M., & Karnani, N. (2022). Machine Learning-Derived Prenatal Predictive Risk Model to Guide Intervention and Prevent the Progression of Gestational Diabetes Mellitus to Type 2 Diabetes: Prediction Model Development Study. *JMIR diabetes*, 7(3), e32366. <https://doi.org/10.2196/32366>
- Lacroix, M., Battista, M. C., Doyon, M., Ménard, J., Ardilouze, J. L., Perron, P., & Hivert, M. F. (2013). Lower adiponectin levels at first trimester of pregnancy are associated with increased insulin resistance and higher risk of developing gestational diabetes mellitus. *Diabetes care*, 36(6), 1577–1583. <https://doi.org/10.2337/dc12-1731>
- Langsenlehner, U., Hofmann, G., Renner, W., Gerger, A., Krenn-Pilko, S., Thurner, E. M., Krippel, P., & Langsenlehner, T. (2015). Association of vascular endothelial growth factor--a gene polymorphisms and haplotypes with breast cancer metastases. *Acta oncologica (Stockholm, Sweden)*, 54(3), 368–376. <https://doi.org/10.3109/0284186X.2014.948056>
- Lappas M. (2014). Markers of endothelial cell dysfunction are increased in human omental adipose tissue from women with pre-existing maternal obesity and gestational diabetes. *Metabolism: clinical and experimental*, 63(6), 860–873. <https://doi.org/10.1016/j.metabol.2014.03.007>
- Lappas, M., Hiden, U., Desoye, G., Froehlich, J., Hauguel-de Mouzon, S., & Jawerbaum, A. (2011). The role of oxidative stress in the pathophysiology of gestational diabetes mellitus. *Antioxidants & redox signaling*, 15(12), 3061–3100. <https://doi.org/10.1089/ars.2010.3765>
- Lappas, M., Hiden, U., Desoye, G., Froehlich, J., Hauguel-de Mouzon, S., & Jawerbaum, A. (2011). The role of oxidative stress in the pathophysiology of gestational diabetes mellitus. *Antioxidants & redox signaling*, 15(12), 3061–3100. <https://doi.org/10.1089/ars.2010.3765>

- Lappas, M., Yee, K., Permezel, M., & Rice, G. E. (2005). Release and regulation of leptin, resistin and adiponectin from human placenta, fetal membranes, and maternal adipose tissue and skeletal muscle from normal and gestational diabetes mellitus-complicated pregnancies. *The Journal of endocrinology*, 186(3), 457–465. <https://doi.org/10.1677/joe.1.06227>
- Law, K. P., Zhang, H., Tam, W. H., & Lau, A. Y. (2017). Gestational diabetes mellitus: Screening, diagnosis and prognosis. *International Journal of Molecular Sciences*, 18(8), 1794. <https://doi.org/10.3390/ijms18081794>
- Leach, L., Gray, C., Staton, S., Babawale, M. O., Gruchy, A., Foster, C., Mayhew, T. M., & James, D. K. (2004). Vascular endothelial cadherin and beta-catenin in human fetoplacental vessels of pregnancies complicated by Type 1 diabetes: associations with angiogenesis and perturbed barrier function. *Diabetologia*, 47(4), 695–709. <https://doi.org/10.1007/s00125-004-1341-7>
- Ledesma, R. D., Valero-Mora, P., & Macbeth, G. (2015). The Scree Test and the Number of Factors: a Dynamic Graphics Approach. *The Spanish journal of psychology*, 18, E11. <https://doi.org/10.1017/sjp.2015.13>
- Lee, E. Y., Chung, C. H., Kim, J. H., Joung, H. J., & Hong, S. Y. (2006). Antioxidants ameliorate the expression of vascular endothelial growth factor mediated by protein kinase C in diabetic podocytes. *Nephrology, dialysis, transplantation : official publication of the European Dialysis and Transplant Association - European Renal Association*, 21(6), 1496–1503. <https://doi.org/10.1093/ndt/gfl022>
- Lever, J., Krzywinski, M., & Altman, N. (2017). Principal component analysis. *Nature Methods*, 14(7), 641-642. <https://doi.org/10.1038/nmeth.4346>
- Li W. (2012). Volcano plots in analyzing differential expressions with mRNA microarrays. *Journal of bioinformatics and computational biology*, 10(6), 1231003. <https://doi.org/10.1142/S0219720012310038>
- Li, J., Cai, Z., Vaites, L. P., Shen, N., Mitchell, D. C., Huttlin, E. L., Paulo, J. A., Harry, B. L., & Gygi, S. P. (2021). Proteome-wide mapping of short-lived proteins in human cells. *Molecular cell*, 81(22), 4722–4735.e5. <https://doi.org/10.1016/j.molcel.2021.09.015>
- Li, P., Hu, S., Zhu, Y., Sun, T., Huang, Y., Xu, Z., Liu, H., Luo, C., Zhou, S., Tan, A., & Liu, L. (2022). Associations of Plasma Fatty Acid Patterns During Pregnancy With Gestational Diabetes Mellitus. *Frontiers in nutrition*, 9, 836115. <https://doi.org/10.3389/fnut.2022.836115>
- Li, Y., Huang, C., Ding, L., Li, Z., Pan, Y., & Gao, X. (2021). Deep learning in bioinformatics: Introduction, application, and perspective in the big data era. *Methods*, 166, 4-21. <https://doi.org/10.1016/j.ymeth.2019.04.008>

- Li, Y., Li, R., Luo, X., Xu, F., Yang, M., Zheng, L., Wu, Q., Jiang, W., & Li, Y. (2023). Vascular endothelial growth factor B regulates insulin secretion in β cells of type 2 diabetes mellitus mice via PLC γ and the IP3R-evoked Ca²⁺/CaMK2 signaling pathway. *Molecular medicine reports*, 28(4), 197. <https://doi.org/10.3892/mmr.2023.13084>
- Lilao-Garzón, J., Valverde-Tercedor, C., Muñoz-Descalzo, S., Brito-Casillas, Y., & Wägner, A. M. (2021). In Vivo and In Vitro Models of Diabetes: A Focus on Pregnancy. *Advances in experimental medicine and biology*, 1307, 553–576. https://doi.org/10.1007/5584_2020_536
- Liu, X., Sun, J., Wen, X., Duan, J., Xue, D., Pan, Y., Sun, J., Zhang, W., Cheng, X., & Wang, C. (2020). Proteome profiling of gestational diabetes mellitus at 16-18 weeks revealed by LC-MS/MS. *Journal of clinical laboratory analysis*, 34(9), e23424. <https://doi.org/10.1002/jcla.23424>
- Liu, X., Sun, J., Wen, X., Duan, J., Xue, D., Pan, Y., Sun, J., Zhang, W., Cheng, X., & Wang, C. (2020). Proteome profiling of gestational diabetes mellitus at 16-18 weeks revealed by LC-MS/MS. *Journal of clinical laboratory analysis*, 34(9), e23424. <https://doi.org/10.1002/jcla.23424>
- Liu, Y., Li, D. Y., Bolatai, A., & Wu, N. (2023). Progress in Research on Biomarkers of Gestational Diabetes Mellitus and Preeclampsia. *Diabetes, metabolic syndrome and obesity : targets and therapy*, 16, 3807–3815. <https://doi.org/10.2147/DMSO.S433179>
- López-Soldado, I., & Herrera, E. (2003). Different diabetogenic response to moderate doses of streptozotocin in pregnant rats, and its long-term consequences in the offspring. *Experimental diabetes research*, 4(2), 107–118. <https://doi.org/10.1155/EDR.2003.107>
- Lowe, W. L., Jr, Scholtens, D. M., Lowe, L. P., Kuang, A., Nodzenski, M., Talbot, O., Catalano, P. M., Linder, B., Brickman, W. J., Clayton, P., Deerochanawong, C., Hamilton, J., Josefson, J. L., Lashley, M., Lawrence, J. M., Lebenthal, Y., Ma, R., Maresh, M., McCance, D., Tam, W. H., ... HAPO Follow-up Study Cooperative Research Group (2018). Association of Gestational Diabetes With Maternal Disorders of Glucose Metabolism and Childhood Adiposity. *JAMA*, 320(10), 1005–1016. <https://doi.org/10.1001/jama.2018.11628>
- Lowe, W. L., Jr, Scholtens, D. M., Lowe, L. P., Kuang, A., Nodzenski, M., Talbot, O., Catalano, P. M., Linder, B., Brickman, W. J., Clayton, P., Deerochanawong, C., Hamilton, J., Josefson, J. L., Lashley, M., Lawrence, J. M., Lebenthal, Y., Ma, R., Maresh, M., McCance, D., Tam, W. H., ... HAPO Follow-up Study Cooperative Research Group (2018). Association of Gestational Diabetes With Maternal Disorders of Glucose Metabolism and Childhood Adiposity. *JAMA*, 320(10), 1005–1016. <https://doi.org/10.1001/jama.2018.11628>

- Lu, W., & Hu, C. (2022). Molecular biomarkers for gestational diabetes mellitus and postpartum diabetes. *Chinese medical journal*, 135(16), 1940–1951. <https://doi.org/10.1097/CM9.0000000000002160>
- Ma, K., Zhang, Y., Zhao, J., Zhou, L., & Li, M. (2024). Endoplasmic reticulum stress: bridging inflammation and obesity-associated adipose tissue. *Frontiers in immunology*, 15, 1381227. <https://doi.org/10.3389/fimmu.2024.1381227>
- Mac-Marcjanek, K., Zieleniak, A., Zurawska-Klis, M., Cypriak, K., Wozniak, L., & Wojcik, M. (2018). Expression Profile of Diabetes-Related Genes Associated with Leukocyte Sirtuin 1 Overexpression in Gestational Diabetes. *International journal of molecular sciences*, 19(12), 3826. <https://doi.org/10.3390/ijms19123826>
- Madazli, R., Tuten, A., Calay, Z., Uzun, H., Uludag, S., & Ocak, V. (2008). The incidence of placental abnormalities, maternal and cord plasma malondialdehyde and vascular endothelial growth factor levels in women with gestational diabetes mellitus and nondiabetic controls. *Gynecologic and obstetric investigation*, 65(4), 227–232. <https://doi.org/10.1159/000113045>
- Maged, A. M., Moety, G. A., Mostafa, W. A., & Hamed, D. A. (2014). Comparative study between different biomarkers for early prediction of gestational diabetes mellitus. *The journal of maternal-fetal & neonatal medicine : the official journal of the European Association of Perinatal Medicine, the Federation of Asia and Oceania Perinatal Societies, the International Society of Perinatal Obstetricians*, 27(11), 1108–1112. <https://doi.org/10.3109/14767058.2013.850489>
- Marcantoni, E., Dovizio, M., O'Gaora, P., Di Francesco, L., Bendaya, I., Schiavone, S., Trenti, A., Guillem-Llobat, P., Zambon, A., Nardelli, G. B., Trevisi, L., Patrignani, P., & Belton, O. (2015). Dysregulation of gene expression in human fetal endothelial cells from gestational diabetes in response to TGF- β 1. *Prostaglandins & other lipid mediators*, 120, 103–114. <https://doi.org/10.1016/j.prostaglandins.2015.03.004>
- Marcantoni, E., Dovizio, M., O'Gaora, P., Di Francesco, L., Bendaya, I., Schiavone, S., Trenti, A., Guillem-Llobat, P., Zambon, A., Nardelli, G. B., Trevisi, L., Patrignani, P., & Belton, O. (2015). Dysregulation of gene expression in human fetal endothelial cells from gestational diabetes in response to TGF- β 1. *Prostaglandins & other lipid mediators*, 120, 103–114. <https://doi.org/10.1016/j.prostaglandins.2015.03.004>
- Martínez, N., Capobianco, E., White, V., Pustovrh, M. C., Higa, R., & Jawerbaum, A. (2008). Peroxisome proliferator-activated receptor alpha activation regulates lipid metabolism in the fetoplacental unit from diabetic rats. *Reproduction (Cambridge, England)*, 136(1), 95–103. <https://doi.org/10.1530/REP-08-0028>

- McIntyre, H. D., Catalano, P., Zhang, C., Desoye, G., Mathiesen, E. R., & Damm, P. (2019). Gestational diabetes mellitus. *Nature reviews. Disease primers*, 5(1), 47. <https://doi.org/10.1038/s41572-019-0098-8>
- Menegazzo, L., Ciciliot, S., Poncina, N., Mazzucato, M., Persano, M., Bonora, B., Albiero, M., Vigili de Kreutzenberg, S., Avogaro, A., & Fadini, G. P. (2015). NETosis is induced by high glucose and associated with type 2 diabetes. *Acta diabetologica*, 52(3), 497–503. <https://doi.org/10.1007/s00592-014-0676-x>
- Menegazzo, L., Ciciliot, S., Poncina, N., Mazzucato, M., Persano, M., Bonora, B., Albiero, M., Vigili de Kreutzenberg, S., Avogaro, A., & Fadini, G. P. (2015). NETosis is induced by high glucose and associated with type 2 diabetes. *Acta diabetologica*, 52(3), 497–503. <https://doi.org/10.1007/s00592-014-0676-x>
- Menegazzo, L., Ciciliot, S., Poncina, N., Mazzucato, M., Persano, M., Bonora, B., Albiero, M., Vigili de Kreutzenberg, S., Avogaro, A., & Fadini, G. P. (2015). NETosis is induced by high glucose and associated with type 2 diabetes. *Acta diabetologica*, 52(3), 497–503. <https://doi.org/10.1007/s00592-014-0676-x>
- Meng, Q., Shao, L., Luo, X., Mu, Y., Xu, W., Gao, L., Xu, H., & Cui, Y. (2016). Expressions of VEGF-A and VEGFR-2 in placentae from GDM pregnancies. *Reproductive biology and endocrinology : RB&E*, 14(1), 61. <https://doi.org/10.1186/s12958-016-0191-8>
- Meng, Q., Shao, L., Luo, X., Mu, Y., Xu, W., Gao, L., Xu, H., & Cui, Y. (2016). Expressions of VEGF-A and VEGFR-2 in placentae from GDM pregnancies. *Reproductive biology and endocrinology : RB&E*, 14(1), 61. <https://doi.org/10.1186/s12958-016-0191-8>
- Merz, K. E., & Thurmond, D. C. (2020). Role of Skeletal Muscle in Insulin Resistance and Glucose Uptake. *Comprehensive Physiology*, 10(3), 785–809. <https://doi.org/10.1002/cphy.c190029>
- Merz, K. E., & Thurmond, D. C. (2020). Role of Skeletal Muscle in Insulin Resistance and Glucose Uptake. *Comprehensive Physiology*, 10(3), 785–809. <https://doi.org/10.1002/cphy.c190029>
- Metzger, B. E., Lowe, L. P., Dyer, A. R., Trimble, E. R., Chaovarindr, U., Coustan, D. R., ... & Sacks, D. A. (2008). Hyperglycemia and adverse pregnancy outcomes. HAPO study cooperative research group. *N Engl J Med*, 358(19), 1991-2002.
- Mishra, P., Kumari, B., & Pandey, S. K. (2020). Advancement and applications of principal component analysis in multivariate analysis. *Biostatistics and Biometrics Open Access Journal*, 9(4), 112-116. <https://doi.org/10.19080/BBOAJ.2020.09.555766>

- Moessinger, C., Nilsson, I., Muhl, L., Zeitelhofer, M., Heller Sahlgren, B., Skogsberg, J., & Eriksson, U. (2020). VEGF-B signaling impairs endothelial glucose transcytosis by decreasing membrane cholesterol content. *EMBO reports*, 21(7), e49343. <https://doi.org/10.15252/embr.201949343>
- Moore, D. S., Notz, W. I., & Flinger, M. A. (2013). *The basic practice of statistics* (6th ed.). New York, NY: W.H. Freeman and Company.
- Moraes-Vieira, P. M., Saghatelian, A., & Kahn, B. B. (2016). GLUT4 Expression in Adipocytes Regulates De Novo Lipogenesis and Levels of a Novel Class of Lipids With Antidiabetic and Anti-inflammatory Effects. *Diabetes*, 65(7), 1808–1815. <https://doi.org/10.2337/db16-0221>
- Moraes-Vieira, P. M., Saghatelian, A., & Kahn, B. B. (2020). GLUT4 expression in adipocytes regulates de novo lipogenesis and levels of a novel class of lipids with antidiabetic and anti-inflammatory effects. *Diabetes*, 69(7), 1518-1531. <https://doi.org/10.2337/db19-0892>
- Moreli, J. B., Morceli, G., De Luca, A. K., Magalhães, C. G., Costa, R. A., Damasceno, D. C., Rudge, M. V., & Calderon, I. M. (2012). Influence of maternal hyperglycemia on IL-10 and TNF- α production: the relationship with perinatal outcomes. *Journal of clinical immunology*, 32(3), 604–610. <https://doi.org/10.1007/s10875-011-9634-3>
- Moreli, J. B., Morceli, G., De Luca, A. K., Magalhães, C. G., Costa, R. A., Damasceno, D. C., Rudge, M. V., & Calderon, I. M. (2012). Influence of maternal hyperglycemia on IL-10 and TNF- α production: the relationship with perinatal outcomes. *Journal of clinical immunology*, 32(3), 604–610. <https://doi.org/10.1007/s10875-011-9634-3>
- Moses, R. G., Morris, G. J., Petocz, P., San Gil, F., & Garg, D. (2011). The impact of potential new diagnostic criteria on the prevalence of gestational diabetes mellitus in Australia. *The Medical journal of Australia*, 194(7), 338–340. <https://doi.org/10.5694/j.1326-5377.2011.tb03001.x>
- Moyce Gruber BL, Dolinsky VW. The Role of Adiponectin during Pregnancy and Gestational Diabetes. *Life*. 2023; 13(2):301. <https://doi.org/10.3390/life13020301>
- Moyce, B. L., & Dolinsky, V. W. (2018). Maternal β -Cell Adaptations in Pregnancy and Placental Signalling: Implications for Gestational Diabetes. *International journal of molecular sciences*, 19(11), 3467. <https://doi.org/10.3390/ijms19113467>
- Mulla, M. J., Salmon, J. E., Chamley, L. W., Brosens, J. J., Boeras, C. M., Kavathas, P. B., & Abrahams, V. M. (2013). A role for uric acid and the Nalp3 inflammasome in antiphospholipid antibody-induced IL-1 β production by human first trimester trophoblast. *PloS one*, 8(6), e65237. <https://doi.org/10.1371/journal.pone.0065237>

- Mulla, M. J., Yu, A. G., Cardenas, I., Guller, S., Panda, B., & Abrahams, V. M. (2009). Regulation of Nod1 and Nod2 in first trimester trophoblast cells. *American journal of reproductive immunology (New York, N.Y. : 1989)*, 61(4), 294–302. <https://doi.org/10.1111/j.1600-0897.2009.00694.x>
- Mwanri, A. W., Kinabo, J., Ramaiya, K., & Feskens, E. J. (2015). Gestational diabetes mellitus in sub-Saharan Africa: systematic review and metaregression on prevalence and risk factors. *Tropical medicine & international health : TM & IH*, 20(8), 983–1002. <https://doi.org/10.1111/tmi.12521>
- Nahavandi, S., Seah, J. M., Shub, A., Houlihan, C., & Ekinici, E. I. (2018). Biomarkers for Macrosomia Prediction in Pregnancies Affected by Diabetes. *Frontiers in endocrinology*, 9, 407. <https://doi.org/10.3389/fendo.2018.00407>
- Nakamura, S., Ito, Y., Hayakawa, H., Aoki, S., Yamagata, T., & Osaka, H. (2023). Establishment of a flow cytometry screening method for patients with glucose transporter 1 deficiency syndrome. *Molecular genetics and metabolism reports*, 34, 100954. <https://doi.org/10.1016/j.ymgmr.2022.100954>
- Nardi, G. M., Ferrara, E., Converti, I., Cesarano, F., Scacco, S., Grassi, R., Gnoni, A., Grassi, F. R., & Rapone, B. (2020). Does Diabetes Induce the Vascular Endothelial Growth Factor (VEGF) Expression in Periodontal Tissues? A Systematic Review. *International journal of environmental research and public health*, 17(8), 2765. <https://doi.org/10.3390/ijerph17082765>
- Narushima, M., Kobayashi, N., Okitsu, T., Tanaka, Y., Li, S. A., Chen, Y., Miki, A., Tanaka, K., Nakaji, S., Takei, K., Gutierrez, A. S., Rivas-Carrillo, J. D., Navarro-Alvarez, N., Jun, H. S., Westerman, K. A., Noguchi, H., Lakey, J. R., Leboulch, P., Tanaka, N., & Yoon, J. W. (2005). A human beta-cell line for transplantation therapy to control type 1 diabetes. *Nature biotechnology*, 23(10), 1274–1282. <https://doi.org/10.1038/nbt1145>
- Natarajan, S., & Remick, D. G. (2008). The ELISA Standard Save: calculation of sample concentrations in assays with a failed standard curve. *Journal of immunological methods*, 336(2), 242–245. <https://doi.org/10.1016/j.jim.2008.04.001>
- National Diabetes Data Group. (1979). Classification and diagnosis of diabetes mellitus and other categories of glucose intolerance. *Diabetes*, 28(12), 1039-1057. <https://doi.org/10.2337/diab.28.12.1039>
- Oludare, G. O., & Iranloye, B. O. (2016). Implantation and pregnancy outcome of Sprague–Dawley rats fed with low and high salt diet. *Middle East Fertility Society Journal*, 21(4), 228-235.

- O'Neil, R. G., Wu, L., & Mullani, N. (2005). Uptake of a fluorescent deoxyglucose analog (2-NBDG) in tumor cells. *Molecular Imaging and Biology*, 7(6), 388-392. <https://doi.org/10.1007/s11307-005-0011-6>
- Orendi, K., Kivity, V., Sammar, M., Grimpel, Y., Gonen, R., Meiri, H., ... & Huppertz, B. (2011). Placental and trophoblastic in vitro models to study preventive and therapeutic agents for preeclampsia. *Placenta*, 32, S49-S54. <https://doi.org/10.1016/j.placenta.2010.11.023>
- Ornoy, A., Becker, M., Weinstein-Fudim, L., & Ergaz, Z. (2021). Diabetes during Pregnancy: A Maternal Disease Complicating the Course of Pregnancy with Long-Term Deleterious Effects on the Offspring. A Clinical Review. *International journal of molecular sciences*, 22(6), 2965. <https://doi.org/10.3390/ijms22062965>
- Ozmen A, Unek G, Kipmen-Korgun D, Korgun ET. The PI3K/Akt and MAPK-ERK1/2 pathways are altered in STZ induced diabetic rat placentas. *Histol Histopathol*. 2014 Jun;29(6):743-56. doi: 10.14670/HH-29.743. Epub 2013 Dec 18. PMID: 24346807.
- Ozmen, A., Unek, G., Kipmen-Korgun, D., & Korgun, E. T. (2014). The PI3K/Akt and MAPK-ERK1/2 pathways are altered in STZ induced diabetic rat placentas. *Histology and histopathology*, 29(6), 743–756. <https://doi.org/10.14670/HH-29.743>
- Palma, C., Lai, A., Scholz-Romero, K., Chittoory, H., Van Haeringen, B., Carrion, F., Handberg, A., Lappas, M., Lakhani, S. R., McCart Reed, A. E., McIntyre, H. D., Nair, S., & Salomon, C. (2024). Differential response of placental cells to high D-glucose and its impact on extracellular vesicle biogenesis and trafficking via small GTPase Ras-related protein RAB-7A. *Journal of extracellular biology*, 3(1), e135. <https://doi.org/10.1002/jex2.135>
- Palviainen, M., Saraswat, M., Varga, Z., Kitka, D., Neuvonen, M., Puhka, M., Joenväärä, S., Renkonen, R., Nieuwland, R., Takatalo, M., & Siljander, P. R. M. (2020). Extracellular vesicles from human plasma and serum are carriers of extravesicular cargo-Implications for biomarker discovery. *PloS one*, 15(8), e0236439. <https://doi.org/10.1371/journal.pone.0236439>
- Pang, Z., Chong, J., Zhou, G., de Lima Morais, D. A., Chang, L., Barrette, M., Gauthier, C., Jacques, P. É., Li, S., & Xia, J. (2021). MetaboAnalyst 5.0: Narrowing the gap between raw spectra and functional insights. *Nucleic Acids Research*, 49(W1), W388-W396. <https://doi.org/10.1093/nar/gkab382>
- Pappa, K. I., Anagnou, N. P., Salamalekis, E., Bikouvarakis, S., Maropoulos, G., Anagnostopoulos, F., & Antsaklis, A. (2011). Gestational diabetes exhibits a lack of adiponectin-mediated enhancement of apolipoprotein B in the third trimester. *Journal of Clinical Endocrinology & Metabolism*, 96(9), 2821–2828.

- Pasek, R. C., & Gannon, M. (2013). Advancements and challenges in generating accurate animal models of gestational diabetes mellitus. *American journal of physiology. Endocrinology and metabolism*, 305(11), E1327–E1338. <https://doi.org/10.1152/ajpendo.00425.2013>
- Pentinat, T., Pernas, M., & Gomez-Anguiano, G. (2018). Mitochondrial dysfunction and gestational diabetes. *Current Medicinal Chemistry*, 25(40), 5594-5609.
- Permana, P. A., Menge, C., & Reaven, P. D. (2006). Macrophage-secreted factors induce adipocyte inflammation and insulin resistance. *Biochemical and biophysical research communications*, 341(2), 507–514. <https://doi.org/10.1016/j.bbrc.2006.01.012>
- Pettitt, D. J., Knowler, W. C., Baird, H. R., & Bennett, P. H. (1980). Gestational diabetes: infant and maternal complications of pregnancy in relation to third-trimester glucose tolerance in the Pima Indians. *Diabetes care*, 3(3), 458–464. <https://doi.org/10.2337/diacare.3.3.458>
- Plows, J. F., Stanley, J. L., Baker, P. N., Reynolds, C. M., & Vickers, M. H. (2018). The pathophysiology of gestational diabetes mellitus. *International Journal of Molecular Sciences*, 19(11), 3342. <https://doi.org/10.3390/ijms19113342>
- Plows, J. F., Stanley, J. L., Baker, P. N., Reynolds, C. M., & Vickers, M. H. (2018). The Pathophysiology of Gestational Diabetes Mellitus. *International journal of molecular sciences*, 19(11), 3342. <https://doi.org/10.3390/ijms19113342>
- Poulsen, M. S., Rytting, E., Mose, T., & Knudsen, L. E. (2009). Modeling placental transport: correlation of in vitro BeWo cell permeability and ex vivo human placental perfusion. *Toxicology in vitro : an international journal published in association with BIBRA*, 23(7), 1380–1386. <https://doi.org/10.1016/j.tiv.2009.07.028>
- Practice Bulletin No. 137: Gestational diabetes mellitus. (2013). *Obstetrics and gynecology*, 122(2 Pt 1), 406–416. <https://doi.org/10.1097/01.AOG.0000433006.09219.f1>
- Prentki, M., & Nolan, C. J. (2006). Islet beta cell failure in type 2 diabetes. *The Journal of clinical investigation*, 116(7), 1802–1812. <https://doi.org/10.1172/JCI29103>
- Prentki, M., & Nolan, C. J. (2006). Islet beta cell failure in type 2 diabetes. *The Journal of clinical investigation*, 116(7), 1802–1812. <https://doi.org/10.1172/JCI29103>
- Qatanani, M., & Lazar, M. A. (2007). Mechanisms of obesity-associated insulin resistance: many choices on the menu. *Genes & development*, 21(12), 1443–1455. <https://doi.org/10.1101/gad.1550907>
- Qiu, C., Sorensen, T. K., Luthy, D. A., & Williams, M. A. (2004). A prospective study of maternal serum C-reactive protein (CRP) concentrations and risk of gestational diabetes mellitus.

Paediatric and perinatal epidemiology, 18(5), 377–384. <https://doi.org/10.1111/j.1365-3016.2004.00578.x>

- Quattrocchi, T., Baviera, G., Pochiero, T., Basile, F., Rizzo, L., Santamaria, A., Corrado, F., & D'Anna, R. (2015). Maternal serum PAPP-A as an early marker of obstetric complications?. *Fetal diagnosis and therapy*, 37(1), 33–36. <https://doi.org/10.1159/000365147>
- Radaelli T, Varastehpour A, Catalano P, Hauguel-de Mouzon S. Gestational diabetes induces placental genes for chronic stress and inflammatory pathways. *Diabetes*. 2003 Dec;52(12):2951-8. doi: 10.2337/diabetes.52.12.2951. PMID: 14633856.
- Raets, L., Beunen, K., & Benhalima, K. (2021). Screening for Gestational Diabetes Mellitus in Early Pregnancy: What Is the Evidence?. *Journal of clinical medicine*, 10(6), 1257. <https://doi.org/10.3390/jcm10061257>
- Rahier, J., Guiot, Y., Goebbels, R. M., Sempoux, C., & Henquin, J. C. (2008). Pancreatic beta-cell mass in European subjects with type 2 diabetes. *Diabetes, obesity & metabolism*, 10 Suppl 4, 32–42. <https://doi.org/10.1111/j.1463-1326.2008.00969.x>
- Räsänen, J. P., Snyder, C. K., Rao, P. V., Mihalache, R., Heinonen, S., Gravett, M. G., Roberts, C. T., Jr, & Nagalla, S. R. (2013). Glycosylated fibronectin as a first-trimester biomarker for prediction of gestational diabetes. *Obstetrics and Gynecology*, 122(3), 586–594. <https://doi.org/10.1097/AOG.0b013e3182a0c88b>
- Ray, G. W., Zeng, Q., Kusi, P., Zhang, H., Shao, T., Yang, T., Wei, Y., Li, M., Che, X., & Guo, R. (2024). Genetic and inflammatory factors underlying gestational diabetes mellitus: a review. *Frontiers in endocrinology*, 15, 1399694. <https://doi.org/10.3389/fendo.2024.1399694>
- Ray, G. W., Zeng, Q., Kusi, P., Zhang, H., Shao, T., Yang, T., Wei, Y., Li, M., Che, X., & Guo, R. (2024). Genetic and inflammatory factors underlying gestational diabetes mellitus: a review. *Frontiers in endocrinology*, 15, 1399694. <https://doi.org/10.3389/fendo.2024.1399694>
- Raza, W., Guo, J., Qadir, M. I., Bai, B., & Muhammad, S. A. (2022). qPCR Analysis Reveals Association of Differential Expression of SRR, NFKB1, and PDE4B Genes With Type 2 Diabetes Mellitus. *Frontiers in endocrinology*, 12, 774696. <https://doi.org/10.3389/fendo.2021.774696>
- Reece, E. A., Leguizamón, G., & Wiznitzer, A. (2009). Gestational diabetes: the need for a common ground. *Lancet (London, England)*, 373(9677), 1789–1797. [https://doi.org/10.1016/S0140-6736\(09\)60515-8](https://doi.org/10.1016/S0140-6736(09)60515-8)
- Ringnér, M. (2008). What is principal component analysis?. *Nature Biotechnology*, 26(3), 303-304. <https://doi.org/10.1038/nbt0308-303>

- Riskin-Mashiah, S., Damti, A., Younes, G., & Auslender, R. (2010). First trimester fasting hyperglycemia as a predictor for the development of gestational diabetes mellitus. *European journal of obstetrics, gynecology, and reproductive biology*, 152(2), 163–167. <https://doi.org/10.1016/j.ejogrb.2010.05.036>
- Rodolaki, K., Pergialiotis, V., Iakovidou, N., Boutsikou, T., Iliodromiti, Z., & Kanaka-Gantenbein, C. (2023). The impact of maternal diabetes on the future health and neurodevelopment of the offspring: a review of the evidence. *Frontiers in endocrinology*, 14, 1125628. <https://doi.org/10.3389/fendo.2023.1125628>
- Rodrigo, N., & Glastras, S. J. (2018). The Emerging Role of Biomarkers in the Diagnosis of Gestational Diabetes Mellitus. *Journal of clinical medicine*, 7(6), 120. <https://doi.org/10.3390/jcm7060120>
- Rose, S., & van der Laan, M. J. (2008). A note on risk prediction for case-control studies.
- Ryu, R. J., Hays, K. E., & Heathcote, S. A. (2015). Placental mitochondrial dysfunction and gestational diabetes mellitus. *Current Diabetes Reports*, 15(10), 92.
- Saeedi, P., Petersohn, I., Salpea, P., Malanda, B., Karuranga, S., Unwin, N., Colagiuri, S., Guariguata, L., Motala, A. A., Ogurtsova, K., Shaw, J. E., Bright, D., Williams, R., & IDF Diabetes Atlas Committee (2019). Global and regional diabetes prevalence estimates for 2019 and projections for 2030 and 2045: Results from the International Diabetes Federation Diabetes Atlas, 9th edition. *Diabetes research and clinical practice*, 157, 107843. <https://doi.org/10.1016/j.diabres.2019.107843>
- Sajewicz-Krukowska, J., Jastrzębski, J. P., Grzybek, M., Domańska-Blicharz, K., Tarasiuk, K., & Marzec-Kotarska, B. (2021). Transcriptome Sequencing of the Spleen Reveals Antiviral Response Genes in Chickens Infected with CAstV. *Viruses*, 13(12), 2374. <https://doi.org/10.3390/v13122374>
- Salomonis N. (2018). Integrative Analysis of Proteomics Data to Obtain Clinically Relevant Markers. *Methods in molecular biology (Clifton, N.J.)*, 1788, 89–111. https://doi.org/10.1007/7651_2017_94
- Saltiel A. R. (2021). Insulin signaling in health and disease. *The Journal of clinical investigation*, 131(1), e142241. <https://doi.org/10.1172/JCI142241>
- Samuel, R. O., Gomes-Filho, J. E., Dezan-Júnior, E., & Cintra, L. T. (2014). Streptozotocin-induced rodent models of diabetes: Protocol comparisons. *Streptozotocin: Uses, mechanism of action and side effects*, 61-80.

- Saraf, S., Gupta, N., Elchalal, U., & Froy, O. (2018). Circulating placental-derived biomarkers in gestational diabetes mellitus. *Clinica Chimica Acta*, 487, 287–292.
- Savage, J. S., Fisher, J. O., & Birch, L. L. (2007). Parental influence on eating behavior: conception to adolescence. *The Journal of law, medicine & ethics : a journal of the American Society of Law, Medicine & Ethics*, 35(1), 22–34. <https://doi.org/10.1111/j.1748-720X.2007.00111.x>
- Schober, P., Boer, C., & Schwarte, L. A. (2018). Correlation coefficients: appropriate use and interpretation. *Anesthesia & Analgesia*, 126(5), 1763-1768. <https://doi.org/10.1213/ANE.0000000000002864>
- Schork, K., Podwojski, K., Turewicz, M., Stephan, C., & Eisenacher, M. (2021). Important Issues in Planning a Proteomics Experiment: Statistical Considerations of Quantitative Proteomic Data. *Methods in molecular biology (Clifton, N.J.)*, 2228, 1–20. https://doi.org/10.1007/978-1-0716-1024-4_1
- Serov AS, Salafia CM, Brownbill P, Grebenkov DS, Filoche M. Optimal villi density for maximal oxygen uptake in the human placenta. *J Theor Biol.* 2015 Jan 7;364:383-96. doi: 10.1016/j.jtbi.2014.09.022. Epub 2014 Sep 27. PMID: 25261730.
- Serov, A. S., Salafia, C. M., Brownbill, P., Grebenkov, D. S., & Filoche, M. (2015). Optimal villi density for maximal oxygen uptake in the human placenta. *Journal of theoretical biology*, 364, 383–396. <https://doi.org/10.1016/j.jtbi.2014.09.022>
- Sharma, A. K., Nayak, N. R., & Jena, M. K. (2024). An in vitro Model to Study Placental Functions in Gestational Diabetes Mellitus. *Trends in Sciences*, 21(1), 7427-7427.
- Sharma, K., Vu, T. T., Cook, W., Naseri, M., Zhan, K., Nakajima, W., Azuma, Y., Livneh, I., Chen, T., Hasegawa, K., Gu, Y., Qi, J., Jiang, C., Fujimori, F., Devkota, S., Jiang, X., Feng, Y., Ruan, H. B., Hu, Y., ... Wan, J. (2021). Caspase-2 cleaves PACT to regulate type I interferon production and promote cGAS-STING-mediated antiviral immunity. *Molecular Cell*, 81(14), 2904-2919.e10. <https://doi.org/10.1016/j.molcel.2021.05.025>
- Shaw, P., Dwivedi, S. K. D., Bhattacharya, R., Mukherjee, P., & Rao, G. (2024). VEGF signaling: Role in angiogenesis and beyond. *Biochimica et biophysica acta. Reviews on cancer*, 1879(2), 189079. <https://doi.org/10.1016/j.bbcan.2024.189079>
- Shiefa, S., Amargandhi, M., Bhupendra, J., Moulali, S., & Kristine, T. (2013). First Trimester Maternal Serum Screening Using Biochemical Markers PAPP-A and Free β -hCG for Down Syndrome, Patau Syndrome and Edward Syndrome. *Indian journal of clinical biochemistry : IJCB*, 28(1), 3–12. <https://doi.org/10.1007/s12291-012-0269-9>

- Shoelson, S. E., Lee, J., & Goldfine, A. B. (2006). Inflammation and insulin resistance. *The Journal of clinical investigation*, 116(7), 1793–1801. <https://doi.org/10.1172/JCI29069>
- Shulman GI. Cellular mechanisms of insulin resistance. *J Clin Invest*. 2000 Jul;106(2):171-6. doi: 10.1172/JCI10583. PMID: 10903330; PMCID: PMC314317.
- Side, L. (2018). A practical guide to sample preparation for liquid chromatography-tandem mass spectrometry in clinical research and toxicology. *Spectroscopy Europe*, 30(6).
- Simmons, R. A., Templeton, L. J., & Gertz, S. J. (2001). Intrauterine growth retardation leads to the development of type 2 diabetes in the rat. *Diabetes*, 50(10), 2279–2286. <https://doi.org/10.2337/diabetes.50.10.2279>
- Sirikunalai, P., Wanapirak, C., Sirichotiyakul, S., Tongprasert, F., Srisupundit, K., Luewan, S., Traisrisilp, K., & Tongsong, T. (2016). Associations between maternal serum free beta human chorionic gonadotropin (β -hCG) levels and adverse pregnancy outcomes. *Journal of obstetrics and gynaecology : the journal of the Institute of Obstetrics and Gynaecology*, 36(2), 178–182. <https://doi.org/10.3109/01443615.2015.1036400>
- Sivan, E., Lee, Y. C., Wu, Y. K., Reece, E. A., & Freeby, M. (2014). Role of insulin-like growth factor axis in the pathogenesis of diabetic nephropathy: A mini review. *The American Journal of the Medical Sciences*, 348(2), 109–113.
- Skajaa, G. O., Fuglsang, J., Knorr, S., Møller, N., Ovesen, P., & Kampmann, U. (2020). Changes in insulin sensitivity and insulin secretion during pregnancy and post partum in women with gestational diabetes. *BMJ open diabetes research & care*, 8(2), e001728. <https://doi.org/10.1136/bmjdr-2020-001728>
- Smilde, A. K., Jansen, J. J., Hoefsloot, H. C., Lamers, R. J., van der Greef, J., & Timmerman, M. E. (2005). ANOVA-simultaneous component analysis (ASCA): a new tool for analyzing designed metabolomics data. *Bioinformatics (Oxford, England)*, 21(13), 3043–3048. <https://doi.org/10.1093/bioinformatics/bti476>
- Solomon, C. G., Willett, W. C., Carey, V. J., Rich-Edwards, J., Hunter, D. J., Colditz, G. A., Stampfer, M. J., Speizer, F. E., Spiegelman, D., & Manson, J. E. (1997). A prospective study of pregravid determinants of gestational diabetes mellitus. *JAMA*, 278(13), 1078–1083.
- Sorice, A., Guerriero, E., Capone, F., Colacurci, N., Bianchi, G., & Longo, L. P. (2019). Placental mitochondrial dysfunction and oxidative stress in gestational diabetes mellitus. *Current Molecular Medicine*, 19(4), 265-273.

- Sriboonvorakul, N., Hu, J., Boriboonhirunsarn, D., Ng, L. L., & Tan, B. K. (2022). Proteomics Studies in Gestational Diabetes Mellitus: A Systematic Review and Meta-Analysis. *Journal of clinical medicine*, 11(10), 2737. <https://doi.org/10.3390/jcm11102737>
- Stojanovska, V., Arnold, S., Bauer, M., Voss, H., Fest, S., & Zenclussen, A. C. (2022). Characterization of Three-Dimensional Trophoblast Spheroids: An Alternative Model to Study the Physiological Properties of the Placental Unit. *Cells*, 11(18), 2884. <https://doi.org/10.3390/cells11182884>
- Straszewski-Chavez, S. L., Abrahams, V. M., Alvero, A. B., Aldo, P. B., Ma, Y., Guller, S., Romero, R., & Mor, G. (2009). The isolation and characterization of a novel telomerase immortalized first trimester trophoblast cell line, Swan 71. *Placenta*, 30(11), 939–948. <https://doi.org/10.1016/j.placenta.2009.08.007>
- Su, M. T., Lin, S. H., Lee, I. W., Chen, Y. C., & Kuo, P. L. (2011). Association of polymorphisms/haplotypes of the genes encoding vascular endothelial growth factor and its KDR receptor with recurrent pregnancy loss. *Human reproduction (Oxford, England)*, 26(4), 758–764. <https://doi.org/10.1093/humrep/deq401>
- Sultan, S. A., Liu, W., Peng, Y., Roberts, W., Whitelaw, D., & Graham, A. M. (2015). The Role of Maternal Gestational Diabetes in Inducing Fetal Endothelial Dysfunction. *Journal of cellular physiology*, 230(11), 2695–2705. <https://doi.org/10.1002/jcp.24993>
- Sun, X., & Li, J. (2013). pairheatmap: comparing expression profiles of gene groups in heatmaps. *Computer methods and programs in biomedicine*, 112(3), 599–606. <https://doi.org/10.1016/j.cmpb.2013.07.010>
- Sweeting, A. N., Wong, J., Appelblom, H., Ross, G. P., Kouru, H., Williams, P. F., Sairanen, M., & Hyett, J. A. (2018). A first trimester prediction model for gestational diabetes utilizing aneuploidy and pre-eclampsia screening markers. *The journal of maternal-fetal & neonatal medicine : the official journal of the European Association of Perinatal Medicine, the Federation of Asia and Oceania Perinatal Societies, the International Society of Perinatal Obstetricians*, 31(16), 2122–2130. <https://doi.org/10.1080/14767058.2017.1336759>
- Sweeting, A. N., Wong, J., Appelblom, H., Ross, G. P., Kouru, H., Williams, P. F., Sairanen, M., & Hyett, J. A. (2018). A first trimester prediction model for gestational diabetes utilizing aneuploidy and pre-eclampsia screening markers. *The journal of maternal-fetal & neonatal medicine : the official journal of the European Association of Perinatal Medicine, the Federation of Asia and Oceania Perinatal Societies, the International Society of Perinatal Obstetricians*, 31(16), 2122–2130. <https://doi.org/10.1080/14767058.2017.1336759>

- Sweeting, A., Park, F., & Hyett, J. (2015). The first trimester: prediction and prevention of the great obstetrical syndromes. *Best practice & research. Clinical obstetrics & gynaecology*, 29(2), 183–193. <https://doi.org/10.1016/j.bpobgyn.2014.09.006>
- Sweeting, A., Wong, J., Murphy, H. R., & Ross, G. P. (2022). A Clinical Update on Gestational Diabetes Mellitus. *Endocrine reviews*, 43(5), 763–793. <https://doi.org/10.1210/edrev/bnac003>
- Syngelaki, A., Kotecha, R., Pastides, A., Wright, A., & Nicolaides, K. H. (2015). First-trimester biochemical markers of placentation in screening for gestational diabetes mellitus. *Metabolism: clinical and experimental*, 64(11), 1485–1489. <https://doi.org/10.1016/j.metabol.2015.07.015>
- Syngelaki, A., Visser, G. H., Krithinakis, K., Wright, A., & Nicolaides, K. H. (2016). First trimester screening for gestational diabetes mellitus by maternal factors and markers of inflammation. *Metabolism: clinical and experimental*, 65(3), 131–137. <https://doi.org/10.1016/j.metabol.2015.10.029>
- Tahergorabi, Z., & Khazaei, M. (2012). A review on angiogenesis and its assays. *Iranian journal of basic medical sciences*, 15(6), 1110–1126.
- Tawfeek, M. A., Alfadhli, E. M., Alayoubi, A. M., El-Beshbishy, H. A., & Habib, F. A. (2017). Sex hormone binding globulin as a valuable biochemical marker in predicting gestational diabetes mellitus. *BMC women's health*, 17(1), 18. <https://doi.org/10.1186/s12905-017-0373-3>
- Taylor, P. D., Matthews, P. A., Khan, I. Y., Rees, D., Itani, N., & Poston, L. (2018). Generation of Maternal Obesity Models in Studies of Developmental Programming in Rodents. *Methods in molecular biology (Clifton, N.J.)*, 1735, 167–199. https://doi.org/10.1007/978-1-4939-7614-0_9
- Teh, W. T., Teede, H. J., Paul, E., Harrison, C. L., Wallace, E. M., & Allan, C. (2011). Risk factors for gestational diabetes mellitus: implications for the application of screening guidelines. *The Australian & New Zealand journal of obstetrics & gynaecology*, 51(1), 26–30. <https://doi.org/10.1111/j.1479-828X.2011.01292.x>
- Troncoso, F., Acurio, J., Herlitz, K., Aguayo, C., Bertoglia, P., Guzman-Gutierrez, E., Loyola, M., Gonzalez, M., Rezgaoui, M., Desoye, G., & Escudero, C. (2017). Gestational diabetes mellitus is associated with increased pro-migratory activation of vascular endothelial growth factor receptor 2 and reduced expression of vascular endothelial growth factor receptor 1. *PloS one*, 12(8), e0182509. <https://doi.org/10.1371/journal.pone.0182509>
- Trout, K.K.; Compher, C.; Durnwald, C.P. Protein vs. Carbohydrate in Gestational Diabetes. *Diabetes* 2019, 68, 753-P. [CrossRef]

- Truvé, K., Parris, T. Z., Vizlin-Hodzic, D., Salmela, S., Berger, E., Ågren, H., & Funa, K. (2020). Identification of candidate genetic variants and altered protein expression in neural stem and mature neural cells support altered microtubule function to be an essential component in bipolar disorder. *Translational psychiatry*, 10(1), 390. <https://doi.org/10.1038/s41398-020-01056-1>
- Tsai, T. H., Wang, M., & Ransom, H. W. (2016). Preprocessing and Analysis of LC-MS-Based Proteomic Data. *Methods in molecular biology* (Clifton, N.J.), 1362, 63–76. https://doi.org/10.1007/978-1-4939-3106-4_3
- Tukey, J. W. (1977). *Exploratory data analysis* (Vol. 2, pp. 131-160)
- Van Assche, F. A., Aerts, L., & De Prins, F. (1978). A morphological study of the endocrine pancreas in human pregnancy. *British journal of obstetrics and gynaecology*, 85(11), 818–820. <https://doi.org/10.1111/j.1471-0528.1978.tb15835.x>
- Vezza, T., Díaz-Pozo, P., Canet, F., de Marañón, A. M., Abad-Jiménez, Z., García-Gargallo, C., Roldan, I., Solá, E., Bañuls, C., López-Domènech, S., Rocha, M., & Víctor, V. M. (2022). The Role of Mitochondrial Dynamic Dysfunction in Age-Associated Type 2 Diabetes. *The world journal of men's health*, 40(3), 399–411. <https://doi.org/10.5534/wjmh.210146>
- Vilotić, A., Nacka-Aleksić, M., Pirković, A., Bojić-Trbojević, Ž., Dekanski, D., & Jovanović Krivokuća, M. (2022). IL-6 and IL-8: An Overview of Their Roles in Healthy and Pathological Pregnancies. *International journal of molecular sciences*, 23(23), 14574. <https://doi.org/10.3390/ijms232314574>
- Virginia Tech. Retro-orbital bleeding in the rat. Available at: https://ouv.vt.edu/content/dam/ouv_vt_edu/sops/small-animal-biomedical/sop-rat-blood-collection-retro-orbital.pdf
- Wang, H., Li, N., Chivese, T., Werfalli, M., Sun, H., Yuen, L., Hoegfeldt, C. A., Elise Powe, C., Immanuel, J., Karuranga, S., Divakar, H., Levitt, N., Li, C., Simmons, D., Yang, X., & IDF Diabetes Atlas Committee Hyperglycaemia in Pregnancy Special Interest Group (2022). IDF Diabetes Atlas: Estimation of Global and Regional Gestational Diabetes Mellitus Prevalence for 2021 by International Association of Diabetes in Pregnancy Study Group's Criteria. *Diabetes research and clinical practice*, 183, 109050. <https://doi.org/10.1016/j.diabres.2021.109050>
- Wang, H., Li, N., Chivese, T., Werfalli, M., Sun, H., Yuen, L., Hoegfeldt, C. A., Elise Powe, C., Immanuel, J., Karuranga, S., Divakar, H., Levitt, N., Li, C., Simmons, D., Yang, X., & IDF Diabetes Atlas Committee Hyperglycaemia in Pregnancy Special Interest Group (2022). IDF Diabetes Atlas: Estimation of Global and Regional Gestational Diabetes Mellitus Prevalence

for 2021 by International Association of Diabetes in Pregnancy Study Group's Criteria. *Diabetes research and clinical practice*, 183, 109050. <https://doi.org/10.1016/j.diabres.2021.109050>

- Wang, Q., Würtz, P., Auro, K., Mäkinen, V. P., Kangas, A. J., Soininen, P., Tiainen, M., Tynkkynen, T., Jokelainen, J., Santalahti, K., Salmi, M., Blankenberg, S., Zeller, T., Viikari, J., Kähönen, M., Lehtimäki, T., Salomaa, V., Perola, M., Jalkanen, S., Järvelin, M. R., ... Ala-Korpela, M. (2016). Metabolic profiling of pregnancy: cross-sectional and longitudinal evidence. *BMC medicine*, 14(1), 205. <https://doi.org/10.1186/s12916-016-0733-0>
- Wang, W. C., Huang, C. H., Chung, H. H., Chen, P. L., Hu, F. R., Yang, C. H., Yang, C. M., Lin, C. W., Hsu, C. C., & Chen, T. C. (2024). Metabolomics facilitates differential diagnosis in common inherited retinal degenerations by exploring their profiles of serum metabolites. *Nature communications*, 15(1), 3562. <https://doi.org/10.1038/s41467-024-47911-3>
- Wang, W., Huang, G., Lin, H., Ren, L., Fu, L., & Mao, X. (2023). Label-free LC-MS/MS proteomics analyses reveal CLIC1 as a predictive biomarker for bladder cancer staging and prognosis. *Frontiers in oncology*, 12, 1102392. <https://doi.org/10.3389/fonc.2022.1102392>
- Wang, Y., Xiao, Y., Zhong, L., Ye, D., Zhang, J., Tu, Y., Bornstein, S. R., Zhou, Z., Lam, K. S., & Xu, A. (2014). Increased neutrophil elastase and proteinase 3 and augmented NETosis are closely associated with β -cell autoimmunity in patients with type 1 diabetes. *Diabetes*, 63(12), 4239–4248. <https://doi.org/10.2337/db14-0480>
- Wei, R., Yang, F., Urban, T. J., Li, L., Chalasani, N., Flockhart, D. A., & Liu, W. (2012). Impact of the Interaction between 3'-UTR SNPs and microRNA on the Expression of Human Xenobiotic Metabolism Enzyme and Transporter Genes. *Frontiers in genetics*, 3, 248. <https://doi.org/10.3389/fgene.2012.00248>
- Weinert L. S. (2010). International Association of Diabetes and Pregnancy Study Groups recommendations on the diagnosis and classification of hyperglycemia in pregnancy: comment to the International Association of Diabetes and Pregnancy Study Groups Consensus Panel. *Diabetes care*, 33(7), e97–e98. <https://doi.org/10.2337/dc10-0544>
- Weir, G. C., Laybutt, D. R., Kaneto, H., Bonner-Weir, S., & Sharma, A. (2001). Beta-cell adaptation and decompensation during the progression of diabetes. *Diabetes*, 50 Suppl 1, S154–S159. <https://doi.org/10.2337/diabetes.50.2007.s154>
- Wice, B., Menton, D., Geuze, H., & Schwartz, A. L. (1990). Modulators of cyclic AMP metabolism induce syncytiotrophoblast formation in vitro. *Experimental Cell Research*, 186(2), 306-316. [https://doi.org/10.1016/0014-4827\(90\)90310-7](https://doi.org/10.1016/0014-4827(90)90310-7)

- Wiśniewski, J. R., Zougman, A., Nagaraj, N., & Mann, M. (2009). Universal sample preparation method for proteome analysis. *Nature methods*, 6(5), 359–362. <https://doi.org/10.1038/nmeth.1322>
- WL Lowe Jr and DM Scholtens. Pathophysiology of gestational diabetes mellitus: The past, present and future. *Diabetic Med.* 2020; 37, 812-20.
- Wold, S., Esbensen, K., & Geladi, P. (1987). Principal component analysis. *Chemometrics and Intelligent Laboratory Systems*, 2(1-3), 37-52. [https://doi.org/10.1016/0169-7439\(87\)80084-9](https://doi.org/10.1016/0169-7439(87)80084-9)
- Wolf, M., Sauk, J., Shah, A., Vossen Smirnakis, K., Jimenez-Kimble, R., Ecker, J. L., & Thadhani, R. (2004). Inflammation and glucose intolerance: a prospective study of gestational diabetes mellitus. *Diabetes care*, 27(1), 21–27. <https://doi.org/10.2337/diacare.27.1.21>
- Xiang, L., Varshney, R., Rashdan, N. A., Shaw, J. H., & Lloyd, P. G. (2014). Placenta growth factor and vascular endothelial growth factor have differential, cell-type specific patterns of expression in vascular cells. *Microcirculation (New York, N.Y. : 1994)*, 21(5), 368–379. <https://doi.org/10.1111/micc.12113>
- Xiao, D., Chenhong, W., Yanbin, X., & Lu, Z. (2018). Gestational diabetes mellitus and first trimester pregnancy-associated plasma protein A: A case-control study in a Chinese population. *Journal of diabetes investigation*, 9(1), 204–210. <https://doi.org/10.1111/jdi.12672>
- Yamada, K., Saito, M., Matsuoka, H., & Inagaki, N. (2007). A real-time method of imaging glucose uptake in single, living mammalian cells. *Nature Protocols*, 2(3), 753-762. <https://doi.org/10.1038/nprot.2007.76>
- Yang, M. T., Chang, W. H., Kuo, T. F., Shen, M. Y., Yang, C. W., Tien, Y. J., Lai, B. Y., Chen, Y. R., Chang, Y. C., & Yang, W. C. (2021). Identification of Novel Biomarkers for Pre-diabetic Diagnosis Using a Combinational Approach. *Frontiers in endocrinology*, 12, 641336. <https://doi.org/10.3389/fendo.2021.641336>
- Yazdani, S., Bilan, P. J., Jaldin-Fincati, J. R., Pang, J., Ceban, F., Saran, E., Brumell, J. H., Freeman, S. A., & Klip, A. (2022). Dynamic glucose uptake, storage, and release by human microvascular endothelial cells. *Molecular biology of the cell*, 33(12), ar106. <https://doi.org/10.1091/mbc.E22-04-0146>
- Yazdani, S., Bilan, P. J., Jaldin-Fincati, J. R., Pang, J., Ceban, F., Saran, E., Brumell, J. H., Freeman, S. A., & Klip, A. (2022). Dynamic glucose uptake, storage, and release by human microvascular endothelial cells. *Molecular biology of the cell*, 33(12), ar106. <https://doi.org/10.1091/mbc.E22-04-0146>

- Yeral, M. I., Ozcan, O., Cetin, Z., & Gunay, V. K. (2019). Mitochondrial dysfunction in gestational diabetes mellitus. *World Journal of Clinical Cases*, 7(23), 3955-3966.
- Yin, Y. N., Cao, L., Wang, J., Chen, Y. L., Yang, H. O., Tan, S. B., Cai, K., Chen, Z. Q., Xiang, J., Yang, Y. X., Geng, H. R., Zhou, Z. Y., Shen, A. N., Zhou, X. Y., Shi, Y., Zhao, R., Sun, K., Ding, C., & Zhao, J. Y. (2023). Proteome profiling of early gestational plasma reveals novel biomarkers of congenital heart disease. *EMBO molecular medicine*, 15(12), e17745. <https://doi.org/10.15252/emmm.202317745>
- Yoshie, M., Tamura, K., Hara, T., & Kogo, H. (2010). Expression of stathmin family genes in human placenta and choriocarcinoma cell lines. *Placenta*, 31(2), 104-110. <https://doi.org/10.1016/j.placenta.2009.11.012>
- Yu, G., Wang, L. G., Meng, X., & He, Q. Y. (2022). ChIPseeker: An R/Bioconductor package for ChIP peak annotation, comparison and visualization. *Bioinformatics*, 38(5), 1465-1467. <https://doi.org/10.1093/bioinformatics/btab826>
- Zhao, C., Zhang, T., Shi, Z., Ding, H., & Ling, X. (2014). MicroRNA-518d regulates PPAR α protein expression in the placentas of females with gestational diabetes mellitus. *Molecular medicine reports*, 9(6), 2085–2090. <https://doi.org/10.3892/mmr.2014.2058>
- Zhao, H., Li, H., Chung, A. C. K., Zhou, G., Luo, Z., Liu, J., Arany, Z., & Lu, Y. (2019). Large-scale longitudinal metabolomics study reveals different trimester-specific alterations of metabolites in relation to gestational diabetes mellitus. *Journal of Proteome Research*, 18(1), 292-300. <https://doi.org/10.1021/acs.jproteome.8b00602>
- Zhou J, Ni X, Huang X, Yao J, He Q, Wang K, Duan T. Potential Role of Hyperglycemia in Fetoplacental Endothelial Dysfunction in Gestational Diabetes Mellitus. *Cell Physiol Biochem*. 2016;39(4):1317-28. doi: 10.1159/000447836. Epub 2016 Sep 8. PMID: 27606810.
- Zhou, F., Ran, X., Song, F., Wu, Q., Jia, Y., Liang, Y., Chen, S., Zhang, G., Dong, J., & Wang, Y. (2024). A stepwise prediction and interpretation of gestational diabetes mellitus: Foster the practical application of machine learning in clinical decision. *Heliyon*, 10(12), e32709. <https://doi.org/10.1016/j.heliyon.2024.e32709>
- Zhou, T., Huang, L., Wang, M., Chen, D., Chen, Z., & Jiang, S. W. (2020). A Critical Review of Proteomic Studies in Gestational Diabetes Mellitus. *Journal of diabetes research*, 2020, 6450352. <https://doi.org/10.1155/2020/6450352>
- Bach, D., Pich, S., Soriano, F. X., Vega, N., Baumgartner, B., Oriola, J., Dugaard, J. R., Lloberas, J., Camps, M., Zierath, J. R., Rabasa-Lhoret, R., Wallberg-Henriksson, H., Laville, M., Palacín, M., Vidal, H., Rivera, F., Brand, M., & Zorzano, A. (2003). Mitofusin-2 determines mitochondrial network architecture and mitochondrial metabolism. A novel regulatory

mechanism altered in obesity. *The Journal of biological chemistry*, 278(19), 17190–17197. <https://doi.org/10.1074/jbc.M212754200>

- Hebert, J. F., & Myatt, L. (2021). Placental mitochondrial dysfunction with metabolic diseases: Therapeutic approaches. *Biochimica et biophysica acta. Molecular basis of disease*, 1867(1), 165967. <https://doi.org/10.1016/j.bbadis.2020.165967>
- Jheng, H. F., Tsai, P. J., Guo, S. M., Kuo, L. H., Chang, C. S., Su, I. J., Chang, C. R., & Tsai, Y. S. (2012). Mitochondrial fission contributes to mitochondrial dysfunction and insulin resistance in skeletal muscle. *Molecular and cellular biology*, 32(2), 309–319. <https://doi.org/10.1128/MCB.05603-11>
- Pentinat, T., Ramon-Krauel, M., Cebria, J., Diaz, R., & Jimenez-Chillaron, J. C. (2018). Transgenerational inheritance of glucose intolerance in a mouse model of neonatal overnutrition. *Endocrinology*, 151(12), 5617-5623.
- Yu, T., Robotham, J. L., & Yoon, Y. (2006). Increased production of reactive oxygen species in hyperglycemic conditions requires dynamic change of mitochondrial morphology. *Proceedings of the National Academy of Sciences of the United States of America*, 103(8), 2653–2658. <https://doi.org/10.1073/pnas.0511154103>
- Zorzano, A., Liesa, M., & Palacín, M. (2009). Mitochondrial dynamics as a bridge between mitochondrial dysfunction and insulin resistance. *Archives of physiology and biochemistry*, 115(1), 1–12. <https://doi.org/10.1080/13813450802676335>

CHAPTER 8

APPENDIX

8. Appendix:

i. 2-NBDG Statistical data (Flow Cytometry):

Depth	Name	Statistic	#Cells
	Q_BeWo 01UT 00001274 951.LMD		8000
>	Cells	76.4	6115
>>	CV : FL1	85.2	
>>	Geometric Mean : FL1	10431	
>>	2-NBDG High	73	4467
>>>	Freq. of Parent	73	
>>	2-NBDG Low	27	1648
>>>	Freq. of Parent	27	
	Q_BeWo 02Control 00001275 952.LMD		8000
>	Cells	75.5	6038
>>	CV : FL1	126	
>>	Geometric Mean : FL1	9816	
>>	2-NBDG High	70.8	4277
>>>	Freq. of Parent	70.8	
>>	2-NBDG Low	29.2	1761
>>>	Freq. of Parent	29.2	
	Q_BeWo 03Test 00001276 953.LMD		8000
>	Cells	69.3	5545
>>	CV : FL1	74.2	
>>	Geometric Mean : FL1	4693	
>>	2-NBDG High	40.5	2248
>>>	Freq. of Parent	40.5	
>>	2-NBDG Low	59.5	3297
>>>	Freq. of Parent	59.5	
	Q_BeWo 04Test+VEGF 00001277 954.LMD		8000
>	Cells	66	5276
>>	CV : FL1	76.7	
>>	Geometric Mean : FL1	5040	
>>	2-NBDG High	43.5	2295
>>>	Freq. of Parent	43.5	
>>	2-NBDG Low	56.5	2981
>>>	Freq. of Parent	56.5	
	Q_BeWo 05WOInsulin 00001278 955.LMD		8000
>	Cells	68.6	5485
>>	CV : FL1	75.9	
>>	Geometric Mean : FL1	4402	
>>	2-NBDG High	38.2	2094
>>>	Freq. of Parent	38.2	
>>	2-NBDG Low	61.8	3391
>>>	Freq. of Parent	61.8	

Unique Proteins-Control

<i>Accession</i>	<i>Description</i>	<i>Coverage [%]</i>	<i># Peptides</i>	<i># Unique Peptides</i>	<i>MW [kDa]</i>	<i>Gene Symbol</i>
Q15059	Bromodomain-containing protein 3 OS=Homo sapiens OX=9606 GN=BRD3 PE=1 SV=1	8	5	1	79.5	BRD3
Q99622	Protein C10 OS=Homo sapiens OX=9606 GN=C12orf57 PE=1 SV=1	12	1	1	13.2	C12orf57
O15127	Secretory carrier-associated membrane protein 2 OS=Homo sapiens OX=9606 GN=SCAMP2 PE=1 SV=2	6	1	1	36.6	SCAMP2
Q9Y4P3	Transducin beta-like protein 2 OS=Homo sapiens OX=9606 GN=TBL2 PE=1 SV=1	3	1	1	49.8	TBL2
P46976	Glycogenin-1 OS=Homo sapiens OX=9606 GN=GYG1 PE=1 SV=4	5	1	1	39.4	GYG1
P42566	Epidermal growth factor receptor substrate 15 OS=Homo sapiens OX=9606 GN=EPS15 PE=1 SV=2	2	1	1	98.6	EPS15
Q8TEQ6	Gem-associated protein 5 OS=Homo sapiens OX=9606 GN=GEMIN5 PE=1 SV=3	1	1	1	168.5	GEMIN5
Q68D06	Schlafen family member 13 OS=Homo sapiens OX=9606 GN=SLFN13 PE=1 SV=1	1	1	1	102	SLFN13
O95070	Protein YIF1A OS=Homo sapiens OX=9606 GN=YIF1A PE=1 SV=2	4	1	1	32	YIF1A
Q5XUX1	F-box/WD repeat-containing protein 9 OS=Homo sapiens OX=9606 GN=FBXW9 PE=1 SV=3	3	1	1	50.7	FBXW9
P17676	CCAAT/enhancer-binding protein beta OS=Homo sapiens OX=9606 GN=CEBPB PE=1 SV=2	3	1	1	36.1	CEBPB
Q86W74	Ankyrin repeat domain-containing protein 46 OS=Homo sapiens OX=9606 GN=ANKRD46 PE=1 SV=2	5	1	1	25.3	ANKRD46
P35754	Glutaredoxin-1 OS=Homo sapiens OX=9606 GN=GLRX PE=1 SV=2	12	1	1	11.8	GLRX

Q96SW2	Protein cereblon OS=Homo sapiens OX=9606 GN=CRBN PE=1 SV=1	6	1	1	50.5	CRBN
P23434	Glycine cleavage system H protein, mitochondrial OS=Homo sapiens OX=9606 GN=GCSH PE=1 SV=2	12	1	1	18.9	GCSH
O60784	Target of Myb protein 1 OS=Homo sapiens OX=9606 GN=TOM1 PE=1 SV=2	2	1	1	53.8	TOM1
P02753	Retinol-binding protein 4 OS=Homo sapiens OX=9606 GN=RBP4 PE=1 SV=3	5	1	1	23	RBP4
P02749	Beta-2-glycoprotein 1 OS=Homo sapiens OX=9606 GN=APOH PE=1 SV=3	3	1	1	38.3	APOH
Q14139	Ubiquitin conjugation factor E4 A OS=Homo sapiens OX=9606 GN=UBE4A PE=1 SV=2	1	1	1	122.5	UBE4A
Q9Y6X5	Bis(5'-adenosyl)-triphosphatase ENPP4 OS=Homo sapiens OX=9606 GN=ENPP4 PE=1 SV=3	2	1	1	51.6	ENPP4
Q9HB19	Pleckstrin homology domain-containing family A member 2 OS=Homo sapiens OX=9606 GN=PLEKHA2 PE=1 SV=2	2	1	1	47.2	PLEKHA2
Q96LD4	E3 ubiquitin-protein ligase TRIM47 OS=Homo sapiens OX=9606 GN=TRIM47 PE=1 SV=2	2	1	1	69.5	TRIM47
Q8WUD4	Coiled-coil domain-containing protein 12 OS=Homo sapiens OX=9606 GN=CCDC12 PE=1 SV=1	8	1	1	19.2	CCDC12
Q09472	Histone acetyltransferase p300 OS=Homo sapiens OX=9606 GN=EP300 PE=1 SV=2	0	1	1	264	EP300
P0C7M7	Acyl-coenzyme A synthetase ACSM4, mitochondrial OS=Homo sapiens OX=9606 GN=ACSM4 PE=2 SV=1	1	1	1	65.7	ACSM4
P51884	Lumican OS=Homo sapiens OX=9606 GN=LUM PE=1 SV=2	3	1	1	38.4	LUM
O00459	Phosphatidylinositol 3-kinase regulatory subunit beta OS=Homo sapiens OX=9606 GN=PIK3R2 PE=1 SV=2	2	1	1	81.5	PIK3R2

Q9H1Z4	WD repeat-containing protein 13 OS=Homo sapiens OX=9606 GN=WDR13 PE=1 SV=2	2	1	1	53.7	WDR13
Q4VNC1	Probable cation-transporting ATPase 13A4 OS=Homo sapiens OX=9606 GN=ATP13A4 PE=2 SV=3	1	1	1	133.9	ATP13A4
Q9HD40	O-phosphoserine-tRNA(Sec) selenium transferase OS=Homo sapiens OX=9606 GN=SEPSECS PE=1 SV=2	2	1	1	55.7	SEPSECS
Q9UJX3	Anaphase-promoting complex subunit 7 OS=Homo sapiens OX=9606 GN=ANAPC7 PE=1 SV=4	2	1	1	66.8	ANAPC7

Unique Proteins-Test

Accession	Description	Coverage [%]	# Peptides	# Unique Peptides	MW [kDa]	Gene Symbol
P29803	Pyruvate dehydrogenase E1 component subunit alpha, testis- specific form, mitochondrial OS=Homo sapiens OX=9606 GN=PDHA2 PE=1 SV=1	11	4	1	42.9	PDHA2
Q9Y4B6	DDB1- and CUL4-associated factor 1 OS=Homo sapiens OX=9606 GN=DCAF1 PE=1 SV=3	2	1	1	168.9	DCAF1
P82094	TATA element modulatory factor OS=Homo sapiens OX=9606 GN=TMF1 PE=1 SV=2	1	1	1	122.8	TMF1
Q96JC1	Vam6/Vps39-like protein OS=Homo sapiens OX=9606 GN=VPS39 PE=1 SV=2	2	1	1	101.7	VPS39
P78537	Biogenesis of lysosome-related organelles complex 1 subunit 1 OS=Homo sapiens OX=9606 GN=BLOC1S1 PE=1 SV=2	7	1	1	17.3	BLOC1S1
Q96D71	RalBP1-associated Eps domain- containing protein 1 OS=Homo sapiens OX=9606 GN=REPS1 PE=1 SV=3	2	1	1	86.6	REPS1
Q9BPZ7	Target of rapamycin complex 2 subunit MAPKAP1 OS=Homo sapiens OX=9606 GN=MAPKAP1	2	1	1	59.1	MAPKAP1

	PE=1 SV=2					
<i>O43314</i>	Inositol hexakisphosphate and diphosphoinositol-pentakisphosphate kinase 2 OS=Homo sapiens OX=9606 GN=PPIP5K2 PE=1 SV=3	1	1	1	140.3	PPIP5K2
<i>Q00765</i>	Receptor expression-enhancing protein 5 OS=Homo sapiens OX=9606 GN=REEP5 PE=1 SV=3	5	1	1	21.5	REEP5
<i>P52732</i>	Kinesin-like protein KIF11 OS=Homo sapiens OX=9606 GN=KIF11 PE=1 SV=2	1	1	1	119.1	KIF11
<i>Q9BYD3</i>	39S ribosomal protein L4, mitochondrial OS=Homo sapiens OX=9606 GN=MRPL4 PE=1 SV=1	4	1	1	34.9	MRPL4
<i>Q9Y5U8</i>	Mitochondrial pyruvate carrier 1 OS=Homo sapiens OX=9606 GN=MPC1 PE=1 SV=1	7	1	1	12.3	MPC1
<i>Q7Z5G4</i>	Golgin subfamily A member 7 OS=Homo sapiens OX=9606 GN=GOLGA7 PE=1 SV=2	8	1	1	15.8	GOLGA7
<i>A6NC98</i>	Coiled-coil domain-containing protein 88B OS=Homo sapiens OX=9606 GN=CCDC88B PE=1 SV=1	1	1	1	164.7	CCDC88B
<i>Q9HAU5</i>	Regulator of nonsense transcripts 2 OS=Homo sapiens OX=9606 GN=UPF2 PE=1 SV=1	1	1	1	147.7	UPF2

Unique Proteins-Test-VEGF

<i>Accession</i>	<i>Description</i>	<i>Coverage [%]</i>	<i># Peptides</i>	<i># Unique Peptides</i>	<i>MW [kDa]</i>	<i>Gene Symbol</i>
P57721	Poly(rC)-binding protein 3 OS=Homo sapiens OX=9606 GN=PCBP3 PE=1 SV=2	20	7	1	39.4	PCBP3
P01877	Immunoglobulin heavy constant alpha 2 OS=Homo sapiens OX=9606 GN=IGHA2 PE=1 SV=4	10	3	1	36.6	IGHA2
Q96RL7	Vacuolar protein sorting-associated protein 13A OS=Homo sapiens OX=9606 GN=VPS13A PE=1 SV=2	1	1	1	360	VPS13A
P01591	Immunoglobulin J chain OS=Homo sapiens OX=9606 GN=JCHAIN PE=1 SV=4	8	1	1	18.1	JCHAIN
Q9HC84	Mucin-5B OS=Homo sapiens OX=9606 GN=MUC5B PE=1 SV=3	1	2	2	596	MUC5B
B9A064	Immunoglobulin lambda-like polypeptide 5 OS=Homo sapiens OX=9606 GN=IGLL5 PE=2 SV=2	7	1	1	23	IGLL5
Q9C040	Tripartite motif-containing protein 2 OS=Homo sapiens OX=9606 GN=TRIM2 PE=1 SV=1	2	1	1	81.5	TRIM2
Q9ULK4	Mediator of RNA polymerase II transcription subunit 23 OS=Homo sapiens OX=9606 GN=MED23 PE=1 SV=2	1	1	1	156.4	MED23
Q9H330	Transmembrane protein 245 OS=Homo sapiens OX=9606 GN=TMEM245 PE=1 SV=3	2	1	1	97.3	TMEM245
O75884	Serine hydrolase RBBP9 OS=Homo sapiens OX=9606 GN=RBBP9 PE=1 SV=2	8	1	1	21	RBBP9
O75151	Lysine-specific demethylase PHF2 OS=Homo sapiens OX=9606 GN=PHF2 PE=1 SV=4	1	1	1	120.7	PHF2
Q8TB61	Adenosine 3'-phospho 5'-phosphosulfate transporter 1 OS=Homo sapiens OX=9606 GN=SLC35B2 PE=1 SV=1	3	1	1	47.5	SLC35B2
H7BZ55	Ciliary rootlet coiled-coil protein 2 OS=Homo sapiens OX=9606	1	2	1	185.5	CROCC2

	GN=CROCC2 PE=1 SV=4					
P31942	Heterogeneous nuclear ribonucleoprotein H3 OS=Homo sapiens OX=9606 GN=HNRNPH3 PE=1 SV=2	3	1	1	36.9	HNRNPH3
Q14966	Zinc finger protein 638 OS=Homo sapiens OX=9606 GN=ZNF638 PE=1 SV=2	1	1	1	220.5	ZNF638
P17544	Cyclic AMP-dependent transcription factor ATF-7 OS=Homo sapiens OX=9606 GN=ATF7 PE=1 SV=3	5	1	1	51.7	ATF7
Q6PD62	RNA polymerase-associated protein CTR9 homolog OS=Homo sapiens OX=9606 GN=CTR9 PE=1 SV=1	1	1	1	133.4	CTR9
Q3V6T2	Girdin OS=Homo sapiens OX=9606 GN=CCDC88A PE=1 SV=2	1	1	1	215.9	CCDC88A
Q70IA6	MOB kinase activator 2 OS=Homo sapiens OX=9606 GN=MOB2 PE=1 SV=1	5	1	1	26.9	MOB2
Q8NEB9	Phosphatidylinositol 3-kinase catalytic subunit type 3 OS=Homo sapiens OX=9606 GN=PIK3C3 PE=1 SV=1	1	1	1	101.5	PIK3C3
Q9UHR5	SAP30-binding protein OS=Homo sapiens OX=9606 GN=SAP30BP PE=1 SV=1	4	1	1	33.9	SAP30BP
P01834	Immunoglobulin kappa constant OS=Homo sapiens OX=9606 GN=IGKC PE=1 SV=2	13	1	1	11.8	IGKC
P22735	Protein-glutamine gamma-glutamyltransferase K OS=Homo sapiens OX=9606 GN=TGM1 PE=1 SV=4	1	1	1	89.7	TGM1
Q7Z6M1	Rab9 effector protein with kelch motifs OS=Homo sapiens OX=9606 GN=RABEPK PE=1 SV=1	6	1	1	40.5	RABEPK
Q9NUY8	TBC1 domain family member 23 OS=Homo sapiens OX=9606 GN=TBC1D23 PE=1 SV=3	1	1	1	78.3	TBC1D23
Q15063	Periostin OS=Homo sapiens OX=9606 GN=POSTN PE=1 SV=2	2	1	1	93.3	POSTN
Q8TAX7	Mucin-7 OS=Homo sapiens OX=9606 GN=MUC7 PE=1 SV=2	2	1	1	39.1	MUC7
Q9H0E2	Toll-interacting protein OS=Homo sapiens OX=9606 GN=TOLLIP PE=1	3	1	1	30.3	TOLLIP

	SV=1					
<i>Q9NXW2</i>	DnaJ homolog subfamily B member 12 OS=Homo sapiens OX=9606 GN=DNAJB12 PE=1 SV=5	3	1	1	41.8	DNAJB12
<i>Q8IUH4</i>	Palmitoyltransferase ZDHHC13 OS=Homo sapiens OX=9606 GN=ZDHHC13 PE=1 SV=3	2	1	1	70.8	ZDHHC13
<i>Q9NPP4</i>	NLR family CARD domain-containing protein 4 OS=Homo sapiens OX=9606 GN=NLRC4 PE=1 SV=2	1	1	1	116.1	NLRC4

T-Test Analysis (Test of Significance): Test Vs Control

Accession	Description	Significance	fold change	logFC	P.Value	Coverage [%]	# Peptides	MW [kDa]	Gene Symbol
P61587	Rho-related GTP-binding protein RhoE OS=Homo sapiens OX=9606 GN=RND3 PE=1 SV=1	+	31.2518 1585	4.96586 8113	3.96E-06	5	1	27.4	RND3
Q9NV31	U3 small nucleolar ribonucleoprotein protein IMP3 OS=Homo sapiens OX=9606 GN=IMP3 PE=1 SV=1	+	19.3354 1585	4.27317 3888	0.00719 8682	8	1	21.8	IMP3
P84243	Histone H3.3 OS=Homo sapiens OX=9606 GN=H3-3A PE=1 SV=2	+	14.5556 5181	3.86350 754	0.00016 8515	65	12	15.3	H3-3A; H3-3B
P55060	Exportin-2 OS=Homo sapiens OX=9606 GN=CSE1L PE=1 SV=3	+	13.8719 8801	3.79410 2652	2.32E-07	26	24	110.3	CSE1L
Q9U0U0	Vesicle transport through interaction with t-SNAREs homolog 1B OS=Homo sapiens OX=9606 GN=VT11B PE=1 SV=3	+	12.7003 9545	3.66680 1514	5.19E-06	4	1	26.7	VT11B
O75962	Triple functional domain protein OS=Homo sapiens OX=9606 GN=TRIO PE=1 SV=2	+	10.7557 3605	3.42703 4351	4.49E-07	2	6	346.7	TRIO
P62304	Small nuclear ribonucleoprotein E OS=Homo sapiens OX=9606 GN=SNRPE PE=1 SV=1	+	9.73470 7135	3.28313 7577	0.00055 0452	17	2	10.8	SNRPE
O15118	NPC intracellular cholesterol transporter 1 OS=Homo sapiens	+	8.54669 7848	3.09536 712	0.00060 4319	1	1	142.1	NPC1

	OX=9606 GN=NPC1 PE=1 SV=2								
P623 08	Small nuclear ribonucleoprotein G OS=Homo sapiens OX=9606 GN=SNRPG PE=1 SV=1	+	7.83068 4334	2.96913 8392	0.02610 9214	16	1	8.5	SNRPG
Q96S 82	Ubiquitin-like protein 7 OS=Homo sapiens OX=9606 GN=UBL7 PE=1 SV=2	+	7.37730 172	2.88309 3241	0.01370 8238	3	1	40. 5	UBL7
P209 36	Ras GTPase- activating protein 1 OS=Homo sapiens OX=9606 GN=RASA1 PE=1 SV=1	+	6.58564 5536	2.71932 4863	0.02141 8139	5	4	11 6.3	RASA1
P184 33	Receptor-type tyrosine-protein phosphatase alpha OS=Homo sapiens OX=9606 GN=PTPRA PE=1 SV=3	+	5.95214 6877	2.57341 0127	3.24E- 05	2	2	90. 7	PTPRA
Q9H9 A6	Leucine-rich repeat- containing protein 40 OS=Homo sapiens OX=9606 GN=LRRC40 PE=1 SV=1	+	5.93466 9889	2.56916 7783	0.00283 2215	4	3	68. 2	LRRC4 0
Q152 57	Serine/threonine- protein phosphatase 2A activator OS=Homo sapiens OX=9606 GN=PTPA PE=1 SV=3	+	5.75100 6156	2.52381 4382	1.90E- 05	15	5	40. 6	PTPA
O149 76	Cyclin-G-associated kinase OS=Homo sapiens OX=9606 GN=GAK PE=1 SV=2	+	5.65187 8985	2.49873 0576	0.04071 0604	2	2	14 3.1	GAK
Q9H4 A6	Golgi phosphoprotein 3 OS=Homo sapiens OX=9606 GN=GOLPH3 PE=1 SV=1	+	5.29505 5954	2.40464 593	0.00015 0493	12	3	33. 8	GOLPH 3
Q8NC N5	Pyruvate dehydrogenase phosphatase regulatory subunit, mitochondrial	+	5.15127 4462	2.36492 9409	0.01576 1527	2	2	99. 3	PDPR

	OS=Homo sapiens OX=9606 GN=PDPR PE=1 SV=2								
Q96P M9	Zinc finger protein 385A OS=Homo sapiens OX=9606 GN=ZNF385A PE=1 SV=2	+	5.05725 3543	2.33835 4109	0.01811 8783	3	1	40. 4	ZNF38 5A
Q96R Q3	Methylcrotonoyl-CoA carboxylase subunit alpha, mitochondrial OS=Homo sapiens OX=9606 GN=MCCC1 PE=1 SV=3	+	4.71049 9379	2.23588 0014	0.00885 7829	1	1	80. 4	MCCC 1
Q8NC 56	LEM domain- containing protein 2 OS=Homo sapiens OX=9606 GN=LEMD2 PE=1 SV=1	+	4.50354 9812	2.17106 2619	0.04819 4666	7	3	56. 9	LEMD2
Q9GZ Y8	Mitochondrial fission factor OS=Homo sapiens OX=9606 GN=MFF PE=1 SV=1	+	4.39379 6676	2.13546 811	0.00027 9326	5	1	38. 4	MFF
P111 71	Protein 4.1 OS=Homo sapiens OX=9606 GN=EPB41 PE=1 SV=4	+	4.32182 5511	2.11164 0826	0.00070 7135	4	4	97	EPB41
Q151 20	[Pyruvate dehydrogenase (acetyl-transferring)] kinase isozyme 3, mitochondrial OS=Homo sapiens OX=9606 GN=PDK3 PE=1 SV=1	+	4.09380 8332	2.03344 3558	0.00901 895	10	3	46. 9	PDK3
Q8TB A6	Golgin subfamily A member 5 OS=Homo sapiens OX=9606 GN=GOLGA5 PE=1 SV=3	+	3.97718 501	1.99174 7675	0.01437 3427	5	4	83	GOLGA 5
Q96P E2	Rho guanine nucleotide exchange factor 17 OS=Homo sapiens OX=9606 GN=ARHGEF17 PE=1 SV=1	+	3.65080 8527	1.86821 6006	0.00011 9614	1	2	22 1.5	ARHGE F17
Q134 25	Beta-2-syntrophin OS=Homo sapiens	+	3.48082 8589	1.79943 0771	6.13E- 05	21	11	57. 9	SNTB2

	OX=9606 GN=SNTB2 PE=1 SV=1								
P027 48	Complement component C9 OS=Homo sapiens OX=9606 GN=C9 PE=1 SV=2	+	3.35167 1973	1.74488 096	0.00244 5463	4	2	63. 1	C9
P412 19	Peripherin OS=Homo sapiens OX=9606 GN=PRPH PE=1 SV=2	+	3.34280 2703	1.74105 8208	0.03985 6933	11	8	53. 6	PRPH
Q153 34	Lethal(2) giant larvae protein homolog 1 OS=Homo sapiens OX=9606 GN=LLGL1 PE=1 SV=3	+	3.12835 088	1.64540 2336	0.03226 2915	4	3	11 5.3	LLGL1
P040 62	Lysosomal acid glucosylceramidase OS=Homo sapiens OX=9606 GN=GBA PE=1 SV=3	+	3.12247 2155	1.64268 8706	0.01337 031	1	1	59. 7	GBA
Q9UJ 50	Calcium-binding mitochondrial carrier protein Aralar2 OS=Homo sapiens OX=9606 GN=SLC25A13 PE=1 SV=2	+	3.08758 2635	1.62647 7749	0.04441 9617	11	8	74. 1	SLC25 A13
Q149 19	Dr1-associated corepressor OS=Homo sapiens OX=9606 GN=DRAP1 PE=1 SV=3	+	3.03715 1484	1.60271 8868	0.01263 6159	9	2	22. 3	DRAP1
Q925 99	Septin-8 OS=Homo sapiens OX=9606 GN=SEPTIN8 PE=1 SV=4	+	3.02837 2966	1.59854 2894	0.01134 9489	16	7	55. 7	SEPTIN 8
Q127 68	WASH complex subunit 5 OS=Homo sapiens OX=9606 GN=WASHC5 PE=1 SV=1	+	2.94890 6832	1.56018 0242	0.00543 9033	1	1	13 4.2	WASH C5
O604 76	Mannosyl- oligosaccharide 1,2- alpha-mannosidase IB OS=Homo sapiens OX=9606 GN=MAN1A2 PE=1	+	2.94011 7172	1.55587 3652	0.00779 5167	3	2	73	MAN1 A2

	SV=1								
Q9NR Y5	Protein FAM114A2 OS=Homo sapiens OX=9606 GN=FAM114A2 PE=1 SV=4	+	2.93930 5289	1.55547 5212	0.03911 1214	3	1	55. 4	FAM11 4A2
P299 72	Aquaporin-1 OS=Homo sapiens OX=9606 GN=AQP1 PE=1 SV=3	+	2.93657 8556	1.55413 6232	0.00152 288	7	1	28. 5	AQP1
Q5JT V8	Torsin-1A-interacting protein 1 OS=Homo sapiens OX=9606 GN=TOR1AIP1 PE=1 SV=2	+	2.75775 5129	1.46349 436	0.00559 0572	2	1	66. 2	TOR1A IP1
Q167 95	NADH dehydrogenase [ubiquinone] 1 alpha subcomplex subunit 9, mitochondrial OS=Homo sapiens OX=9606 GN=NDUFA9 PE=1 SV=2	+	2.70068 0269	1.43332 2851	0.03856 2634	5	2	42. 5	NDUFA 9
Q96S 99	Pleckstrin homology domain-containing family F member 1 OS=Homo sapiens OX=9606 GN=PLEKHF1 PE=1 SV=3	+	2.68616 5109	1.42554 7985	0.04468 9264	5	1	31. 2	PLEKH F1
Q8NE 86	Calcium uniporter protein, mitochondrial OS=Homo sapiens OX=9606 GN=MCU PE=1 SV=1	+	2.66373 8575	1.41345 25	0.00839 5305	6	2	39. 8	MCU
P497 48	Very long-chain specific acyl-CoA dehydrogenase, mitochondrial OS=Homo sapiens OX=9606 GN=ACADVL PE=1 SV=1	+	2.54813 6014	1.34944 2288	0.00046 8799	6	4	70. 3	ACADV L

Q562 R1	Beta-actin-like protein 2 OS=Homo sapiens OX=9606 GN=ACTBL2 PE=1 SV=2	+	2.50853 9843	1.32684 7852	0.02650 547	18	9	42	ACTBL 2
Q9UN L2	Translocon-associated protein subunit gamma OS=Homo sapiens OX=9606 GN=SSR3 PE=1 SV=1	+	2.46400 5144	1.30100 5268	0.00741 0222	12	3	21. 1	SSR3
P684 00	Casein kinase II subunit alpha OS=Homo sapiens OX=9606 GN=CSNK2A1 PE=1 SV=1	+	2.44626 0515	1.29057 8052	0.01105 4495	33	10	45. 1	CSNK2 A1
Q9H9 J2	39S ribosomal protein L44, mitochondrial OS=Homo sapiens OX=9606 GN=MRPL44 PE=1 SV=1	+	2.42994 7207	1.28092 497	0.04575 3882	3	1	37. 5	MRPL4 4
O001 61	Synaptosomal-associated protein 23 OS=Homo sapiens OX=9606 GN=SNAP23 PE=1 SV=1	+	2.42739 1155	1.27940 6606	0.00028 476	7	1	23. 3	SNAP2 3
P106 20	Microsomal glutathione S-transferase 1 OS=Homo sapiens OX=9606 GN=MGST1 PE=1 SV=1	+	2.41250 0322	1.27052 9135	0.03304 4227	22	2	17. 6	MGST1
O606 45	Exocyst complex component 3 OS=Homo sapiens OX=9606 GN=EXOC3 PE=1 SV=3	+	2.31888 7481	1.21343 2818	0.00236 0679	5	3	85. 5	EXOC3
Q8ND Z4	Divergent protein kinase domain 2A OS=Homo sapiens OX=9606 GN=DIPK2A PE=1 SV=1	+	2.29026 4271	1.19551 4079	0.02368 3868	5	2	49. 5	DIPK2 A

Q765 P7	Protein MTSS 2 OS=Homo sapiens OX=9606 GN=MTSS2 PE=1 SV=1	+	2.27185 6109	1.18387 1463	0.03148 8136	1	1	79. 9	MTSS2
Q86T 29	Zinc finger protein 605 OS=Homo sapiens OX=9606 GN=ZNF605 PE=2 SV=1	+	2.24180 9729	1.16466 3836	0.01853 3709	1	1	74. 3	ZNF60 5
Q9Y6 76	28S ribosomal protein S18b, mitochondrial OS=Homo sapiens OX=9606 GN=MRPS18B PE=1 SV=1	+	2.21678 0837	1.14846 6145	0.03784 3415	3	1	29. 4	MRPS1 8B
P068 58	Lipoprotein lipase OS=Homo sapiens OX=9606 GN=LPL PE=1 SV=1	+	2.19586 1174	1.13478 6848	0.00625 3343	8	3	53. 1	LPL
Q9Y2 23	Bifunctional UDP-N- acetylglucosamine 2- epimerase/N- acetylmannosamine kinase OS=Homo sapiens OX=9606 GN=GNE PE=1 SV=1	+	2.17391 5063	1.12029 5574	0.02738 209	3	2	79. 2	GNE
C9JL W8	Mapk-regulated corepressor- interacting protein 1 OS=Homo sapiens OX=9606 GN=MCRIP1 PE=1 SV=1	+	2.16114 5664	1.11179 6315	0.02345 8281	23	2	10. 9	MCRIP 1
Q8N3 C0	Activating signal cointegrator 1 complex subunit 3 OS=Homo sapiens OX=9606 GN=ASCC3 PE=1 SV=3	+	2.16077 4112	1.11154 8261	0.01305 4128	2	3	25 1.3	ASCC3
Q9BP X6	Calcium uptake protein 1, mitochondrial OS=Homo sapiens OX=9606 GN=MICU1 PE=1 SV=1	+	2.11935 337	1.08362 4155	0.00730 7642	3	2	54. 3	MICU1
P293	Protein S100-G	+	2.10811	1.07595	0.03118	9	1	9	S100G

77	OS=Homo sapiens OX=9606 GN=S100G PE=1 SV=2		3679	2665	1673				
P274 82	Calmodulin-like protein 3 OS=Homo sapiens OX=9606 GN=CALML3 PE=1 SV=2	+	2.07305 2429	1.05175 6604	0.02715 4557	32	4	16. 9	CALML 3
Q129 81	Vesicle transport protein SEC20 OS=Homo sapiens OX=9606 GN=BNIP1 PE=1 SV=3	+	2.07212 9769	1.05111 4356	0.00190 8595	12	3	26. 1	BNIP1
O152 58	Protein RER1 OS=Homo sapiens OX=9606 GN=RER1 PE=1 SV=1	+	2.05980 0067	1.04250 431	0.00527 1174	24	4	22. 9	RER1
Q9HC 35	Echinoderm microtubule- associated protein- like 4 OS=Homo sapiens OX=9606 GN=EML4 PE=1 SV=3	+	2.03001 8411	1.02149 2812	0.01129 6758	6	5	10 8.8	EML4
Q8IX M6	Nurim OS=Homo sapiens OX=9606 GN=NRM PE=1 SV=1	+	2.01899 1859	1.01363 5093	0.00336 7327	11	2	29. 4	NRM
O760 24	Wolframin OS=Homo sapiens OX=9606 GN=WFS1 PE=1 SV=2	+	2.00641 8527	1.00462 2575	0.01543 7012	1	1	10 0.2	WFS1
P420 25	Beta-actin OS=Homo sapiens OX=9606 GN=ACTR1B PE=1 SV=1	+	2.00064 158	1.00046 2728	0.03810 9995	26	9	42. 3	ACTR1 B
Q996 14	Tetratricopeptide repeat protein 1 OS=Homo sapiens OX=9606 GN=TTC1 PE=1 SV=1	+	1.98557 1674	0.98955 4439	0.01321 0781	7	2	33. 5	TTC1
Q8N2 01	Integrator complex subunit 1 OS=Homo sapiens OX=9606 GN=INTS1 PE=1 SV=2	+	1.97216 7498	0.97978 2087	0.00371 71	1	3	24 4.1	INTS1
P356 10	Sterol O- acyltransferase 1 OS=Homo sapiens OX=9606 GN=SOAT1	+	1.96968 6596	0.97796 6095	0.03052 043	2	1	64. 7	SOAT1

	PE=1 SV=3								
Q96IX 5	ATP synthase membrane subunit K, mitochondrial OS=Homo sapiens OX=9606 GN=ATP5MK PE=1 SV=1	+	1.96327 7645	0.97326 4212	0.00268 7606	19	2	6.5	ATP5 MK
Q9NR Y4	Rho GTPase- activating protein 35 OS=Homo sapiens OX=9606 GN=ARHGAP35 PE=1 SV=3	+	1.92812 0619	0.94719 5306	0.02301 5192	3	5	17 0.4	ARHG AP35
Q7L0 14	Probable ATP- dependent RNA helicase DDX46 OS=Homo sapiens OX=9606 GN=DDX46 PE=1 SV=2	+	1.92667 0828	0.94611 0108	0.00139 8865	21	21	11 7.3	DDX46
Q150 84	Protein disulfide- isomerase A6 OS=Homo sapiens OX=9606 GN=PDIA6 PE=1 SV=1	+	1.90389 039	0.92895 0423	0.00356 032	25	9	48. 1	PDIA6
P121 07	Collagen alpha-1(XI) chain OS=Homo sapiens OX=9606 GN=COL11A1 PE=1 SV=4	+	1.88478 8162	0.91440 2383	0.02729 9869	2	3	18 1	COL11 A1
Q161 86	Proteasomal ubiquitin receptor ADRM1 OS=Homo sapiens OX=9606 GN=ADRM1 PE=1 SV=2	+	1.87987 6068	0.91063 7554	0.00659 5934	4	2	42. 1	ADRM 1
Q5W 0V3	FHF complex subunit HOOK interacting protein 2A OS=Homo sapiens OX=9606 GN=FHIP2A PE=1 SV=1	+	1.87954 9133	0.91038 6629	0.00957 5981	1	1	86. 5	FHIP2A
Q142 89	Protein-tyrosine kinase 2-beta OS=Homo sapiens OX=9606 GN=PTK2B	+	1.87479 2773	0.90673 1138	0.00183 3411	3	3	11 5.8	PTK2B

	PE=1 SV=2								
P497 70	Translation initiation factor eIF-2B subunit beta OS=Homo sapiens OX=9606 GN=EIF2B2 PE=1 SV=3	+	1.87088 1609	0.90371 8267	0.01942 2356	2	1	39	EIF2B2
Q9HD 20	Endoplasmic reticulum transmembrane helix translocase OS=Homo sapiens OX=9606 GN=ATP13A1 PE=1 SV=2	+	1.86829 7252	0.90172 4011	0.02980 8687	8	8	13 2.9	ATP13 A1
P175 16	Aldo-keto reductase family 1 member C4 OS=Homo sapiens OX=9606 GN=AKR1C4 PE=1 SV=3	+	1.86607 2503	0.90000 5041	0.02261 2703	3	1	37	AKR1C 4
P509 93	Sodium/potassium-transporting ATPase subunit alpha-2 OS=Homo sapiens OX=9606 GN=ATP1A2 PE=1 SV=1	+	1.84487 8488	0.88352 5797	0.01518 4556	13	12	11 2.2	ATP1A 2
Q96II 8	DISP complex protein LRCH3 OS=Homo sapiens OX=9606 GN=LRCH3 PE=1 SV=2	+	1.84406 6985	0.88289 1062	0.02917 4883	2	1	86	LRCH3
Q96J B1	Dynein axonemal heavy chain 8 OS=Homo sapiens OX=9606 GN=DNAH8 PE=1 SV=2	+	1.83354 3226	0.87463 4278	0.00352 3121	0	1	51 4.3	DNAH 8
Q929 97	Segment polarity protein dishevelled homolog DVL-3 OS=Homo sapiens OX=9606 GN=DVL3 PE=1 SV=2	+	1.81491 0498	0.85989 8404	0.01114 2537	4	3	78	DVL3
P607 09	Actin, cytoplasmic 1 OS=Homo sapiens	+	1.81289 9623	0.85829 9048	0.03262 1085	78	30	41. 7	ACTB

	OX=9606 GN=ACTB PE=1 SV=1								
P557 95	Heterogeneous nuclear ribonucleoprotein H2 OS=Homo sapiens OX=9606 GN=HNRNPH2 PE=1 SV=1	+	1.80581 0149	0.85264 6225	0.00646 6881	21	7	49. 2	HNRN PH2
Q9NQ P4	Prefoldin subunit 4 OS=Homo sapiens OX=9606 GN=PFDN4 PE=1 SV=1	+	1.79024 9959	0.84016 1034	0.01433 7148	11	1	15. 3	PFDN4
Q9UP N6	SR-related and CTD- associated factor 8 OS=Homo sapiens OX=9606 GN=SCAF8 PE=1 SV=1	+	1.78738 597	0.83785 1205	0.00535 7783	1	1	14 0.4	SCAF8
P563 85	ATP synthase subunit e, mitochondrial OS=Homo sapiens OX=9606 GN=ATP5ME PE=1 SV=2	+	1.77612 1796	0.82873 0517	0.00189 6948	17	2	7.9	ATP5 ME
O001 16	Alkyldihydroxyaceton ephosphate synthase, peroxisomal OS=Homo sapiens OX=9606 GN=AGPS PE=1 SV=1	+	1.77456 6761	0.82746 6851	0.00279 1112	7	4	72. 9	AGPS
Q9H0 A0	RNA cytidine acetyltransferase OS=Homo sapiens OX=9606 GN=NAT10 PE=1 SV=2	+	1.75929 814	0.81499 999	0.01227 5533	5	5	11 5.7	NAT10
Q9Y6 13	FH1/FH2 domain- containing protein 1 OS=Homo sapiens OX=9606 GN=FHOD1 PE=1 SV=3	+	1.74285 8291	0.80145 5271	0.00352 0321	3	4	12 6.5	FHOD1
Q9Y6 08	Leucine-rich repeat flightless-interacting protein 2 OS=Homo sapiens OX=9606 GN=LRRFIP2 PE=1 SV=1	+	1.74178 8734	0.80056 9646	0.00218 9086	4	3	82. 1	LRRFIP 2

Q135 86	Stromal interaction molecule 1 OS=Homo sapiens OX=9606 GN=STIM1 PE=1 SV=3	+	1.71539 7114	0.77854 2599	0.00521 9278	8	4	77. 4	STIM1
Q86U E4	Protein LYRIC OS=Homo sapiens OX=9606 GN=MTDH PE=1 SV=2	+	1.71277 5962	0.77633 6453	0.04815 9924	14	5	63. 8	MTDH
Q9Y2 82	Endoplasmic reticulum-Golgi intermediate compartment protein 3 OS=Homo sapiens OX=9606 GN=ERGIC3 PE=1 SV=1	+	1.70682 7302	0.77131 7093	0.04941 9988	7	3	43. 2	ERGIC 3
P515 31	Probable global transcription activator SNF2L2 OS=Homo sapiens OX=9606 GN=SMARCA2 PE=1 SV=2	+	1.70645 6161	0.77100 3352	0.02829 9915	7	9	18 1.2	SMAR CA2
Q9HD 33	39S ribosomal protein L47, mitochondrial OS=Homo sapiens OX=9606 GN=MRPL47 PE=1 SV=2	+	1.69774 0362	0.76361 5842	0.03905 1147	4	1	29. 4	MRPL4 7
Q9UB P6	tRNA (guanine-N(7)-)-methyltransferase OS=Homo sapiens OX=9606 GN=METTL1 PE=1 SV=1	+	1.68964 576	0.75672 0812	0.02684 8138	3	1	31. 5	METTL 1
P143 14	Glucosidase 2 subunit beta OS=Homo sapiens OX=9606 GN=PRKCSH PE=1 SV=2	+	1.68120 5442	0.74949 6032	0.04386 2814	7	5	59. 4	PRKCS H
Q96B P3	Peptidylprolyl isomerase domain and WD repeat-containing protein 1 OS=Homo sapiens OX=9606 GN=PPWD1 PE=1 SV=1	+	1.67076 2824	0.74050 6947	0.03753 6546	4	2	73. 5	PPWD 1

Q15173	Membrane-associated progesterone receptor component 2 OS=Homo sapiens OX=9606 GN=PGRMC2 PE=1 SV=1	+	1.65422078	0.726151796	0.01593846	17	4	23.8	PGRMC2
Q9NR15	Disrupted in schizophrenia 1 protein OS=Homo sapiens OX=9606 GN=DISC1 PE=1 SV=3	+	1.652593519	0.724731915	0.021442067	1	1	93.6	DISC1
Q9Y6A4	Cilia- and flagella-associated protein 20 OS=Homo sapiens OX=9606 GN=CFAP20 PE=1 SV=1	+	1.646424967	0.719336765	0.03917482	21	4	22.8	CFAP20
Q14410	Glycerol kinase 2 OS=Homo sapiens OX=9606 GN=GK2 PE=2 SV=2	+	1.632901012	0.707437336	0.003516911	1	1	60.6	GK2
O43772	Mitochondrial carnitine/acylcarnitine carrier protein OS=Homo sapiens OX=9606 GN=SLC25A20 PE=1 SV=1	+	1.622041032	0.697810315	0.005366037	11	4	32.9	SLC25A20
P08697	Alpha-2-antiplasmin OS=Homo sapiens OX=9606 GN=SERPINF2 PE=1 SV=3	+	1.618482546	0.694641807	0.026981582	2	1	54.5	SERPINF2
Q9NYL4	Peptidyl-prolyl cis-trans isomerase FKBP11 OS=Homo sapiens OX=9606 GN=FKBP11 PE=1 SV=1	+	1.617349995	0.693631912	0.048003133	9	3	22.2	FKBP11
O15260	Surfeit locus protein 4 OS=Homo sapiens OX=9606 GN=SURF4 PE=1 SV=3	+	1.614503028	0.691090147	0.021151033	17	4	30.4	SURF4
Q7LBR1	Charged multivesicular body protein 1b OS=Homo	+	1.611199602	0.688135232	0.026333702	9	2	22.1	CHMP1B

	sapiens OX=9606 GN=CHMP1B PE=1 SV=1								
Q754 31	Metaxin-2 OS=Homo sapiens OX=9606 GN=MTX2 PE=1 SV=1	+	1.60455 3876	0.68217 2232	0.01717 9399	8	2	29. 7	MTX2
Q925 45	Transmembrane protein 131 OS=Homo sapiens OX=9606 GN=TMEM131 PE=1 SV=3	+	1.60335 4111	0.68109 3089	0.03211 2269	1	1	20 5	TMEM 131
O147 37	Programmed cell death protein 5 OS=Homo sapiens OX=9606 GN=PDCD5 PE=1 SV=3	+	1.59550 049	0.67400 9052	0.01513 6335	46	5	14. 3	PDCD5
P467 83	40S ribosomal protein S10 OS=Homo sapiens OX=9606 GN=RPS10 PE=1 SV=1	+	1.59011 3023	0.66912 9314	0.00580 0304	42	12	18. 9	RPS10
Q86T B9	Protein PAT1 homolog 1 OS=Homo sapiens OX=9606 GN=PATL1 PE=1 SV=2	+	1.57910 0077	0.65910 2607	0.04789 4578	3	2	86. 8	PATL1
Q9Y3 B7	39S ribosomal protein L11, mitochondrial OS=Homo sapiens OX=9606 GN=MRPL11 PE=1 SV=1	+	1.57475 1276	0.65512 398	0.00825 1252	6	1	20. 7	MRPL1 1
Q6PI7 8	Transmembrane protein 65 OS=Homo sapiens OX=9606 GN=TMEM65 PE=1 SV=2	+	1.57391 4424	0.65435 7101	0.03101 8044	5	1	25. 5	TMEM 65
Q96S 59	Ran-binding protein 9 OS=Homo sapiens OX=9606 GN=RANBP9 PE=1 SV=1	+	1.56992 7423	0.65069 7866	0.02951 882	3	2	77. 8	RANBP 9
Q759 55	Flotillin-1 OS=Homo sapiens OX=9606 GN=FLOT1 PE=1 SV=3	+	1.56790 0997	0.64883 4465	0.02713 8299	17	6	47. 3	FLOT1

Q130 84	39S ribosomal protein L28, mitochondrial OS=Homo sapiens OX=9606 GN=MRPL28 PE=1 SV=4	+	1.56776 5326	0.64870 9623	0.01948 5257	5	1	30. 1	MRPL2 8
Q8IYB 8	ATP-dependent RNA helicase SUPV3L1, mitochondrial OS=Homo sapiens OX=9606 GN=SUPV3L1 PE=1 SV=1	+	1.56526 2474	0.64640 4598	0.03544 8938	2	1	87. 9	SUPV3 L1
Q96Q D8	Sodium-coupled neutral amino acid transporter 2 OS=Homo sapiens OX=9606 GN=SLC38A2 PE=1 SV=2	+	1.56144 01	0.64287 7226	0.03889 7936	4	1	56	SLC38 A2
Q7LG A3	Heparan sulfate 2-O-sulfotransferase 1 OS=Homo sapiens OX=9606 GN=HS2ST1 PE=1 SV=1	+	1.55281 7717	0.63488 8484	0.01270 2658	6	2	41. 9	HS2ST 1
Q5JR X3	Presequence protease, mitochondrial OS=Homo sapiens OX=9606 GN=PITRM1 PE=1 SV=3	+	1.54746 07	0.62990 277	0.02765 1057	9	7	11 7.3	PITRM 1
Q7Z7 D3	V-set domain-containing T-cell activation inhibitor 1 OS=Homo sapiens OX=9606 GN=VTCN1 PE=1 SV=1	+	1.54214 7251	0.62494 0527	0.00603 934	2	1	30. 9	VTCN1
O438 15	Striatin OS=Homo sapiens OX=9606 GN=STRN PE=1 SV=4	+	1.53511 3314	0.61834 5152	0.00755 0742	9	5	86. 1	STRN
P082 40	Signal recognition particle receptor subunit alpha OS=Homo sapiens OX=9606 GN=SRPRA PE=1 SV=2	+	1.53096 3731	0.61444 0106	0.01063 7318	12	7	69. 8	SRPRA

P610 09	Signal peptidase complex subunit 3 OS=Homo sapiens OX=9606 GN=SPCS3 PE=1 SV=1	+	1.52951 5887	0.61307 5092	0.00741 7604	22	4	20. 3	SPCS3
Q135 57	Calcium/calmodulin-dependent protein kinase type II subunit delta OS=Homo sapiens OX=9606 GN=CAMK2D PE=1 SV=3	+	1.52884 1483	0.61243 8829	0.00850 6895	19	8	56. 3	CAMK 2D
P049 20	Anion exchange protein 2 OS=Homo sapiens OX=9606 GN=SLC4A2 PE=1 SV=4	+	1.51682 3147	0.60105 2885	0.01663 9972	1	1	13 6.9	SLC4A 2
O949 73	AP-2 complex subunit alpha-2 OS=Homo sapiens OX=9606 GN=AP2A2 PE=1 SV=2	+	1.51440 0516	0.59874 6807	0.01214 0937	21	19	10 3.9	AP2A2
Q9P2 X3	Protein IMPACT OS=Homo sapiens OX=9606 GN=IMPACT PE=1 SV=2	+	1.51268 1604	0.59710 8354	0.02750 7245	4	1	36. 5	IMPAC T
Q9B W27	Nuclear pore complex protein Nup85 OS=Homo sapiens OX=9606 GN=NUP85 PE=1 SV=1	+	1.50922 3087	0.59380 6074	0.03746 5545	5	3	75	NUP85
P547 60	Ephrin type-B receptor 4 OS=Homo sapiens OX=9606 GN=EPHB4 PE=1 SV=2	+	1.50603 1288	0.59075 1743	0.03181 2601	2	1	10 8.2	EPHB4
Q9UN P4	Lactosylceramide alpha-2,3-sialyltransferase OS=Homo sapiens OX=9606 GN=ST3GAL5 PE=1 SV=4	+	1.50469 8314	0.58947 4262	0.03711 115	2	1	48	ST3GA L5
Q6U WH4	Golgi-associated kinase 1B OS=Homo	+	1.49760 6985	0.58265 9069	0.03962 2848	2	1	57. 5	GASK1 B

	sapiens OX=9606 GN=GASK1B PE=2 SV=1								
Q8W XE9	Stonin-2 OS=Homo sapiens OX=9606 GN=STON2 PE=1 SV=1	+	1.49525 3719	0.58039 0306	0.00629 4505	1	1	10 1.1	STON2
Q003 25	Phosphate carrier protein, mitochondrial OS=Homo sapiens OX=9606 GN=SLC25A3 PE=1 SV=2	+	1.48791 3365	0.57329 0527	0.03101 1175	20	10	40. 1	SLC25 A3
P432 46	DNA mismatch repair protein Msh2 OS=Homo sapiens OX=9606 GN=MSH2 PE=1 SV=1	+	1.47999 7125	0.56559 4373	0.01798 784	6	6	10 4.7	MSH2
Q149 97	Proteasome activator complex subunit 4 OS=Homo sapiens OX=9606 GN=PSME4 PE=1 SV=2	+	1.47869 038	0.56432 0001	0.02152 9211	4	7	21 1.2	PSME4
Q141 81	DNA polymerase alpha subunit B OS=Homo sapiens OX=9606 GN=POLA2 PE=1 SV=2	+	1.47170 0479	0.55748 4084	0.02170 731	2	1	65. 9	POLA2
Q8N3 U4	Cohesin subunit SA-2 OS=Homo sapiens OX=9606 GN=STAG2 PE=1 SV=3	+	1.47088 0611	0.55668 0151	0.01688 3709	8	10	14 1.2	STAG2
P577 40	Nuclear pore complex protein Nup107 OS=Homo sapiens OX=9606 GN=NUP107 PE=1 SV=1	+	1.46555 5894	0.55144 7991	0.03373 6494	3	3	10 6.3	NUP10 7
Q53H 12	Acylglycerol kinase, mitochondrial OS=Homo sapiens OX=9606 GN=AGK PE=1 SV=2	+	1.45130 9697	0.53735 5411	0.01184 4436	6	2	47. 1	AGK
Q9Y5 K8	V-type proton ATPase subunit D OS=Homo sapiens OX=9606	+	1.44617 5957	0.53224 3096	0.01868 394	18	4	28. 2	ATP6V 1D

	GN=ATP6V1D PE=1 SV=1								
Q969 N2	GPI transamidase component PIG-T OS=Homo sapiens OX=9606 GN=PIGT PE=1 SV=1	+	1.44438 0046	0.53045 0395	0.04779 2297	3	2	65.7	PIGT
P094 88	Glutathione S-transferase Mu 1 OS=Homo sapiens OX=9606 GN=GSTM1 PE=1 SV=3	+	1.44108 4066	0.52715 4498	0.02675 2635	19	5	25.7	GSTM1
Q9619 9	Succinate--CoA ligase [GDP-forming] subunit beta, mitochondrial OS=Homo sapiens OX=9606 GN=SUCLG2 PE=1 SV=2	+	1.44066 3376	0.52673 3277	0.03560 1789	11	5	46.5	SUCLG 2
O004 87	26S proteasome non-ATPase regulatory subunit 14 OS=Homo sapiens OX=9606 GN=PSMD14 PE=1 SV=1	+	1.43656 9783	0.52262 8075	0.03107 4638	28	9	34.6	PSMD 14
P103 01	Ras-related protein R-Ras OS=Homo sapiens OX=9606 GN=RRAS PE=1 SV=1	+	1.43136 5946	0.51739 2562	0.02287 186	16	3	23.5	RRAS
Q134 02	Unconventional myosin-VIIa OS=Homo sapiens OX=9606 GN=MYO7A PE=1 SV=2	+	1.42953 4542	0.51554 5481	0.03557 7639	1	3	25 4.2	MYO7 A
Q9UB F2	Coatomer subunit gamma-2 OS=Homo sapiens OX=9606 GN=COPG2 PE=1 SV=1	+	1.42565 0569	0.51162 0416	0.04357 3862	13	11	97.6	COPG2
Q9BY D6	39S ribosomal protein L1, mitochondrial OS=Homo sapiens OX=9606 GN=MRPL1 PE=1 SV=2	+	1.42284 7752	0.50878 1298	0.03611 8375	2	1	36.9	MRPL1

P570 88	Transmembrane protein 33 OS=Homo sapiens OX=9606 GN=TMEM33 PE=1 SV=2	+	1.42213 8755	0.50806 2232	0.01394 8299	9	2	28	TMEM 33
O146 57	Torsin-1B OS=Homo sapiens OX=9606 GN=TOR1B PE=1 SV=2	+	1.41935 8468	0.50523 8997	0.04267 4265	2	1	38	TOR1B
Q134 80	GRB2-associated-binding protein 1 OS=Homo sapiens OX=9606 GN=GAB1 PE=1 SV=2	+	1.39847 4898	0.48385 4358	0.03392 8708	3	2	76. 6	GAB1
O148 28	Secretory carrier-associated membrane protein 3 OS=Homo sapiens OX=9606 GN=SCAMP3 PE=1 SV=3	+	1.39666 4624	0.48198 5634	0.04024 1363	15	3	38. 3	SCAMP 3
P220 33	Methylmalonyl-CoA mutase, mitochondrial OS=Homo sapiens OX=9606 GN=MMUT PE=1 SV=4	+	1.39243 4344	0.47760 9303	0.01798 6791	16	10	83. 1	MMUT
Q9NX 47	E3 ubiquitin-protein ligase MARCHF5 OS=Homo sapiens OX=9606 GN=MARCHF5 PE=1 SV=1	+	1.38579 9187	0.47071 8215	0.03227 3714	17	4	31. 2	MARCH F5
P518 12	Ribosomal protein S6 kinase alpha-3 OS=Homo sapiens OX=9606 GN=RPS6KA3 PE=1 SV=1	+	1.38418 5631	0.46903 7433	0.02154 0719	21	14	83. 7	RPS6K A3
Q014 15	N-acetylgalactosamine kinase OS=Homo sapiens OX=9606 GN=GALK2 PE=1 SV=1	+	1.38387 6612	0.46871 5316	0.03731 0321	3	2	50. 3	GALK2
Q969 23	Mitochondrial amidoxime reducing	+	1.38061 5962	0.46531 2069	0.02426 564	7	3	38	MTAR C2

	component 2 OS=Homo sapiens OX=9606 GN=MTARC2 PE=1 SV=1								
Q9Y2 77	Voltage-dependent anion-selective channel protein 3 OS=Homo sapiens OX=9606 GN=VDAC3 PE=1 SV=1	+	1.37996 0678	0.46462 7158	0.01524 7272	55	12	30. 6	VDAC3
P0C8 70	Bifunctional peptidase and (3S)- lysyl hydroxylase JMJD7 OS=Homo sapiens OX=9606 GN=JMJD7 PE=1 SV=1	+	1.37784 3847	0.46241 2395	0.02590 4422	3	1	35. 9	JMJD7
P112 16	Glycogen phosphorylase, brain form OS=Homo sapiens OX=9606 GN=PYGB PE=1 SV=5	+	1.37642 9329	0.46093 0539	0.03319 6988	21	16	96. 6	PYGB
O958 65	N(G),N(G)- dimethylarginine dimethylaminohydroly ase 2 OS=Homo sapiens OX=9606 GN=DDAH2 PE=1 SV=1	+	1.37527 7994	0.45972 3269	0.03732 4225	31	8	29. 6	DDAH2
P138 04	Electron transfer flavoprotein subunit alpha, mitochondrial OS=Homo sapiens OX=9606 GN=ETFA PE=1 SV=1	+	1.37032 9679	0.45452 3024	0.02555 2974	26	7	35. 1	ETFA
Q8IVF 7	Formin-like protein 3 OS=Homo sapiens OX=9606 GN=FMNL3 PE=1 SV=3	+	1.36463 8029	0.44851 8326	0.03266 9111	1	1	11 7.1	FMNL3
O004 22	Histone deacetylase complex subunit SAP18 OS=Homo sapiens OX=9606 GN=SAP18 PE=1 SV=1	+	1.35855 3895	0.44207 1799	0.01969 0561	29	6	17. 6	SAP18
Q141 08	Lysosome membrane protein 2 OS=Homo	+	1.35838 5947	0.44189 3439	0.02050 2905	8	5	54. 3	SCARB 2

	sapiens OX=9606 GN=SCARB2 PE=1 SV=2								
Q96I2 5	Splicing factor 45 OS=Homo sapiens OX=9606 GN=RBM17 PE=1 SV=1	+	1.35461 6966	0.43788 497	0.04889 3004	16	7	44. 9	RBM1 7
O606 84	Importin subunit alpha-7 OS=Homo sapiens OX=9606 GN=KPNA6 PE=1 SV=1	+	1.35416 3015	0.43740 1422	0.03280 7633	14	6	60	KPNA6
P352 22	Catenin beta-1 OS=Homo sapiens OX=9606 GN=CTNNB1 PE=1 SV=1	+	1.35304 2777	0.43620 7451	0.02839 6456	35	24	85. 4	CTNNB 1
P381 17	Electron transfer flavoprotein subunit beta OS=Homo sapiens OX=9606 GN=ETFB PE=1 SV=3	+	1.33726 9745	0.41929 0505	0.03781 5913	22	6	27. 8	ETFB
Q9UG 18	Testin OS=Homo sapiens OX=9606 GN=TES PE=1 SV=1	+	1.33632 54	0.41827 1352	0.02602 0274	22	9	48	TES
P502 81	Matrix metalloproteinase-14 OS=Homo sapiens OX=9606 GN=MMP14 PE=1 SV=3	+	1.33059 9803	0.41207 6726	0.04655 7678	8	5	65. 9	MMP1 4
Q96C S3	FAS-associated factor 2 OS=Homo sapiens OX=9606 GN=FAF2 PE=1 SV=2	+	1.32697 8245	0.40814 4719	0.04076 1888	15	6	52. 6	FAF2
Q6DD 88	Atlastin-3 OS=Homo sapiens OX=9606 GN=ATL3 PE=1 SV=1	+	1.32185 5475	0.40256 4449	0.02488 8824	15	7	60. 5	ATL3
Q71U 36	Tubulin alpha-1A chain OS=Homo sapiens OX=9606 GN=TUBA1A PE=1 SV=1	+	1.31548 3406	0.39559 305	0.03945 9467	63	26	50. 1	TUBA1 A
P219 12	Succinate dehydrogenase [ubiquinone] iron- sulfur subunit,	+	1.31443 7849	0.39444 5928	0.04500 5529	15	4	31. 6	SDHB

	mitochondrial OS=Homo sapiens OX=9606 GN=SDHB PE=1 SV=3								
Q134 23	NAD(P) transhydrogenase, mitochondrial OS=Homo sapiens OX=9606 GN=NNT PE=1 SV=3	+	1.30903 3622	0.38850 2153	0.04735 9606	19	20	11 3.8	NNT
Q2M 389	WASH complex subunit 4 OS=Homo sapiens OX=9606 GN=WASHC4 PE=1 SV=2	+	1.29843 5718	0.37677 4592	0.04258 4885	2	2	13 6.3	WASH C4
Q8TB 72	Pumilio homolog 2 OS=Homo sapiens OX=9606 GN=PUM2 PE=1 SV=2	+	1.29320 949	0.37095 6	0.04674 1645	4	5	11 4.1	PUM2
P050 26	Sodium/potassium- transporting ATPase subunit beta-1 OS=Homo sapiens OX=9606 GN=ATP1B1 PE=1 SV=1	+	1.29137 8091	0.36891 1456	0.03178 9504	17	6	35	ATP1B 1
P264 40	Isovaleryl-CoA dehydrogenase, mitochondrial OS=Homo sapiens OX=9606 GN=IVD PE=1 SV=2	+	1.28720 695	0.36424 402	0.04324 1652	6	3	46. 6	IVD

T-Test Analysis (Test of Significance): Test-VEGF Vs Control

Accession	Description	Significance	fold change	logFC	P.Value	Coverage [%]	# Unique Peptides	MW [kDa]	Gene Symbol
P61587	Rho-related GTP-binding protein RhoE OS=Homo sapiens OX=9606 GN=RND3 PE=1 SV=1	+	31.2518 1585	4.96586 8113	3.96E- 06	5	1	27. 4	RND3
Q9NV31	U3 small nucleolar ribonucleoprotein protein IMP3 OS=Homo sapiens OX=9606 GN=IMP3 PE=1 SV=1	+	19.3354 1585	4.27317 3888	0.0071 98682	8	1	21. 8	IMP3
P84243	Histone H3.3 OS=Homo sapiens OX=9606 GN=H3-3A PE=1 SV=2	+	14.5556 5181	3.86350 754	0.0001 68515	65	2	15. 3	H3-3A; H3-3B
P55060	Exportin-2 OS=Homo sapiens OX=9606 GN=CSE1L PE=1 SV=3	+	13.8719 8801	3.79410 2652	2.32E- 07	26	24	11 0.3	CSE1L
Q9JEU0	Vesicle transport through interaction with t-SNAREs homolog 1B OS=Homo sapiens OX=9606 GN=VTI1B PE=1 SV=3	+	12.7003 9545	3.66680 1514	5.19E- 06	4	1	26. 7	VTI1B
O75962	Triple functional domain protein OS=Homo sapiens OX=9606 GN=TRIO PE=1 SV=2	+	10.7557 3605	3.42703 4351	4.49E- 07	2	6	34 6.7	TRIO
P62304	Small nuclear ribonucleoprotein E OS=Homo sapiens OX=9606 GN=SNRPE PE=1 SV=1	+	9.73470 7135	3.28313 7577	0.0005 50452	17	2	10. 8	SNRPE
O15118	NPC intracellular cholesterol transporter 1 OS=Homo sapiens OX=9606 GN=NPC1 PE=1 SV=2	+	8.54669 7848	3.09536 712	0.0006 04319	1	1	14 2.1	NPC1
P62308	Small nuclear ribonucleoprotein G OS=Homo sapiens OX=9606 GN=SNRPG PE=1 SV=1	+	7.83068 4334	2.96913 8392	0.0261 09214	16	1	8.5	SNRPG
Q08257	Quinone oxidoreductase OS=Homo sapiens		7.49907 5593	2.90671 2766	0.0541 71805	3	1	35. 2	CRYZ

	OX=9606 GN=CRYZ PE=1 SV=1								
Q96S82	Ubiquitin-like protein 7 OS=Homo sapiens OX=9606 GN=UBL7 PE=1 SV=2	+	7.37730 172	2.88309 3241	0.0137 08238	3	1	40. 5	UBL7
P20936	Ras GTPase-activating protein 1 OS=Homo sapiens OX=9606 GN=RASA1 PE=1 SV=1	+	6.58564 5536	2.71932 4863	0.0214 18139	5	4	11 6.3	RASA1
P18433	Receptor-type tyrosine- protein phosphatase alpha OS=Homo sapiens OX=9606 GN=PTPRA PE=1 SV=3	+	5.95214 6877	2.57341 0127	3.24E- 05	2	2	90. 7	PTPRA
Q9H9A 6	Leucine-rich repeat- containing protein 40 OS=Homo sapiens OX=9606 GN=LRRRC40 PE=1 SV=1	+	5.93466 9889	2.56916 7783	0.0028 32215	4	3	68. 2	LRRRC40
Q15257	Serine/threonine-protein phosphatase 2A activator OS=Homo sapiens OX=9606 GN=PTPA PE=1 SV=3	+	5.75100 6156	2.52381 4382	1.90E- 05	15	5	40. 6	PTPA
O14976	Cyclin-G-associated kinase OS=Homo sapiens OX=9606 GN=GAK PE=1 SV=2	+	5.65187 8985	2.49873 0576	0.0407 10604	2	2	14 3.1	GAK
Q9H4A 6	Golgi phosphoprotein 3 OS=Homo sapiens OX=9606 GN=GOLPH3 PE=1 SV=1	+	5.29505 5954	2.40464 593	0.0001 50493	12	3	33. 8	GOLPH 3
Q8NCN 5	Pyruvate dehydrogenase phosphatase regulatory subunit, mitochondrial OS=Homo sapiens OX=9606 GN=PDPR PE=1 SV=2	+	5.15127 4462	2.36492 9409	0.0157 61527	2	2	99. 3	PDPR
Q96PM 9	Zinc finger protein 385A OS=Homo sapiens OX=9606 GN=ZNF385A PE=1 SV=2	+	5.05725 3543	2.33835 4109	0.0181 18783	3	1	40. 4	ZNF385 A
Q96RQ 3	Methylcrotonoyl-CoA carboxylase subunit alpha, mitochondrial OS=Homo sapiens OX=9606 GN=MCCC1 PE=1 SV=3	+	4.71049 9379	2.23588 0014	0.0088 57829	1	1	80. 4	MCCC1
P01037	Cystatin-SN OS=Homo sapiens OX=9606 GN=CST1 PE=1 SV=3		4.56040 6403	2.18916 2397	0.2035 97029	26	3	16. 4	CST1

Q8NC5 6	LEM domain-containing protein 2 OS=Homo sapiens OX=9606 GN=LEMD2 PE=1 SV=1	+	4.50354 9812	2.17106 2619	0.0481 94666	7	3	56. 9	LEMD2
Q9GZY 8	Mitochondrial fission factor OS=Homo sapiens OX=9606 GN=MFF PE=1 SV=1	+	4.39379 6676	2.13546 811	0.0002 79326	5	1	38. 4	MFF
P11171	Protein 4.1 OS=Homo sapiens OX=9606 GN=EPB41 PE=1 SV=4	+	4.32182 5511	2.11164 0826	0.0007 07135	4	3	97	EPB41
Q15120	[Pyruvate dehydrogenase (acetyl-transferring)] kinase isozyme 3, mitochondrial OS=Homo sapiens OX=9606 GN=PDK3 PE=1 SV=1	+	4.09380 8332	2.03344 3558	0.0090 1895	10	3	46. 9	PDK3
Q8TBA 6	Golgin subfamily A member 5 OS=Homo sapiens OX=9606 GN=GOLGA5 PE=1 SV=3	+	3.97718 501	1.99174 7675	0.0143 73427	5	4	83	GOLGA 5
Q96PE2	Rho guanine nucleotide exchange factor 17 OS=Homo sapiens OX=9606 GN=ARHGEF17 PE=1 SV=1	+	3.65080 8527	1.86821 6006	0.0001 19614	1	2	22 1.5	ARHGE F17
P13646	Keratin, type I cytoskeletal 13 OS=Homo sapiens OX=9606 GN=KRT13 PE=1 SV=4		3.54601 5148	1.82619 8699	0.1402 63084	45	15	49. 6	KRT13
Q13425	Beta-2-syntrophin OS=Homo sapiens OX=9606 GN=SNTB2 PE=1 SV=1	+	3.48082 8589	1.79943 0771	6.13E- 05	21	11	57. 9	SNTB2
Q9Y211	Nischarin OS=Homo sapiens OX=9606 GN=NISCH PE=1 SV=3		3.41861 6862	1.77341 2743	0.0702 90677	1	1	16 6.5	NISCH
P02748	Complement component C9 OS=Homo sapiens OX=9606 GN=C9 PE=1 SV=2	+	3.35167 1973	1.74488 096	0.0024 45463	4	2	63. 1	C9
P41219	Peripherin OS=Homo sapiens OX=9606 GN=PRPH PE=1 SV=2	+	3.34280 2703	1.74105 8208	0.0398 56933	11	2	53. 6	PRPH
Q8NFH 5	Nucleoporin NUP35 OS=Homo sapiens OX=9606 GN=NUP35 PE=1 SV=1		3.33517 0189	1.73776 0382	0.0607 84274	10	2	34. 8	NUP35
Q13509	Tubulin beta-3 chain OS=Homo sapiens OX=9606 GN=TUBB3 PE=1 SV=2		3.31071 9822	1.72714 4924	0.0565 30355	34	1	50. 4	TUBB3

Q15334	Lethal(2) giant larvae protein homolog 1 OS=Homo sapiens OX=9606 GN=LLGL1 PE=1 SV=3	+	3.12835 088	1.64540 2336	0.0322 62915	4	3	11 5.3	LLGL1
P04062	Lysosomal acid glucosylceramidase OS=Homo sapiens OX=9606 GN=GBA PE=1 SV=3	+	3.12247 2155	1.64268 8706	0.0133 7031	1	1	59. 7	GBA
Q9UJS0	Calcium-binding mitochondrial carrier protein Aralar2 OS=Homo sapiens OX=9606 GN=SLC25A13 PE=1 SV=2	+	3.08758 2635	1.62647 7749	0.0444 19617	11	2	74. 1	SLC25A 13
O60488	Long-chain-fatty-acid--CoA ligase 4 OS=Homo sapiens OX=9606 GN=ACSL4 PE=1 SV=2		3.06740 4646	1.61701 8497	0.0652 56975	6	3	79. 1	ACSL4
Q14919	Dr1-associated corepressor OS=Homo sapiens OX=9606 GN=DRAP1 PE=1 SV=3	+	3.03715 1484	1.60271 8868	0.0126 36159	9	2	22. 3	DRAP1
Q92599	Septin-8 OS=Homo sapiens OX=9606 GN=SEPTIN8 PE=1 SV=4	+	3.02837 2966	1.59854 2894	0.0113 49489	16	4	55. 7	SEPTIN 8
Q9UKG 9	Peroxisomal carnitine O-octanoyltransferase OS=Homo sapiens OX=9606 GN=CROT PE=1 SV=2		3.00571 4464	1.58770 7963	0.1836 87687	1	1	70. 1	CROT
Q12768	WASH complex subunit 5 OS=Homo sapiens OX=9606 GN=WASHC5 PE=1 SV=1	+	2.94890 6832	1.56018 0242	0.0054 39033	1	1	13 4.2	WASHC 5
O60476	Mannosyl-oligosaccharide 1,2-alpha-mannosidase IB OS=Homo sapiens OX=9606 GN=MAN1A2 PE=1 SV=1	+	2.94011 7172	1.55587 3652	0.0077 95167	3	2	73	MAN1A 2
Q9NRY 5	Protein FAM114A2 OS=Homo sapiens OX=9606 GN=FAM114A2 PE=1 SV=4	+	2.93930 5289	1.55547 5212	0.0391 11214	3	1	55. 4	FAM11 4A2
P29972	Aquaporin-1 OS=Homo sapiens OX=9606 GN=AQP1 PE=1 SV=3	+	2.93657 8556	1.55413 6232	0.0015 2288	7	1	28. 5	AQP1
Q9Y3Q 8	TSC22 domain family protein 4 OS=Homo sapiens OX=9606 GN=TSC22D4 PE=1 SV=2		2.92305 7573	1.54747 8245	0.2576 84828	3	1	41	TSC22D 4

Q9BYD 2	39S ribosomal protein L9, mitochondrial OS=Homo sapiens OX=9606 GN=MRPL9 PE=1 SV=2		2.82695 3652	1.49924 8231	0.1204 85264	7	2	30. 2	MRPL9
P11217	Glycogen phosphorylase, muscle form OS=Homo sapiens OX=9606 GN=PYGM PE=1 SV=6		2.80958 544	1.49035 7273	0.2156 64659	8	1	97	PYGM
Q5JTV8	Torsin-1A-interacting protein 1 OS=Homo sapiens OX=9606 GN=TOR1AIP1 PE=1 SV=2	+	2.75775 5129	1.46349 436	0.0055 90572	2	1	66. 2	TOR1AI P1
Q9BSU 1	Phagosome assembly factor 1 OS=Homo sapiens OX=9606 GN=PHAF1 PE=1 SV=1		2.74182 5516	1.45513 6764	0.1050 6083	2	1	47. 5	PHAF1
Q16795	NADH dehydrogenase [ubiquinone] 1 alpha subcomplex subunit 9, mitochondrial OS=Homo sapiens OX=9606 GN=NDUFA9 PE=1 SV=2	+	2.70068 0269	1.43332 2851	0.0385 62634	5	2	42. 5	NDUFA 9
P78386	Keratin, type II cuticular Hb5 OS=Homo sapiens OX=9606 GN=KRT85 PE=1 SV=1		2.69006 7384	1.42764 2311	0.1572 56838	2	2	55. 8	KRT85
Q96599	Pleckstrin homology domain-containing family F member 1 OS=Homo sapiens OX=9606 GN=PLEKHF1 PE=1 SV=3	+	2.68616 5109	1.42554 7985	0.0446 89264	5	1	31. 2	PLEKHF 1
Q8NE8 6	Calcium uniporter protein, mitochondrial OS=Homo sapiens OX=9606 GN=MCU PE=1 SV=1	+	2.66373 8575	1.41345 25	0.0083 95305	6	2	39. 8	MCU
P09228	Cystatin-SA OS=Homo sapiens OX=9606 GN=CST2 PE=1 SV=1		2.64187 2285	1.40156 0725	0.0796 85438	18	3	16. 4	CST2
Q0ZGT 2	Nexilin OS=Homo sapiens OX=9606 GN=NEXN PE=1 SV=1		2.63445 2701	1.39750 3278	0.0824 65531	5	4	80. 6	NEXN
Q8WYH 8	Inhibitor of growth protein 5 OS=Homo sapiens OX=9606 GN=ING5 PE=1 SV=1		2.61957 388	1.38933 2151	0.1030 51784	5	1	27. 7	ING5
A0A0B4 J2D5	Putative glutamine amidotransferase-like class 1 domain-containing protein 3B, mitochondrial OS=Homo sapiens OX=9606 GN=GATD3B PE=5 SV=1		2.57133 4266	1.36251 7168	0.1655 90069	12	2	28. 1	GATD3 B

P49748	Very long-chain specific acyl-CoA dehydrogenase, mitochondrial OS=Homo sapiens OX=9606 GN=ACADVL PE=1 SV=1	+	2.54813 6014	1.34944 2288	0.0004 68799	6	4	70. 3	ACADV L
Q562R1	Beta-actin-like protein 2 OS=Homo sapiens OX=9606 GN=ACTBL2 PE=1 SV=2	+	2.50853 9843	1.32684 7852	0.0265 0547	18	1	42	ACTBL2
P51570	Galactokinase OS=Homo sapiens OX=9606 GN=GALK1 PE=1 SV=1		2.48356 0269	1.31240 9758	0.0918 43007	6	2	42. 2	GALK1
Q96Q0 5	Trafficking protein particle complex subunit 9 OS=Homo sapiens OX=9606 GN=TRAPPC9 PE=1 SV=2		2.47348 5382	1.30654 5373	0.1469 90858	1	1	12 8.4	TRAPPC 9
Q9UNL 2	Translocon-associated protein subunit gamma OS=Homo sapiens OX=9606 GN=SSR3 PE=1 SV=1	+	2.46400 5144	1.30100 5268	0.0074 10222	12	3	21. 1	SSR3
P68400	Casein kinase II subunit alpha OS=Homo sapiens OX=9606 GN=CSNK2A1 PE=1 SV=1	+	2.44626 0515	1.29057 8052	0.0110 54495	33	9	45. 1	CSNK2 A1
O60306	RNA helicase aquarius OS=Homo sapiens OX=9606 GN=AQR PE=1 SV=4		2.43056 8536	1.28129 3815	0.4539 49932	2	3	17 1.2	AQR
Q9H9J2	39S ribosomal protein L44, mitochondrial OS=Homo sapiens OX=9606 GN=MRPL44 PE=1 SV=1	+	2.42994 7207	1.28092 497	0.0457 53882	3	1	37. 5	MRPL4 4
O00161	Synaptosomal-associated protein 23 OS=Homo sapiens OX=9606 GN=SNAP23 PE=1 SV=1	+	2.42739 1155	1.27940 6606	0.0002 8476	7	1	23. 3	SNAP23
Q9HCG 8	Pre-mRNA-splicing factor CWC22 homolog OS=Homo sapiens OX=9606 GN=CWC22 PE=1 SV=3		2.41698 8994	1.27321 0904	0.0636 59502	3	3	10 5.4	CWC22
P10620	Microsomal glutathione S-transferase 1 OS=Homo sapiens OX=9606 GN=MGST1 PE=1 SV=1	+	2.41250 0322	1.27052 9135	0.0330 44227	22	2	17. 6	MGST1
Q8N8S 7	Protein enabled homolog OS=Homo sapiens OX=9606 GN=ENAH PE=1 SV=2		2.40837 2637	1.26805 8631	0.2659 81112	11	6	66. 5	ENAH

Q68E01	Integrator complex subunit 3 OS=Homo sapiens OX=9606 GN=INTS3 PE=1 SV=1		2.40572 728	1.26647 3104	0.3331 49085	3	3	11 8	INTS3
O60645	Exocyst complex component 3 OS=Homo sapiens OX=9606 GN=EXOC3 PE=1 SV=3	+	2.31888 7481	1.21343 2818	0.0023 60679	5	3	85. 5	EXOC3
Q7KZ85	Transcription elongation factor SPT6 OS=Homo sapiens OX=9606 GN=SUPT6H PE=1 SV=2		2.31238 87	1.20938 3927	0.0613 56949	4	5	19 8.9	SUPT6H
Q8NDZ 4	Divergent protein kinase domain 2A OS=Homo sapiens OX=9606 GN=DIPK2A PE=1 SV=1	+	2.29026 4271	1.19551 4079	0.0236 83868	5	2	49. 5	DIPK2A
P23443	Ribosomal protein S6 kinase beta-1 OS=Homo sapiens OX=9606 GN=RPS6KB1 PE=1 SV=2		2.28649 2816	1.19313 6387	0.0894 85097	3	1	59. 1	RPS6KB 1
Q765P7	Protein MTSS 2 OS=Homo sapiens OX=9606 GN=MTSS2 PE=1 SV=1	+	2.27185 6109	1.18387 1463	0.0314 88136	1	1	79. 9	MTSS2
P62979	Ubiquitin-40S ribosomal protein S27a OS=Homo sapiens OX=9606 GN=RPS27A PE=1 SV=2		2.25584 5563	1.17366 8303	0.1221 38591	51	13	18	RPS27A
P25311	Zinc-alpha-2-glycoprotein OS=Homo sapiens OX=9606 GN=AZGP1 PE=1 SV=2		2.25123 2082	1.17071 4793	0.1067 45572	7	2	34. 2	AZGP1
Q86T29	Zinc finger protein 605 OS=Homo sapiens OX=9606 GN=ZNF605 PE=2 SV=1	+	2.24180 9729	1.16466 3836	0.0185 33709	1	1	74. 3	ZNF605
O14672	Disintegrin and metalloproteinase domain-containing protein 10 OS=Homo sapiens OX=9606 GN=ADAM10 PE=1 SV=1		2.23828 8194	1.16239 5805	0.0505 06954	3	2	84. 1	ADAM1 0
P08754	Guanine nucleotide-binding protein G(i) subunit alpha-3 OS=Homo sapiens OX=9606 GN=GNAI3 PE=1 SV=3		2.22662 156	1.15485 6376	0.0534 57238	27	2	40. 5	GNAI3
P33947	ER lumen protein-retaining receptor 2 OS=Homo sapiens OX=9606 GN=KDELR2 PE=1 SV=1		2.22618 0585	1.15457 0627	0.0701 5031	9	2	24. 4	KDELR2

Q9NW13	RNA-binding protein 28 OS=Homo sapiens OX=9606 GN=RBM28 PE=1 SV=3		2.217780546	1.149116615	0.058056621	7	5	85.7	RBM28
Q9Y676	28S ribosomal protein S18b, mitochondrial OS=Homo sapiens OX=9606 GN=MRPS18B PE=1 SV=1	+	2.216780837	1.148466145	0.037843415	3	1	29.4	MRPS18B
Q9Y673	Dolichyl-phosphate beta-glucosyltransferase OS=Homo sapiens OX=9606 GN=ALG5 PE=1 SV=1		2.214272476	1.146832763	0.158894122	10	2	36.9	ALG5
Q9HCJ6	Synaptic vesicle membrane protein VAT-1 homolog-like OS=Homo sapiens OX=9606 GN=VAT1L PE=1 SV=2		2.210112525	1.144119824	0.203771826	3	1	45.9	VAT1L
P09001	39S ribosomal protein L3, mitochondrial OS=Homo sapiens OX=9606 GN=MRPL3 PE=1 SV=1		2.206475771	1.141743906	0.148802528	3	1	38.6	MRPL3
P06858	Lipoprotein lipase OS=Homo sapiens OX=9606 GN=LPL PE=1 SV=1	+	2.195861174	1.134786848	0.006253343	8	3	53.1	LPL
P61626	Lysozyme C OS=Homo sapiens OX=9606 GN=LYZ PE=1 SV=1		2.193464577	1.133211408	0.054597749	14	2	16.5	LYZ
P10586	Receptor-type tyrosine-protein phosphatase F OS=Homo sapiens OX=9606 GN=PTPRF PE=1 SV=2		2.18968009	1.130720109	0.187100196	1	1	212.7	PTPRF
Q6UW68	Transmembrane protein 205 OS=Homo sapiens OX=9606 GN=TMEM205 PE=1 SV=1		2.181804593	1.125521897	0.19507835	5	1	21.2	TMEM205
Q9Y223	Bifunctional UDP-N-acetylglucosamine 2-epimerase/N-acetylmannosamine kinase OS=Homo sapiens OX=9606 GN=GNE PE=1 SV=1	+	2.173915063	1.120295574	0.02738209	3	2	79.2	GNE
P04792	Heat shock protein beta-1 OS=Homo sapiens OX=9606 GN=HSPB1 PE=1 SV=2		2.167873507	1.116280579	0.262154455	30	5	22.8	HSPB1

C9JLW8	Mapk-regulated corepressor-interacting protein 1 OS=Homo sapiens OX=9606 GN=MCRI1 PE=1 SV=1	+	2.16114 5664	1.11179 6315	0.0234 58281	23	2	10. 9	MCRI1
Q8N3C0	Activating signal cointegrator 1 complex subunit 3 OS=Homo sapiens OX=9606 GN=ASCC3 PE=1 SV=3	+	2.16077 4112	1.11154 8261	0.0130 54128	2	3	25 1.3	ASCC3
Q53F19	Nuclear cap-binding protein subunit 3 OS=Homo sapiens OX=9606 GN=NCBP3 PE=1 SV=2		2.15887 9772	1.11028 2902	0.1425 66364	4	2	70. 5	NCBP3
Q9H6F5	Coiled-coil domain-containing protein 86 OS=Homo sapiens OX=9606 GN=CCDC86 PE=1 SV=1		2.14614 4456	1.10174 7186	0.0652 34323	2	1	40. 2	CCDC86
P07384	Calpain-1 catalytic subunit OS=Homo sapiens OX=9606 GN=CAPN1 PE=1 SV=1		2.13345 5193	1.09319 1812	0.0906 76578	6	4	81. 8	CAPN1
Q9BPX6	Calcium uptake protein 1, mitochondrial OS=Homo sapiens OX=9606 GN=MICU1 PE=1 SV=1	+	2.11935 337	1.08362 4155	0.0073 07642	3	2	54. 3	MICU1
P29377	Protein S100-G OS=Homo sapiens OX=9606 GN=S100G PE=1 SV=2	+	2.10811 3679	1.07595 2665	0.0311 81673	9	1	9	S100G
Q9UPT8	Zinc finger CCCH domain-containing protein 4 OS=Homo sapiens OX=9606 GN=ZC3H4 PE=1 SV=3		2.10526 5877	1.07400 2445	0.1918 11664	1	1	14 0.2	ZC3H4
Q9Y6K0	Choline/ethanolaminephosphotransferase 1 OS=Homo sapiens OX=9606 GN=CEPT1 PE=1 SV=1		2.07998 8664	1.05657 5666	0.1283 40872	3	1	46. 5	CEPT1
P27482	Calmodulin-like protein 3 OS=Homo sapiens OX=9606 GN=CALML3 PE=1 SV=2	+	2.07305 2429	1.05175 6604	0.0271 54557	32	2	16. 9	CALML3
Q5T5P2	Sickle tail protein homolog OS=Homo sapiens OX=9606 GN=KIAA1217 PE=1 SV=2		2.07256 764	1.05141 9186	0.0819 43639	1	1	21 4	KIAA1217
Q12981	Vesicle transport protein SEC20 OS=Homo sapiens OX=9606 GN=BNIP1 PE=1	+	2.07212 9769	1.05111 4356	0.0019 08595	12	3	26. 1	BNIP1

	SV=3								
O15258	Protein RER1 OS=Homo sapiens OX=9606 GN=RER1 PE=1 SV=1	+	2.059800067	1.04250431	0.005271174	24	4	22.9	RER1
Q13322	Growth factor receptor-bound protein 10 OS=Homo sapiens OX=9606 GN=GRB10 PE=1 SV=2		2.036981818	1.026433103	0.056455673	2	1	67.2	GRB10
Q14643	Inositol 1,4,5-trisphosphate receptor type 1 OS=Homo sapiens OX=9606 GN=ITPR1 PE=1 SV=3		2.034884125	1.024946643	0.065229882	1	2	313.7	ITPR1
Q9HC35	Echinoderm microtubule-associated protein-like 4 OS=Homo sapiens OX=9606 GN=EML4 PE=1 SV=3	+	2.030018411	1.021492812	0.011296758	6	5	108.8	EML4
Q8IXM6	Nurim OS=Homo sapiens OX=9606 GN=NRM PE=1 SV=1	+	2.018991859	1.013635093	0.003367327	11	2	29.4	NRM
P12035	Keratin, type II cytoskeletal 3 OS=Homo sapiens OX=9606 GN=KRT3 PE=1 SV=3		2.00752797	1.005420088	0.311339054	34	8	64.4	KRT3
Q99700	Ataxin-2 OS=Homo sapiens OX=9606 GN=ATXN2 PE=1 SV=2		2.007234784	1.005209377	0.069198254	4	4	140.2	ATXN2
O76024	Wolframin OS=Homo sapiens OX=9606 GN=WFS1 PE=1 SV=2	+	2.006418527	1.004622575	0.015437012	1	1	100.2	WFS1
P42025	Beta-centractin OS=Homo sapiens OX=9606 GN=ACTR1B PE=1 SV=1	+	2.00064158	1.000462728	0.038109995	26	2	42.3	ACTR1B
Q99614	Tetratricopeptide repeat protein 1 OS=Homo sapiens OX=9606 GN=TTC1 PE=1 SV=1	+	1.985571674	0.989554439	0.013210781	7	2	33.5	TTC1
Q01629	Interferon-induced transmembrane protein 2 OS=Homo sapiens OX=9606 GN=IFITM2 PE=1 SV=2		1.980645535	0.985970713	0.061981496	12	1	14.6	IFITM2
Q9H4G0	Band 4.1-like protein 1 OS=Homo sapiens OX=9606 GN=EPB41L1 PE=1 SV=2		1.978611475	0.984488349	0.063206459	2	1	98.4	EPB41L1
Q8N201	Integrator complex subunit 1 OS=Homo sapiens OX=9606	+	1.972167498	0.979782087	0.0037171	1	3	244.1	INTS1

	GN=INTS1 PE=1 SV=2								
P35610	Sterol O-acyltransferase 1 OS=Homo sapiens OX=9606 GN=SOAT1 PE=1 SV=3	+	1.96968 6596	0.97796 6095	0.0305 2043	2	1	64. 7	SOAT1
Q96IX5	ATP synthase membrane subunit K, mitochondrial OS=Homo sapiens OX=9606 GN=ATP5MK PE=1 SV=1	+	1.96327 7645	0.97326 4212	0.0026 87606	19	2	6.5	ATP5M K
Q725L9	Interferon regulatory factor 2-binding protein 2 OS=Homo sapiens OX=9606 GN=IRF2BP2 PE=1 SV=2		1.95298 805	0.96568 3121	0.2685 70852	2	1	61	IRF2BP 2
Q96GM 5	SWI/SNF-related matrix- associated actin- dependent regulator of chromatin subfamily D member 1 OS=Homo sapiens OX=9606 GN=SMARCD1 PE=1 SV=2		1.94966 4376	0.96322 5793	0.1020 05255	4	2	58. 2	SMARC D1
Q15173	Serine/threonine-protein phosphatase 2A 56 kDa regulatory subunit beta isoform OS=Homo sapiens OX=9606 GN=PPP2R5B PE=1 SV=1		1.94761 3747	0.96170 7589	0.3168 7975	3	1	57. 4	PPP2R5 B
P27707	Deoxycytidine kinase OS=Homo sapiens OX=9606 GN=DCK PE=1 SV=1		1.94289 0722	0.95820 4759	0.2168 47717	3	1	30. 5	DCK
Q9NRY 4	Rho GTPase-activating protein 35 OS=Homo sapiens OX=9606 GN=ARHGAP35 PE=1 SV=3	+	1.92812 0619	0.94719 5306	0.0230 15192	3	4	17 0.4	ARHGA P35
Q7L014	Probable ATP-dependent RNA helicase DDX46 OS=Homo sapiens OX=9606 GN=DDX46 PE=1 SV=2	+	1.92667 0828	0.94611 0108	0.0013 98865	21	21	11 7.3	DDX46
P62861	40S ribosomal protein S30 OS=Homo sapiens OX=9606 GN=FAU PE=1 SV=1		1.90401 3193	0.92904 3475	0.0801 10162	20	3	6.6	Fau; FAU
Q15084	Protein disulfide- isomerase A6 OS=Homo sapiens OX=9606 GN=PDIA6 PE=1 SV=1	+	1.90389 039	0.92895 0423	0.0035 6032	25	9	48. 1	PDIA6

Q6KC79	Nipped-B-like protein OS=Homo sapiens OX=9606 GN=NIPBL PE=1 SV=2		1.88992 8854	0.91833 1925	0.0908 46405	2	5	31 5.9	NIPBL
P40937	Replication factor C subunit 5 OS=Homo sapiens OX=9606 GN=RFC5 PE=1 SV=1		1.88613 2009	0.91543 0653	0.0661 00645	10	3	38. 5	RFC5
P12107	Collagen alpha-1(XI) chain OS=Homo sapiens OX=9606 GN=COL11A1 PE=1 SV=4	+	1.88478 8162	0.91440 2383	0.0272 99869	2	1	18 1	COL11A 1
Q15750	TGF-beta-activated kinase 1 and MAP3K7-binding protein 1 OS=Homo sapiens OX=9606 GN=TAB1 PE=1 SV=1		1.88123 7882	0.91168 2289	0.1201 65738	2	1	54. 6	TAB1
Q16186	Proteasomal ubiquitin receptor ADRM1 OS=Homo sapiens OX=9606 GN=ADRM1 PE=1 SV=2	+	1.87987 6068	0.91063 7554	0.0065 95934	4	2	42. 1	ADRM1
Q5W0V 3	FHF complex subunit HOOK interacting protein 2A OS=Homo sapiens OX=9606 GN=FHIP2A PE=1 SV=1	+	1.87954 9133	0.91038 6629	0.0095 75981	1	1	86. 5	FHIP2A
Q8WVY 7	Ubiquitin-like domain- containing CTD phosphatase 1 OS=Homo sapiens OX=9606 GN=UBLCP1 PE=1 SV=2		1.87885 4921	0.90985 3671	0.1076 66537	14	5	36. 8	UBLCP1
Q14289	Protein-tyrosine kinase 2- beta OS=Homo sapiens OX=9606 GN=PTK2B PE=1 SV=2	+	1.87479 2773	0.90673 1138	0.0018 33411	3	2	11 5.8	PTK2B
P49770	Translation initiation factor eIF-2B subunit beta OS=Homo sapiens OX=9606 GN=EIF2B2 PE=1 SV=3	+	1.87088 1609	0.90371 8267	0.0194 22356	2	1	39	EIF2B2
Q9NZ4 5	CDGSH iron-sulfur domain- containing protein 1 OS=Homo sapiens OX=9606 GN=CISD1 PE=1 SV=1		1.86868 6939	0.90202 4895	0.2483 80701	14	1	12. 2	CISD1
Q9HD2 0	Endoplasmic reticulum transmembrane helix translocase OS=Homo sapiens OX=9606 GN=ATP13A1 PE=1 SV=2	+	1.86829 7252	0.90172 4011	0.0298 08687	8	8	13 2.9	ATP13A 1

P17516	Aldo-keto reductase family 1 member C4 OS=Homo sapiens OX=9606 GN=AKR1C4 PE=1 SV=3	+	1.86607 2503	0.90000 5041	0.0226 12703	3	1	37	AKR1C4
Q9UBF 8	Phosphatidylinositol 4-kinase beta OS=Homo sapiens OX=9606 GN=PI4KB PE=1 SV=1		1.85193 1461	0.88903 0706	0.1182 40195	3	2	91. 3	PI4KB
Q8TBQ 9	Protein kish-A OS=Homo sapiens OX=9606 GN=TMEM167A PE=1 SV=1		1.84804 7676	0.88600 1976	0.3478 95763	13	1	8.1	TMEM1 67A
Q9ULE4	Protein FAM184B OS=Homo sapiens OX=9606 GN=FAM184B PE=2 SV=3		1.84545 3899	0.88397 5699	0.0740 45827	1	1	12 1	FAM18 4B
P50993	Sodium/potassium-transporting ATPase subunit alpha-2 OS=Homo sapiens OX=9606 GN=ATP1A2 PE=1 SV=1	+	1.84487 8488	0.88352 5797	0.0151 84556	13	1	11 2.2	ATP1A2
Q96I18	DISP complex protein LRCH3 OS=Homo sapiens OX=9606 GN=LRCH3 PE=1 SV=2	+	1.84406 6985	0.88289 1062	0.0291 74883	2	1	86	LRCH3
Q96JB1	Dynein axonemal heavy chain 8 OS=Homo sapiens OX=9606 GN=DNAH8 PE=1 SV=2	+	1.83354 3226	0.87463 4278	0.0035 23121	0	1	51 4.3	DNAH8
Q9H1A 3	Protein-L-histidine N-pros-methyltransferase OS=Homo sapiens OX=9606 GN=METTL9 PE=1 SV=1		1.81883 7578	0.86301 6716	0.0732 86764	4	1	36. 5	METTL 9
Q9P035	Very-long-chain (3R)-3-hydroxyacyl-CoA dehydratase 3 OS=Homo sapiens OX=9606 GN=HACD3 PE=1 SV=2		1.81643 7192	0.86111 1482	0.2376 04395	3	1	43. 1	HACD3
Q92997	Segment polarity protein dishevelled homolog DVL-3 OS=Homo sapiens OX=9606 GN=DVL3 PE=1 SV=2	+	1.81491 0498	0.85989 8404	0.0111 42537	4	1	78	DVL3
P60709	Actin, cytoplasmic 1 OS=Homo sapiens OX=9606 GN=ACTB PE=1 SV=1	+	1.81289 9623	0.85829 9048	0.0326 21085	78	1	41. 7	ACTB
Q9NY9 3	Probable ATP-dependent RNA helicase DDX56 OS=Homo sapiens OX=9606 GN=DDX56 PE=1		1.81247 8526	0.85796 3902	0.0632 76579	10	4	61. 6	DDX56

	SV=1								
P50542	Peroxisomal targeting signal 1 receptor OS=Homo sapiens OX=9606 GN=PEX5 PE=1 SV=3		1.81176 7665	0.85739 7961	0.2180 42009	7	3	70. 8	PEX5
P55795	Heterogeneous nuclear ribonucleoprotein H2 OS=Homo sapiens OX=9606 GN=HNRNPH2 PE=1 SV=1	+	1.80581 0149	0.85264 6225	0.0064 66881	21	3	49. 2	HNRNP H2
P01111	GTPase NRas OS=Homo sapiens OX=9606 GN=NRAS PE=1 SV=1		1.80292 653	0.85034 0607	0.3606 02527	17	2	21. 2	NRAS
Q81V48	3'-5' exoribonuclease 1 OS=Homo sapiens OX=9606 GN=ERI1 PE=1 SV=3		1.79938 1598	0.84750 1174	0.1210 76552	2	1	40	ERI1
O43583	Density-regulated protein OS=Homo sapiens OX=9606 GN=DENR PE=1 SV=2		1.79855 6721	0.84683 9658	0.2028 54215	4	1	22. 1	DENR
Q9NQP 4	Prefoldin subunit 4 OS=Homo sapiens OX=9606 GN=PFDN4 PE=1 SV=1	+	1.79024 9959	0.84016 1034	0.0143 37148	11	1	15. 3	PFDN4
P61923	Coatmer subunit zeta-1 OS=Homo sapiens OX=9606 GN=COPZ1 PE=1 SV=1		1.78862 5546	0.83885 1386	0.1633 8409	22	4	20. 2	COPZ1
Q9UPN 6	SR-related and CTD-associated factor 8 OS=Homo sapiens OX=9606 GN=SCAF8 PE=1 SV=1	+	1.78738 597	0.83785 1205	0.0053 57783	1	1	14 0.4	SCAF8
P56385	ATP synthase subunit e, mitochondrial OS=Homo sapiens OX=9606 GN=ATP5ME PE=1 SV=2	+	1.77612 1796	0.82873 0517	0.0018 96948	17	2	7.9	ATP5M E
O00116	Alkylidihydroxyacetonephosphate synthase, peroxisomal OS=Homo sapiens OX=9606 GN=AGPS PE=1 SV=1	+	1.77456 6761	0.82746 6851	0.0027 91112	7	4	72. 9	AGPS
P51809	Vesicle-associated membrane protein 7 OS=Homo sapiens OX=9606 GN=VAMP7 PE=1 SV=3		1.76755 6173	0.82175 6065	0.2080 6552	13	3	24. 9	VAMP7

Q8N5Z5	BTB/POZ domain-containing protein KCTD17 OS=Homo sapiens OX=9606 GN=KCTD17 PE=1 SV=3		1.766698865	0.821056152	0.063547502	4	1	35.6	KCTD17
Q9H0A0	RNA cytidine acetyltransferase OS=Homo sapiens OX=9606 GN=NAT10 PE=1 SV=2	+	1.75929814	0.81499999	0.012275533	5	5	115.7	NAT10
O94829	Importin-13 OS=Homo sapiens OX=9606 GN=IPO13 PE=1 SV=3		1.754557684	0.81110738	0.176106771	1	1	108.1	IPO13
P29353	SHC-transforming protein 1 OS=Homo sapiens OX=9606 GN=SHC1 PE=1 SV=4		1.745464814	0.803611275	0.291979295	4	2	62.8	SHC1
Q9Y613	FH1/FH2 domain-containing protein 1 OS=Homo sapiens OX=9606 GN=FHOD1 PE=1 SV=3	+	1.742858291	0.801455271	0.003520321	3	4	126.5	FHOD1
Q9Y608	Leucine-rich repeat flightless-interacting protein 2 OS=Homo sapiens OX=9606 GN=LRRFIP2 PE=1 SV=1	+	1.741788734	0.800569646	0.002189086	4	2	82.1	LRRFIP2
P30043	Flavin reductase (NADPH) OS=Homo sapiens OX=9606 GN=BLVRB PE=1 SV=3		1.737910389	0.797353695	0.201057045	17	2	22.1	BLVRB
Q96FN9	D-aminoacyl-tRNA deacylase 2 OS=Homo sapiens OX=9606 GN=DTD2 PE=1 SV=1		1.733339823	0.793554524	0.323428542	5	1	18.6	DTD2
Q12769	Nuclear pore complex protein Nup160 OS=Homo sapiens OX=9606 GN=NUP160 PE=1 SV=3		1.719339308	0.781854285	0.419907532	2	3	162	NUP160
P55212	Caspase-6 OS=Homo sapiens OX=9606 GN=CASP6 PE=1 SV=2		1.716850916	0.779764767	0.179355893	3	1	33.3	CASP6
Q13586	Stromal interaction molecule 1 OS=Homo sapiens OX=9606 GN=STIM1 PE=1 SV=3	+	1.715397114	0.778542599	0.005219278	8	4	77.4	STIM1
Q86UE4	Protein LYRIC OS=Homo sapiens OX=9606 GN=MTDH PE=1 SV=2	+	1.712775962	0.776336453	0.048159924	14	5	63.8	MTDH
O15400	Syntaxin-7 OS=Homo sapiens OX=9606 GN=STX7 PE=1 SV=4		1.710513237	0.774429269	0.156986408	36	7	29.8	STX7

Q9Y282	Endoplasmic reticulum-Golgi intermediate compartment protein 3 OS=Homo sapiens OX=9606 GN=ERGIC3 PE=1 SV=1	+	1.70682 7302	0.77131 7093	0.0494 19988	7	3	43. 2	ERGIC3
P51531	Probable global transcription activator SNF2L2 OS=Homo sapiens OX=9606 GN=SMARCA2 PE=1 SV=2	+	1.70645 6161	0.77100 3352	0.0282 99915	7	2	18 1.2	SMARCA2
Q9UII2	ATPase inhibitor, mitochondrial OS=Homo sapiens OX=9606 GN=ATP5IF1 PE=1 SV=1		1.70027 1765	0.76576 536	0.1877 27896	8	1	12. 2	ATP5IF1
Q9H492	Microtubule-associated proteins 1A/1B light chain 3A OS=Homo sapiens OX=9606 GN=MAP1LC3A PE=1 SV=2		1.69884 9036	0.76455 7657	0.2169 08738	17	1	14. 3	MAP1LC3A
Q9HD33	39S ribosomal protein L47, mitochondrial OS=Homo sapiens OX=9606 GN=MRPL47 PE=1 SV=2	+	1.69774 0362	0.76361 5842	0.0390 51147	4	1	29. 4	MRPL47
Q9BPX3	Condensin complex subunit 3 OS=Homo sapiens OX=9606 GN=NCAPG PE=1 SV=1		1.69348 8113	0.75999 7861	0.0711 61279	4	4	11 4.3	NCAPG
Q7RTS9	Dymeclin OS=Homo sapiens OX=9606 GN=DYM PE=1 SV=1		1.69066 7666	0.75759 3098	0.0970 63707	3	2	75. 9	DYM
Q9UBP6	tRNA (guanine-N(7)-methyltransferase OS=Homo sapiens OX=9606 GN=METT1 PE=1 SV=1	+	1.68964 576	0.75672 0812	0.0268 48138	3	1	31. 5	METT1
P07954	Fumarate hydratase, mitochondrial OS=Homo sapiens OX=9606 GN=FH PE=1 SV=3		1.68910 5285	0.75625 9257	0.1348 40993	11	5	54. 6	FH
P14314	Glucosidase 2 subunit beta OS=Homo sapiens OX=9606 GN=PRKCSH PE=1 SV=2	+	1.68120 5442	0.74949 6032	0.0438 62814	7	5	59. 4	PRKCSH
P08727	Keratin, type I cytoskeletal 19 OS=Homo sapiens OX=9606 GN=KRT19 PE=1 SV=4		1.67382 5758	0.74314 9354	0.1961 66392	63	17	44. 1	KRT19
Q96BP3	Peptidylprolyl isomerase domain and WD repeat-containing protein 1 OS=Homo sapiens	+	1.67076 2824	0.74050 6947	0.0375 36546	4	2	73. 5	PPWD1

	OX=9606 GN=PPWD1 PE=1 SV=1								
Q14232	Translation initiation factor eIF-2B subunit alpha OS=Homo sapiens OX=9606 GN=EIF2B1 PE=1 SV=1		1.67002 1349	0.73986 6546	0.0513 2117	8	2	33. 7	EIF2B1
O75477	Erlin-1 OS=Homo sapiens OX=9606 GN=ERLIN1 PE=1 SV=2		1.66510 7912	0.73561 5679	0.2453 47864	17	2	39. 1	ERLIN1
Q99986	Serine/threonine-protein kinase VRK1 OS=Homo sapiens OX=9606 GN=VRK1 PE=1 SV=1		1.66509 4681	0.73560 4214	0.1171 49686	10	4	45. 4	VRK1
P15848	Arylsulfatase B OS=Homo sapiens OX=9606 GN=ARSB PE=1 SV=1		1.66054 8531	0.73165 9887	0.0863 88279	1	1	59. 6	ARSB
O15173	Membrane-associated progesterone receptor component 2 OS=Homo sapiens OX=9606 GN=PGRMC2 PE=1 SV=1	+	1.65422 078	0.72615 1796	0.0159 3846	17	4	23. 8	PGRMC 2
P46926	Glucosamine-6-phosphate isomerase 1 OS=Homo sapiens OX=9606 GN=GNPDA1 PE=1 SV=1		1.65293 8482	0.72503 3032	0.1023 8487	11	2	32. 6	GNPDA 1
Q8N8A 2	Serine/threonine-protein phosphatase 6 regulatory ankyrin repeat subunit B OS=Homo sapiens OX=9606 GN=ANKRD44 PE=1 SV=3		1.65270 6649	0.72483 0673	0.0688 10502	3	2	10 7.5	ANKRD 44
Q9NRI5	Disrupted in schizophrenia 1 protein OS=Homo sapiens OX=9606 GN=DISC1 PE=1 SV=3	+	1.65259 3519	0.72473 1915	0.0214 42067	1	1	93. 6	DISC1
Q14694	Ubiquitin carboxyl-terminal hydrolase 10 OS=Homo sapiens OX=9606 GN=USP10 PE=1 SV=2		1.65145 4543	0.72373 7259	0.1405 49435	5	3	87. 1	USP10
P62273	40S ribosomal protein S29 OS=Homo sapiens OX=9606 GN=RPS29 PE=1 SV=2		1.64967 6371	0.72218 3028	0.1263 67596	46	3	6.7	RPS29
Q9Y6A 4	Cilia- and flagella-associated protein 20 OS=Homo sapiens OX=9606 GN=CFAP20 PE=1 SV=1	+	1.64642 4967	0.71933 6765	0.0391 7482	21	4	22. 8	CFAP20

Q86U70	LIM domain-binding protein 1 OS=Homo sapiens OX=9606 GN=LDB1 PE=1 SV=2		1.64183701	0.715310913	0.111682393	4	1	46.5	LDB1
---------------	--	--	-------------------	--------------------	-------------	----------	---	------	------

ii. ONE WAY ANOVA:

Ordinary one-way ANOVA ANOVA results						
1	Table Analyzed	Treatments2				
2	Data sets analyzed	A-D				
3						
4	ANOVA summary					
5	F	147.6				
6	P value	<.001				
7	P value summary	***				
8	Significant diff. among means (P < 0.05)?	Yes				
9	R squared	0.9823				
10						
11	Brown-Forsythe test					
12	F (DFn, DFd)	0.5572 (3, 8)				
13	P value	.858				
14	P value summary	ns				
15	Are SDs significantly different (P < 0.05)?	No				
16						
17	Bartlett's test					
18	Bartlett's statistic (corrected)					
19	P value					
20	P value summary					
21	Are SDs significantly different (P < 0.05)?					
22						
23	ANOVA table	SS	DF	MS	F (DFn, DFd)	P value
24	Treatment (between columns)	1403	3	467.7	F (3, 8) = 147.6	P<.001
25	Residual (within columns)	25.35	8	3.169		
26	Total	1428	11			
27						
28	Data summary					
29	Number of treatments (columns)	4				
30	Number of values (total)	12				

iii. Standard Curve and interpolation:

Interpolation Table of results		A Absorbance (450nm)
1	Sigmoidal, 4PL, X is concentration	
2	Best-fit values	
3	Bottom	0.1448
4	Top	2.991
5	IC50	40.47
6	HillSlope	2.245
7	logIC50	1.607
8	Span	2.847
9	95% CI (asymptotic)	
10	Bottom	0.1024 to 0.1871
11	Top	2.937 to 3.046
12	IC50	39.09 to 41.86
13	HillSlope	2.090 to 2.400
14	logIC50	1.592 to 1.622
15	Span	2.774 to 2.920
16	Goodness of Fit	
17	Degrees of Freedom	11
18	R squared	0.9993
19	Adjusted R squared	0.9991
20	Sum of Squares	0.01232
21	Replicates test for lack of fit	
22	SD replicates	0.03507
23	SD lack of fit	0.004028
24	Discrepancy (F)	0.01319
25	P value	.911
26	Evidence of inadequate model?	No
27		
28	Number of points	
29	# of X values	15
30	# Y values analyzed	15

CHAPTER 9

LIST OF PUBLICATIONS

9. List of Publications:

(a)



Review

Deep Insight of the Pathophysiology of Gestational Diabetes Mellitus

Amarish Kumar Sharma ¹, Sanjeev Singh ¹, Himanshu Singh ¹, Deviyani Mahajan ¹, Prachetha Kolli ²,
Gowtham Mandadapu ³, Bimlesh Kumar ⁴, Dharmendra Kumar ⁵, Sudarshan Kumar ⁶
and Manoj Kumar Jena ^{1,*}

- ¹ Department of Biotechnology, School of Bioengineering and Biosciences, Lovely Professional University, Phagwara 144411, Punjab, India
 - ² Microgen Health Inc., 14225 Sullyfield Cir Suite E, Chantilly, VA 20151, USA
 - ³ Devansh Lab Werks, 234 Aquarius Drive, Homewood, AL 35209, USA
 - ⁴ School of Pharmaceutical Sciences, Lovely Professional University, Phagwara 144411, Punjab, India
 - ⁵ Animal Physiology and Reproduction Division, ICAR-Central Institute for Research on Buffaloes, Hisar 125001, Haryana, India
 - ⁶ Animal Biotechnology Centre, ICAR-National Dairy Research Institute, Karnal 132001, Haryana, India
- * Correspondence: manoj.20283@lpu.co.in

Abstract Diabetes mellitus is a severe metabolic disorder, which consistently requires medical care and self-management to restrict complications, such as obesity, kidney damage and cardiovascular diseases. The subtype gestational diabetes mellitus (GDM) occurs during pregnancy, which severely affects both the mother and the growing foetus. Obesity, uncontrolled weight gain and advanced gestational age are the prominent risk factors for GDM, which lead to high rate of perinatal mortality and morbidity. Zn in-depth understanding of the molecular mechanism involved in GDM will help researchers to design drugs for the optimal management of the condition without affecting the mother and foetus. This review article is focused on the molecular mechanism involved in the pathophysiology of GDM and the probable biomarkers, which can be helpful for the early diagnosis of the condition. The early diagnosis of the metabolic disorder, most preferably in first trimester of pregnancy, will lead to its effective long-term management, reducing foetal developmental complications and mortality along with safety measures for the mother.

Keywords: gestational diabetes mellitus; VEGF; pregnancy; pathophysiology; biomarker



Citation: Sharma, A.K.; Singh, S.; Singh, H.; Mahajan, D.; Kolli, P.; Mandadapu, G.; Kumar, B.; Kumar, D.; Kumar, S.; Jena, M.K. Deep Insight of the Pathophysiology of Gestational Diabetes Mellitus. *Cells* **2022**, *11*, 2672. <https://doi.org/10.3390/cells11172672>

Academic Editor: Georg Boker

(b)

An *in vitro* Model to Study Placental Functions in Gestational Diabetes Mellitus

Amarish Kumar Sharma¹, Nihar Ranjan Nayak² and Manoj Kumar Jena^{1,*}

¹*Department of Biotechnology, School of Bioengineering and Biosciences, Lovely Professional University, Punjab 144411, India*

²*Department of Obstetrics and Gynecology, UMKC School of Medicine, Missouri 64108, United States of America*

(*Corresponding author's e-mail: manoj.20283@lpu.co.in)

Received: 25 August 2023, Revised: 8 September 2023, Accepted: 15 September 2023, Published: 20 October 2023

Abstract

Background: Gestational diabetes mellitus (GDM) is a serious pregnancy complication that affects around 14 % of pregnancies worldwide. It not only causes short-term complications in the mother and child but also significantly increases the risks of several chronic diseases, including cardiovascular diseases and diabetes. An excess production of the soluble vascular endothelial growth factor (VEGF) receptor 1 in the placenta, which is a natural inhibitor of VEGF, has been linked to various pregnancy complications. However, placentas affected by GDM often exhibit increased vascularization, suggesting that the role of VEGF in GDM differs from its impact on typical pregnancy complications. Unfortunately, limited studies on placental functions in GDM have been conducted due to a lack of reliable culture models. **Methods:** In this study, we developed an *in vitro* model of GDM using the human choriocarcinoma trophoblast cell line BeWo and examined the effects of VEGF on glucose uptake. The BeWo cells were treated with a high glucose-containing (25 mM) syncytialization differentiation medium to produce insulin-resistant cells. Insulin resistance was assessed by a glucose uptake assay using the fluorescent glucose analog 2-NBDG and flow cytometry analysis. **Results:** The cells treated with high glucose exhibited a significant decrease in glucose uptake, suggesting the successful development of glucose resistance in these cells. However, VEGF treatment did not show a significant impact on glucose uptake in high glucose-treated cells. **Conclusions:** It is important to note that glucose homeostasis is a complex process involving multiple cell types, and further studies are necessary to fully understand the functions of VEGF on GDM placentas. Nevertheless, the *in vitro* model we have developed and validated will be a valuable tool for studying placental pathophysiology in GDM and evaluating the effectiveness of potential therapeutic agents.

Keywords: Gestational diabetes mellitus, Biomarker, Trophoblast, Insulin resistance, BeWo cells, VEGF, Flow cytometry

CHAPTER 10

LIST OF CONFERENCES

10. List of conferences

Oral Presentations:

- (a) Oral presentation on the title “Effect of exogenous Vascular Endothelial Growth Factor on the Glucose Homeostasis in an Insulin Resistant Gestation Diabetes Mellitus (GDM) Cell Model” with Co-author/s: Manoj Kumar Jena at International Conference on Recent Advances in Biotechnology (icRAB -2022) on 2nd-4th December 2022



- (b) Oral Presentation on the topic entitled Establishment of In-vitro Insulin Resistant model for Evaluation of Glucose Transport in Gestation Diabetes Mellitus Study in the International Conference on Bioengineering and Biosciences (ICBB-2022) held on 18-19 November 2022 organized by the Department of Biotechnology, School of Bio-engineering and Biosciences in association with the Society of Bioinformatics for Experimenting Scientists (Bioclues) organized at Lovely Professional University, Punjab.

